

**IMPACT OF COMBINED
MECHANICAL DAMAGE ON
THE INTEGRITY OF PIPELINES**

BY
HUSAIN MUHAMMED AL-MUSLIM

A Dissertation Presented to the
DEANSHIP OF GRADUATE STUDIES

KING FAHD UNIVERSITY OF PETROLEUM & MINERALS

DHAHRAN, SAUDI ARABIA

In Partial Fulfillment of the
Requirements for the Degree of

DOCTOR OF PHILOSOPHY

In

MECHANICAL ENGINEERING

MAY 2010

**KING FAHD UNIVERSITY OF PETROLEUM AND MINERALS
DHAHRAN 31261, SAUDI ARABIA**

DEANSHIP OF GRADUATE STUDIES

This dissertation, written by **Mr. Husain Muhammed Al-Muslim** under the direction of his dissertation advisor and approved by his dissertation committee, has been presented to and accepted by the Dean of Graduate Studies, in partial fulfillment of the requirements for the degree of **DOCTOR OF PHILOSOPHY IN MECHANICAL ENGINEERING**.

Dissertation Committee



Prof. Dr. Abul Fāzal M. Arif
Dissertation Advisor



Prof. Dr. Abdel Salam M. Eleiche, **Member**



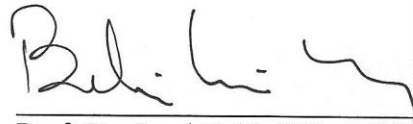
Dr. Amro Al-Qutub
Chairman, Mechanical Engineering



Prof. Dr. Anwar Khalil Sheikh, **Member**



Dr. Salam A. Zummo
Dean of Graduate Studies



Prof. Dr. Sami Bekir Yilbas, **Member**



Dr. Muhammad Kalimur Rahman, **Member**

Date: 24/9/20

Dedicated to
my beloved sister
AMAL

ACKNOWLEDGMENT

In the name of Allah, Most Gracious, Most Merciful, "My welfare is only in Allah. In Him I trust and unto Him I turn" Sourat Hood (S. 11), Ayah 88, The Holy Quran.

First and above all, all praise to Allah, Who gave us the gift of mind and inspired me with the will to accomplish this work. And second, prayers and peace upon His Prophet, Mohammed. I ask Allah to accept my efforts and make this work beneficial to me and others.

The support provided by the King Fahd University of Petroleum and Minerals is highly acknowledged. Also, I would like to appreciate the full support by my Company, Saudi Aramco, for sponsoring my residency period in the university.

I would like to extend my profound gratitude to my Dissertation Chairman Prof. Dr. Abul Fazal Arif whose knowledge, guidance, advice, encouragement and care raised my spirit to accomplish such jobs. Throughout the years of my PhD program, and even before starting the dissertation work, Dr. Arif supported me in overcoming many hurdles in the way.

Appreciation words are not enough, but are the least to give to the members of my Dissertation Committee. I would like to extend my appreciation to Prof. Dr. Abdel Salam Eleiche, Prof. Dr. Anwar Sheikh, Prof. Dr. Sami Yilbas, and Dr. Muhammad Kalimur Rahman. Their guidance during the work, and their valuable comments, enriched my knowledge and improved my work.

Special thanks to those people behind the scenes; the engineers and technicians in KFUPM facilities, Mr. Abdul Abdulaziz Al-Abdullatif, Mr. Muhammad Al-Hamdan, Mr. Saber Ali, Mr. Kamal (ME shop), Mr. Saleh Al-Abbas (material lab), Mr. Omar (CE), and Mr. Esam Khoja (IT HPC) for their assistance.

I would like also to thank my management and colleagues in Saudi Aramco, Consulting Services Department for their support especially Mr. Nadhir Al-Nasri and Mr. Tony Dib. I am due of special thanks to Mr. Tareq Al-Nuaim, Mr. Khalifah Al-Yahyai and Mr. Allan Cavaletto for their support of my sponsorship for the residency period in KFUPM.

To the reason of my existence, to the persons who are behind all of this, I kiss the hands of my parents who raised me well and planted the seed of love of education and science in my hearts. I also appreciate the love and support from my brothers, sisters, relatives and friends especially to me beloved sister, Amal, my Allah bless her soul.

Finally, no matter what I say, I cannot thank my dear wife enough for her love, patience, encouragement, understanding and support. No such work could ever been accomplished without her support. Thanks also to my children Ali, Amal, and Mariya for giving me the laughter and enjoyment during the rest periods.

TABLE OF CONTENTS

Acknowledgment	iv
Table of Contents	v
List of Tables	xiii
List of Figures	xvi
Abstract (English)	xxii
Abstract (Arabic)	xxiii
1. INTRODUCTION	1
1.1 Background	1
1.1.1 Pipeline Failure History	1
1.1.2 Pipeline Integrity Management System (PIMS)	3
1.1.3 Classification of mechanical damage	9
1.1.4 Definitions of terms related to mechanical damage	10
1.1.5 Detection tool techniques	11
1.1.6 Modes of failures	13
1.1.7 Parameters of the mechanical damage	15
1.2 Current dissertation work	17
1.2.1 Motivation and Significance of the Proposed Work	17
1.2.2 Objectives and Scope of Work	19
1.2.3 Dissertation Tasks	22
2. LITERATURE REVIEW	25
2.1 Ground research (prior to year 2000)	25

2.2 Recent research (2000-2008)	27
2.2.1 Critical Review of Available Assessment Models	27
2.2.2 Assessment application by Pipeline Operators	28
2.2.3 Simulating the Denting Process	29
2.2.4 Damage Assessment Using S-N Curve	30
2.2.5. Damage Assessment Using Fatigue Crack Growth (Paris Law)	31
2.2.6 Damage Assessment Using Strain-Based Approach	33
2.2.7 Damage Assessment Using Fracture Mechanics and Importance of Residual Stresses	34
2.2.8 Damage Assessment Using Probabilistic Design	36
2.3 Active research program	38
2.4 Assessment and acceptance criteria by local and international Codes	41
3. MATERIAL CHARACTERIZATION OF DAMAGED PIPES	44
3.1 Introduction	44
3.2 Test plan and procedures	45
3.3 Sample preparations and testing	49
3.3.1 Tensile Test Specimen	51
3.3.2 Impact Test Specimen	54
3.3.3 Hardness Test Specimen	54
3.3.4 Microscopic Test Specimen	59
3.4 Results and discussion	59
3.4.1 Visual Inspection	59
3.4.2 Tensile Test	65

3.4.3 Impact Test	70
3.4.4 Hardness Test	74
3.4.5 Microscopic Tests	74
3.5 Summary	77

4. DEVELOPMENT AND VALIDATION OF 3D FINITE ELEMENT

MODEL	81
4.1 Introduction	81
4.2 Material modeling of plastic behavior	84
4.2.1 Isotropic Hardening Rule	86
4.2.2 Kinematic Hardening Rule	86
4.2.3 Hill's Potential Theory for Anisotropy Material	88
4.2.4 Combined Material Models	89
4.3 Description of the problem	89
4.3.1 Geometry and Boundary Conditions	89
4.3.2 Loading: Static Indentation and Cyclic Pressurization	90
4.3.3 Pipe Material Properties	90
4.4 Description of the numerical model	93
4.4.1 Material Modeling	95
4.4.2 FE Model	99
4.5 Results and discussion	100
4.5.1 Strain Profiles	100
4.5.2 Stress-Based Fatigue Analysis	109
4.5.3 Transferability Tests	110

6.3.1 FE Model	165
6.3.2 Material Model	165
6.4 Deterministic Analysis of the Base Case	167
6.4.1 Strain Fields at End of Indentation Phase	167
6.4.2 Stress Fields at End of Indentation Phase	171
6.4.3 Stress Range at End of Pressure Cycle and Fatigue Analysis	171
6.5 Probabilistic analysis	174
6.5.1 Random Input Variables	174
6.5.2 Probability Analysis Loops	176
6.5.3 Probability Analysis Results	177
6.5.4 Regression Analysis	179
6.6 Summary	181
7. IMPACT OF INTERACTION OF TWO DENTS	185
7.1 Introduction	185
7.2 Description of the Problem	187
7.3 Description of the Numerical Model	187
7.3.1 FE Model	190
7.3.2 Material Model	190
7.4 Deterministic Analysis of 2 Indenters	193
7.4.1 Strain fields at end of indentation phase	193
7.4.2 Stress Fields at End of Indentation Phase	197
7.4.3 Stress Range at End of Pressure Cycle and Fatigue Analysis	201
7.5 Probabilistic Analysis	204

7.5.1 Random Input Variables	204
7.5.2 Probability Analysis Loops	205
7.5.3 Probability Analysis Results	205
7.5.4 Regression Analysis	211
7.6 Summary	213
8. IMPACT OF INTERACTION OF DENT WITH METAL LOSS	218
8.1 Introduction	218
8.2 Description of the Problem	219
8.3 Description of the Numerical Model	219
8.3.1 FE Model	221
8.3.2 Material Model	221
8.4 Deterministic Analysis of Dent with Metal Loss	221
8.4.1 Strain fields at End of Indentation Phase	222
8.4.2 Stress Fields at End of Indentation Phase	222
8.4.3 Stress Range at End of Pressure Cycle and Fatigue Analysis	228
8.5 Probabilistic analysis	228
8.5.1 Random Input Variables	229
8.5.2 Probability Analysis Loops	229
8.5.3 Probability Analysis Results	229
8.5.4 Regression Analysis	234
8.6 Summary	235

9. IMPACT OF INTERACTION OF DENT WITH RESIDUAL STRESSES OF	
WELDS	239
9.1 Introduction	239
9.2 Description of the Problem	241
9.3 Description of the Numerical Model	245
9.3.1 FE Model	245
9.3.2 Material Model	245
9.4 Deterministic Analysis of Dent with Weld Residual Stress	247
9.4.1 Strain fields at End of Indentation Phase	247
9.4.2 Stress Fields at End of Indentation Phase	253
9.4.3 Stress Range at End of Pressure Cycle and Fatigue Analysis	253
9.5 Probabilistic Analysis	258
9.5.1 Random Input Variables	258
9.5.2 Probability Analysis Loops	259
9.5.3 Probability Analysis Results	260
9.5.4 Regression Analysis	267
9.6 Summary	268
CONCLUSIONS AND RECOMMENDATIONS	273
10.1 Conclusions	273
10.2 Recommendations	274
NOMENCLATURE	276
APPENDIX A: INSPECTION DATA OF MECHANICAL DAMAGE	280

APPENDIX B: DETAILED INPUT AND RESULTS OF PROBABILITY

DESIGN ANALYSIS	288
REFERENCES	327
VITA	340

LIST OF TABLES

<u>Table</u>	<u>Page</u>
3.1. Summary of test plan	48
3.2. List of equipment required for the various planned mechanical and microscopic tests	50
3.3. Photographs of damaged pipes	62
3.4. Recording of dent dimensions damaged pipes	66
3.5. Tensile properties at pipe dent peak, dent edge and undamaged sections	69
3.6. Impact test results at pipe dent peak, dent edge and undamaged sections	72
3.7. Optical microscopy at 50 magnifications of microstructure of different sections of damaged pipe	78
3.8. SEM microscopy at 900 magnifications of microstructure of different sections of damaged pipe	79
4.1. Summary of eight material models utilized in this paper	97
4.2. Percentage errors for each FEA material model in comparison with experimental results	104
4.3. Fatigue life calculation for various FEA material models	111
4.4. Comparison of numerical and experimental fatigue cycles for three different indentation/pressurization loads	112
5.1 Compare two samples of mechanical damage data (local vs. external)	136
5.2. Types and parameters of statistical distributions	138
5.3 Hit rate for specific surveyed pipelines and generic pipeline population	159
5.4 Cumulative number of dents vs. cumulative exposure	160
6.1. Stress range and fatigue cycles at different locations of dent	175

7.1 Comparison of results between single dent and 2 dents	198
7.2. Comparison of results between single dent and 2 dents for shallow dent depth	203
7.3 Probability percentage of failure for pipe with 2 dents	208
8.1 Comparison of results between no-metal loss case with 12.5% and 50% metal loss cases	225
8.2 Probability percentage of failure for combined damage of dent and metal loss	232
9.1 Comparison of results between no-weld case and longitudinal and girth weld cases	252
9.2 Probability percentage of failure for dents interacting with welds	263
A.1. Inspection data of dents from local company	281
A.2. Sample of mechanical damage survey data by PRCI	285
B.1.1. List of random input variables and their statistical distribution for single dent	289
B.1.2. Output parameters and their statistical distribution for single dent	290
B.1.3. Rank order Spearman Correlation factors between output and input parameters for single dent	291
B.1.4. Regression analysis- Coefficients and R^2 value for single dent	293
B.2.1. List of random input variables and their statistical distribution for interaction of 2 dents	294
B.2.2. Output parameters and their statistical distribution for interaction of 2 dents	296
B.2.3. Rank order Spearman Correlation factors between output and input parameters for interaction of 2 dents	297
B.2.4. Regression analysis- Coefficients and R^2 value for interaction of 2 dents	299
B.3.1. List of random input variables and their statistical distribution for interaction of dent with metal loss	302
B.3.2. Output parameters and their statistical distribution for interaction of dent with metal loss	304

B.3.3. Rank order Spearman Correlation factors between output and input parameters for interaction of dent with metal loss	306
B.3.4. Regression analysis- Coefficients and R^2 value for interaction of dent with metal loss	308
B.4.1. List of random input variables and their statistical distribution for interaction of dent with longitudinal weld	311
B.4.2. Output parameters and their statistical distribution for interaction of dent with longitudinal weld	313
B.4.3. Rank order Spearman Correlation factors between output and input parameters for interaction of dent with longitudinal weld	314
B.4.4. Regression analysis- Coefficients and R^2 value for interaction of dent with longitudinal weld	316
B.5.1. List of random input variables and their statistical distribution for interaction of dent with girth weld	319
B.5.2. Output parameters and their statistical distribution for interaction of dent with girth weld	321
B.5.3. Rank order Spearman Correlation factors between output and input parameters for interaction of dent with girth weld	322
B.5.4. Regression analysis- Coefficients and R^2 value for interaction of dent with girth weld	324

LIST OF FIGURES

<u>Figure</u>	<u>Page</u>
1.1. Mechanical damage due to third party activities	2
1.2. Mechanical damage in offshore pipeline	2
1.3. Mechanical damage due to pipe movement	4
1.4. Pipe collapse under sleeve because of hydrogen trap	4
1.5. Illustration of pipeline dent and its dimensions	5
1.6. Elements of the Pipeline Integrity Management System (PIMS)	6
1.7. Picture of (a) Caliper ILI tool. (b) Sensor arm.	14
1.8. Picture of MFL tool	14
1.9. Picture of (a) UT tool. (b) ultrasonic transducer	14
1.10. Parameters of the mechanical damage	16
3.1. Measurement of dent depth in damaged pipe before cutting	46
3.2. Preparation of tensile specimen (a) selected locations for tensile test (b) dimensions of tensile specimen	52
3.3. Installation of strain gauge on tensile specimen (a) tools needed (b) installed gauge	53
3.4. Mounting the specimen on the tensile testing machine	55
3.5. Preparation of impact specimen (a) selected locations for impact test (b) dimensions of impact specimen	56
3.6. Equipment for impact testing (a) temperature controller (b) impact test machine	57
3.7. Microhardness test preparation (a) cut strip along axial direction (b) cut strip along transverse direction (c) cut cube sample (d) location of microhardness measurement	58

3.8 Sample preparation for microscopy (a) mounting (b) grinding (c) polishing (d) gold plating (c) final specimen	60
3.9. Equipment for microscopic analysis (a) optical microscopy (b) SEM/EDS	61
3.10. Stress-strain curves for tensile specimens from pipe no. 3 (a) full range (b) initial yield range	67
3.11. Stress-strain curves for tensile specimens from pipe no. 9 (a) full range (b) initial yield range	68
3.12. Regression fit for elastic modulus of P3-undamaged with estimate of error limits	71
3.13. Hardness results along pipe dented area (a) transverse direction (b) longitudinal direction	75
3.14. EDS Analysis of damaged pipe specimen	76
4.1. Yield surface for isotropic and anisotropic materials.	85
4.2. Stress-strain curves for different hardening rules.	87
4.3. Progressive development of yield surface for isotropic and kinematic hardening rules	87
4.4. Cross-section of problem at the pipe mid-span	91
4.5. Monotonic and cyclic stress-strain curves of the pipe material (a) full range (b) zoom at elastic and initial plastic portion	92
4.6. Quarter symmetry model of the pipe indentation FEA model	94
4.7. Mesh of indentation problem (a) overall (b) finer mesh closer to indenter	101
4.8. Convergence check of Von Mises strains at the dent peak	102
4.9. Comparison of circumferential strain history between FEA runs and experimental results	106
4.10. Comparison of axial strain history between FEA runs and experimental results	107
5.1. Illustration of dummy caliper run	119

5.2 Graphical illustration for Kolmogorov-Smirnov distance test for goodness of fit	130
5.3 Comparison of two samples of D/t (local vs. external)	
(a) frequency histogram (b) density traces (c) quantile plot	133
5.4 Cumulative probability of sample data and fitted distribution for D/t ratio	
(a) local company (b) external companies	137
5.5. Comparison of two samples of d/D% (local vs. external)	
(a) frequency histogram (b) density traces (c) quantile plot	139
5.6. Cumulative probability of sample data and fitted distribution for d/D% ratio	
(a) local company (b) external companies	142
5.7 Comparison of two samples of l/d (local vs. external)	
(a) frequency histogram (b) density traces (c) quantile plot	143
5.8 Cumulative probability of sample data and fitted distribution for l/d ratio	
(a) local company (b) external companies	146
5.9 Comparison of two samples of SMYS (local vs. external)	
(a) frequency histogram (b) density traces (c) quantile plot	147
5.10 Cumulative probability of sample data and fitted distribution for SMYS	
(a) local company (b) external companies	149
5.11 Comparison of two samples of age (local vs. external)	
(a) frequency histogram (b) density traces (c) quantile plot	151
5.12 Cumulative probability of sample data and fitted distribution for pipe age	
(a) local company (b) external companies	154
5.13 Statistical distributions of pipe manufacturing seam type	155
5.14 Statistical distributions of pipe product type	157
5.15. Linear regression fit of hit rate trend (a) fitted line and prediction intervals	
(b) plot of residuals	161
6.1. Full and 3-point approximation of stress-strain curves of the pipe material	
(a) full range (b) zoom at elastic and initial plastic portion	166
6.2. Axial strain profile at (a) top shell (b) bottom shell	168
6.3. Hoop strain profile at (a) top shell (b) bottom shell	169

6.4. Axial strain profile along longitudinal axis from dent peak	170
6.5. Axial stress profile at (a) top shell (b) bottom shell	172
6.6. Hoop stress profile at (a) top shell (b) bottom shell	173
6.7. Sample history of axial strain at dent peak	178
6.8. Sensitivity plot of axial strain at dent peak	178
6.9. Scatter plot of axial strain at dent peak vs. percentage of dent-to-diameter ratio	180
6.10. Regression fit curve for axial strain at dent peak	182
6.11. Regression fit curve for axial stress at dent peak	184
6.12. Regression fit curve for natural log of fatigue life	184
7.1. Illustration of pipe with two indenters (a) full pipe (b) zoom at indentation area	188
7.2. Boundary conditions for pipe with 2 indenters	189
7.3. FE mesh at the indentation area for 2 indenters (a) general (b) zoom at dent peak	191
7.4. Convergence check of pipe with 2 indenters (a) Von Mises strains at dent peak (b) Von Mises stresses at dent peak	192
7.5. Axial strain profile for 2 dents at (a) top shell (b) bottom shell	194
7.6. Hoop strain profile for 2 dents at (a) top shell (b) bottom shell	195
7.7. Strain profile along longitudinal axis from dent peak (a) 2 dents (b) single dent	196
7.8. Axial stress profile for 2 dents at (a) top shell (b) bottom shell	199
7.9. Hoop stress profile for 2 dents at (a) top shell (b) bottom shell	200
7.10. Stress profile along longitudinal axis from dent peak (a) 2 dents (b) single dent	202
7.11. Sample history of natural log of fatigue life of pipe with 2 dents	206
7.12. Histogram of natural log of fatigue life of pipe with 2 dents	206
7.13. Sensitivity plot of natural log of fatigue life for pipe with 2 dents	209

7.14. Scatter plot of fatigue life vs. orientation angle between 2 indenters	210
7.15. Scatter plot of fatigue life vs. distance between 2 indenters	210
7.16. Sensitivity plot of stresses at the midpoint between 2 dents (a) mean stress (b) stress range	212
7.17. Regression fit curve for axial strain at dent peak for interaction of 2 dents	214
7.18. Regression fit curve for axial stress at dent peak for interaction of 2 dents	214
7.19. Regression fit curve for natural log of fatigue life for interaction of 2 dents	215
7.20. Regression fit curve for stresses at midpoint between the 2 indenters (a) mean stress (b) stress range	216
8.1. Illustration of pipe with combined damage of dent with metal loss	220
8.2. Axial strain profile for dent with metal loss at (a) top shell (b) bottom shell	223
8.3. Hoop strain profile for dent with metal loss at (a) top shell (b) bottom shell	224
8.4. Axial stress profile for dent with metal loss at (a) top shell (b) bottom shell	226
8.5. Hoop stress profile for dent with metal loss at (a) top shell (b) bottom shell	227
8.6. Sample history of natural log of fatigue life for dent with metal loss	231
8.7. Histogram natural log of fatigue life for dent with metal loss	231
8.8. Sensitivity plot of fatigue life for dent with metal loss	233
8.9. Scatter plot of fatigue life vs. percentage of metal loss	233
8.10. Regression fit curve for axial strain at dent peak for dent with metal loss	236
8.11. Regression fit curve for axial stress at dent peak for dent with metal loss	236
8.12. Regression fit curve for natural log of fatigue life for dent with metal loss	237
9.1. Illustration of interaction of dent with (a) longitudinal weld (b) girth weld	242
9.2. Residual stress distribution for double-groove weld in pipes (a) longitudinal welds (b) girth welds	243

9.3. Residual stress distribution along weld lines before dent and pressure loading (a) longitudinal weld (b) girth weld	246
9.4. Axial strain profile for dent with longitudinal weld at (a) top shell (b) bottom shell	248
9.5. Hoop strain profile for dent with longitudinal weld at (a) top shell (b) bottom shell	249
9.6. Axial strain profile for dent with girth weld at (a) top shell (b) bottom shell	250
9.7. Hoop strain profile for dent with girth weld at (a) top shell (b) bottom shell	251
9.8. Axial stress profile for dent with longitudinal weld at (a) top shell (b) bottom shell	254
9.9. Hoop stress profile for dent with longitudinal weld at (a) top shell (b) bottom shell	255
9.10. Axial stress profile for dent with girth weld at (a) top shell (b) bottom shell	256
9.11. Hoop stress profile for dent with girth weld at (a) top shell (b) bottom shell	257
9.12. Sample history of natural log of fatigue life of interaction of dent with (a) longitudinal weld (b) girth weld	261
9.13. Histogram natural log of fatigue life of interaction of dente with (a) longitudinal weld (b) girth weld	262
9.14. Sensitivity plot of fatigue life for interaction of dent with (a) longitudinal weld (b) girth weld	265
9.15. Scatter plot of fatigue life vs. residual stress value for dent interacting with (a) longitudinal weld (b) girth weld	266
9.16. Regression fit curve for axial strain at dent peak for dent interacting with (a) longitudinal weld (b) girth weld	269
9.17. Regression fit curve for axial stress at dent peak for dent interacting with (a) longitudinal weld (b) girth weld	270
9.18. Regression fit curve for natural log of fatigue life for dent interacting with (a) longitudinal weld (b) girth weld	271

DISSERTATION ABSTRACT

Name: Husain Muhammed Al-Muslim
Title of Study: Impact of Combined Mechanical Damage on Integrity of Pipelines
Major Field: Applied Materials and Manufacturing
Date of Degree: May 2010

Mechanical damage in transportation pipelines is a threat to its structural integrity. Failure in oil and gas pipelines is catastrophic as it leads to personal fatalities, injuries, property damage, loss of production and environmental pollution. Therefore, it is important to pipeline operators, government and regulatory agencies, and local communities to develop appropriate tools and procedures for assessment. There are many parameters that affect the severity of the mechanical damage related to the pipe geometry and material properties, the defect geometry and boundary conditions, and the pipe state of strain and stress. Moreover, the mechanical damage may be combined with another defect such as metal loss or weld. It is impossible to cover all combination of input parameters whether by full-scale tests or FEA as the parameters values and their combinations are random. Therefore, the use of probabilistic design analysis offers an excellent way to study the problem. The main objective of the current study is to assess the interaction of combined mechanical damage on the structural integrity of transportation pipelines under static and cyclic pressure loading using FEA and probabilistic design analysis. The scope of the study includes multiple dents, dents with metal loss, and dents interacting with residual stresses of welds. To simulate real-life situation, 500 cases are randomly generated using Monte Carlo simulations. All of those cases are analyzed using FEA to find the strain and stress fields as well as the stress range and fatigue life for every case. The statistical distribution of output parameters and correlation between output and input variables is presented. Moreover, regression analysis is conducted to derive mathematical formulas of the output variables in terms of practically measured variables. The results can be used into strain based assessment. Moreover, they can be coupled with fracture mechanics to assess cracks. Furthermore, the derived probabilities of failure can be used in risk assessment. The outcome of the study is practical qualitative and quantitative assessment criteria that can be applied by the pipeline operators to design against mechanical damage, assess severity of mechanical damage, rank and prioritize maintenance activities. The criteria developed have two features, input data are easily gathered by In-Line-Inspection tools and the assessment mathematical formulation can be automated.

DOCTOR OF PHILOSOPHY DEGREE
King Fahd University of Petroleum and Minerals
Dhahran, Saudi Arabia
May, 2010

ملخص بحث

درجة الدكتوراه في الفلسفة

الإسم: حسين محمد المسلم
عنوان الرسالة: أثر الإصابات الناجمة عن ضربات ميكانيكية على سلامة خطوط الأنابيب
التخصص: هندسة ميكانيكية – علوم المواد و التطبيق
تاريخ التخرج: مايو 2010

إن الإصابات الناجمة عن ضربات ميكانيكية تشكل خطرا على سلامة خطوط الأنابيب، و حيث أن انفجار أنابيب النفط و الغاز يؤدي الى اضرار بليغة على الإنسان و الاقتصاد و البيئة، أولت الهيئات الحكومية و الشركات العاملة في هذا المجال اهتماما خاصا لتحديد و تطوير الاليات التي يعتمد عليها لتقييم هذه الاصابات. هناك عدة عوامل تؤثر على شدة الضرر التي تسببه الإصابة الميكانيكية منها ما هو مرتبط بخواص الأنبوب المتضرر سواء مقاساته الهندسية او خصائص المادة الفولاذية المصنع منها، كما أن لمقاسات الإصابة الناتجة من عمق و طول و عرض أثرها الواضح، و كذلك الظروف التشغيلية مثل الضغط التشغيلي الثابت و المتغير لأثرها المباشر على الجهد و الانفعال. كما أن مما يزيد الأمور تعقيدا أن تكون الإصابة مركبة كأن يكون هناك هناك انبعاجا في موقع متصدئ او في موقع لحام. و لذلك فإنه من المستحيل تغطية جميع الحالات المحتملة للإصابات الميكانيكية البسيطة و المركبة سواء بالتجارب العملية او بالمحاكاة الرقمية، و هنا تبرز إمكانية استخدام التحليل المبني على المعلومات الاحصائية و دراسة الاحتمالات. إن الهدف من هذه الرسالة هو دراسة و تقييم أثر الإصابات المركبة على سلامة خطوط الأنابيب الفولاذية تحت عوامل الضغط التشغيلي الثابت و المتغير باستخدام تقنيات المحاكاة الرقمية بطريقة العنصر المحدد و كذلك التحليل المبني على دراسة الاحتمالات. إن نطاق البحث يشتمل على دراسات الانبعاجات الإحادية و المتعددة، و الانبعاجات الواقعة في منطقة متصدئة، و الانبعاجات الواقعة في منطقة لحام. و لمحاكاة الظروف الطبيعية، سيتم توليد 500 حالة مختلفة عشوائيا باستخدام تقنية مونتى كارلو و تحليلها رقما بطريقة العنصر المحدد و ذلك لايجاد الجهود و الانفعالات و العمر الافتراضي لكل حالة على حدة. و سيتم تجميع النتائج و تحليلها احصائيا لايجاد العلاقات القائمة بين المدخلات و المخرجات من التحليل في صيغة علاقات رياضية. إن النتائج المستخلصة ممكن أن تستخدم في عمليات تقييم الضرر لإصابة محددة سواء المبنية على الجهد أو على الانفعال. كما إن احتمالات الفشل المستخلصة من دراسة الاحتمالات يمكن استخدامها في دراسة إدارة الخطر للأنابيب قيد الإنشاء. إن محصلة هذه الدراسة يجب أن تكون معايير عملية قابلة للتطبيق بواسطة مشغلي خطوط الأنابيب و لذلك لا بد أن تتوفر على ميزتين: الأولى أن تكون المعطيات المطلوبة ممكنة الجمع عن طريق أجهزة الفحص التي تمر داخل خطوط الأنابيب و الثانية أن تكون المعايير بصيغة رياضية يمكن تطبيقها اليا في برامج حاسوبية.

درجة الدكتوراه في الفلسفة

جامعة الملك فهد للبترول و المعادن

الظهران- المملكة العربية السعودية

مايو 2010

CHAPTER 1

INTRODUCTION

1.1 BACKGROUND

1.1.1 Pipeline Failure History

Mechanical damage has been reported to be the most common reason of failure of transportation pipelines worldwide. United States Department of Transportation (DOT) has reported that 20-40% of serious incidents are due to mechanical damage (Kiefner et al. 2000). Similarly, a statistical study for a major oil company in Saudi Arabia has concluded that 19% of the reported incident failures between 1985 and 2003 were attributed to mechanical damage (Advantica 2004).

Mechanical damage is mainly caused by third party activities, which is common terminology in pipeline industry that refers to the work of other than pipeline operation and maintenance. It mainly implies excavation work for community development like laying electric cables, building new roads, expanding telephone networks, etc (Fig. 1.1). In offshore pipelines, third party damage can take place due to impact of ship anchors or other foreign objects (Fig. 1.2).

Mechanical damage can also occur during construction due to improper handling of the pipeline during lifting, stacking, laying, etc. A common cause of damage during construction of the pipeline is where hard rocks can penetrate the pipe bottom during laying or pipe top during backfilling.

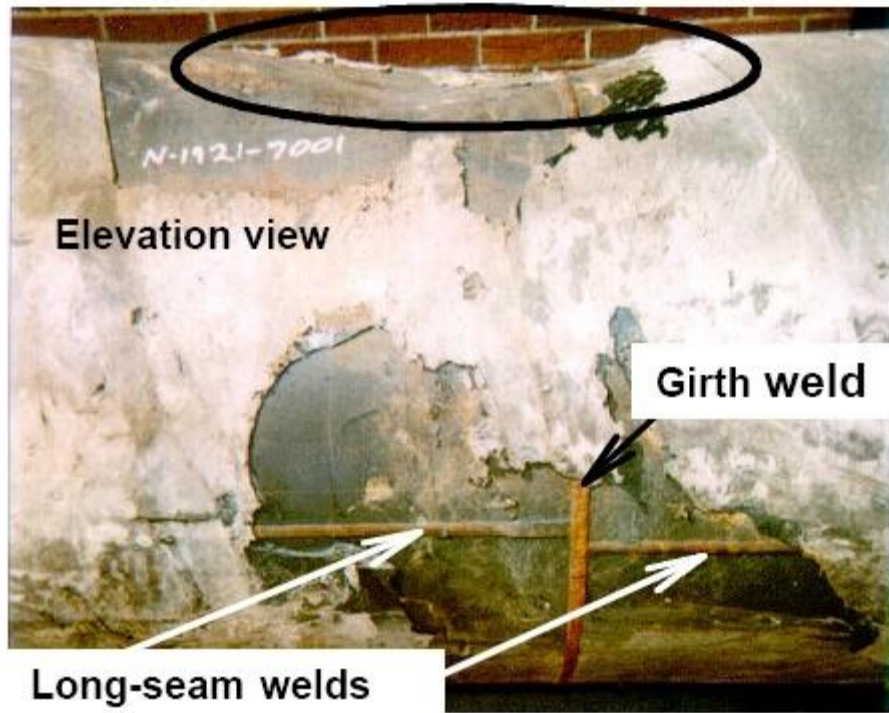


Figure 1.1. Mechanical damage due to third party activities (Leis and Francini 1999)



Figure 1.2. Mechanical damage in offshore pipeline

Mechanical damage can also happen as a result of pipe movement due to surge forces resulting from operational upsets (Fig. 1.3). Another unique example of mechanical damage is the collapse of pipeline under repair sleeve due to accumulation of hydrogen in the annulus area (Fig. 1.4). A similar collapse can happen and has been reported during the hydrotest of hot-tap sleeve.

The impact forces imposed on the pipe yield plastic deformation in the form of a dent as Figure 1.5 illustrates. This dent might be plain or it might be associated with a gouge, i.e. local metal removal by the action of the excavator machine for example. The dent might also coincide with the longitudinal or circumferential welds. In some cases, immediate failure in terms of rupture will take place if the damage is excessive. In other cases, the damage will be less such that the pipeline is still sustaining the pressure, but a concern to the pipeline operators is the probability of reduced fatigue life due to the localized stress-strain distribution in the dent area.

1.1.2 Pipeline Integrity Management System (PIMS)

Due to the serious consequences of pipeline failure in terms of fatalities or serious injuries, economical due to loss of production or damage of properties, and environmental, pipeline operators are implementing the so called “Pipeline Integrity Management System (PIMS)”. As Fig. 1.6 illustrates, this method is implemented throughout the pipeline life cycle covering design, material specification, manufacturing, construction, operation, inspection, maintenance and repair. The implementation can be as simple as following the Code and conducting periodic inspection and repair and can be a complex one with fully integrated software that has all the pipeline data, pipeline



Figure 1.3. Mechanical damage due to pipe movement. (Courtesy, Saudi Aramco)



Figure 1.4. Pipe collapse under sleeve because of hydrogen trap. Shown also is a stuck pipeline scraper. (Courtesy, Saudi Aramco)

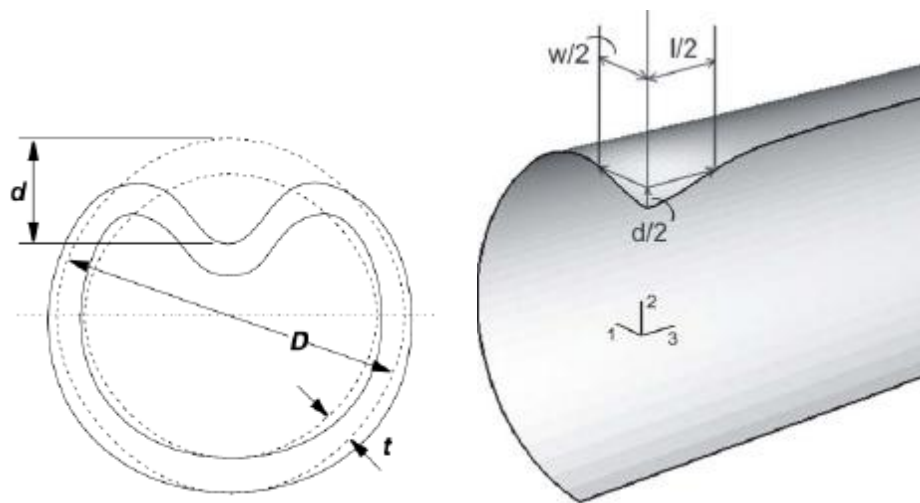


Figure 1.5. Illustration of pipeline dent and its dimensions

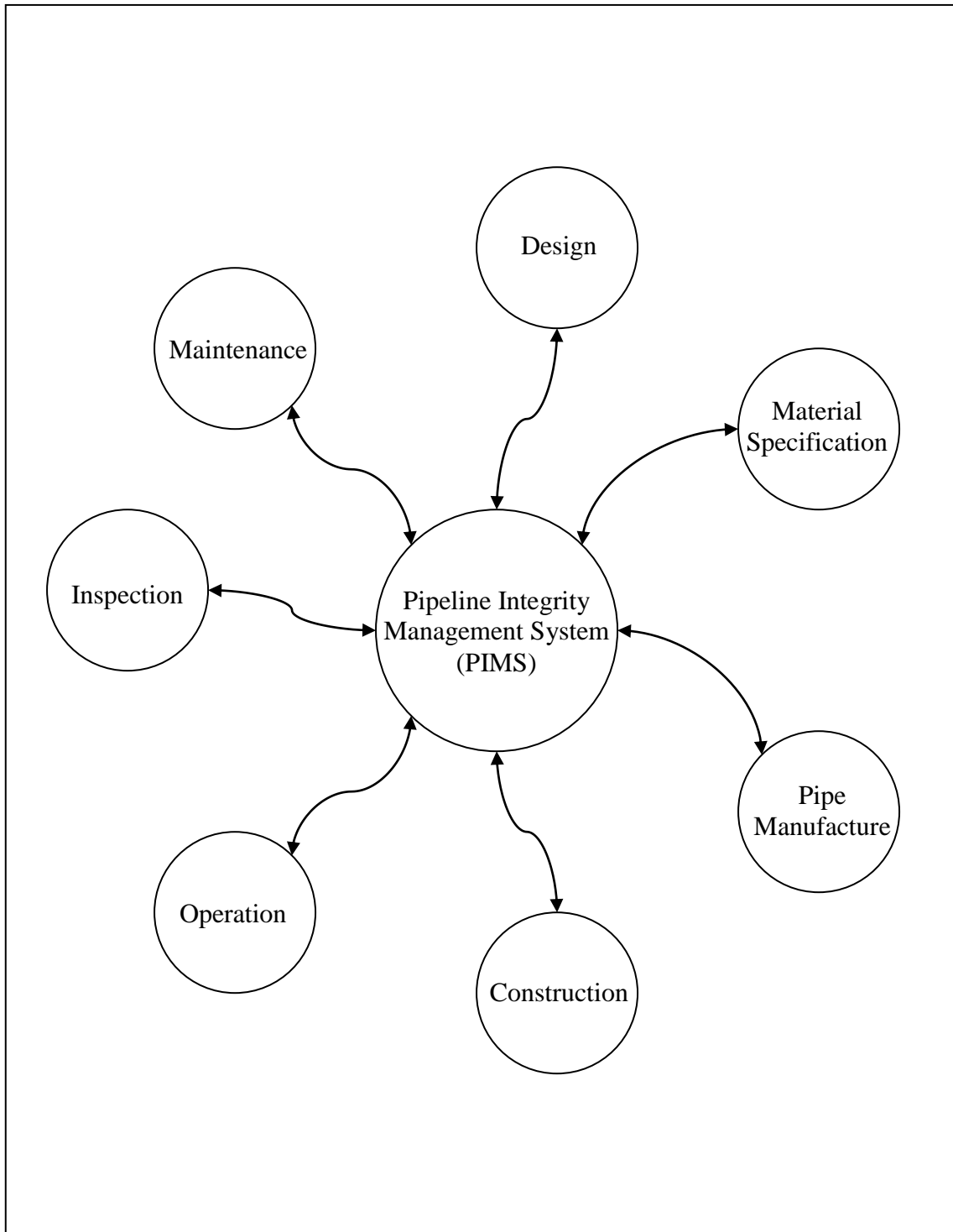


Figure 1.6. Elements of the Pipeline Integrity Management System (PIMS)

coordinates using Global Point System (GPS), online process monitoring, leak detection system, stored data base of inspection runs, and automated decision making of repair. Some pipeline operators are even piloting satellite-based imaging to monitor the activities nearby the pipelines to prevent the potential third party damage (O'Neil et al. 2002).

As the PIMS has a variety of elements all associated with cost, optimization of the system is a continuous process. Imagining the PIMS as a computer, any improvement in the input will lead to improvement in the output. Similarly, advancement in the processing capabilities will enhance the PIMS. For the input, there are variables that are once selected are fixed, e.g. pipeline diameter and thickness, pipeline material properties, etc. There are also variables that are driven by demand like the pipeline pressure. However, there are inputs that can be improved like the inspection data. Intelligent scrapers known as In-Line-Inspection (ILI) are launched through the pipeline to collect information about the pipeline immediately after construction (baseline) and in periodic intervals, e.g. five years. There are three types of ILI scrapers, caliper, magnetic flux leakage (MFL), and ultrasonic (UT). The caliper measures the geometry of the pipe and thus can detect dents. The MFL and UT measure the wall thickness and thus monitor the corrosion progress. A huge amount of research and development has been invested leading to high resolution generation of the ILI. The new generation has lower uncertainties, can detect cracks, and can detect multiple defects, e.g. dent with gouge.

The enhancement in the processing techniques is another means of improving the PIMS. For example, quantitative risk assessment (QRA) has been used extensively by Pipeline Operators. The risk is calculated by the probability of failure time the consequences. To determine the probability of failure, an engineering assessment method

is needed. Engineering assessment might be based on code criteria, fracture mechanics, finite element, etc. It might also be coupled with probabilistic design to take advantage of the actual higher than nominal values of pipe properties.

Enbridge Pipeline Inc. presented a case study of Dent Management Program implemented for their system of transportation pipelines. The main objective of the program is to prioritize the dents that should be excavated and/or repaired. The approach includes two stages of prioritizations. The first stage depends on the general qualitative screening of rocky terrain, large occurrence of third party damage, and history of dents and failures. The second stage uses “Dent Characterization criteria” which is a function of dent geometry, pipe material properties, and historical pressure to predict the remaining service life for each dent. According to the results, the selected dents will be excavated for examination and possible repairs. The engineering assessment is done by applying a recently development assessment model for dent characterization. The paper notes that many models were developed recently, but few were actually implemented by Pipeline Operators. The results are prioritized list for excavation, and determination of the re-inspection intervals. (Ironsides and Carroll 2002, McCoy and Ironsides 2004)

TransCanada PipeLines Limited presented another case study for the dent management program. The program was triggered by the advancement in ILI tools, development of assessment models, and recent flexibility of code requirement in dent acceptability. The assessment program utilizes 3D high resolution tools to collect the required geometry inputs. It also utilizes 1D low resolution tools complemented with statistical and probabilities analysis to fill the gaps in the parameters needed. The assessment is done based on geometry characterization factors of dent depth, curvature

angle, and dent width. The pressure cycle history is used in the fatigue analysis to determine the remaining service life which is the basis for prioritization the dent excavation and repair. The authors highlight a difficulty in identification of dents associate with other defects like corrosion, stress corrosion cracking, gouges and welds as there is no single ILI tool that will detect all these types of defects. Moreover, coupling the results of different ILI tools is not accurate. (Adams and Zhou 2004)

1.1.3 Classification of Mechanical Damage

The mechanical damage is classified based on the physical changes it creates in the pipelines cross-section shape, wall thickness, material properties due to micro-structural transformation and strain hardening, fracture initiation toughness, and their combination.

Accordingly, there are four basic types of mechanical damage:

- a) Dent which involves only shape change in the pipeline cross section.
- b) Gouge which involves wall metal loss
- c) Dent and gouge which is a combination of shape change and metal loss
- d) Plain dent where the shape change is smooth and does not have stress risers.

There is a second classification based on re-rounding response to pressure and falls into two categories: constrained vs. un-constrained. The constrained conditions are when the dent is fixed and does not re-round due to pressure because of the pipeline weight or the backfill weight. A third classification is based on the consequences of contact, i.e. leak or rupture which depends on the growth of the damage. A fourth and final classification is dependent on the timeframe for failure whether instant (burst) or delayed (fatigue). (Leis et al. 2004)

1.1.4 Definitions of Terms Related to Mechanical Damage

Francini and Yoosef-Ghodsi (2008) summarized in their report to PRCI the definitions of terms related to mechanical damage. The objective is to have consistency between users as the terms are qualitative in nature. The definitions below are quoted from the report.

Dent- a depression which produces a gross disturbance in the curvature of the pipe wall, caused by contact with a foreign body resulting in plastic deformation of the pie wall.

Smooth dent- a dent which causes a smooth change in the curvature of the pipe wall (radius of the curvature is more than 5 times the thickness of the pipe)

Kinked or creased dent- a dent which causes an abrupt change in the curvature of the pipe wall (radius of the curvature is less than 5 times the thickness of the pipe)

Plain dent- a smooth dent that contains no wall thickness reductions (such as gouge or crack) and does not change the curvature of an adjacent girth weld or seam weld.

Unconstrained dent- a dent that is free to rebound elastically (spring back) when the indenter is removed and is free to reround as the internal pressure changes.

Constrained Dent- a dent that is not free to rebound or reround because the indenter is not removed (a rock dent is an example of a constrained dent).

Gouge- surface damage to a pipeline caused by contact with a foreign object that has scrapped (gouged) material out of the pipe, resulting in a metal loss defect.

Dent depth- the maximum reduction in dent depth due to elastic unloading that occurs when the indenter is removed from the pipe.

Spring back- the reduction in dent depth due to elastic unloading hat occurs when the indenter is removed from the pipe.

Rerounding- the change in dent depth under internal pressure.

Top of line (TOL) dent- is located in the upper two-thirds of the pipeline circumference, i.e. above the 8 and 4 o'clock positions.

Bottom of line (BOL) dent- is located in the lower third of the pipeline circumference, i.e. below the 8 and 4 o'clock positions.

Additionally, definitions of terms used related to failure and risk and are commonly used in this dissertation are given below:

Fatigue life - the number of applied repeated stress or strain cycles a material can endure before failure.

Failure rate (failure frequency) - the probability of failure per unit of time of engineering components in operation; sometimes estimated as a ratio of the number of failures to the accumulated operating time for the components.

Risk - the product of probability of hazard (like pipeline failure) times the consequences of the hazard (like fatality, property damage, etc.).

Risk management - the overall systematic approach to analyzing risk and implementing measures to eliminate or mitigate the risk.

Probability of failure: the percentage of failing engineering components in a given sample size.

1.1.5 Detection Tool Techniques

The detection and measurement of the defect can be visual and direct. The Inspector will check the mechanical damage and look for signs of cracks, gouges, corrosion, etc. The Inspector will also report if it coincides or near the weld. Measurement tools like

ruler, micro gauges, etc. will be used to measure the depth, length and width of the damage or dent. Manual ultrasonic probe might be used to measure the remaining wall thickness if necessary. However, since most of the pipelines are buried, excavation or digging in the location of the defect is necessary. Even for exposed pipelines, it is not effective to walk tens of kilometers to measure wall thickness and look for damages manually. Therefore, all Pipeline Operators use In-Line Inspection (ILI) tools.

ILI tools are instrumented tools that are inserted into the pipeline through a pipe section at the beginning of the pipeline called the Scraper Trap Launcher. They run through the pipeline by the pressure differential across the tool and they measure and store various data like pipeline geometry, wall thickness, etc. They are finally captured at the end of pipeline in a Scraper Trap Receiver. This inspection operation is called Pipeline Scraping or Pigging and it is conducted at regular intervals, e.g. every five years. There are three main techniques of ILI each with its own advantages and limitations: caliper, magnetic flux leakage and ultrasonic.

Caliper tools

The Caliper ILI are used for geometry measurement of the pipeline, i.e. the inside diameter and detection of dents. The Caliper tool has mechanical arms covering all over the circumference of the pipeline (Fig. 1.7). Each arm sends a signal to indicate its position. The mechanical design of the arm allows it to adapt to the contour of the pipeline, and thus the signal changes recording the change in the measured dimensions. (Rosen 2007, RoGeo·Xt)

Magnetic Flux Leakage (MFL) tools

The main function of the MFL is to detect metal loss due to corrosion. The principle of the MFL is to measure the magnetic flux across two points. The density of the magnetic flux is a function of the metal wall thickness. The MFL tool is equipped with two sets of sensors. Each set has coverage all over the circumference of the pipeline (Fig. 1.8). The magnetic flux is measured between each two sensors stationed axially and thus the metal wall thickness is determined as any loss in the metal wall will cause the saturated magnetic flux to leak. (Rosen 2007, CDP)

Ultrasonic (UT) tools

The main function of the UT is to detect crack-like flaws as well as defects in the coating. The principle of the UT is to generate electromagnetic waves inside the pipeline. The wave is reflected back in a return echo to the transducer (Fig. 1.9). The presence of crack-like flaws causes a disturbance in the reflected (echoed) wave. By measuring the time and intensity of the echo, the condition of the pipe wall and the presence of cracks can be determined. (ROSEN 2007, RoCD²)

1.1.6 Modes of Failures

The failure of dents and gouges involve high plastic strain, thinning of wall, dent movement, initiation of crack, ductile tearing, plastic flow, micro-crack at the base, and material property change (Seevam et al. 2008). The mechanical damage can cause instant catastrophic failure, but can also cause failure after period of time. The time, or rate, between the damage incident and the failure is dependent on factor like stable-tearing,



(a)



(b)

Figure 1.7. Picture of (a) Caliper ILI tool. (b) Sensor arm. (Rosen 2007, RoGeo-Xt)



Figure 1.8. Picture of MFL tool (ROSEN 2007, CDP)



(a)



(b)

Figure 1.9. Picture of (a) UT tool. (b) ultrasonic transducer. (ROSEN 2007, RoCD²)

fatigue or other time- and/or cycle-dependent process. (Leis et al. 2004) Cracks may occur at the surface during the re-rounding process. The defect might not cause immediate rupture, but is not stable. Some circumstances might lower the failure pressure like pressure variations, metal loss, environmentally simulated cracking as defects are associated with coating damage. (Semiga, December 2007)

Leis and Francini (1999) classified the consequences of pipeline denting into four categories:

- Instantaneous failure by plastic collapse or cracking at the inside diameter of the pipe during contact.
- Instantaneous failure by plastic collapse or cracking at outside diameter during re-rounding of the pipe.
- Delayed failure due to fatigue at cyclic pressure.
- No failure or threat to pipeline during its life cycle.

1.1.7 Parameters of the Mechanical Damage

There are many factors and parameters that characterize the mechanical damage and determine its effect on the structural integrity of the pipe (Fig. 1.10). The factors are related to the pipe, the defect, the operating conditions and the boundary conditions. The pipe geometry parameters are usually defined by the dimensionless diameter-to-thickness ratio. Also of importance are the pipe material properties including yield strength, tensile strength, and fracture toughness. Moreover, residual stresses resulting from the pipe manufacturing processes of bending and welding play a decisive role. The defect geometry includes the depth which is the most critical. However, other parameters of

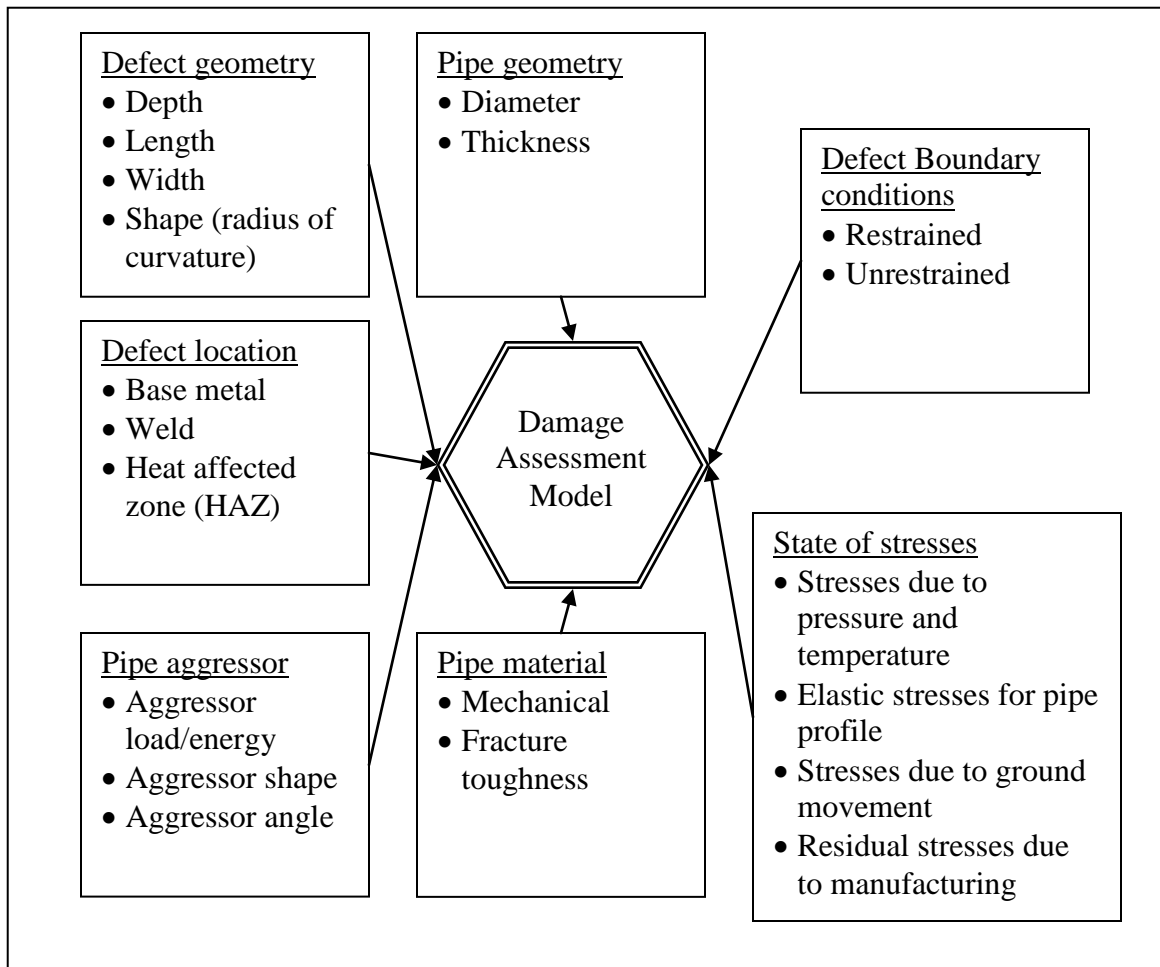


Figure 1.10. Parameters of the mechanical damage

width, length, and radius of curvature are also important as they will determine the maximum strain in the dent. The boundary conditions of the dent are also deterministic factor as unrestrained dents are more likely to fail than restrained dents. The damage creator or pipe aggressor parameters of shape, angle, and load/energy of impact are directly related to the severity of damage. The state of the stresses of the pipe due to its operating pressure and temperature and their variation is a vital element in the assessment. Finally, the boundary conditions of the pipe itself whether above-ground unrestrained or underground fully-strained is a factor.

Fowler et al. (1992) determined that the most important variable in a plain dent is the ratio of the dent depth over the pipeline diameter. This ratio has been and is still being used for the acceptance vs. repair. However, as Pipeline Operators tend to optimize and prioritize maintenance and repair activities, the other parameters must be considered in the assessment. Therefore, proper understanding of the effect of each of the parameters is necessary.

1.2 CURRENT DISSERTATION WORK

1.2.1 Motivation and Significance of the Proposed Work

The motivation of this active research can be attributed to shortcomings of the existing criteria due to the previous limitations on full-scale tests and the expanded use of statistical approaches such as quantitative risk assessment and probabilistic design.

The existing assessment model has started in 1981 with almost no change since then. There has been a lot of investment in improvement of inspection techniques, and risk analysis methods, but little investment on the improvement of the assessment model,

which is now the weak link. (Seevam et al. 2008) The existing assessment models have significant elements of uncertainty which must be incorporated into the probabilistic analysis approaches. (Jandu et al. 2008)

One of the main shortcomings of the existing criteria for dent for example is that it is only based on single parameter of dent depth. This led to unnecessary excavation and repair of dents deeper than 6% but with low strains. On the other hand, it led to missing dents of lesser depth but with high strain due to their overall dimensions and sharp shapes. Failures were also reported for dents of less than 3% depth. This led to the assessment based on strain rate, but created a new challenge of how to measure the strain rate both in terms of field measurement and mathematical formulation. (Gao et al. 2008)

Pipeline Research Council International (PRCI) launched an extensive research program for all aspects of instantaneous and delayed failure (Jandu et al. 2008). Part of the program is to conduct full scale tests with comprehensive instrumentations including strain gauges at various locations and directions. Their objective is to avail experimental data for researchers to develop appropriate mechanistic model for validation of analytical and numerical analyses. There is no numerical model published yet that uses this data for validation.

The second major motivation to active research in assessment of mechanical damage is increasing use of statistical analysis such as quantitative risk assessment and probabilistic design. Quantitative risk assessment needs the frequency of failure. To estimate failure frequency, input data for mechanical damage are generated using statistics of historical data and damage assessment is conducted using empirical relations to determine the failure rate (Wolvert et al., 2004; Vieth et al., 2004). However, There is

no published that combined numerical analysis and probabilistic analysis in one module. This module is available in ANSYS (2007) and has the advantage of analyzing each random case numerically which reduces the uncertainty resulting from using the empirical relations.

1.2.2 Objectives and Scope of Work

Mechanical damage affects the pipeline by introducing additional stresses and strains. Moreover, it can introduce stress risers such as gouges and cracks. To maintain the structural integrity of the pipeline, the new state of stress must be assessed to ensure that the pipeline will fit for its operating conditions, mainly pressure containment, for its intended service life. If the damage is severe such that it is a threat to cause pipe leak or rupture, pipeline repair must be scheduled.

The mechanical damage can be a stand-alone defect such as plain dents in the base metal of the pipe. However, it might interact with another localized effect in the pipe. This will make the developed state of stress more complex and the damage assessment more involved. For example, a group of dents might be created in close proximity due to multiple-teeth excavator hitting the pipe. The dent might also coincide with structural discontinuity which will act as stress riser such as welds. Welds are not only stress risers, but they have residual stress profile that will add to the mechanical damage stresses. Other localized effect of the mechanical damage is the metal loss. Metal loss can be natural due to corrosion either externally or internally. It can also be intentional to remove gouges associated with mechanical damage which is an acceptable method of repair.

It is impossible to cover all possible combination of input parameters of geometry, material, and operating conditions whether by full-scale tests or FEA as the parameters values as well as their combination are random. Moreover, each nominal value of these parameters has its own variability due to manufacturing tolerances, measurement uncertainties, etc. Therefore, the use of probabilistic design analysis offers an excellent way to study the problem and determine the sensitivity of the strain and stress fields to each of those input parameters.

The main objective of the current study is to assess the interaction of combined mechanical damage on the structural integrity of transportation pipelines. To simulate real-life situation, probabilistic design analysis is implanted to generate 500 random cases of combined mechanical damage. All of those cases are analyzed using FEA to find the strain and stress fields as well as the stress range and fatigue life for every case. Then, the output is analyzed using statistical analysis to find correlation between input and output parameters. The outcome of the study should be practical assessment criteria that can be applied by the Pipeline Operators. Therefore, it must have two features, input data are easily gathered by ILI and assessment model can be automated. Therefore, general regression formulas of quadratic polynomial are developed for the different cases of mechanical damage where the input parameters can be easily gathered by the pipeline operator. The scope of work includes multiple dents, dents with metal loss, and dents interacting with residual stresses of welds.

Multiple dents

All current codes and practices deal with the assessment of isolated dents. This is despite the fact that multiple dents common since most of the excavation equipment, which normally causes the mechanical damage, are multiple-tooth. For the literature reviewed, only one paper provides the separation distance ($2\sqrt{(Dt/2)}$) to consider the dents isolated (Francini and Yoosef-Ghodsi, 2008). Another paper characterizes multiple dents based on the maximum peak depth (Dinovitzer et al., 2008). In this study, the effect of distance and orientation between two dents will be evaluate to determine the impact of interaction them on the integrity of pipelines.

Dents with metal loss

Metal loss can occur gradually in the dented pipe due to corrosion which is usually accelerated as the protective coating layer is also damaged. It can also happen intentionally as gouges associated with dents are normally removed by grinding. The current codes and practice conduct separate assessments for dents with metal loss, i.e. the dent is assessed based on the maximum depth or maximum strain criteria while the metal loss is assessed based on the metal loss depth and length. Some codes limit the maximum metal loss to 12.5% of the original thickness. However, there are no assessment procedures that consider the dent with metal loss as single defect. In this study, a combined damage of dent with metal loss will be analyzed to determine the acceptance criteria.

Dents with initial weld residual stresses

Initial residual stresses can exist in the pipe due to manufacturing processes such as rolling and welding. The interaction of dent with the weld has always been considered a

threat to the pipeline and was studied by many researchers. However, all of the reviewed literature did not combine the dent and weld features in one numerical model. Moreover, none of the reviewed literature has considered the effect of interaction of dent with the residual stresses of welds. High residual stresses exist in the vicinity of the weld line reaching values up to the yield stress of the pipe. In this study, the impact of interaction of dent with the residual stresses of longitudinal welds and girth welds on the integrity of pipelines will be evaluated.

1.2.3 Dissertation Tasks

The following tasks describe the work plan to achieve the objective of this thesis based on a modular approach.

Task I: Literature review

- Literature review of pioneer and ground research work.
- Literature review of research work in the last 10 years.
- Communication with active research projects.

Task II: Study of damaged pipe

- Statistical analysis:
 - Collection of a local company damage inspection data for pipelines.
 - Collection international companies' damage inspection data for pipelines.
 - Conduction statistical analysis to determine the representative defect parameters.
- Metallurgical and microscopic analysis:

- Collection of damaged pipes from a local company.
- Visual inspection for cracks and their location.
- Preparation of samples for microscopic analysis and mechanical testing.
- Mapping of the material property profile to the dent profile.

Task III: Development of 3D finite element model

- Numerical analysis:
 - Numerical modeling using commercial software (ANSYS)
 - Model optimization (symmetry, mesh size, element type, etc.)
 - Model validation by comparison with full-scale test from PRCI.

Task IV: Determination of relative significance of defect parameters

- Numerical analysis:
 - Analysis of 100 cases different combination of geometry and material parameters using ANSYS PDA Module
 - Determination of stress and strain profiles
- Statistical analysis:
 - Determination of the relative significance of defect parameters using sensitivity.
 - Develop general formula using regression analysis

Task V: Investigating interaction of mechanical damage

- Numerical analysis:

- Analysis of 100 cases of multiple dents at various separating distances using ANSYS PDA Module.
- Analysis of 100 cases of different combinations of dent with metal loss using ANSYS PDA Module.
- Analysis of 100 cases of different combination of dent with residual stress of longitudinal weld using ANSYS PDA Module.
- Analysis of 100 cases of different combination of dent with residual stress of girth weld using ANSYS PDA Module.
- Determination of stress and strain profile as well as stress range and fatigue life.
- Statistical analysis:
- Determination of the relative significance of defect parameters using sensitivity.
- Develop general formula using regression analysis

CHAPTER 2

LITERATURE REVIEW

2.1 GROUND RESEARCH (PRIOR TO YEAR 2000)

The first dent-gouge assessment model was developed by Hopkins and Cairns in 1981. It considers membrane and bending stresses at the base of dent and uses a collapse modified strip-yield fracture mechanics model. The model was calibrated using a large number of models and vessel burst tests with notched dents.

Fowler et al. (1992) studied plain dents under cyclic internal pressure loading (fatigue) in offshore gas pipelines using numerical analysis and full-scale tests. Previous research showed that the presences of gouges or gouges with dents are deterministic to the burst pressure of pipelines while plain dents are not. However, the plain dents increase the stresses locally when pressure is applied. With cyclic pressure loads, this could lead eventually to fatigue failure. To determine the parameters of the study, a review of failure histories and survey of pipeline operators were conducted to determine the most common dents profiles. They conducted dimensional analysis and determined that the dent depth, pipeline pressure to stress ratio, and pipeline diameter to thickness ratio are the most critical parameter. Depth was selected to be 5%, 10% and 20% of the diameter which thought to be the most representative. The study concluded that the current regulations, at that time, are too conservative as they require repair of dents in

welds, repair of dents with gouges, and repair dents more 2%. The study found that plain dents less than 5% are acceptable as they have fatigue life much more than the expected pipeline service life.

The study was extended in a subsequent research project by Fowler et al. (1994) to cover plain dents, dents with gouges, and dents with welds under cyclic pressure leading to fatigue. They conducted full-scale tests to determine the number of cycles to failure of various damage features to come up with screening criteria for immediate repair, repair at later stage, or no repair. The study found that plain smooth dents less than 5% of the diameter are of no concern unless the cyclic pressure is very severe. For dents with gouges, it was recommended to grind the gouges up to 15% of the wall thickness as immediate repair. The position of dents was found not to affect the longitudinal weld, but was detrimental to girth welds

Rosenfeld (1997) simulated by analytical model the denting/loading process of plain shallow unrestrained dents. The re-rounding phenomenon due to indenter removal was studied and a relation between the final measured depth and the initial depth was estimated. The bending stresses were calculated at the apex of the dent in minimum and maximum pressure cycles to estimate the fatigue life and the results were given in simplified fatigue rating curves in terms of pipe and dent geometry, material properties, and frequency of full operating pressure cycles. In general, the fatigue life decreases with increasing D/t , increasing strength level, and increasing initial depth and width.

The previous work was continued to include plain shallow unrestrained dents in girth welds (Rosenfeld et al. 1997, Rosenfeld 1999). The objective was to develop more relaxed guidelines compared to the existing ones (at 1999) that require repair of any dent

on girth welds. The authors conducted analytical analysis to calculate the remaining fatigue life based on the accumulated damage theory, stress concentration factor, and appropriate S-N curve based on weld quality. The study concluded that shallow dent in girth welds could be left and repaired at convenient time if they do not contain mechanical damage, in a weld of high quality, and cyclic pressure is not severe.

Leis and Francini (1999) conducted an evaluation of the available assessment criteria for mechanical damage and found that they have a wide scatter. The authors highlighted on possible reason was that the full scale testing experiments had wide approaches and cannot be compared. They proposed a different evaluation approach based on Ductile-Flaw-Growth-Model (DFGM) to predict flaw initiation and propagation in pipelines which they thought to be more accurate as it depended on first engineering principles. The other objective of the study was to find how to design against mechanical damage by assessing installation of mechanical crack barriers vs. high-toughness pipeline material internally resistance to crack. The authors also looked into how to prevent against mechanical damage by comparing the construction equipment differences between Europe and North America.

2.2 RECENT RESEARCH (2000-2008)

2.2.1 Critical Review of Available Assessment Models

Cosham and Hopkins published the Pipeline Defect Assessment Manual (PDAM) in 2002 which covered different types of mechanical damage as well as corrosion. The authors conducted critical review of the best available assessment methods of defected pipelines into one document; and highlighted their range of application and limitation.

The authors pointed that the available assessment methods are based on fracture mechanics or limit-state (collapse) theory. There are generic assessment fitness for service such as BS7910 and API 579, but they are considered conservative for pipelines. This is because the generic models depend on 1D fracture mechanics parameter measured in conditions not applicable to pipeline in terms of constraint and ductile tearing. However, the authors recommended using more sophisticated 2D fracture mechanics parameter to eliminate the conservatism of the analysis.

Leis et al. (2004) evaluated the criticality of the dent in more general parameters than the simple depth, which was the main controlling parameter in the available assessment then. The focus of the paper was is plain dents under cyclic load (fatigue). The research introduced new material properties are introduced including true-fracture ductility and fracture-initiation toughness in the assessment. The authors found that the current code criteria are very conservative and that restrained dents do not impact the integrity of the pipeline unlike the unrestrained dents. Therefore, the best repair of dents is to sleeve them with stiff filler material. They highlighted that severity of dents based on measure final depth without the history of deformation can mislead the analysis and overestimate the life of shallow dents. They recommended future work to find the characterizing parameters of dents which might include dent depth in addition to wall thickness reduction or curvature.

2.2.2 Assessment application by Pipeline Operators

Rosenfeld et al. (2006) conducted a deterministic assessment based of minor mechanical damage of Trans Alaska Pipeline System. The ILI revealed 77 locations with

suspected minor mechanical damage, 42 of which were excavated. The assessment was based on the characteristic of the observed damage, material properties of the pipe, and fatigue environment leading to development of empirical constants of the crack growth equation to assess the remaining life. The assessment concluded that 33 out of 35 damages were minor, which led to considerable savings without sacrificing the safety and integrity of the pipelines.

Warman et al. (2006) presented another case study which showed the importance of viable damage assessment criteria for Pipeline Operators to manage the mechanical damage. The authors used a simple approach of semi-empirical formulas and qualitative criteria, yet were able to produce a prioritized list of mechanical damage for optimum planning of maintenance and repair decisions. They highlighted that such approaches are very handy to operators as they can automate it with the ILI results.

2.2.3 Simulating the Denting Process

Hertz-Clemens (2006) modeled the process of dent creation numerically and experimentally. They extended the depth of the dent up to 30% and considered wider range of D and t than previous work. Accordingly, the paper highlighted that the current criteria which depends on the dent depth only is not sufficient and that the Importance of the various geometry parameters of the dent (depth, length, width) is not well defined. Therefore, they recommended future work to conduct parametric study of these dent geometry dimensions to correlate those parameters with the integrity of the indented pipe (stresses and strains).

Le Bastard (2006) simulated the denting process to find a relation between the measured depth (under pressure) and the initial depth (without pressure). He was able to find a coefficient to relate the two.

Mannucci et al. (2002) noticed that the basis of available assessment methods of dents on gouges is idealized defects. They considered this as shortage especially with the modern design techniques that are reliably based on actual conditions. To fill this gap, the authors built full-scale labs of actual excavator under controlled conditions. The developed experimental procedure was able to re-produce the real excavator damage. This will help in classifying the seriousness of the damage based on the excavator type.

Brock et al. (2008) conducted full-scale tests to create 12 plain dent specimens. The specimens were later put under pressure cycles to fatigue failure. This was the first phase of comprehensive PRCI project towards a validated pipeline dent integrity assessment model. Detailed experimental data were recorded including indentation force, applied internal pressure, pipe wall strains and the number of cycles to failure.

2.2.4 Damage Assessment Using S-N Curve

Dawson et al. (2006) proposed a new analytical formula to assess plain dents under static and cyclic loads, which is based on the dent profile and not the depth only. The paper pointed out that the strain based formulas such as that of ASME B31.8 are limited to static failure only. They described a procedure of assessing dents under cyclic load which involves basic screening as first level assessment and FEA as second level assessment to calculate the stress range. The S-N curve is then used to estimate the fatigue life. The authors recommended for future work to be conducted investigating the

applicability of the non-dimensional volumetric dent parameter to estimate fatigue life. They highlighted that if this is successful, it will eliminate the need to run FEA.

Pinheiro et al. (2006 and 2008) conducted experimental and numerical analysis to determine the stress concentration factors of dented pipelines to be used in high cycle fatigue evaluation using S-N curves. The authors emphasized that numerical analysis is not practical for field engineering, and therefore, analytical formulas are needed. Therefore, parametric analysis was conducted for different pipe geometry, dent geometry, and accordingly, analytical formulas were developed to calculate the stress concentration factor K_t . The study recommends for future work to determine notch sensitivity factor q .

2.2.5. Damage Assessment Using Fatigue Crack Growth (Paris Law)

Keifner et al. (2004) highlighted their experience over a decade of assessing pipe line fatigue life. They pointed out that it is a great tool to determine the appropriate inspection intervals. They stated that they found pitfall in implementing fatigue life assessment method. Although the basic principles are sound, application requires in-depth understanding. The authors admitted that they did not have confidence that they could model the effect of dent on fatigue crack growth. However, the authors noted that not all defects are deterministic to pipeline integrity, but of the critical ones are dents with gouges and dents with stress corrosion cracks. The authors recommend using Paris Law but without implementing the bulging factor suggested by BS 7910. Rather they implemented bending stresses due to eccentricity.

Lazer and Verbit (2004) utilized the pipeline operating history to predict the remaining life of an example pipeline. The analytical approach of Paris Law was

implemented per the recommendations of BS7910 where a bulging factor is applied to the crack defect. The authors depended on the data logging system, called SCADA, to find the pressure profile over a representative period. This was integrated into the calculations using rain flow counting techniques. The authors suggested this procedure to be used as an integral part of a pipeline integrity management program to determine the inspection intervals or risk of failure.

The work by Jinheng et al. (2004) enhanced the prediction of the fatigue life by applying the elastic-plastic fracture mechanics based on Failure Assessment Diagram (FAD). The paper developed an algorithm for calculating the fatigue life by first applying the Paris Law for the elastic stress intensity. This stress intensity is updated for every increment in crack length by calculating the primary stresses and the secondary stresses. Accordingly, new fatigue life is calculated. The proposed methodology was verified by full scale tests and found to predict life of half the actual. This was accepted by the authors as conservative and practical estimate.

Been et al. (2006) studied the effect of the presence of dents in the environmental cracking services on the crack growth. They used numerical model to calculate the stress intensification factor near a dent, and they superimposed the results on analytical crack growth model using Paris Law with constants based on corrosion fatigue. The authors were able to develop a combined dent assessment model (DAM) and mechanical fatigue function which incorporates: dent depth, dent shoulder slope, dent acuity, multiple-peak dents, grade of material, presence of cracks and corrosion flaws or welds, and operating pressure fluctuations.

2.2.6 Damage Assessment Using Strain-Based Approach

Gao et al. (2008) compared the available formulas to calculate the strain of a plain dent (directional and effective) and found conflicts which they tried to resolve. The review included the formula in ASME B31.8 and others in open literature. Utilizing numerical and analytical analyses, they proposed different alternative to calculate the strain noting that negative strains are not damaging compared to tensile strains. They suggested to have a strain-limit criterion in addition to the effective strain criteria and to relate the effective strains to positive strains only. Furthermore, the paper noted that for fatigue assessment, the stress hot spots must be evaluated which not necessarily overlap with the maximum effective strain. This hot stress spot include areas of maximum membrane and bending stresses and/or residual stresses.

Noronha Jr. et al. (2006) developed a method to calculate the strain based on the fourth-order B-spline curves to approximate the dent profile which was validate by finite element analysis. They emphasized that Strain-based approach is a step forward and eliminates a number of unnecessary repairs based on depth criteria. They also noted that the equations of Appendix R of ASME B31.8 contained errors: the thickness should be divided by 2, the plain-strain assumption should be plastic strain. In 2008, they extended the work to study the effect of ILI resolution on the calculation of the strain. The objective was to find the minimum number of sensors needed in ILI to be used for a reliable strain-calculation. The resolution of the ILI significantly affects the calculation of the strain which is similar to the conclusion by Westwood and Hopkins (2004) on the effect of ILI on the metal loss defect integrity assessment.

Belanger and Narayanan (2008) utilized kinematics analytical approach (tensors) to develop an analytical formula to calculate the strains based on ILI data. The analytical formulas were verified against numerical analysis. The authors highlighted that it is not practical to use finite element method to analyze each dent in a pipeline, and therefore, analytical models that directly relate the radial displacement measured by the ILI tool to strains is of great importance. Therefore, they planned to extend their new approach to account for factors such as fatigue, residual stresses and environmental conditions.

Cunha et al. (2006) simulated metal loss, such as caused by corrosion or removal of gouge, by volumetric flow in two shapes axisymmetric and narrow axially oriented. They studied the mechanical behavior of two strain modes: bending strain of axisymmetric flow and membrane strain of narrow axially oriented flow. They used analytical linear elastic shell solution, which was verified by FEA modeling and 3" lab scale tests of two material of different plasticity; carbon steel and stainless steel. They developed a set of equations to predict the failure pressure due to plastic instability.

2.2.7 Damage Assessment Using Fracture Mechanics and Importance of Residual Stresses

Jandu et al. (2008) used fracture mechanics to assess dent dent/gouge combination under instantaneous failure conditions. They applied fracture mechanic model based on Failure Assessment Diagram (FAD) to express the ratio of elastic J-integral to plastic J-integral. The authors highlighted that the fit parameters of the existing model do not reconcile in view of the modern elastic-plastic fracture mechanics theory. There is a model which assumes plastic collapse of the remaining ligament in the pipe-wall at the

root of the gouge. This model needed additional term depending on fracture toughness to be used to match full-scale tests. The other model which treats gouge as crack-like defect is not accurate. The proposed a new model on the postulation that micro-crack is present in the root of the gouge. The main assumptions (postulations) in their model were: gouging and denting processes will result in micro-cracking a sub-layer of material adjacent to the surface; and micro-cracking will depend on the level of denting and slip band of the material. Furthermore, their new fracture mechanics model, which needs to be verified by testing, that incorporates residual stresses by the denting process, stress concentration factor due to gouge, stress intensification factor due to crack, and depth of crack.

As determining the residual stress should be addressed in the failure assessment of structures to find its detrimental effect on the integrity. is important in the integrity assessment of piping, Lee et al. (2004) developed a method to calculate the residual stress profile resulting from welding in several joint types and residual stresses resulting from cold-forming of pipes. The paper presented a comprehensive set of transverse linear residual stress profiles. To measure the residual stresses in the field, Choi et al. (2002) developed non-destructive technique to measure residual stresses of pipeline in-service to assist in the integrity assessment. The concept is applying a load by a spherical indenter to create mechanical deformation in three stages: elastic, elastic-plastic and fully plastic. The loading unloading curve is analyzed to find the specimen tensile properties as well as the residual stresses. Clapham et al. (2002) highlighted that the residual stresses could be detected by ILI that uses magnetic flux leakage technique. The authors noted that magnetic field is affected by residual elastic stresses as well as geometric changes.

However, due to the complex stress distribution, the interpretation of the signal is difficult. Therefore, they conducted experiments to better characterize the effect of residual stresses on magnetic flux leakage and magnetic noise fields. The authors were able to separate the geometry effects from the stress effects in the denting process. The issue of residual stresses can even discourage Pipeline Operators from using a pipeline, that would be otherwise economically attractive, i.e. spirally-welded pipe. Knoop and Sommer (2004) mentioned that the Pipeline Operators tend to have reservations on spiral-welded pipe or completely reject to use it. This is due to past poor experience with this type of pipes. However, due to low capital cost and encouragement of building local pipe mills, the number of spiral-welded pipes has increased. Accordingly, it is critical to qualify this type of pipe to fit for purpose. One issue that had not received attention before is the assessment of dents interacting with spiral weld. This is due to the fact that historically longitudinally seamed pipes are the predominant used in pipeline companies.

2.2.8 Damage Assessment Using Probabilistic Design

In an effort to develop a quick technique to estimate the remaining life of dented pipe with parameter of dent geometry, pressure history, pipe material properties; Dinovitzer et al. (2002) conducted sensitivity analysis and probabilistic design on hundreds of various models of plain dents under cyclic loads. They defined a dent relative risk factor which has a relation between the geometry of the dent and service life, the relative importance of each parameter, and evaluation of the potential of quick model. The paper highlighted the effect of seam weld: surface discontinuity (notch), residual stress field, effect of mean stress, dent shape, and response to pressure.

Veith et al. (2004) also applied probabilistic approach to calculate the probability of failure instead of deterministic approach. The authors highlighted that the deterministic approach uses the minimum values of the material properties while the pipe actually have higher values. Moreover, the only way to account for the variability of input data such as pressure cycles and defect size is the probabilistic approach. The authors conducted Monte Carlo simulation of the input variables and they counted the number of failures in a certain period of time, e.g. they found 2% probability of failure in 10 years. They compared the results for a history of failures and concluded that this approach is promising and has many advantages primarily to rank and prioritize the defects to be repaired.

Seevam et al. (2008) used probabilistic methods to determine the effect of the dent/gouge assessment models on the probability of pipeline failure in a range of pipeline geometry with the help of available full-scale database. Moreover, they conducted gap analysis on the models to identify and recommend research areas for improvement. The authors stated that the existing models have a wide variability which makes them conservative and not closely matching with test data. They emphasized that the variation in the models does not help the pipeline quantitative risk analysis, which is heavily used nowadays, in predicting the failure frequency as an unnecessary conservative dent-gouge assessment model will give very risks of failure. Based on the assessment, the authors stated that the method of API 579 has a wide scatter which has been thought by some workers to be inaccurate. Therefore, Advantica (2005) improved the model by using the Failure Assessment Diagram (FAD). Also, it addressed limitations by explicitly adding the effect of micro-cracking and residual stress known to develop around the gouge. This

is accomplished by including several fit parameters, by iterative procedure, in the model to quantify these effects. The authors concluded with recommendations to improve the too simple stress model, and use 3D stress intensification factor instead of the current 2D one.

2.3 ACTIVE RESEARCH PROGRAM

The Pipeline Research Council International (PRCI) has launched a comprehensive and extensive research program to address mechanical damage in pipelines from all aspects. The program aims improve the characterization and profiling of the mechanical damage which is the input to the assessment models. By improving the input, as well as improving the analysis models, the output will be a more reliable and trusted decision to repair immediately, schedule later, or leave untouched. The program is divided into several independent, but interrelated projects covering inspection tools (MD-1), screening and ranking (MD-2), assessment modeling based on full-scale tests (MD-4), and inspection and repair procedures (MD-5). The full list of projects is given in the references of active project. Some projects submitted progress report to PRCI, and their findings are summarized in the following paragraphs.

Semiga (December 2007) surveyed pipeline operators to collect data of damage reported by ILI as well field dig inspection. The information gathered were: type of mechanical damage, pipeline geometry details and material properties, soil details, ILI reported damage details, dig reported damage details, possible source of damage, significance of the defect (leak, rupture, no release), and frequency of detection relevant to various sizes and grades. The objective of the survey is to gather inventory and

develop trends of mechanical damage in gas and oil pipelines to ensure that models that are being developed or used to predict the pipe behavior are applicable and capable. Moreover, results will be used in a related project (MD-2-2) to develop a model for ranking ILI indications of mechanical damage to help pipeline operators in prioritizing their maintenance. One of the major findings of the survey were that measures of dent depth by ILI and field-dig tend to agree on top-side dents, but the field-dig underestimate the depth of the bottom-side dents. This could be explained by the spring-back effect of removing the soil restraint during excavation. Another finding was that rock dents are more frequent than third-party dents. Third-party dents result in plain dents or dents with gouges, while rock dents result in plain dents or dents with corrosion. The survey also revealed that majority of the dents was found on the bottom of the pipe (42%) then the side (32%) then the top. The study could not find a trend between the dent geometry and pipeline statistics. This might be due to the limited range of data.

Francini and Yoosef-Ghodsi (2008) developed a model that predicts the severity (qualitative screening criteria) of mechanical damage based on ILI data to allow the Pipeline Operator to rank and prioritize investigation by excavation and repair and defend decisions to Management and Regulatory Authorities. The levels are: serious where schedule investigation as soon as possible, questionable which should be investigated on scheduled basis, and benign which needs monitoring but no investigation is required. The assessment is a simplified model directly linked with the ILI data and based on empirical and experiential knowledge which will be validated in the next phase of the project.

Dinovitzer et al. (2008) have developed a detailed project scope to assist in the development of new mechanistic models which will better assess the mechanical damage

and eventually increase safety, minimize unnecessary maintenance cost, and improve pipeline standards and codes. The scope of the project is mechanical damage reported with secondary features (gouges, corrosion and welds) under static and cyclic loads. Full-scale experiments with detailed recording and instrumentation are conducted as part of this project to establish a comprehensive database that could be used in the development and validation of assessment models of mechanical damage.

Zarea et al. presented their work progress on the modeling of dent and gouge damage in February 2008. The Pipe Aggression Rig (PAR) was already designed and constructed. The testing will be conducted on a total of five defects: three defect types of one grade of steel (X52) and two defect types of another grade of steel (X70). Detailed experimental data will be recorded of the five samples for different objectives: one sample for stress-strain characterization, one sample for failure under static load, one sample for failure under fatigue load, one sample for characterization of ILI, and one sample for repairs.

Comprehensive data of full scale tests of plain dents was reported by Semiga in November 2007. The tests on the plain dents are the first phase of the project. The second phase includes dents on girth welds, dents on electric resistance long seam welds, and dents with simulated metal loss. The full scale experiments were instrumented to produce detailed recording of denting process, loading, and failure including dent depth profiles at various stages of the indentation and pressure cycling processes and pipe wall strain measurement. Moreover, detailed material property were tested and recorded

2.4 ASSESSMENT AND ACCEPTANCE CRITERIA BY LOCAL AND INTERNATIONAL CODES

The basic criteria for assessment of mechanical damage is to measure the depth of the dent, taking into account the spring back effect, and relate it to the diameter of the pipe. Moreover, the interaction of dents with localized effect such as metal loss, gouge, and welds must be considered. Historically, plain dents were accepted up to a depth of 6%. Repair was required for deeper dents, dents with gouges and dents on welds. However, due to the active research in this area, the criteria are being updated regularly. The following paragraphs give the requirements of the latest editions of the relevant codes.

The PRCI updated Pipeline Repair Manual (August 28, 2006) accepts 6% plain dent and 2% dent on girth welds unless the dent is subjected to very large pressure cycles or the dents interferes with ILI passage. The manual warns that any dent with stress riser such as gouge, crack, groove, score, etc. is a threat to pipeline. It states that Operators reported leaks of plain dents less than 6% but with sharp profiles. Research showed that a strain higher than 12% would be serious. Therefore, the code limited the strain to 6% and provided appendix for calculation.

ASME B31.4 (2006) requires that during Construction, all dents more than 6% shall be removed. Similarly, all dents with gouges, scores, etc. and all dents on welds shall be removed. For dents found during the service life of the pipeline and for the purpose of integrity assessment, the following dents shall be removed or repaired unless qualified by engineering assessment: dents with gouges, scores, etc.; dents with more than 12.5% metal loss (nominal wall thickness); dents on girth of longitudinal welds, and dents more

than 6% depth. Dents with gouge can be repaired by grinding only to remove the gouge, it shall not exceed 12.5% of the nominal wall thickness.

ASME B31.8 (2007) requires that during Construction: All dents more than 2% shall be removed if the stress is 40% of the yield stress or more. All dents with gouges, scores, etc. shall be removed as well as all dents on welds. For integrity assessment of pipeline in operation, plain dents are considered injurious if they exceed 6% depth. Plain dent of any depth is acceptable if strain is less than 6% per Appendix R. Dents that prevent ILI must be removed regardless if they are threat to pipeline. Dents with metal loss are injurious if they exceed 6% or the corrosion exceeds the code criteria. Dents on welds (girth or seam) are injurious if they exceed 2% depth. This might be 4% strain for high quality welds. It is worth mentioning that the strain formulas of Appendix R were corrected and the thickness was divided by 2 compared to the previous edition of 2003.

CSA Z662 (2003) requires engineering assessment of plain dents exceeding 6% depth, plain dents on welds exceeding 2% depth, dents with stress concentration such as gouge, groove, crack, etc, and dents with metal loss more than 40% of the thickness or as low as 10% if corrosion defect length exceed the maximum allowable by the code. The code give safety precautions relating to the spring back effect. It warns that consideration should be given before excavating a pipeline to inspect dent on the top side. Moreover, it recommends, lowering the pipeline pressure to minimum feasible before removing racks indenting pipes on the bottom side.

API 1156 (1999) covers smooth dents and rock dents in pipelines under burst and fatigue loads and it provides guidelines for the pipeline operators. The code highlights that it would be very rare to find dents in excess of 5% depth in pipelines operating with

more than 72% SMYS due to re-rounding of un-constrained pipelines. It states that smooth dents should not be a concern unless they are subject to aggressive pressure cycles or contain stress risers such as gouges, scores, etc. The code warns that the interaction between two close dents will flatten the pipe and might lead to leak. The code also points out that rock dents are not of concern from fatigue point of view because they are constrained. However, they are concern for puncturing the pipe or accelerating corrosion. Similar to other codes, API 1156 mentions that dents on welds are concern if they are more than 2% deep.

API 579 (2005) section 8 provides assessment procedure of plain dents by considering them as out of roundness defect. Level 1 assessment is not applicable for cyclic conditions. Moreover, it is for code acceptance only where ASME B31.3 does not have dent acceptance. Level 2 has assessment based on dent depth and minimum radius at the depth (gouge). Level 2 also accounts for interaction between dents of the distance is less than $1.8\sqrt{Dt}$. The cyclic pressure should not be server and is limited to 500, i.e. start-up and shutdown only. Moreover, stresses due to other than pressure should not significant. The assessment is not applicable if the dent is located in weld. It is also not applicable to dents with gouges.

Saudi Aramco Engineering Procedure SAEP-310 requires repairing all dents that violate the applicable Code criteria. The repair can be with a metallic or non-metallic sleeve. The gap between the dented pipe and the repair sleeve must be filled with hardenable material. Saudi Aramco is very conservative for dents that result from construction and handling activities and reject all damaged pipes although this is not explicitly spelled out in the construction standard SAES-L-450.

CHAPTER 3

MATERIAL CHARACTERIZATION OF DAMAGED PIPES

3.1 INTRODUCTION

Material properties play a decisive role in improving the resistance of damaged pipes to failure. This is not limited only the pipe material yield stress which will determine the pipe general thickness based on the applied pressure hoop stress. Other mechanical properties like hardness and impact toughness as well as chemical composition and microstructure also are essential. Industry standards set requirements for these properties depending on the service. For example, the maximum hardness level allowed is 250 Vickers to avoid hydrogen embrittlement (01-SAMSS-035, 2009). . The impact toughness for pipes carrying gases must be higher than pipes carrying liquids such that the pipe can resist the gas decomposition and fracture velocity. The minimum toughness is determined based on the gas composition, gas temperature, gas pressure, diameter and wall thickness of pipe, pipe strength and design pressure (SAES-L-131, 2009). Also, the chemical composition must be controlled. Example is the limitation of carbon equivalent to 0.43 to maintain good weldability of the pipe joints during installation (01-SAMSS-035, 2009). API 5L (2007) sets the requirements of pipe microstructure to be of fine grain.

The knowledge of material characteristic and behavior is also critical for the purpose of development and validation of a mechanistic approach for assessment of damaged

pipes. In order to define a material model in the FEA to closely resemble the actual pipe behavior, detailed material properties must be available through regressive testing. Pipeline Research Council International has launched a comprehensive program to study the pipe mechanical damage from all aspects. One of the tasks of the program is to conduct full material characterization (Carroll, 2007). This will be discussed in details in Chapter 4 for the development and validation of the FEA model. However, these tests are concerned with the global behavior of the pipe as they are conducted on un-damaged pipes. There was no reporting on the literature of material testing conducted on damaged pipes.

The objective of this chapter is to conduct material characterization of damaged pipes from a real case. Detailed mechanical testing including tensile, impact and hardness will be conducted as well as chemical and microstructure examination. Comparison of properties between the damaged and undamaged sections of the pipe will be made to determine if any significance change to be considered in the numerical model.

3.2 TEST PLAN AND PROCEDURES

A total of 10 damaged pipes were collected from a local source. The pipes were damaged during mishandling at the storehouse transportation before transportation to the construction site. Measurement of dent depth was conducted by the project inspection (Fig. 3.1) and accordingly those damaged sections were cut and rejected as they exceeded the maximum allowed dent depth as per the project specifications. The cut sections of the 10 damaged pipes were transported from the project material yard to KFUPM Mechanical Shop.



(a)



(b)

Figure 3.1. Measurement of dent depth in damaged pipe before cutting

A detailed test plan was developed to maximize the use of the 10 pipes to cover all aspects of mechanical and microscopic analysis (Table 3.1). Also, repeatability was considered to ensure validity of the results, and therefore each test is repeated twice. Below are the detailed test procedures:

Part I: Visual

- Mark each sample clearly for identification.
- Take several photographs for each damaged section from different angles.
- Measure and record the outside diameter of the pipe (d) and the thickness (t).
- Measure and record dimensions for each dent including length (l), width (w) and depth (d).
- Examine visually each dent and record observations such as gouge, crack.

Part II: Mechanical Testing

- Cut 3 samples for tensile testing from each pipe as described in section 3.3.1.
 - Attach strain gauges on the samples for strain measurement.
 - Measure the tensile specimen gauge length before the tensile test.
 - Conduct the tensile test on the specimens.
- Cut 4 samples for impact testing from each pipe as described in section 3.3.2.
 - Put the samples in the temperature controller to reach 0 degrees Celsius.
 - Conduct the Charpy impact testing and record the energy values.
- Cut samples for hardness measurement in 3 locations in each pipe as described in section 3.3.3.

Table 3.1. Summary of test plan

Pipe #	PART I: VISUAL				PART II: MECHANICAL TESTING			PART III: MICROSCOPIC	
	Photos	Pipe dimensions	Dent dimensions	Visual for crack	Tensile	Impact	Hardness	Microscopic	SEM/EDS
1	√	√	√	√					
2	√	√	√	√					
3	√	√	√	√	√				
4	√	√	√	√			√(XT)	√	√
5	√	√	√	√		√			
6	√	√	√	√			√(XL)		
7	√	√	√	√					
8	√	√	√	√		√			
9	√	√	√	√	√				
10	√	√	√	√					

- Measure the hardness in every sample in equally spaced distances along the sample two perpendicular directions.

Part III: Microscopic

- Cut samples for microscopic analysis from three locations on the pipe as described in section 3.3.4.
- Mount the samples and grind and polish to provide the appropriate surface finish for analysis.
- Apply gold plating to prevent the samples from corrosion.
- Conduct optical microscopy, scanning electron microscopy (SEM), and energy dispersive spectroscopy (EDS) analysis on the samples.

Special equipments are needed for each type of the planned tests. These equipments are available in a number of KFUPM laboratories including material lab, corrosion lab, and structural lab. Table 3.2 lists the equipment type and models required for the different planned tests.

3.3 SAMPLE PREPARATIONS AND TESTING

The sample preparation was conducted in KFUPM Mechanical Shops utilizing saw, lathe, and CNC machines. It was necessary to conduct several machining steps to reach final desired sample shape. The first step was to saw-cut the cylindrical pipe section into rectangular coupons containing the defect so that the coupons can be easily handled in subsequent required machining. Then, lathe and CNC machining was necessary for the

Table 3.2. List of equipment required for the various planned mechanical and microscopic tests

Test	Equipment description	Equipment model
Tensile	Tensile test machine	Instron 1196, Model # A212-201
Impact	Temperature controller	Fridge, FTS Systems
	Charpy impact testing machine	Tinius Olsen Testing Machine
Hardness	Hardness testing machine	Buehler, Type: 1600-6303
Microscopic	Mounting press machine	IPA Evolution
	Grinding tool	Buehler, Model Handimet
	Polishing machine	Buehler, Model Polimet
	Gold plating machine	JEOL, Fine Coat, Ion Spotter, JFC-1100
	Optical microscope	MEIJI Techno Co. Ltd., Model: Mx7100
	SEM/EDS machine	JEOL, Model JSM-6460 LV

final dimensions and tolerances. The following sections give detailed description of the sample preparation and testing.

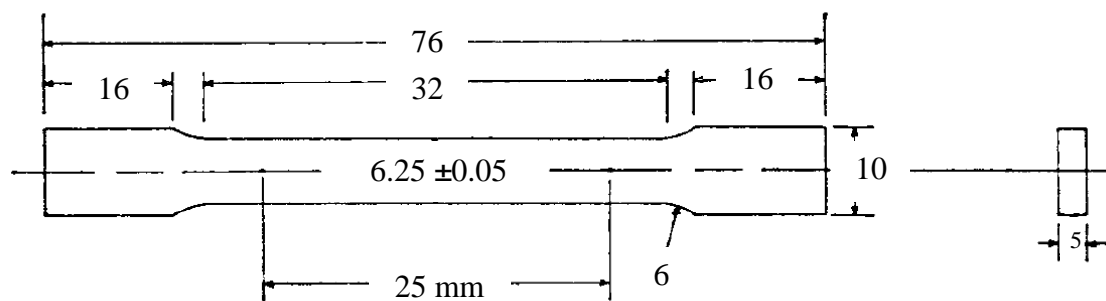
3.3.1 Tensile Test Specimen

Three samples are intended to be tested from each pipe: at the dent peak, at the dent edge and at undamaged location as illustrated in Fig. 3.2.a. The curvature the pipe section and the limited region of damage made it not possible to prepare tensile specimen in accordance with the standard dimensions of ASTM A370 (2009). It was then necessary to choose non-standard size that can be extracted from the desired pipe sections as shown in Fig. 3.2.b. Furthermore, and due to the small specimen size, it is necessary to utilize strain gauges to measure the strains developed during the tensile testing. The following steps are necessary for the correct mounting of the strain gauge.

- a) Polish the intended area for installation with sand paper to remove burrs resulting from machining.
- b) Use light acid like acetone to clean the intended area from any debris and lubricants.
- c) Attach the strain gauge on the back of a scotch tape.
- d) Apply one drop of super glue to the strain gauge.
- e) Install the strain gauge in the intended area and parallel the axis of the tensile test.
- f) Press the strain gauge for a minimum of 1 minute.
- g) Leave the stain gauge for about 20 minutes to ensure curing of the glue.



(a)



(b)

Figure 3.2. Preparation of tensile specimen (a) selected locations for tensile test
(b) dimensions of tensile specimen



(a)



(b)

Figure 3.3. Installation of strain gauge on tensile specimen
(a) tools needed (b) installed gauge

The tools required to complete the installation procedure is shown in Fig. 3.3. After that, the 25-mm gauge length is marked by light indenters on the side of the tensile specimen. Also, it is very important to measure the exact width and thickness of the specimen to account for tolerances during the machining process. Then, the specimen is mounted on the tensile test machine and the test is conducted (Fig. 3.4). After the test is completed, the gauge length is measured again to determine the total elongation of the specimen.

3.3.2 Impact Test Specimen

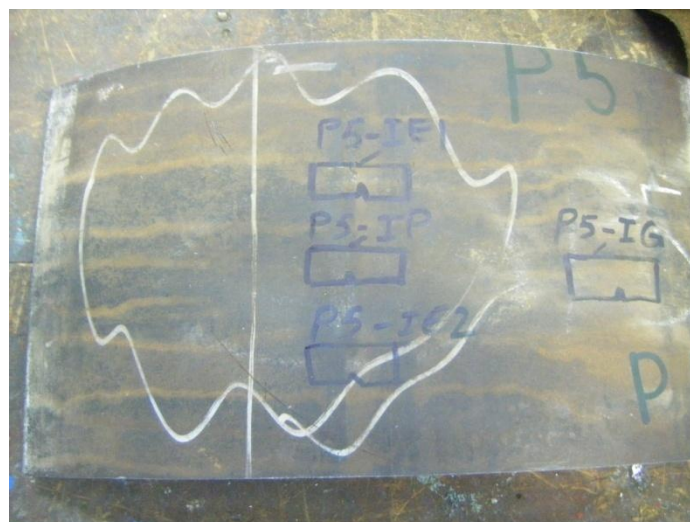
The locations of the specimens for the impact test are shown in Fig. 3.5.a. Four samples are intended to be tested from each pipe: at the dent peak, at each dent edge and at undamaged location. Due to the thickness of the pipe being only 9 mm, the specimen thickness is selected to be 5 mm while maintaining the other standard dimensions of ASTM A370 (2009) as illustrated in Fig. 3.5.b. The specimens are first cooled in a temperature controller until they reach temperature of 0 degrees Celsius (Fig. 3.6.a). This temperature is selected according to international specifications API 5L (2007). Then, they are impacted with the Charpy Impact machine (Fig 3.6.b). The absorbed energy value is recorded and the fracture surface is examined to determine the shear surface area.

3.3.3 Hardness Test Specimen

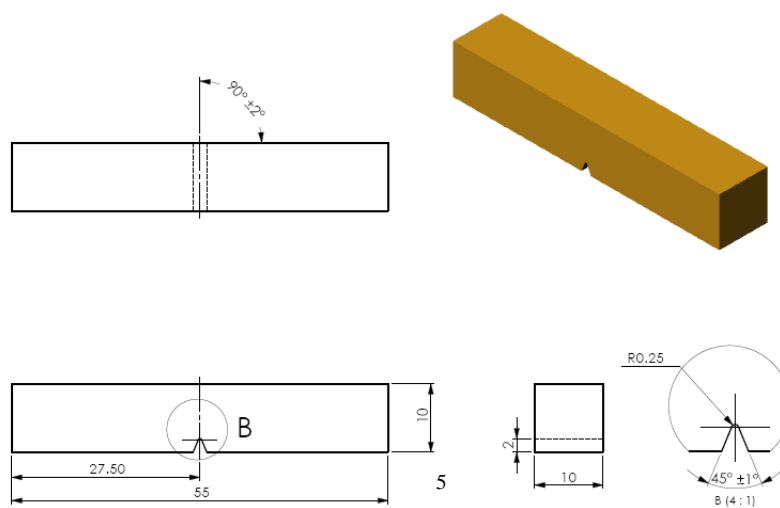
A 10-mm strip is cut from the pipe coupons: one along the pipe axial direction and the other along the pipe transverse direction (Fig. 3.7). Then, three cube samples each of 10 mm width are cut in the pipe dent peak, dent edge and undamaged section.



Figure 3.4. Mounting the specimen on the tensile testing machine



(a)



(b)

Figure 3.5. Preparation of impact specimen
 (a) selected locations for impact test (b) dimensions of impact specimen



(a)



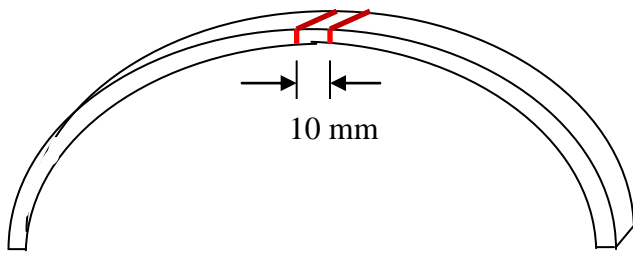
(b)

Figure 3.6. Equipment for impact testing
(a) temperature controller (b) impact test machine

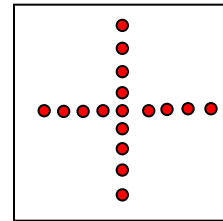


(a)

(b)



(c)



(d)

Figure 3.7. Microhardness test preparation (a) cut strip along axial direction (b) cut strip along transverse direction (c) cut cube sample (d) location of microhardness measurement

Microhardness measurements are taken in equal distances along a line starting from the pipe outer diameter to the inner diameter as well as along a perpendicular line (Fig 3.7.d).

3.3.4 Microscopic Test Specimen

The three cube samples prepared from pipe no. 4 for microhardness are also utilized for the microscopic test. Extensive sample preparation is required by the specimen can be utilized for microscopic analysis. First, the sample is mounted on plastic holder for ease of handling (Fig. 3.8.a). Then, hand grinding is performed to smoothen the surface in 4 stages at 240, 320, 400, and 600 mm (Fig. 3.8.b). After that, fine polishing is made to produce mirror-like surface (Fig. 3.8.c). Finally, the finished surface is gold plated to protect from corrosion (Fig. 3.8.d). The final prepared specimens are shown in Fig. 3.8.e.

The specimens are first examined under optical microscopy (Fig. 3.9.a) at magnification of 50 times the original size to see the general microstructure. Then, the specimens are entered in the SED/EDS machine (Fig. 3.9.b) to find the chemical composition and the fine microstructure. Defects in form of change of microstructure or presence of microcracks due to the mechanical damage are investigated.

3.4 RESULTS AND DISCUSSION

3.4.1 Visual Inspection

Detailed photography is taken for all damaged pipes and they are summarized in Table 3.3. Two of the damaged pipes (Pipe No. 2 and Pipe No. 3) have two dents aligned in the transverse direction while the other 8 pipes have a single dent. The impact of interaction of 2 dents is investigated in detail in Chapter 7. Moreover, one pipe (Pipe No. 10) has a combined damage of dent and gouge. One way to repair the damage is to



(a)

(b)

(c)



(d)



(e)

Figure 3.8 Sample preparation for microscopy
(a) mounting (b) grinding (c) polishing (d) gold plating (e) final specimen



(a)



(b)

Figure 3.9. Equipment for microscopic analysis (a) optical microscopy (b) SEM/EDS

Table 3.3. Photographs of damaged pipes






Pipe number	Outside	inside
1		
2 combined		
2A		
2B		

Table 3.3 (continued). Photographs of damaged pipes










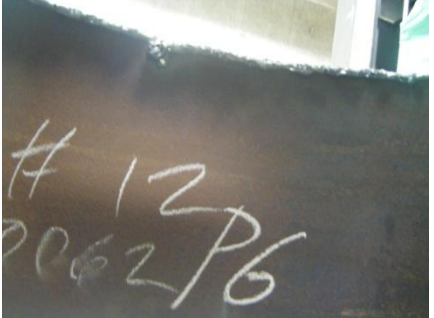





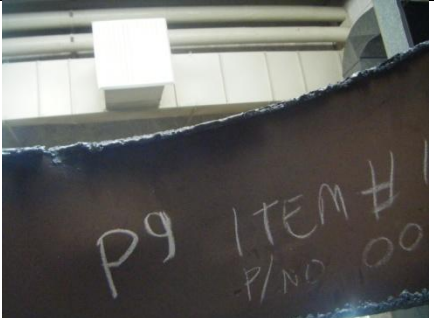


3 combined	 A photograph of a cylindrical pipe section. The pipe is heavily rusted and has several white chalk-like markings. The letters 'P3' are written in two locations. A ruler is placed horizontally across the middle of the pipe section.	 A close-up photograph of a pipe section. The surface is dark and rusted. Handwritten in white chalk are the words 'ITEM' and 'P3 P110'.
3A	 A close-up photograph of a pipe section. A large, white chalk scribble is drawn on the surface, resembling a stylized 'A' or a similar symbol.	
3B	 A close-up photograph of a pipe section. The letters 'P3' are written on the left side, and a large white chalk scribble resembling the letter 'B' is in the center.	
4	 A close-up photograph of a pipe section. A ruler is placed horizontally across the pipe. The letters 'P2' are written in white chalk on the right side.	 A close-up photograph of a pipe section. The letters 'P2' are written in white chalk on the surface.
5	 A close-up photograph of a pipe section. A ruler is placed horizontally across the pipe. The letters 'P5' are written in white chalk on the right side.	 A close-up photograph of a pipe section. The surface is dark and rusted. There are some faint white markings, but they are not clearly legible.

Table 3.3 (continued). Photographs of damaged pipes

6		
7		
8		
9		
10		

remove the gouge by grinding. However, the impact of interaction of dent with metal loss must be evaluated which is done in Chapter 8. Also, one pipe (Pipe No. 7) has the dent at the same location of longitudinal weld. The impact of interaction of dent with welds is studied in Chapter 9. There are no cracks that can be detected visually in any the 10 damaged pipes, and therefore, the assumption of no-crack will be used in the analysis in the subsequent chapters.

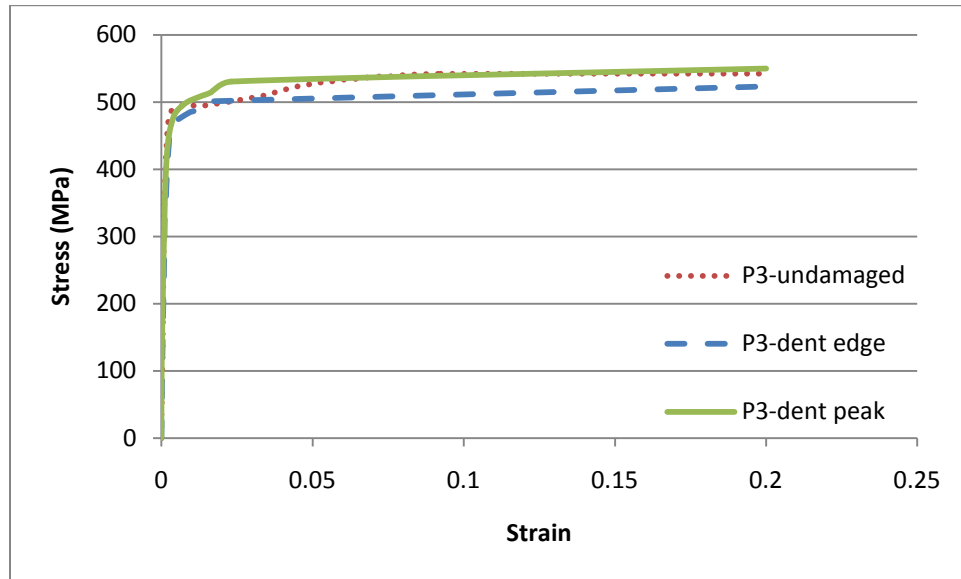
The dimensions of the dents are given in Table 3.4. The dent depth varies between 2.8 mm to 12.1 mm. The dent length has a range between 34 and 320 mm while the dent width has a range between 39 to 189 mm. There is a great scatter in the dent dimensions. Therefore, statistical analysis to define the distribution functions of the dent dimensions is recommended and is conducted in Chapter 5. Moreover, the evaluation of dent severity based on probabilistic design analysis is presented in Chapter 6.

3.4.2 Tensile Test

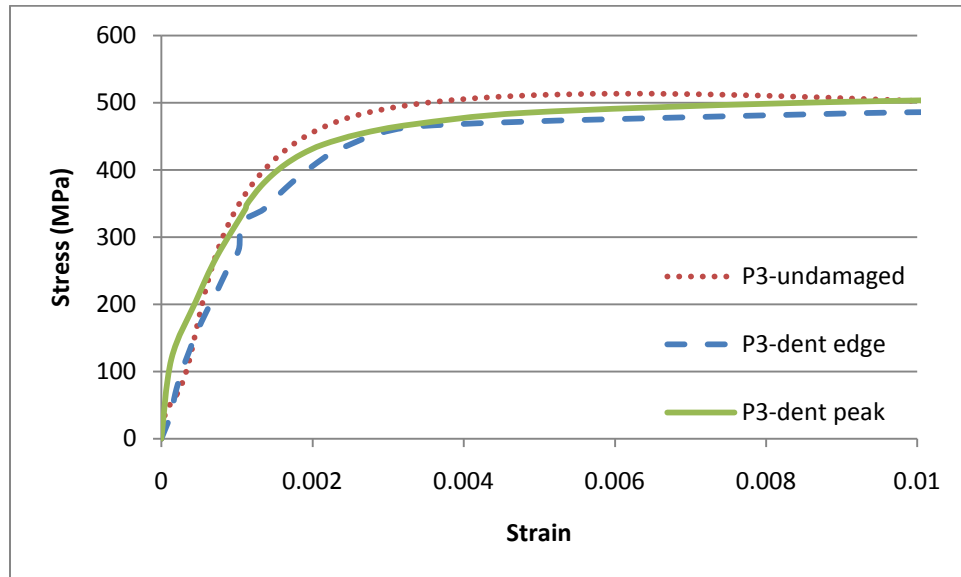
The stress-strain curves of the tensile specimens from the dent peak, dent edge and undamaged section of pipe no. 3 are presented in Fig. 3.10 while the specimens from pipe no. 9 are presented in Fig. 3.11. The overall behavior is typical for a metallic specimen with initial linear vertically-steep section for the elastic elongation, followed by almost flat line after the yield point. However, by zooming into the initial yield range, it is noticed that there is no definite line in the elastic portion that should define the modulus of elasticity. This behavior of initial non-linear stress-strain curve is more pronounced in the dent peak specimen especially for pipe no. 9. This might not make a lot of differences for the acceptability of the damaged pipe from tensile properties points, In Table 3.5, it is

Table 3.4. Recording of dent dimensions damaged pipes (dimensions in mm)

PIPE NO	Pipe dimensions		Dent dimensions				Gouge dimensions (if any)	
	D	t	d	L	W	d/D (%)	L _g	d _g
1	610	10.2	5.7	172	176	0.9	-	-
2A	610	11.4	9.1	121	189	1.5	-	-
2B	610	11.4	6.7	162	197	1.1	-	-
3A	610	11.0	2.8	34	39	0.5	-	-
3B	610	11.0	4.2	78	76	0.7	-	-
4	610	10.2	8.0	151	143	1.3	-	-
5	610	10.5	7.8	192	158	1.3	-	-
6	610	11.1	8.4	147	176	1.4	-	-
7	610	10.4	6.7	170	143	1.1	-	-
8	610	11.0	7.8	134	132	1.3	-	-
9	610	11.3	7.6	87	129	1.2	-	-
10	510	8.2	12.1	320	108	2.4	199	1.8

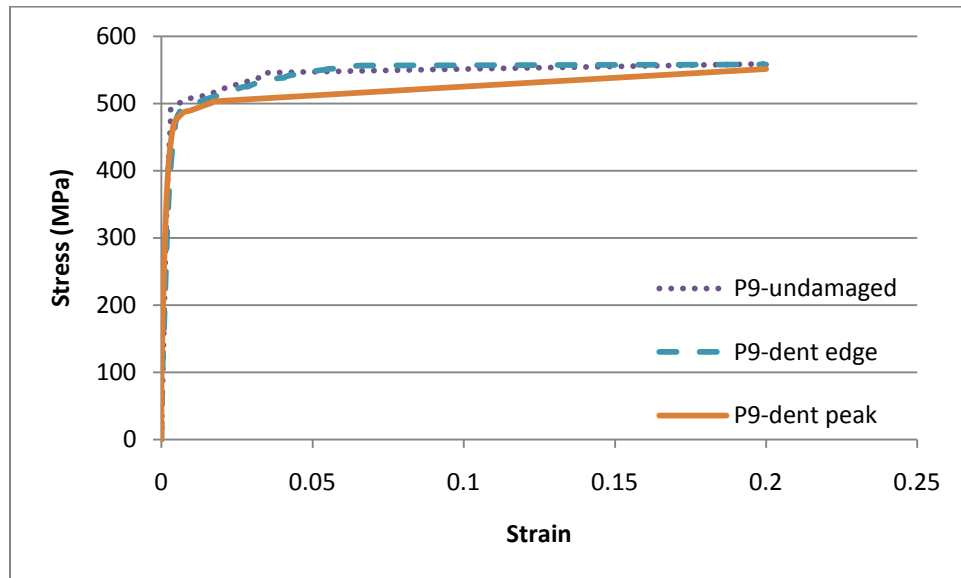


(a)

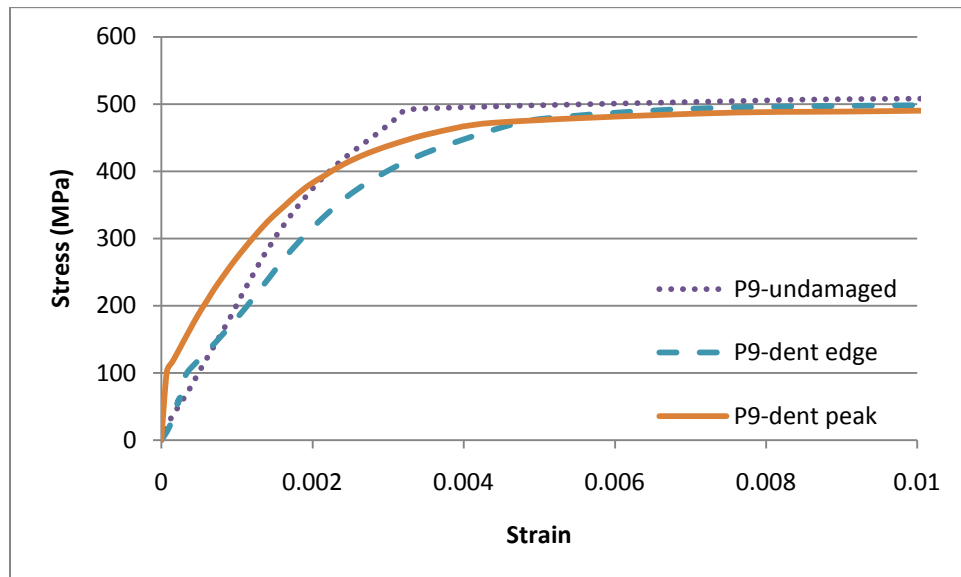


(b)

Figure 3.10. Stress-strain curves for tensile specimens from pipe no. 3 (a) full range (b) initial yield range



(a)



(b)

Figure 3.11. Stress-strain curves for tensile specimens from pipe no. 9 (a) full range (b) initial yield range

Table 3.5. Tensile properties at pipe dent peak, dent edge and undamaged sections

Specimen location	E (MPa)		σ_y (MPa)	S_{ut} (MPa)
	Estimated value	Estimated error		
Standard requirements for grade X65 (API 5L, 2007)	-		450-600	535-670
P3-undamaged	1.65×10^5	2.5%	486	542
P3-dent edge	2.05×10^5	4.6%	474	540
P3-dent peak	2.05×10^5	5.3%	485	550
P9-undamaged	1.85×10^5	0.5%	499	559
P9-dent edge	1.60×10^5	2.6%	478	558
P9-dent peak	1.94×10^5	5.6%	479	551
Average value	1.86×10^5		484	550
Standard deviation	0.20×10^5		8.8	7.8
Coefficient of variation	10.5%		1.8%	1.4%

shown that the yield strength and tensile strength of all tensile specimens meet the API 5L (2007) requirements. However, this makes a lot of difference for the sake of proper numerical model as the FEA is sensitive to the modulus of elasticity defined. Table 3.5 shows high variability in the modulus of elasticity with standard deviation of around 11%. The standard deviation is much smaller for the yield and tensile strengths as it is limited to 2% only. The variability in the modulus of elasticity cannot be attributed to instrument accuracy as it is limited to 0.5% for the strain gauge and 1% for the tensile force. Moreover, the variability cannot be attributed to the error in estimated the modulus of elasticity due to data scatter which is presented graphically in Fig. 3.12 and summarized in Table 3.5 as the maximum error is only half the 11% variability of the modulus of elasticity. Similar observation of high variability in the modulus of elasticity has been reported by Carroll (2007) in the material characterization for PRCI project. The affect of the initial non-linear behavior of the stress-strain cure on the numerical modeling will be investigated in detail in Chapter 4. Moreover, the effect of variability of material properties will be studied in detail in Chapter 6.

3.4.3 Impact Test

The absorbed energy values as well as the fracture surface of the impact test specimens are shown Table 3.6. The absorbed energy ranges between 72 to 94 joules. The variability is expected in the impact test results and it is not attributed to the dent. The measured value exceed the minimum requirements of API 5L (2007), which is 52 joules. The fracture surface for all specimens is 100% ductile shear, and there is not brittle fracture area. This exceeds the requirements of API 5L (2007) in having a

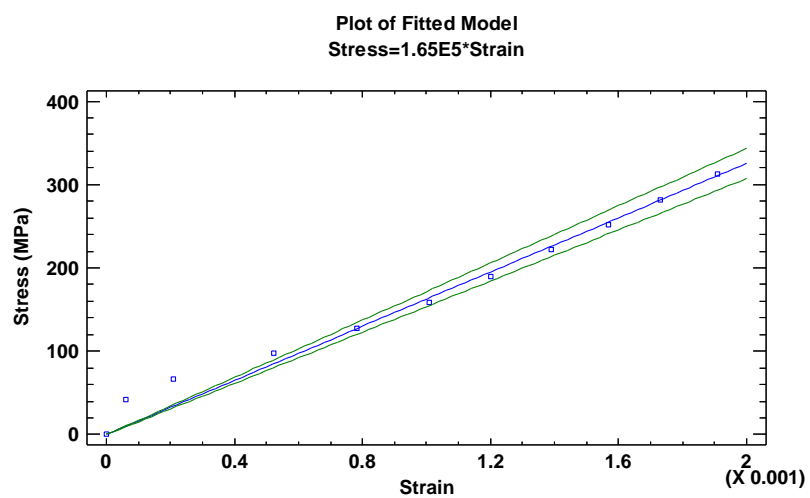


Figure 3.12. Regression fit for elastic modulus of P3-undamaged with estimate of error limits

Table 3.6. Impact test results at pipe dent peak, dent edge and undamaged sections

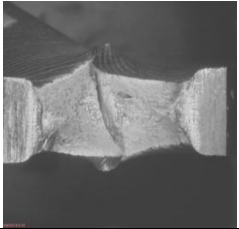
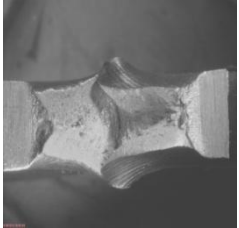
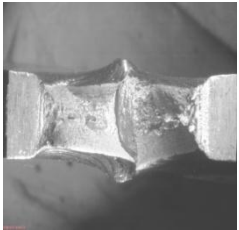
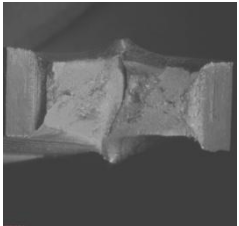
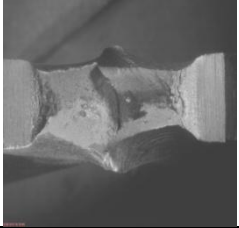

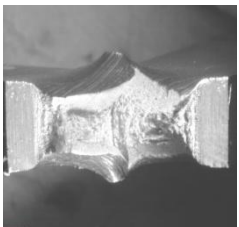
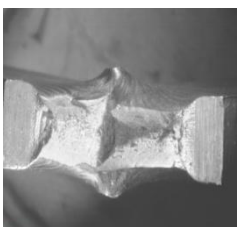
Sample ID	Impact Energy Value (Joules)	Fracture surface
P5-undamaged	80	
P5-dent edge 1	90	
P5-dent edge 2	72	
P5-dent peak	74	

Table 3.6 (continued). Impact test results at pipe dent peak, dent edge and undamaged sections

Sample ID	Impact Energy Value (Joules)	Fracture surface
P8-undamaged	83	
P8-dent edge 1	85	
P8-dent edge 2	90	
P8-dent peak	94	

minimum of 85% shear fracture area. In accordance with the results of the impact test, the denting process does not affect the toughness of the ductile fracture resistance of the pipe, and therefore, the integrity assessment in the subsequent chapters will not consider fracture toughness in the analysis.

3.4.4 Hardness Test

The results of hardness measurements along the dent profile are illustrated in Fig. 3.13 for both the transverse and longitudinal directions. The hardness values range between 177 to 222 Vickers, equivalent to 159 to 211 Brinnell, which converts to tensile strength of 557 to 739 MPa using the empirical relation $S_{ut} \sim 3.5 \times Hb$. The values are in agreement with the tensile test results presented in Table 3.5. There is a slight increase observed in the hardness values in the samples from the transverse strip in the direction from the surface subject to compressive stresses to the surface subject to tensile stresses. At the dent peak, the increase is from the outer diameter to the inner diameter, while at the dent edge, the increase is from the inner diameter to the outer diameter. No similar trend is observed in the longitudinal strip. In any case, since the increase is marginal, and the hardness values are still less than 250 Vickers, which is the onset of hydrogen embrittlement, the hardening due to denting process is not considered in the integrity assessment of dented pipes.

3.4.5 Microscopic Tests

Figure 3.14 shows the chemical composition of the pipe material as determined by the ESD analysis. The pipe has low carbon content with an average of 0.27% by weight

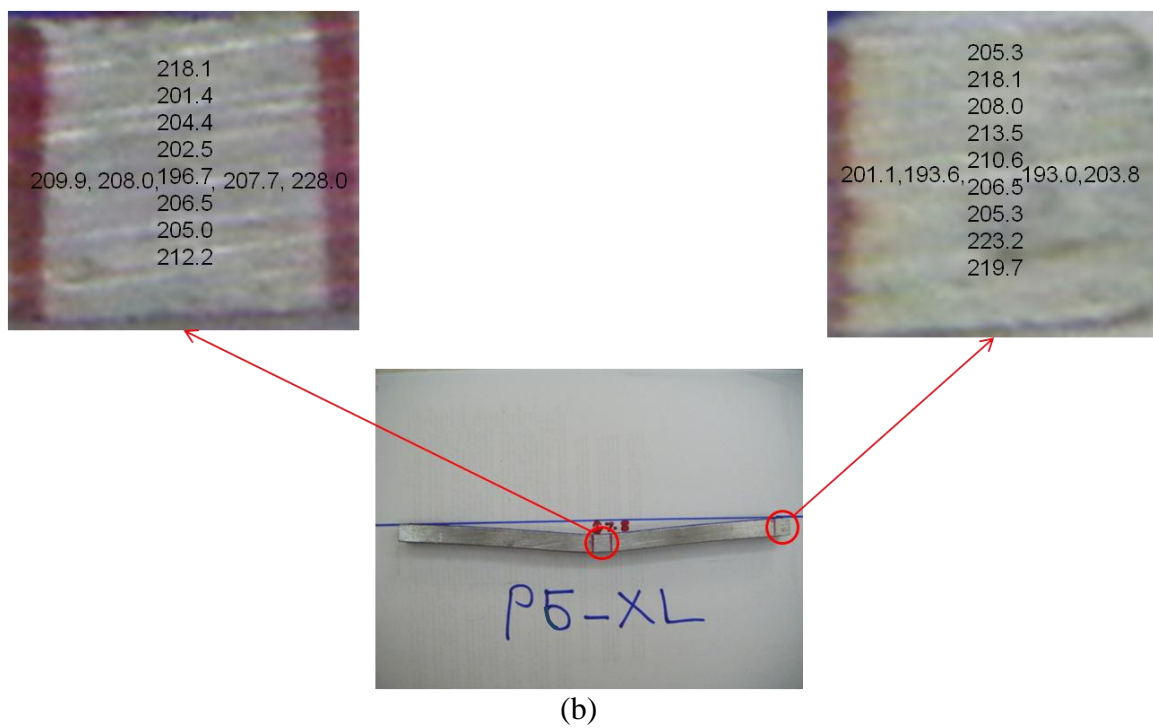
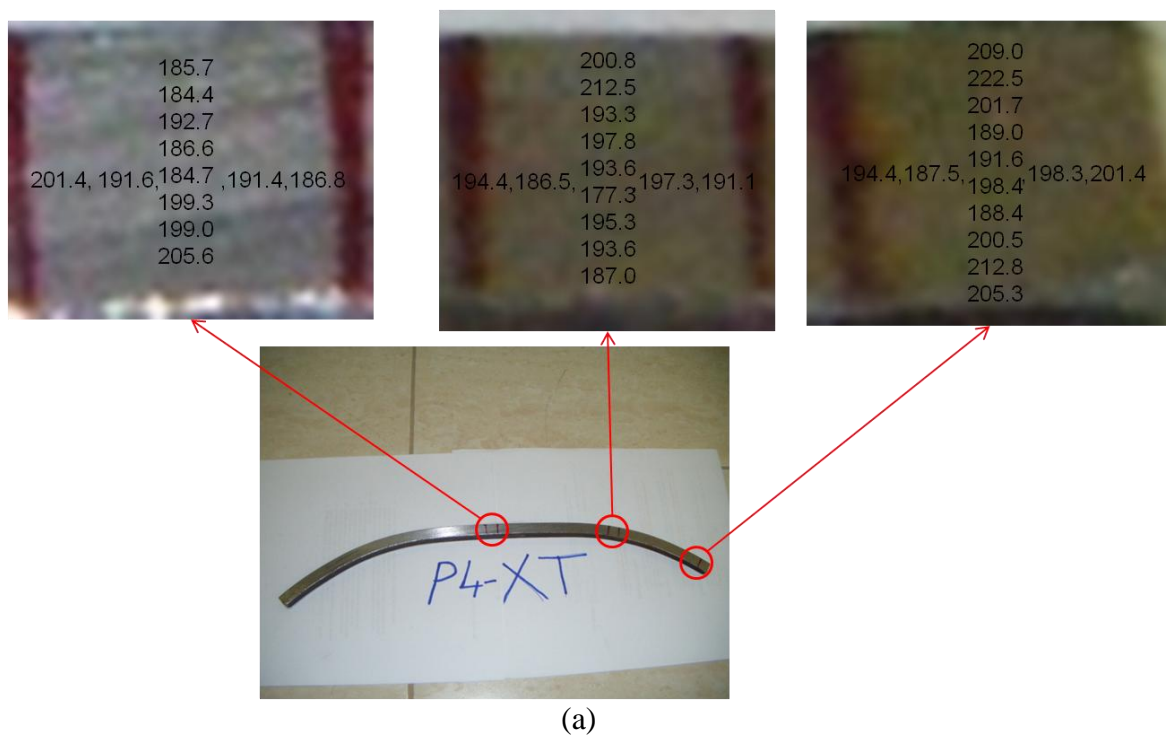
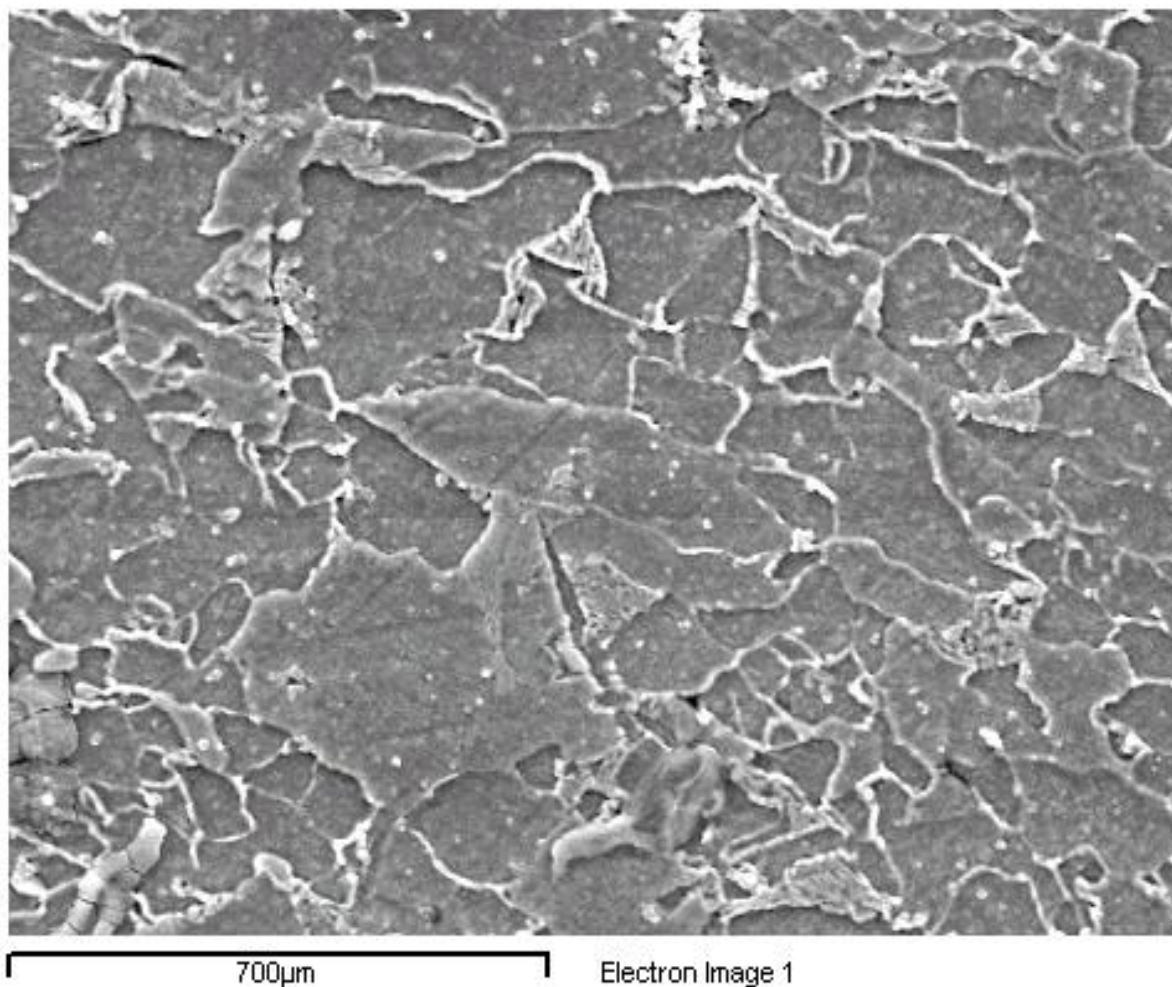


Figure 3.13. Hardness results along pipe dented area
 (a) transverse direction (b) longitudinal direction



Spectrum	C	O	Si	Mn	Fe	Total
Spectrum 1	0.28	3.31		1.02	95.39	100.00
Spectrum 2	0.31	1.20		1.00	97.49	100.00
Spectrum 3	0.23	2.74	0.00	1.11	95.92	100.00

Figure 3.14. EDS Analysis of damaged pipe specimen

which is less than the requirement of API 5L (2007) PSL1 pipes. There is no hard element spots detected in the sample. The microstructure of the damaged pipes is investigated in a number of locations using both optical microscopy (Table 3.7) and SEM microscopy (Table 3.8). The microstructure of the outer diameter, middle shell, and inner diameter is compared in the dent peak, dent edge and undamaged section. All the samples showed a microstructure of ferrite/pearlite with fine grain size. These iron phases are of ductile nature, which supports the conclusion of sections 3.4.2 and 3.4.3. It was noticed from the SEM, that the grain size in the middle shell is smaller than that of the outer and inner diameters. This is attributed to the rolling operation to produce the plates used in the production of line pipes. In conclusion, no special effect from the microstructure shall be considered in the numerical analysis or the integrity assessment.

3.5 SUMMARY

In this chapter, material characterization of damaged pipes from was conducted for a case study of pipes rejected from a pipeline project due to the presence of dents. Detailed testing including visual, tensile, impact and hardness was performed as well as chemical and microstructure examination. The visual examination revealed that multiple dents, dent interacting with welds, and dents with metal loss all existed in this case study, and therefore, presence of evaluation criteria is of extreme importance. Moreover, measurement of the dent dimensions showed great scatter which support the use of probabilistic analysis for the dent geometry. Moreover, the tensile test showed also variation in the material properties supporting the use of probabilistic analysis for material properties as well. The tensile test also revealed that the initial range of the

Table 3.7. Optical microscopy at 50 magnifications of microstructure of different sections of damaged pipe










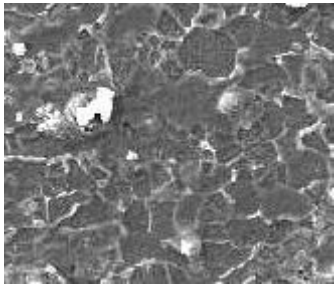
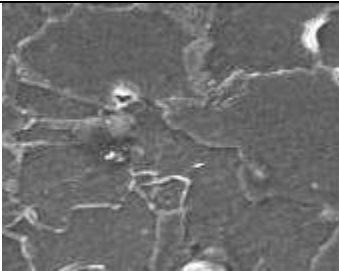
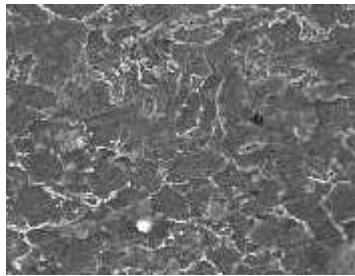
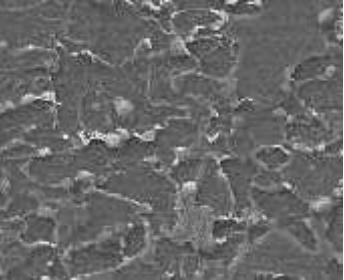
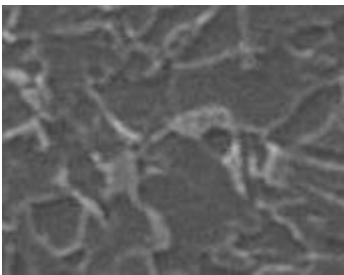
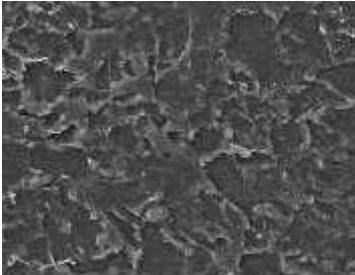
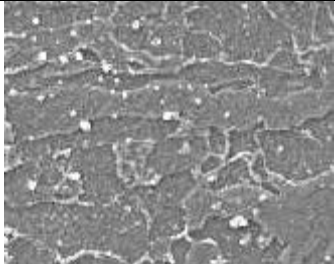
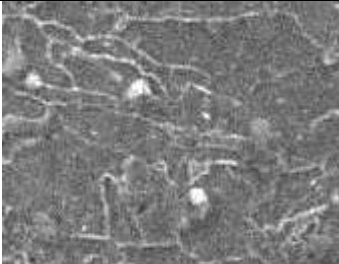
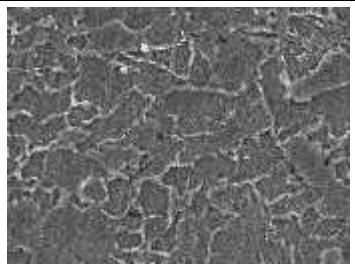
	Top	Middle	Bottom
Undamaged			
Dent edge			
Dent peak			

Table 3.8. SEM microscopy at 900 magnifications of microstructure of different sections of damaged pipe

	Top	Middle	Bottom
Undamaged			
Dent edge			
Dent peak			

stress-strain curve is not truly linear especially for the specimen from the dent peak. Therefore, the affect of the initial non-linear behavior of the stress-strain cure on the numerical modeling must be investigated.

CHAPTER 4

DEVELOPMENT AND VALIDATION OF 3D FINITE ELEMENT MODEL

4.1 INTRODUCTION

There are many parameters that affect the severity of the mechanical damage related to the pipe geometry and material properties, the defect geometry and boundary conditions, the loading cycle, and the pipe state of stress. To understand the effects of those parameters, different full-scale tests were conducted (Fowler et al. 1992, Fowler et al. 1994, API 1999), but it is too expensive to run tests that cover all different aspects of the problem with full ranges. Therefore, the utilization of numerical finite element analysis has been widely used based on the full-scale tests and to extend their limitations. As the actual pipe material exhibits a number of special features including non-linear elasticity, anisotropy, and cyclic softening which needs advanced material modeling techniques. However, the success of the numerical material model to actually simulate the pipe material behavior could not be studied previously in details due to insufficient experimental data especially in cyclic pressure loading.

Leis et al. (2004) simulated the indentation and re-rounding spherical and cylindrical indenters on a pipeline to evaluate the non-linearity of the problem due to geometry and material response. For the material model, isotropic hardening was implemented, but no

details about the stress-strain curve were given. The effect of the pressure during indentation phase on the initial and final indentation depth was discussed. The results were discussed qualitatively as no experimental test was conducted to validate the data. The influence of internal pressure on the final depth of a dent was also studied numerically and validated experimentally by Le Bastard (2006). For the material model, a relationship of the form $\sigma = k\epsilon^n$ where implemented where the constants k and n were determined from the results of tensile tests. Although, isotropic hardening rule was used for the plastic material model, the author recommended investigating kinematic hardening rule for the case of cyclic loading.

Pinheiro et al. (2006 and 2008) conducted FEA to determine the stress concentration factor of dent under cyclic pressure loading which was simulated by small-scale pipe with strain gauges. The process included indentation plus two cycles of pressure loads. To model the plastic behavior, the von Mises yield function with combined isotropic and kinematic hardening was assumed. However, the cyclic uniaxial tensile test was not conducted but estimated by the FEA routine. The authors indicated that first pressure cycle was non-linear while the second pressure cycle was linear after a phenomenon known as shakedown. Thereafter the stress concentration factor is calculated based on elastic model. The observation of the need of few pressure cycles to reach elastic behavior before calculating the stress range was also cited by Dawson et al. (2006). However, there was not a description of the material model assumed. The validation was relative by finding that the estimated life by the stress range from the FEA is comparable in magnitude to a pipe in service with similar dent profile. Jandu et al. (2008) in their work assumed the material model was bi-linear stress-strain with kinematic hardening.

Dinovitzer et al. (2007) conducted comprehensive sensitivity study to understand the aspects of the numerical model on the behavior of pipe indentation problems. For validation, they depended on API 1156 (1999) which did not have strain measurements or detailed material properties. Therefore, relative comparisons between the different FEA models were conducted to show effects of each aspect. The parameters studies were element type, element size, contact assumption and material properties. The authors concluded that material properties had decisive role on the stress values and would greatly affect the stress-based assessments. Moreover, the numerical analysis greatly over predicted the final dent depth after cyclic loading compared to the experimental part due to the unknown material properties. The issue of material properties was one of the key observations by Carroll et al. (2006) on previous dent test programs in three areas. First, most of researchers depend on the transverse orientation flattened strap tensile test data to characterize the pipe material properties while other tests like round bar, pressure vessel, ring expansion, etc. give variability in the yield stress value, stress-strain curve shape, and to less extent the tensile stress value. The second is cyclic stress-strain curve and hardening rule. The third is anisotropy as almost all models assume isotropic material properties which in fact is not true for pipes as the transverse properties is usually higher than the axial ones.

Pipeline Research Council Institute (PRCI) has been running detailed and fully-instrumented full-scale tests to overcome the deficiencies discussed in the previous models (Semiga 2007, Bolton et al. 2008). Part of the work also was to conduct detailed material characterization task with different tensile tests in transverse and axial directions

(Carroll 2007). This chapter utilizes the available data from this work for the validation of the numerical model.

The objective of this chapter is to investigate the effect of material modeling using finite element analysis (FEA) on the integrity assessment of dented pipe under static and cyclic loading by simulating pipe denting followed by subsequent pressure cycles. For validation purposes, the strain results of the FEA are compared to the experimental strain measurements of full-scale tests. Moreover, the calculated fatigue cycles to failure based on FEA stress range will be compared to the experimental cycles to failure.

4.2 MATERIAL MODELING OF PLASTIC BEHAVIOR

A brief of material modeling for plastic behavior is discussed here to give the reader a quick reference to understand the different material models used in this chapter (Ansys 2007). The discussion in this section is limited to rate-independent plastic yielding.

The plasticity model is generally composed of three elements: the yield criterion, the flow rule and the hardening rule. The yield criterion is a function that determines the yield surface so that when the equivalent stress is within the yield surface, the material response is elastic. On the other hand, when the equivalent stress is on the yield surface, plastic strain occurs. Examples of yield surfaces for isotropic and anisotropic materials are given in Fig. 4.1. The flow rule determines the direction of the plastic strain increment when yielding starts. Finally the hardening rule describes the change in the yield surface with progressive yielding. There are two basic hardening rules: isotropic hardening where the yield surface increases in size but retains its center, and kinematic hardening where the yield surface maintains its magnitude but shifts its center. The two hardening modes can be combined to simulate more complex material behavior. The

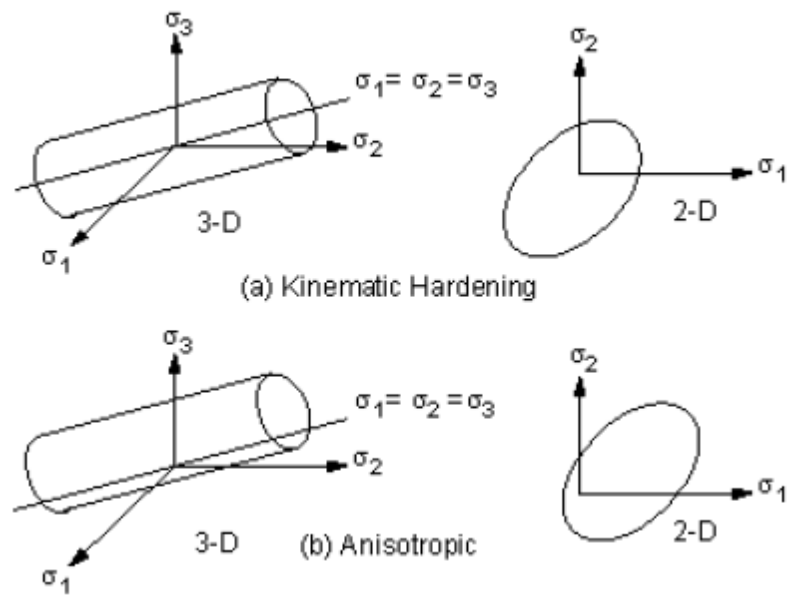


Figure 4.1. Yield surface for isotropic and anisotropic materials. (ANSYS 2007)

stress-strain behaviors of different hardening rules are given Figure 4.2, while Figure 4.3 illustrates the yield surface development. The following sections give the mathematical formulation of the yield function for the different material models used in this chapter as well as the required material parameters to be determined for the material properties.

4.2.1 Isotropic Hardening Rule

The yield criterion is defined as

$$F = \left[\frac{3}{2} \{S\}^T [M] \{S\} \right]^{1/2} - R \quad (4.1)$$

Where $\{S\}$ is the deviatoric stress and R is the yield stress determined based on the stress-strain points of the material response curve in case of multi-linear isotropic hardening. In the case of non-linear isotropic hardening, a power law is used to define the current yield stress as follows:

$$R = K + R_0 \hat{\varepsilon}^{pl} + R_\infty \left(1 - e^{-b \hat{\varepsilon}^{pl}} \right) \quad (4.2)$$

where K , R_0 , R_∞ and b are material constants that must be determined in accordance with the material properties.

4.2.2 Kinematic Hardening Rule

The yield criterion is defined as:

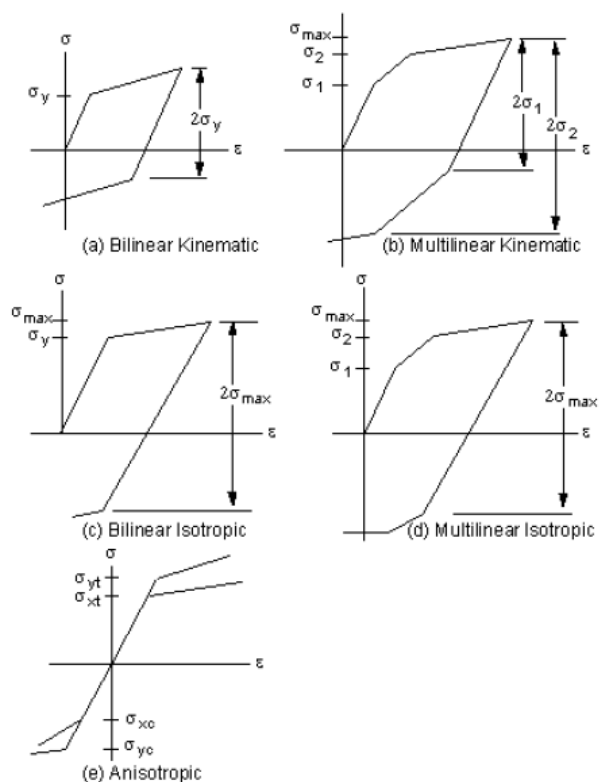


Figure 4.2. Stress-strain curves for different hardening rules. (Ansys 2007)

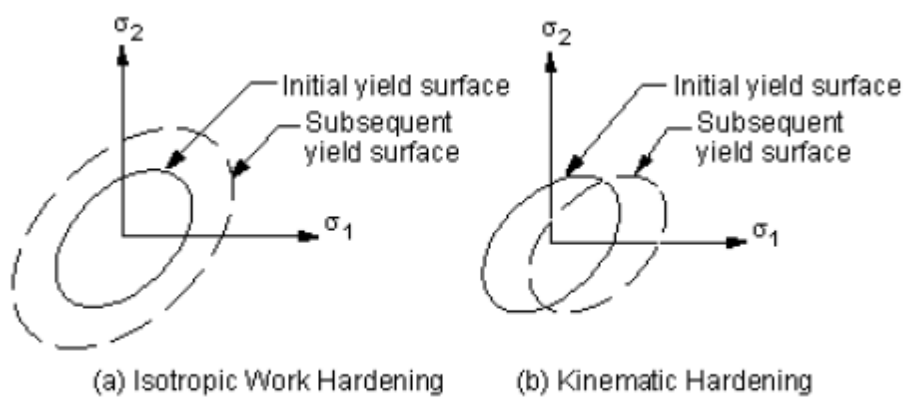


Figure 4.3. Progressive development of yield surface for isotropic and kinematic hardening rules (Ansys 2007)

$$F = \left[\frac{3}{2} (\{S\} - \{\alpha\})^T [M] (\{S\} - \{\alpha\}) \right]^{1/2} - R \quad (4.3)$$

$$\{\alpha\} = \int C d\varepsilon^{pl} \quad (4.4)$$

R again is determined from direct reading of the stress-strain curve of the material, C is material parameter that depends on the slope of the stress-strain curve. The kinematic hardening model can be also defined by a non-linear function using the Chaboche model. In this case, the back stress α is composed of several kinematic hardening models up to 5 and it is defined by the following functions.

$$\{\alpha\} = \sum_{i=1}^n \{\alpha_i\} \quad (4.5)$$

$$\{\Delta\alpha\}_i = \frac{2}{3} C_i \{\Delta\varepsilon^{pl}\} - \gamma_i \{\alpha_i\} \Delta\varepsilon^{pl} \quad (4.6)$$

The model parameters C_i and γ_i need to be determined. However, they are not physical material properties, and therefore, special procedures are needed for calibration of the model. (Chaboche 2008, Broggiato et al. 2008)

4.2.3 Hill's Potential Theory for Anisotropy Material

The matrix M in equations (1) and (3) is for equivalent stress formulation and takes the following format for the case of Von Mises equivalent stress for isotropic materials

$$M = \begin{bmatrix} 1 & 0 & 0 & 0 & 0 & 0 \\ 0 & 1 & 0 & 0 & 0 & 0 \\ 0 & 0 & 1 & 0 & 0 & 0 \\ 0 & 0 & 0 & 2 & 0 & 0 \\ 0 & 0 & 0 & 0 & 2 & 0 \\ 0 & 0 & 0 & 0 & 0 & 2 \end{bmatrix} \quad (4.7)$$

This matrix can be modified to account for anisotropy using the Hill's potential theory. In this model, the diagonal values are determined based on relationships of the stress-to-the stress reference ratios r_{xx} , r_{yy} , r_{zz} , r_{xy} , r_{xz} , r_{yz} . Both the state reference and the constants must be defined depending on the material properties.

4.2.4 Combined Material Models

Different material models can be combined to simulate complex material behavior. For examples, the Hill's potential theory with different any hardening model to account for the anisotropy in the material. Moreover, non-linear kinematic hardening and non-linear isotropic hardening can be combined in the Chaboche model to simulate the effect of cyclic hardening or softening of the material.

4.3 DESCRIPTION OF THE PROBLEM

The problem parameters discussed hereafter were selected to match the experimental set-up of PRCI full scale tests for model validation (Semiga 2007, Bolton et al. 2008).

4.3.1 Geometry and Boundary Conditions

The specific problem geometry under consideration in this paper is of a 610-mm cylindrical pipe supported at the middle of its span as well as its two ends. The pipe wall thickness is 7.9 mm, i.e. the diameter-to-thickness ratio is 76. The pipe section length is

3,000 mm which is equivalent to 4.9 times the pipe diameter. The length was selected by the experiment protocol to ensure that the pipe length does not affect the results of the indented area. The two pipe ends are enclosed by pipe caps to contain the pressure.

4.3.2 Loading: Static Indentation and Cyclic Pressurization

An indentation displacement-controlled load is applied by a spherical indenter of 60 mm diameter (Fig. 4.4). The displacement is increased gradually until it reaches a maximum depth of 46 mm, i.e. 7.5% of the pipe diameter. This value is slightly higher than the general practice of the 6% threshold considered by Industry to be acceptable with the additional conditions that the dent is smooth and there is no severe cyclic pressure expected in the pipe life.

The indenter is kept at its maximum displacement in the so-called restrained condition. This is to simulate indentation created by rocks for example when lowering pipes in trenches during the construction process. Subsequently pressure cycles are applied until leak due to fatigue occurs and the number of cycles to failure is recorded. The first pressure cycle starts from 0 to 9.27 MPaG to generate a stress equivalent to 100% of the specified minimum yield stress (SMYS) to simulate the hydrotest pressure cycle. The subsequent cycles range from 0.944 to 7.44 MPaG which is equivalent to 10% to 80% SMYS which is the maximum stress allowed by few Codes where majority limits the maximum stress to 72% SMYS only.

4.3.3 Pipe Material Properties

The monotonic and cyclic true stress-true strain curves in the pipe longitudinal and transverse directions based on tensile strip tests are plotted in Fig. 4.5. They were

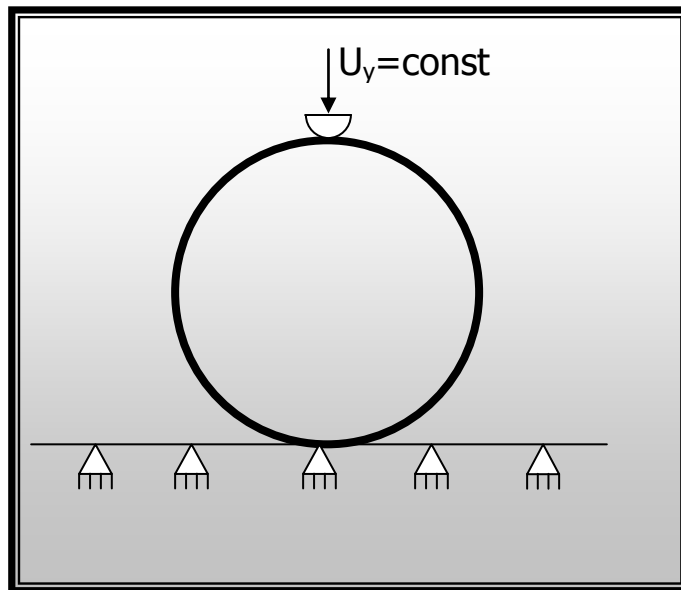
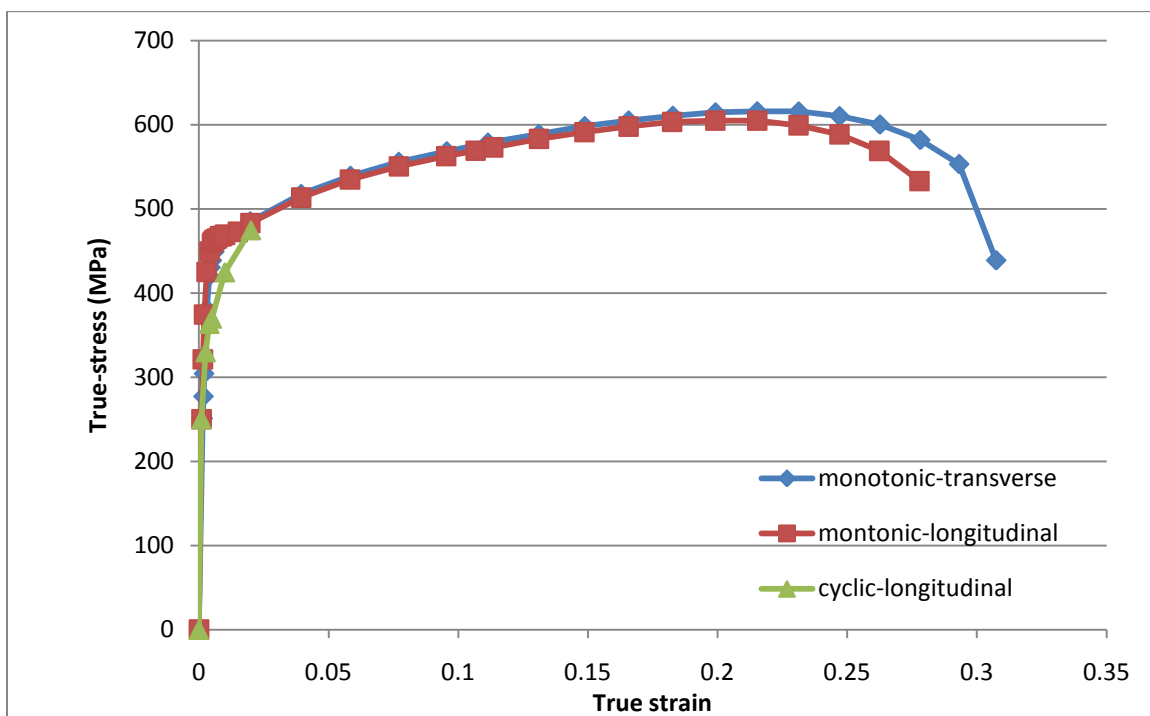
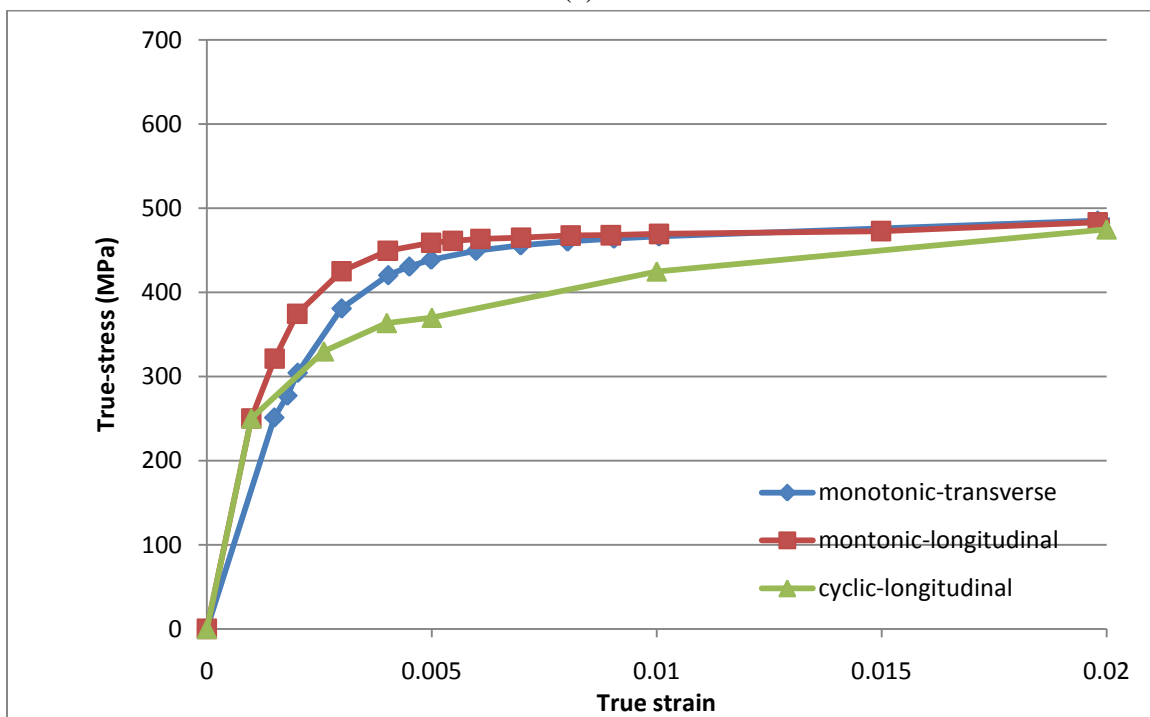


Figure 4.4. Cross-section of problem at the pipe mid-span



(a)



(b)

Figure 4.5. Monotonic and cyclic stress-strain curves of the pipe material (a) full range (b) zoom at elastic and initial plastic portion (Carroll 2007)

generated as a task of PRCI program to fully characterize pipe mechanical damage (Carroll 2007). Several important aspects shall be highlighted. The first aspect is the considerable difference between the end of the proportional limit of the material and the 0.5% yield point characterizing a significant portion of the material behavior of non-linear elasticity. The second is the anisotropy of the material where the properties in the transverse direction are different from that of the longitudinal direction especially in the elastic region up to the 0.5% yield. This is attributed to the directional strain hardening as the pipes are manufactured from cold-rolled steel plates. The third is the cyclic softening of the material is pronounced at small strains less than 2% and diminishes thereafter.

4.4 DESCRIPTION OF THE NUMERICAL MODEL

Finite Element Analysis (FEA) is conducted using commercial software (ANSYS) to simulate the indentation process as well as the eight pressure cycles described in Section 4.3. The problem is non-linear in geometry, boundary conditions, and material. For geometry, large displacements are imposed. For boundary conditions, two contact pairs are present: one for indenter-pipe pair and the other for the pipe-support pair. For material, the pipe in contact with the indenter undergoes plastic deformation.

A quarter of the pipe is used due to the symmetry in geometry, loading and boundary conditions (Fig. 4.6). The geometry dimensions are matching the experimental set-up described in 4.3.1. Symmetry boundary conditions are applied in the two symmetry planes. The two bottom supports are modeled by zero displacement loads in the vertical direction instead of contact elements. This was reported by Dinovitzer et al. (2007) to have negligible effects on the results while greatly improving the solution time. In

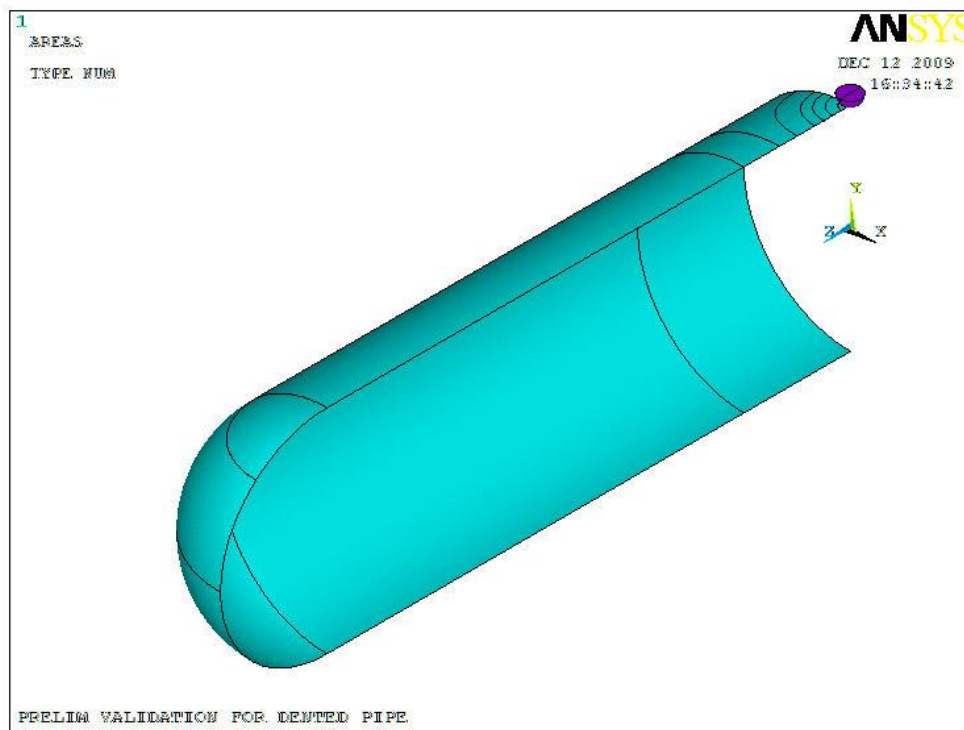


Figure 4.6. Quarter symmetry model of the pipe indentation FEA model

addition, a single node at the bottom intersection of the two symmetry planes is fixed in all degrees of freedom to prevent rigid body motion and to ensure numerical stability.

The indentation process is modeled by a contact pair of rigid target with pilot node. A vertical load displacement is applied on the target in small load steps until it reached the target depth of 56 mm. The contact parameters are 0.1 contact stiffness, 0.1 penetration factor and 0 friction factor. The contact parameters were not varied in this report as they were investigated in details by Dinovitzer et al. (2007). After that, the first pressure cycle up to 9.27 MPaG is implemented in small load steps as well as small unloading steps to 0 gauge pressure. Subsequently, the next pressure cycles are simulated in two load steps of minimum and maximum pressure except for the eighth pressure cycle which is incremented in six load steps to enable capturing the strain values at each load step and compare it with experimental strain measurements.

4.4.1 Material Modeling

There is no FEA material model that has all the features that the actual pipe material exhibits; i.e. non-linear elasticity, anisotropy, and cyclic softening. Therefore, more than 20 single and combined material models were tested to find which model best matches the actual behavior of the pipe. In some instances, two material models were implemented in the same FEA model: one in the highly plastic indented area, and the other in the remaining bulk of the pipe. This is because the aforementioned features are pronounced in the low strain region up to 0.5% while they diminish in higher strains. Out of the many material models investigated, eight material models are presented in this paper as they produced the closest results and they can be used to illustrate the impact on

the strain and stress results, and thus, integrity assessment of the dented pipe. The features and parameters of the eight models are summarized in Table 4.1.

The anisotropy effect on the accuracy of the results is evaluated by assuming the first four models to be isotropic. The first two models Mat_1 and Mat_2 assume isotropic properties of the pipe material based on the actual pipe material transverse properties while the third one is based on the longitudinal properties. To investigate the effect of plastic hardening rule, the first two models are of exactly the same material properties, but the first one (Mat_1) assume isotropic hardening where the second one (Mat_2) assume kinematic hardening. All the remaining models also assume kinematic hardening rule.

The fourth model (Mat_4) is a modification of Mat_3, but assuming that the elastic linear response is continued up to the 0.2% strain point This is to overcome the challenge with the non-linear material response is that all material plasticity models assume that the end of the proportional limit coincides with the yield point meaning that the initial non-linear response is also neglected. This does not make much difference if the two points in the actual material stress-strain response are close, but this is not the case for the pipe material under study.

The next four models all incorporate anisotropy effect utilizing orthotropic linear elastic model as well as Hill's potential theory. In Hill's model, it is assumed that the ratio of the transverse-to-longitudinal yields is constant in the whole range of the material response curve. This not the case here as Fig. 4.5 showed that the ratio is around 0.75 at initial yielding and approaches unity beyond true strain value of 0.02. With several trials on a simple FEA tensile test model for calibration of the Hill's ratio parameters, it was

Table 4.1. Summary of eight material models investigated

	Elastic Model		Plastic Model	
Model No.	Model description	Material Parameters	Model description	Material parameters
Mat_1	Isotropic linear elastic	$E=1.68 \times 10^5$ MPa $\nu=0.3$	Multi-linear isotropic hardening	Fig. 3, <i>transverse</i> curve.
Mat_2	Isotropic linear elastic	$E=1.68 \times 10^5$ MPa $\nu=0.3$	Multi-linear kinematic hardening	Fig.e 3, <i>transverse</i> curve.
Mat_3	Isotropic linear elastic	$E=2.52 \times 10^5$ MPa $\nu=0.3$	Multi-linear kinematic hardening	Fig. 3, <i>longitudinal</i> curve.
Mat_4	Isotropic linear elastic	$E=1.86 \times 10^5$ MPa $\nu=0.3$ (assume linear elastic response up to the 0.2% strain)	Multi-linear kinematic hardening	Fig. 3, <i>longitudinal</i> curve.
Mat_5	Orthotropic linear elastic	$E_t=1.68 \times 10^5$ MPa $\nu_t=0.3$ $E_l=2.52 \times 10^5$ MPa $\nu_l=0.3$	Multi-linear kinematic hardening coupled with Hill's potential theory	Fig. 3, <i>longitudinal</i> curve. $r_{xx}=r_{yy}=r_{zz}=1$ $r_{xy}=r_{xz}=r_{yz}=1$
Mat_6	Orthotropic linear elastic	$E_t=1.51 \times 10^5$ MPa $\nu_t=0.3$ $E_l=1.86 \times 10^5$ MPa $\nu_l=0.3$ (assume linear elastic response up to the 0.2% strain)	Multi-linear kinematic hardening coupled with Hill's potential theory	Fig. 3, <i>longitudinal</i> curve. $r_{xx}=r_{yy}=r_{zz}=1$ $r_{xy}=r_{xz}=r_{yz}=1$

Table 4.1 (continued). Summary of eight material models investigated

	Elastic Model		Plastic Model	
Model No.	Model description	Material Parameters	Model description	Material parameters
Mat_7	Indentation and high plastic deformation region			
	Orthotropic linear elastic	$E_t=1.68 \times 10^5$ MPa $\nu_t=0.3$ $E_l=2.52 \times 10^5$ MPa $\nu_l=0.3$	Multi-linear kinematic hardening coupled with Hill's potential theory	Fig. 3, <i>longitudinal</i> curve. $r_{xx}=r_{yy}=r_{zz}=1$ $r_{xy}=r_{xz}=r_{yz}=1$
	Low plastic deformation region (pipe bulk)			
	Non-linear elastic	$E=1.68 \times 10^5$ MPa $\nu=0.3$ Fig. 3, <i>transverse</i> curve.	None	-
Mat_8	Orthotropic linear elastic	$E_t=1.51 \times 10^5$ MPa $\nu_t=0.3$ $E_l=1.86 \times 10^5$ MPa $\nu_l=0.3$ (assume linear elastic response up to the 0.2% strain)	Multi-linear Chaboche kinematic hardening combined with non-linear isotropic hardening power law and Hill's potential theory.	$K=374$ MPa $C_1=5.72 \times 10^5$ MPa $\gamma_1=600$ $C_2=6.89 \times 10^4$ MPa $\gamma_2=45$ $C_3=6.89 \times 10^3$ MPa $\gamma_3=4.5$ $R_0=0$ $R_\infty=-110$ MPa $b=100$

found that using the unity values presented in Table 1 give matching results of the actual material stress-strain response. Mat_5 defines the stress-strain points for multi-linear kinematic hardening model based on the actual material properties. Mat_6 and Mat_7 are modifications of Mat_5 to account for the initial non-linear elastic response of the material. Mat_6 tackles this by assuming a linear elastic response up to the 0.2% strain. Mat_7 utilizes different approach as it has two material models in the same FEA model. It implements non-linear elastic model in the bulk pipe away from the dented area where strains are below 0.5%.

Finally, Mat_8 implements a combined Chaboche model of non-linear kinematic hardening, non-linear isotropic hardening to simulate the cyclic softening of the pipe material. In addition, Mat_8 combined the Hill's model to account for anisotropy. Moreover, the linear elastic response is assumed up to the 0.2% strain. Therefore, this model takes all features of the actual material pipe behavior into consideration. The challenge of this model is the calibration of the parameters of the Chaboche model as well as the non-linear isotropic model to reproduce the actual material monotonic and cyclic stress-strain curves. Moreover, the Chaboche model is sensitive to the strain point of calibration, and therefore, the calibration points should be close to the expected strain range in the problem. Several trials on a simple FEA tensile test model were conducted for the calibration purposes and only the final model is presented in this paper.

4.4.2 FE Model

Elements used are shell element 181 (4-nodes) in the majority of the FEA models, which is recommended by Dinovitzer (2007). However, this element does not support the

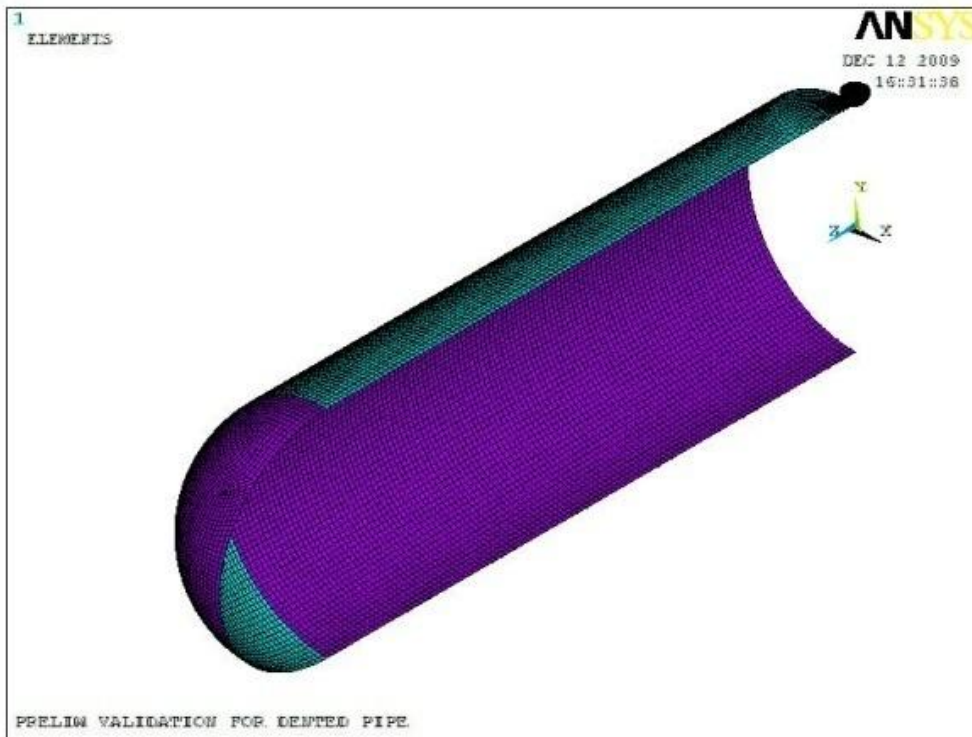
material model of non-linear elastic response; shell element 43 was used in this instance. For the contact pair, the indenter is modeled with Target 170 while the contact areas are modeled with Contact 174. The contact area is defined for quarter circle with the center at the top intersection of the planes of symmetry and of radius 50 mm to ensure covering the radius of the indenter (30 mm) and optimize the contact problem solution time.

The generated mesh is shown in Fig. 4.7. Square mapped mesh of 12.5 mm edge size was used in the areas away from the indentation. As the indentation process imposes large displacements as well as displacement gradient and thus strain, very fine mesh must be used. Therefore, mapped mesh of circular angular divisions of 5 degrees were applied leading to very small element of edge size of 0.25 mm at the dent peak and gradually increasing in size to the 12.5 mm edge away from the indenter. The aspect ratio of the elements was maintained around one as much as practical. The selection of the appropriate element size was done through a series of convergence checks by increasing the number of elements in the indentation region and until convergence in maximum strains and maximum stresses are reached (Fig. 4.8).

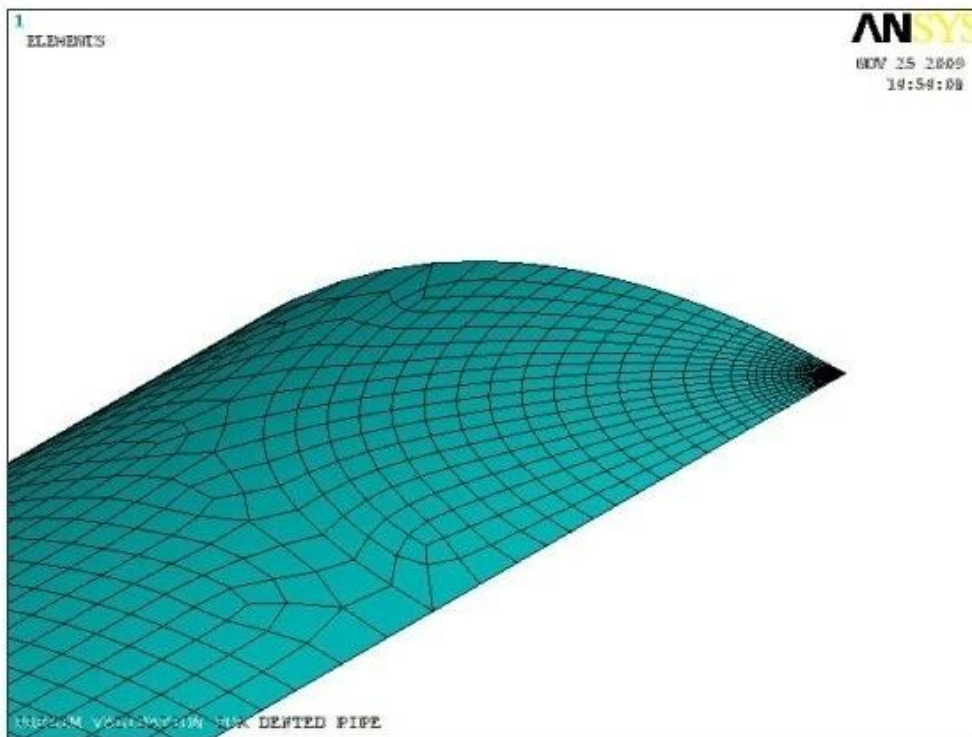
4.5 RESULTS AND DISCUSSION

4.5.1 Strain Profiles

The strain profiles results of the eight FEA material models were compared with that of measured experimental strains in terms of percentage difference. The attention was focused on the strain profiles at the end of indentation phase, end of the first pressurization cycle and end of the eighth pressurization cycle. The results are given in



(a)



(b)

Figure 4.7. Mesh of indentation problem (a) overall (b) finer mesh closer to indenter

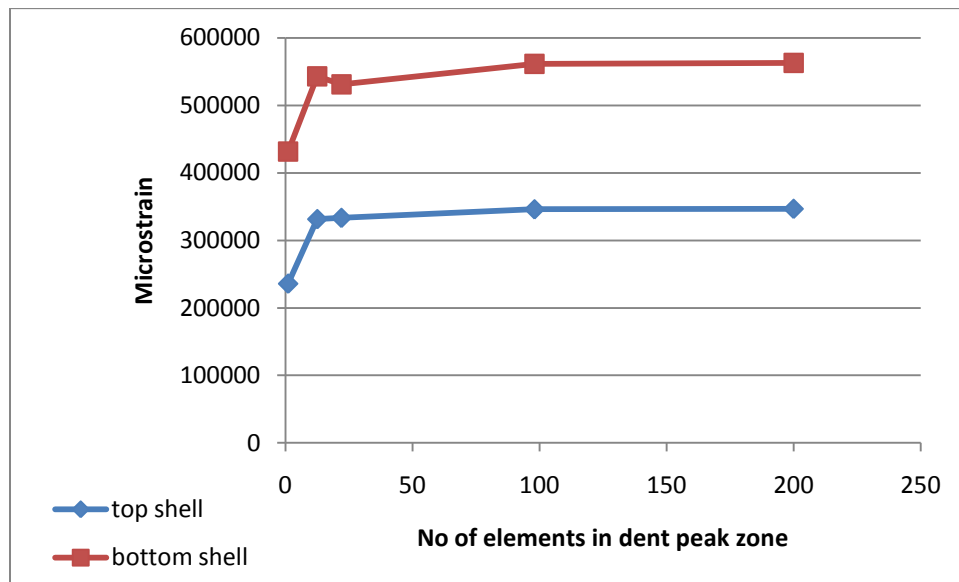


Figure 4.8. Convergence check of Von Mises strains at the dent peak

Table 4.2. The table clearly shows that all FEA models have a certain advantage at point where minimum error for all models is close to zero. However, the models diverge significantly at the high maximum error.

There was no material model that gave the best results in all points as each model has its strengths and weaknesses in terms of approximating the real material behavior. This is because the problem nature creates complicated states of strain-stress cycles in the whole pipe. For example, the indentation area undergoes high compressive plastic strains during indentation; however, the strains in the far region are purely linear elastic. Moreover, the indentation load creates compressive strains in the circumferential direction and longitudinal ones in the axial direction. Then, in the first pressure cycle, the strains are reversed in the circumferential direction from compressive to tensile while they continue to grow in magnitude in the axial direction. Moreover, as the hoop stresses resulting from the end of the first pressure cycles exceed the proportional limit, the whole pipe now experience non-linear material response. Finally, as the subsequent pressure cycles are less than the first one, the strains continue reversal in almost linear elastic manner.

To make the comparison between the different FEA models easier, few trends are observed. During the indentation phase, the different FEA models give close results averaging between 15 and 20%. This is because the strains in the whole pipe are going in one direction whether tensile or compression. This means that non-linear elasticity is not affecting the pipe response; neither does the cyclic stress-strain behavior. From anisotropy point of view, the model based on transverse isotropy properties (Mat_1) gives close results to that of anisotropy models (Mat_6 and Mat_8). Therefore, it can be concluded that anisotropy can be approximated with transverse isotropy properties during

Table 4.2. Percentage errors for each FEA material model in comparison with experimental results

	Axial distance from indenter	Percentage error							
		Mat_1	Mat_2	Mat_3	Mat_4	Mat_5	Mat_6	Mat_7	Mat_8
Circumferential strains		Indentation cycle							
	4	10	11	23	13	22	12	15	12
	6	21	25	33	24	34	25	29	24
	24	19	18	1	12	3	14	18	13
	48	13	11	9	7	2	11	13	10
		1 st pressure cycle							
	4	0	3	11	5	7	2	1	1
	6	17	6	54	35	25	18	6	9
	24	30	32	16	3	14	0	32	0
	48	15	15	21	9	21	8	15	8
		8 th pressure cycle							
	4	16	2	12	6	8	3	4	1
	6	17	10	49	34	26	20	17	15
	24	1	38	15	6	11	3	13	3
	48	10	17	21	12	20	11	1	11
	Axial strains		Indentation cycle						
4		18	18	4	11	9	17	18	16
6		6	10	32	16	26	13	12	15
		1 st pressure cycle							
6		21	12	9	14	4	10	9	9
24		24	24	38	28	6	7	19	7
48		32	31	51	38	6	10	26	10
		8 th pressure cycle							
6		26	11	8	13	4	10	6	9
24		15	24	37	27	7	8	23	8
48		15	33	52	40	8	12	34	12
	Min	0	2	1	3	2	0	1	0
	Max	32	38	54	40	34	25	34	24

indentation stage. It is worth mentioning here that errors during indentation stage are quite high due to the experiment conditions. The pressure inside the pipe increased gradually (due to compressed water as volume of pipe got smaller due to indentation) and it reached 0.5 MPaG at the end of the indentation. In the FEA simulation, pressure was assumed 0 during the indentation stage which would result in differences especially in the far regions where strains are low.

During the pressurization phase, the percentage difference diverges between the different models. This indicates that accuracy of the FEA material model is decisive in the cyclic loading. The models that give the least errors are Mat_6 and Mat_8 averaging between 5 and 10% with slightly better results for Mat_8. These models take account for non-linear elastic behavior, anisotropy as well as cyclic softening for Mat_8. This comparison indicates that Mat_6 and Mat_8 are the best models of the eight considered. The maximum error of these two material models is only 25% whereas in the rest of the models, it exceeds 32% up to 54%.

The strain profiles are further investigated for Mat_6 and Mat_8 by plotting the strain history during the first pressure cycle and eighth pressure cycle and comparing it with the experimental results at different strain gauges. This is to ensure that the material model really reflects the actual pipe behavior time-wise and space-wise. The results are only presented for Mat_8 for clarity of figures as both gave very close values with a slight advantage for Mat_8. Figure 4.9 gives the circumferential strains at different axial location from the indenter as well as at 90 degrees in the transverse direction from the indenter. Figure 4.10 gives the axial strains. Before discussing the results, it shall be

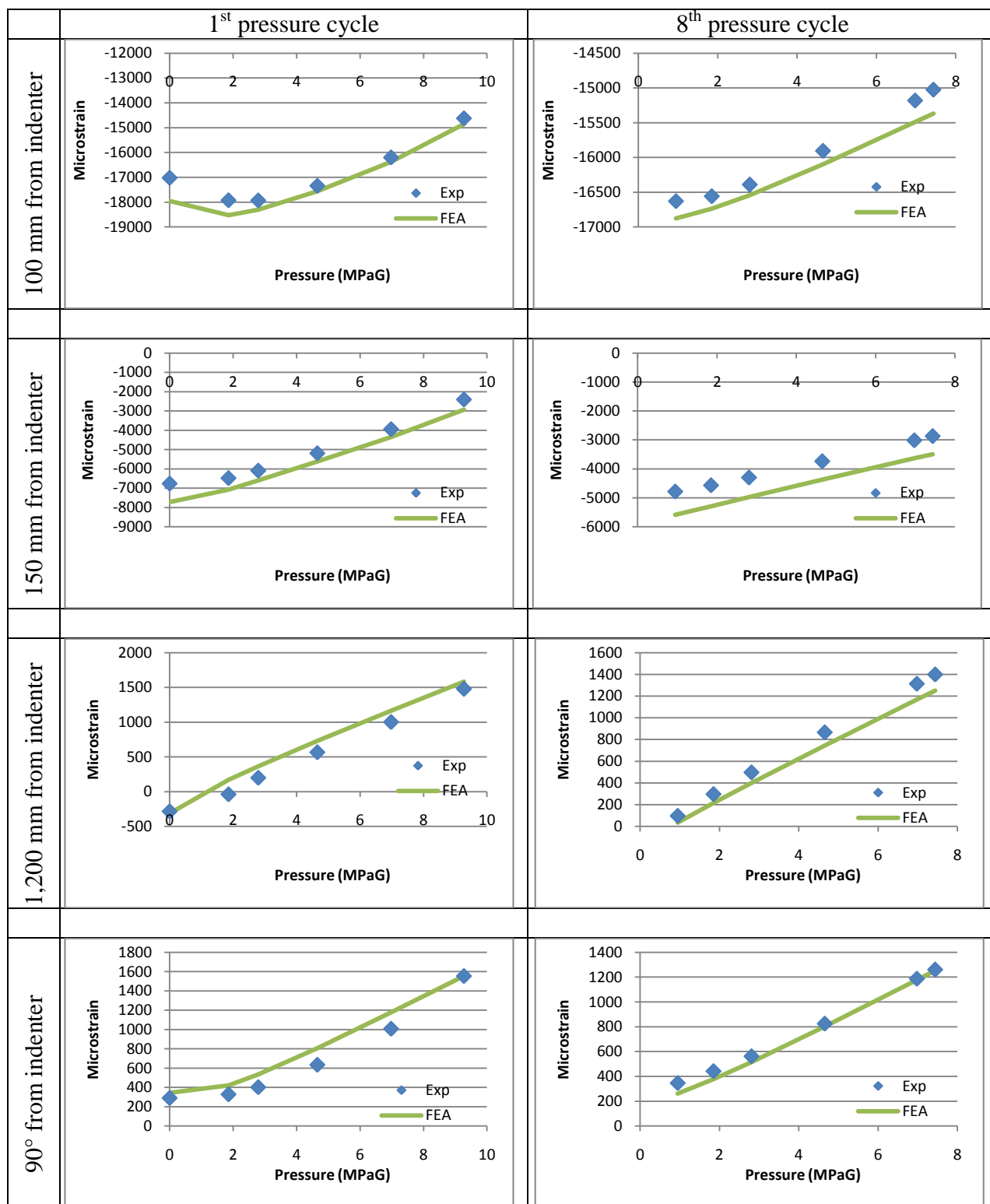


Figure 4.9. Comparison of circumferential strain history between FEA runs and experimental results

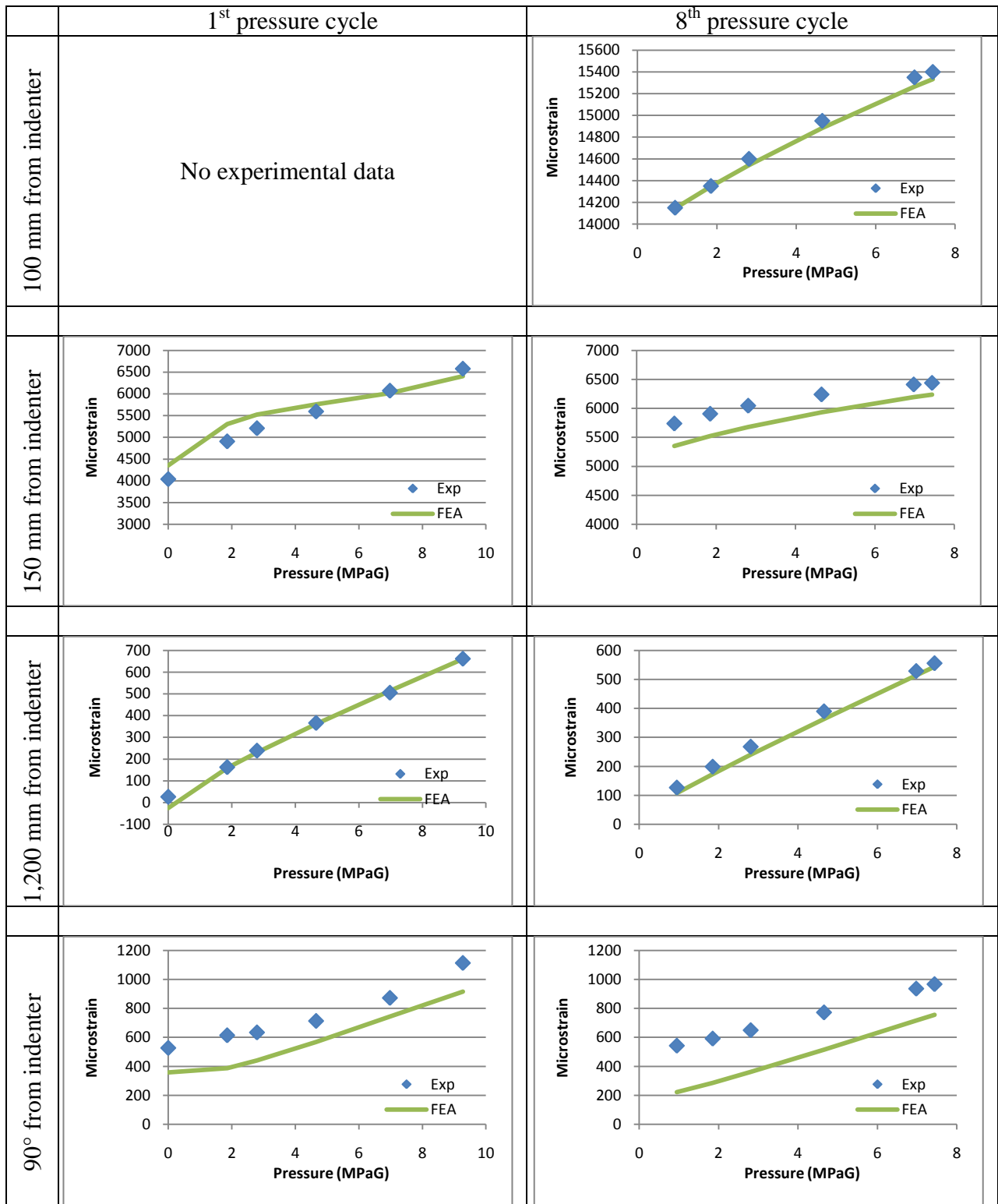


Figure 4.10. Comparison of axial strain history between FEA runs and experimental results

highlighted that strain gauges were also placed at 50 mm axial and transverse failed during the experiment due to high strains.

The strain history results of FEA model (Mat_8) are in very good agreement with the experimental results. The strain trends are also matching between all FEA and experimental for all strain gauge locations. The highest deviation in strain values is observed at 150 mm from axial direction and is attributed due to the level of strain being close to 0.5% which is the transition point into the full plastic region. Another deviation in strain values was found in the axial strains at 90 degrees in transverse direction while the circumferential strains at the same location gave very good results. This could be attributed to change in material properties during plate rolling to form the pipe as this is the center point for bending the plate into the pipe circular direction.

It is also observed that during the first pressure cycle, the strain-pressure profile is non linear because of change of pipe geometry (retain circular cross section after ovalization) and material response. The non-linear response is highest at close to indenter and diminishes far away at 1,200 mm. The strain-pressure profile of the eighth cycle is linear due to elastic shake-down behavior observed in both experimental and FEA results.

In conclusion, both Mat_6 and Mat_8 are proven to successfully duplicate the actual pipe material behavior time-wise (during indentation and pressurization phases) and space-wise (close by and far from indentation). The two models approximate the initial non-linear response by assuming a linear response up to the 0.2% strain, and thus, they reduce the elastic modulus. They both use the Hill's potential to model anisotropy. Mat_8 has the extra advantage of using Chaboche model to simulate the cyclic softening of the material. The effect of anisotropy and non-linear elastic response and is the most

significant on the model accuracy. The effect of cyclic softening is less significant as it gives slightly better results.

4.5.2 Stress-Based Fatigue Analysis

It is shown from the previous section that pressure cycles after the first few ones follow linear response due to elastic shake-down. The elastic stress range of the various FEA models conducted can be used for fatigue analysis to estimate the cycles based on the following Equation (4.8). Due to bi-axial stress condition, the Von Mises stresses at the dent peak are considered. The mean stress effect is including by using Goodman Equation (4.9). The fatigue strength of the material is estimated based on the monotonic true stress-strain curve to be 612 MPa. The material constant b is estimated by Equation (4.10-4.11) to be -0.084. These equations are adopted from Shigley and Mischke (1989)

$$N_f = \frac{1}{2} \left(\frac{\sigma_{ar}}{\sigma_f} \right)^{1/b} \quad (4.8)$$

$$\sigma_{ar} = \frac{\sigma_a}{1 - (\sigma_m / \sigma_f)} \quad (4.9)$$

$$b = -\frac{1}{3} \log \frac{0.9S_{ut}}{S_e} \quad (4.10)$$

$$S_e \approx 0.504S_{ut} \quad (4.11)$$

The fatigue analysis results are summarized in Table 4.3 for all eight FEA material models and compared with the experimental results. Due to the many factors involve in fatigue failure, comparison of the fatigue cycles between FEA and experiment should only be made to the order of magnitude. This was clearly proven by conducting the same experimental set-up twice. The fatigue happened after 6,948 cycles in the first specimen while it took 38,865 cycles in the second specimen.

Once again, Mat_6 and Mat_8 give results within the range of the experimental results indicating that these two material models not only give good approximation not only for the strains, but also does for the stress values. Mat_1 which is the only one assuming isotropic hardening gave very low fatigue life in the order of 1% of the experimental which indicates that this mode of hardening rule shall not be used in dented pipes problem for cyclic pressure loads. Mat_2, Mat_3 and Mat_4 which assume isotropic properties with kinematic hardening rule overestimate the fatigue life by a factor of 2-4. Therefore, using isotropic properties in fatigue life for cyclic loading is not a conservative approach and must be companied by a safety factor of minimum 4 if the anisotropy properties are not available. Mat_5 and Mat_7 which both use the modulus of elasticity same as that of the real material linear proportional limit give reasonable life values less than the experimental ones, and thus, neglecting the initial non-linear elastic response is a conservative approach.

4.5.3 Transferability Tests

To check the material model validity under different loading conditions, both Mat_6 and Mat_8 are implemented in two different indentation specimens. Table 4.4 compares

Table 4.3. Fatigue life calculation for various FEA material models ($N_{\text{exp}} = 38,865$)

FEA No.	σ_{max} (MPa)	σ_{min} (MPa)	σ_a (MPa)	σ_m (MPa)	$N_{\text{calculated}}$	% error
Mat_1	524	197	164	361	85	-100
Mat_2	375	63	156	219	127,231	229
Mat_3	363	92	135	228	337,917	774
Mat_4	387	17	185	202	71,489	85
Mat_5	353	105	124	229	6,485	-83
Mat_6	384	117	133	251	29,727	-23
Mat_7	407	31	188	219	3,289	-91
Mat_8	420	143	138	281	16,260	-58

Table 4.4. Comparison of numerical and experimental fatigue cycles for three different indentation/pressurization loads

Spec#	Indenter diameter	Initial depth	Hydro pressure	Press range	N (exp)	N (Mat_6)	N (Mat_8)
	(mm)	(% OD)	(SMYS)	(SMYS)			
1	50	7.50%	100%	10-80%	38,685	29,727	16,260
2	100	10%	100%	10-80%	16,234	47,995	37,573
3	100	10%	80%	10-80%	3,359	941	1,193

the calculated fatigue cycles to failure with the experimental results where specimen 1 refers to the one already studied in detail and specimens 2 and 3 are new analysis. The pipe geometry and boundary conditions are the same while the indenter diameter and indentation depth are different. The table shows that the two models successfully predicted the experimental life order of magnitude as it is not possible to predict the exact value since fatigue failure is dependent on many factors which are clear from the difference between the results of the two identical specimens. Mat_8 gave closer results to experimental in all 3 specimens although from order of magnitude the difference can be neglected. Mat_8 predicted lower fatigue cycles than Mat_6 in specimen 1 while higher fatigue cycles in specimen 2 and 3. This is because the strain levels are higher in specimen 1 which indicates that Mat_8 which has the feature of cyclic behavior can simulate better the effect of maximum strain values during indentation on the fatigue life.

4.6 SUMMARY

The effect of material model using FEA on the integrity assessment of dented pipes under static and cyclic pressure loading was investigated. The actual pipe material properties exhibit special features of non-linear elasticity, anisotropy and cyclic softening, and therefore, needs advanced material modeling techniques. Eight different material models were presented and evaluated in this paper, and they were compared to experimental results in terms of strain values as well as fatigue cycles to failure.

The results of this research showed that a combined material model simulating all special features of non-linear elasticity, anisotropy, and cyclic softening gave very close representation of experimental data. Comparing the different material models, the results

were close at the indentation phase, but they diverged at the cyclic pressurization phase. Moreover, it was found that anisotropy has the most impact on the results where as cyclic softening had the least impact.

The material model plays decisive rule on the accuracy of the FEA results especially in the case of cyclic pressure loading. Therefore, detailed material properties are needed to conduct appropriate integrity assessment of dented pipes under such cyclic conditions to calculate the expected cycles to failure. If those material properties are not available, appropriate safety factor must be included. It is intended to utilize the material model developed and validated in this paper for future parametric study of dent geometry and material properties to find a general integrity assessment approach.

CHAPTER 5

STATISTICAL ANALYSIS OF MECHANICAL DAMAGE INSPECTION DATA

5.1 INTRODUCTION

Assessing the risk that a certain pipeline poses to the surrounding community is of primary interest to the Pipeline Operators and in some cases mandatory by Government Regulations (Lyons et al., 2008). The standard definition of risk is the product of probability of failure of pipeline times the consequences of failure. Determination of failure rate due to mechanical damage is of special challenge as mechanical damage occurrence does not depend on the pipeline age and its rate cannot be lowered by regular maintenance. This is in contrast with failure due to corrosion where corrosion rate can be anticipated and regular maintenance can reduce the probability of failure. (Caleyo et al., 2006) Therefore, utilization of statistical analysis of real-life damage data has been used extensively to improve the accuracy of the prediction of failure of mechanical damage. Accordingly, Government Regulations require Pipeline Operators to report all failure incidents with enough data to characterize the failure. Such data include pipeline geometry, material properties, damage dimensions, and type of failure (small leak, large leak, or rupture). Examples of those are the reports generated by the US Department of Transportation (Kiefner et al., 2000), the United Kingdom Onshore Pipeline Operators

Association (Arunakumar, 2007), the European Gas Pipeline Incident Data Group (EGIG, 1999), and Saudi Aramco (Advantica, 2004).

The general approach to determine the probability of failure is to conduct statistical analysis of the real-life input data to generate their distribution. The input data with their appropriate distribution is then evaluated using structural integrity assessment model whether theoretical, or semi-empirical to determine failure vs. non-failure cases. Accordingly, the distribution of failure cases is used to define the probability of failure. If the mechanical damage rate is available, it is multiplied by the probability of failure to determine the failure frequency of pipeline system(s).

Fuglem et al. (2001) developed a design check tool based on probabilistic analysis that correlates the probability of failure of mechanical damage to the pipeline design parameters (e.g. diameter, wall thickness, material grade, pressure and location class) as well as the preventive measures against mechanical damage (e.g. depth of burial, excavation procedures, and frequency of patrol surveillance). Although Monte Carlo simulation was used to generate the analysis input parameters, the results of probability of failures were validated with incident data of DOT and EGIG.

Wolvert et al. (2004) indicated the importance of using pipeline surveys in generating the necessary input data for probabilistic assessment of pipeline resistance to third party damage. They tested two statistical distributions of excavator masses one based on sales data and the other based on actual survey of excavation work around pipelines. They concluded that the high sensitivity of probability of failure to the input data, in this case the excavator mass, strongly supports the use of real-life statistical distribution to produce reliable results.

Rosenfeld et al. (2006) have presented a case study where the probabilistic analysis led to optimization of maintenance work by elimination of excavation of minor mechanical damage due to low probability of failure. Caleyó et al. (2006) has proposed a methodology of how to process failure data from different pipeline systems and when it is appropriate to merge data to reduce uncertainties. Different systems are defined based on different pipeline operator, different service (gas, liquid), and different usage (transmission, gathering). Accordingly, the authors were able to estimate the failure rate of a pipeline population based on historical failure data merged from multiple pipeline systems.

Seevam et al. (2008) conducted a study to find the effect of the structural integrity assessment model on probability of failure and they tested to models for this purpose. In both models, the input parameters of damage dimensions were based on probability distributions obtained from UKOPA (2007) database of pipeline incident. This database was also utilized by Lyons et al. (2008) to predict the pipeline failure frequency due to external interference.

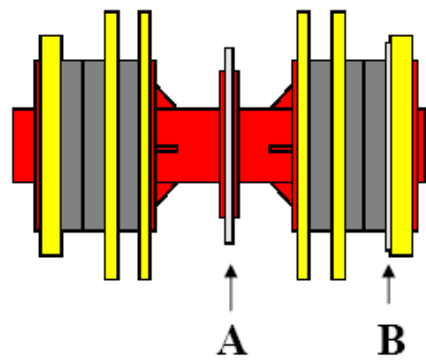
In this chapter, comprehensive statistical analysis is conducted on mechanical damage data of plain dents for a major oil and local company and is benchmarked to data collected from external companies. There are two objectives from this analysis. The first objective is to investigate if the statistical distribution of a local company is similar or different from external companies. Accordingly, differences are explained in terms of comparison of design, installation and operation conditions. The second one is to find statistical distribution of dent parameters such as geometry of dented pipe, material of

dented pipe, and geometry of the dent to be used in failure probabilistic analysis according to the approach outline later in Chapter 6.

5.2 DATA SOURCES

The data of the local company is collected from In-Line-Inspection (ILI) geometry caliper runs conducted for 9 different pipelines for the period between 2005 and 2009. The data consists of a total of 134 dents whose details are given in Table A.1 of Appendix A. It is worth highlighting that it is not a standard practice to run Caliper ILI for pipelines of this local company. It is only required to pass a dummy mechanical caliper which is illustrated in Fig. 5.1 before the magnetic flux ILI run to ensure it will have smooth passage. If the dummy caliper shows indication of change of geometry of the pipe inside diameter of more than 2%, Caliper ILI will be run. In 2008, only 4% of the ILI inspected pipelines needed Caliper ILI.

The external data are taken from a report by Semiga (December 2007) who collected data of 161 defects of mechanical damage from 5 pipeline operators and 1 consulting company. The total number of pipelines in the survey was 80. Out of the 161 defects, 39 were plain dents, 9 were dents in weld areas, 58 were dents with gouges and 65 were dents with corrosion. The questionnaire sheet demands a lot of details of the pipeline and the mechanical damage, and therefore, the responses varied between basic and detailed. Some data are based on ILI tools while others are collected from field digging. A representative sample of the survey data is given in Table A.2 of Appendix A.



Dimensions:
A: 940 mm
B: 1091 mm

A			<p>Observations: Bend Plate: Slight bent back in two locations.</p>
B			<p>Observations: Gauge Plate: Bent forward in one location with one heavy pinch mark and one slight pinch mark. Smallest Dia. = 1072 mm</p>

Wear:	Minimal concentric wear in both of the sealing & guiding discs.
Debris:	None on the product but there is bits of pcs. of guiding discs.

NOTE: These results need further assessments.

Figure 5.1. Illustration of dummy caliper run

5.3 METHOD OF STATISTICAL ANALYSIS

The data are analyzed with the help of the software STATGRAPHICS Centurion XVI (Statgraphics, 2010). The software has many applications for data analysis amongst which are comparing two independent samples, fitting sample data, conducting regression analysis. The applications are supported by the appropriate statistical test such as null hypothesis test to compare two samples, Kolmogorov-Smirnov test goodness of fitted distribution. Moreover, it allows several graphical presentations of data including frequency histogram, density traces, fitted probability distribution function as well as cumulative distribution function. The software uses spreadsheet to input the raw data which is compatible with Excel spreadsheet.

Statistical comparison between two independent samples of the local company and external companies is conducted for a number of variables related to pipe mechanical damage. The objective is to find the statistical parameters for each group (minimum, maximum, mean, standard deviation and coefficient of variance) and to determine if the parameters are significantly different between the two groups based on statistical tests. The variables under study include: pipe diameter-to-thickness ratio (D/t), dent percent ($d/D\%$), dent sharpness (l/D), pipe material grade (SMYS), and pipe age.

Furthermore, distribution fitting of the sample data for each group is conducted. As the fit distributions available are wide, the following logic is used to make the data analysis consistent. First, the distribution functions are limited to the common ones that are available in ANSYS PDA Module (2007) which include: normal, lognormal, inverse Gaussian, Weibull, triangular, and uniform. Second, the same distribution type is used for the same variable, e.g. dented pipe age, for rational comparison between the local

company data and external companies' data. Third, the fitted distribution must pass the appropriate statistical goodness of fit test.

5.3.1 Mathematical Definitions of General Statistics

There are two basic measures to characterize a sample of data: center point and dispersion. For each measure, several statistical parameters exist. In this chapter, the average or arithmetic mean is used to characterize the center point of the sample data. Standard deviation and coefficient of variance are used to characterize the dispersion of the sample data. (Hines and Montgomery, 1990)

The arithmetic mean is defined as:

$$\mu = \frac{\sum_{i=1}^n x_i}{n} \quad (5.1)$$

The variance which measures the average square of deviation around the sample mean is defined as:

$$S = \frac{\sum_{i=1}^n (x_i - \mu)^2}{n-1} \quad (5.2)$$

The standard deviation is the square root of the variance and defined as:

$$\sigma = \sqrt{S} = \sqrt{\frac{\sum_{i=1}^n (x_i - \mu)^2}{n-1}} \quad (5.3)$$

The coefficient of variance is the percentage ratio of the variance to the mean:

$$COV = \frac{S}{\mu} \times 100\% \quad (5.4)$$

5.3.2 Comparison of Two Samples

The direct number to number comparison between two sample parameters might imply that the two samples are different. However, the difference might be attributed to the limited size of the sample, while a large sample population would yield that the two samples are equivalent. Therefore, statistical tests have been developed to test whether the parameters of two samples are statistically different. The basic approach in those tests is to assume null hypothesis that the parameter of the two samples are the same and test if this hypothesis is true at a desired significance level (Hines and Montgomery, 1990). In this chapter, the two samples are compared in terms of the standard deviation, mean, and distribution.

5.3.2.1 Comparison of Standard Deviation

The comparison is conducted by conducting an F-test on the ratio of variance between the two samples. The null hypothesis assumes that the ratio is unity, and thus, there is not statistically significance difference between the standard deviation of the two samples. The alternative hypothesis is that the ratio does not equal unity, and thus, there is a statistically significance difference between the two samples. The mathematical definition of the test is as follows: (Hines and Montgomery, 1990)

Ratio between the variances of the two samples:

$$\omega = \frac{s_1}{s_2} \quad (5.5)$$

The null hypothesis is defined as:

$$\omega = \omega_0 = 1 \quad (5.6)$$

The alternative hypothesis is defined as:

$$\omega \neq 1 \quad (5.7)$$

The F-test is defined as:

$$F = \frac{\omega}{\omega_0} = \frac{s_1/s_2}{1} = \frac{s_1}{s_2} \quad (5.8)$$

The P-value is then calculated from F tables (Hines and Montgomery, 1990) for degrees of freedom of n_1-1 and n_2-1 . The P-value is the probability of rejecting the null hypothesis while it is true. If the calculated P-value is greater than the specified significance level, the null hypothesis cannot be rejected and the standard deviations of the two samples are not significantly different. Otherwise, if the P-value is less than the

specified significance level, the two samples have significantly different values of standard deviation. The significance level of the test α is usually defined at 0.01, 0.05, and 0.1. A significance level of 0.05 is assumed, which is very common, means that the probability of rejecting the null hypothesis if it is true must be 0.05 or less so that the two samples can be considered significantly different.

Another method to determine if the difference between the standard deviation of two samples is statistically significant is by establishing the confidence interval of the variance ratio as follows:

$$\left[\frac{S_1}{S_2} \frac{1}{F_{\alpha/2, n_1-1, n_2-1}}, \frac{S_1}{S_2} F_{\alpha/2, n_2-1, n_1-1} \right] \quad (5.9)$$

If the confidence interval contains the unity ratio, the standard deviations of the two samples are not significantly different at the significance level α . Otherwise, if the confidence interval does not contain the unity ratio, the standard deviations of the two samples are significantly different.

5.3.2.2 Comparison of Means

The comparison is conducted by conducting a t-test on the difference between the two samples. The null hypothesis assumes that the difference is zero, and thus, there is not statistically significance difference between the standard deviation of the two samples. The alternative hypothesis is that the ratio does not equal to zero, and thus, there is a

statistically significance difference between the two samples. The mathematical definition of the test is as follows: (Hines and Montgomery, 1990)

Difference between the mean of the two samples:

$$\Delta = \mu_1 - \mu_2 \quad (5.10)$$

The null hypothesis is defined as:

$$\Delta = \Delta_0 = 0 \quad (5.11)$$

The alternative hypothesis is defined as:

$$\Delta \neq 0 \quad (5.12)$$

The t-test is defined as:

$$t = \frac{\Delta - \Delta_0}{\sqrt{\frac{s_1 + s_2}{n_1 + n_2}}} = \frac{(\mu_1 - \mu_2) - 0}{\sqrt{\frac{s_1 + s_2}{n_1 + n_2}}} = \frac{(\mu_1 - \mu_2)}{\sqrt{\frac{s_1 + s_2}{n_1 + n_2}}} \quad (5.13)$$

Degrees of freedom of the t-test is defined by v:

$$\frac{1}{v} = \frac{c^2}{n_1 - 1} + \frac{(1 - c)^2}{n_2 - 1} \quad (5.14)$$

Where:

$$c = \frac{S_1/n_1}{S_1/n_1 + S_2/n_2} \quad (5.15)$$

If the F-test from the previous section shows that there is no significance difference between the standard deviation of the two samples, the variance is assumed equal and the t-test is defined as:

$$\hat{t} = \frac{(\mu_1 - \mu_2)}{S_P \times \sqrt{\frac{1}{n_1} + \frac{1}{n_2}}} \quad (5.16)$$

Where:

$$S_P = \sqrt{\frac{(n_1 - 1)S_1 + (n_2 - 1)S_2}{n_1 + n_2 - 2}} \quad (5.17)$$

The P-value is then calculated from t-distribution tables (Hines and Montgomery, 1990) for degrees of freedom of v (Eq. 5.14) for not equal variance (Eq. 5.13) and degrees of freedom $n_1 + n_2 - 2$ for equal variance (Eq. 5.16). The P-value is the probability of rejecting the null hypothesis while it is true. If the calculated P-value is greater than the specified significance level, the null hypothesis cannot be rejected and the standard deviations of the two samples are not significantly different. Otherwise, if the P-value is less than the specified significance level, the two samples have significantly different values of sample mean. The significance level of the test α is usually defined at 0.01, 0.05, and 0.1. A significance level of 0.05 is assumed, which is very common, means that the probability of rejecting the null hypothesis if it is true must be 0.05 or less so that the two samples can be considered significantly different.

Another method to determine if the difference between the means of two samples is statistically significant is by establishing the confidence interval of the difference as follows:

For not equal variance:

$$(\mu_1 - \mu_2) \pm t_{\alpha/2, v} \times \sqrt{\frac{S_1}{n_1} + \frac{S_2}{n_2}} \quad (5.18)$$

For equal variance

$$(\mu_1 - \mu_2) \pm t_{\alpha/2, n_1+n_2-2} \times S_p \times \sqrt{\frac{1}{n_1} + \frac{1}{n_2}} \quad (5.19)$$

If the confidence interval contains zero, the means of the two samples are not significantly different at the significance level α . Otherwise, if the confidence interval does not contain zero, the means of the two samples are significantly different.

5.3.3 Comparison of Fitted Distribution

In this chapter, three types of distribution will be fit for the two sample data, local and external, for each of the related damage variables. These three distributions are: the normal distribution, the lognormal distribution, and the Weibull distribution. Those distributions were selected as they are common and for consistency of comparison. Moreover, the lognormal and Weibull distributions can only take positive value which is in line with the physics of the problem.

5.3.3.1 Mathematical Formulation of Fitted Distribution

If x defines the random quantity of any selected dent feature, the probability density functions of the selected distributions are given below (Hines and Montgomery, 1990):

Normal

$$f(x) = (\sigma\sqrt{2\pi})^{-1} \exp\left(-\frac{1}{2}\left(\frac{x-\mu}{\sigma}\right)^2\right) \quad (5.20)$$

Lognormal

$$f(x) = (x\sigma_l\sqrt{2\pi})^{-1} \exp\left(-\frac{1}{2}\left(\frac{\ln x - \mu_l}{\sigma_l}\right)^2\right) \quad x > 0 \quad (5.21)$$

Weibull

$$f(x) = \frac{\beta}{\delta} \left(\frac{x-\gamma}{\delta}\right)^{\beta-1} \exp\left(-\left(\frac{x-\gamma}{\delta}\right)^\beta\right) \quad x \geq \gamma \quad (5.22)$$

5.3.3.2 Kolmogorov-Smirnov (K-S) Test for Fitted Distribution and Comparison of Two Distribution

To test that the fitted distribution of the data is appropriate or not, graphical evaluation of the fitted curve versus the data points should give a qualitative assessment hint. However, statistical tests are also available so that the assessment is based on quantitative measures. The statistical tests are either based on the probability distribution function (PDF) or the cumulative distribution function. In this chapter, the Kolmogorov-

Smirnov test is adopted due to its versatility as it can be used for any continuous distribution. Moreover, the test can be assessed due to the availability of the critical values at different significant levels α (Kececioglu, 2002). Accordingly, the P-value can be also calculated by the tables of formulas. The calculated P-value must be higher than the desired significance level α so that we can consider that the theoretical distribution is a good fit of the sample data. Otherwise, if the P-value is less than the desired significance level α , the hypothesis that the fitted distribution is a good fit of the sample data is rejected.

The test finds the maximum distance between the empirical step distribution function, defined by the data points, and the assumed theoretical distribution function, defined by the distribution function parameters such as the mean and standard deviation. The test is illustrated graphically in Fig. 5.2 and mathematically by the following equations (D'Agostino and Stephens, 1986):

The theoretical cumulative distribution function F_0 is defined as

$$F_0(X_i) = CDF(X_i) = \text{probability of } (X \leq X_i) \quad (5.23)$$

The empirical cumulative distribution function F_n which is a step function is defined as

$$F_n(X_i) = \text{probability of } (X \leq X_i) = \frac{i}{n}, i = 1, 2, \dots, n \quad (5.24)$$

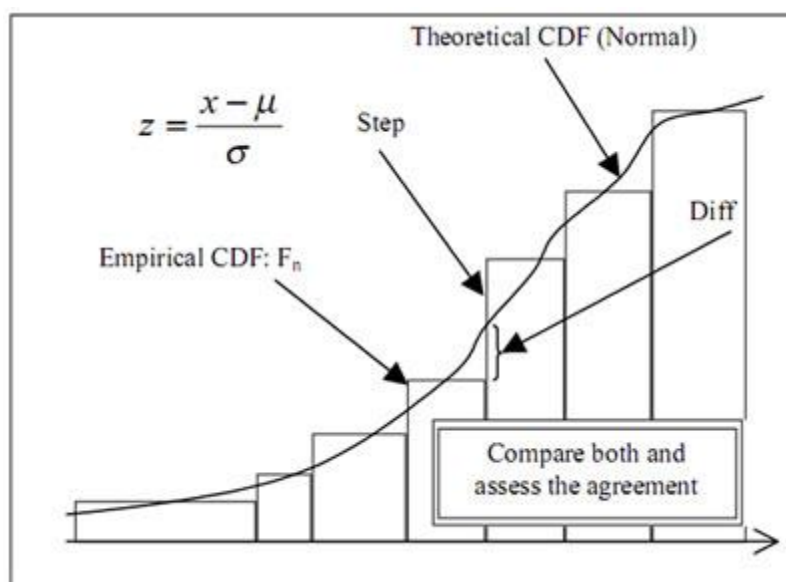


Figure 5.2. Graphical illustration for Kolmogorov-Smirnov distance test for goodness of fit

The maximum distance of the empirical distribution function above the fitted function is defined as:

$$KSD^+ = \max\{F_n(X_i) - F_0(X_i)\}, i = 1, 2, \dots, n - 1 \quad (5.25)$$

The maximum distance of the empirical distribution function below the fitted function is defined as:

$$KSD^- = \max\{F_0(X_i) - F_n(X_{i-1})\}, i = 2, 3, \dots, n \quad (5.26)$$

The overall maximum distance between the empirical function and the fitted function is defined as:

$$KSD = \max(KSD^+, KSD^-) \quad (5.27)$$

The KSD is then compared to the critical values at the desired significance level α .

Alternatively, the P-value can be calculated according to the following formulas:

$$\text{Let } \theta = KSD \times \sqrt{n} \quad (5.28)$$

$$P - \text{value} = \begin{cases} 1 & \text{if } \theta < 0.22 \\ 1 - \frac{\sqrt{2\pi}}{\theta} \exp\left(\frac{-\pi^2}{8\theta^2}\right) & 0.22 \leq \theta \leq 0.80 \\ 2e^{-2\theta^2} + e^{-8\theta^2} - e^{-18\theta^2} & 0.80 < \theta \leq 3.15 \\ 0 & \text{if } \theta > 3.15 \end{cases} \quad (5.29)$$

The same test can also be used to evaluate if the distribution of two sample data is significantly different. In this case, the maximum distance between the empirical distributions of the two samples is calculated:

$$KSD = \max\{F_1(X) - F_2(X)\}, X_{min} \leq X \leq X_{max} \quad (5.30)$$

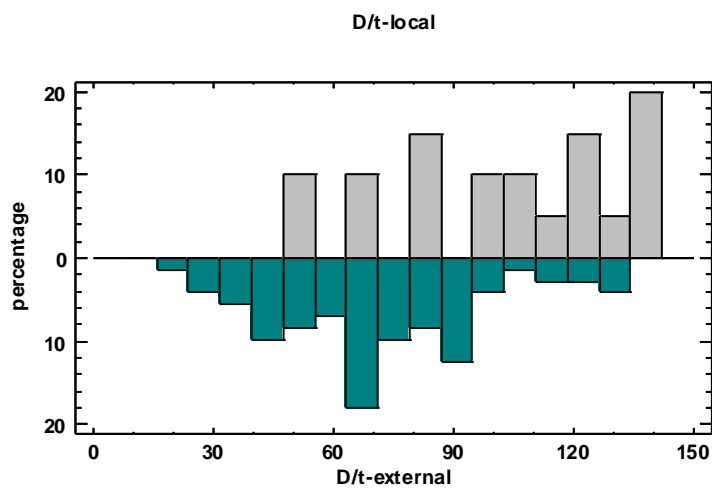
The K-S statistic is defined as

$$K - S = KSD \times \sqrt{\frac{n_1 n_2}{n_1 + n_2}} \quad (5.31)$$

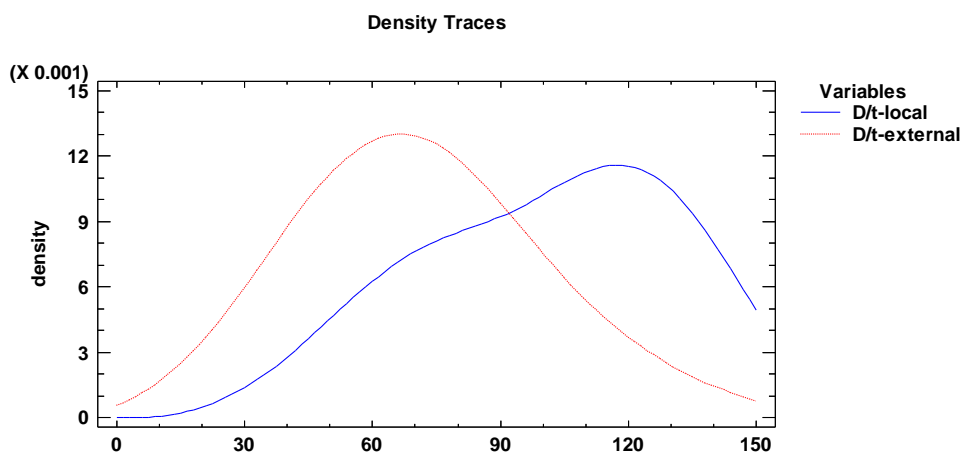
The P-value can be calculated by Eq. (5.29) and letting θ equals the K-S statistic. If the P-value is greater than the specified significance level α , the two samples are considered to come from the same population distribution. Otherwise, if the P-value is less than the significance level α , the two samples are considered to come from statistically different distributions.

5.4 RESULTS AND DISCUSSION

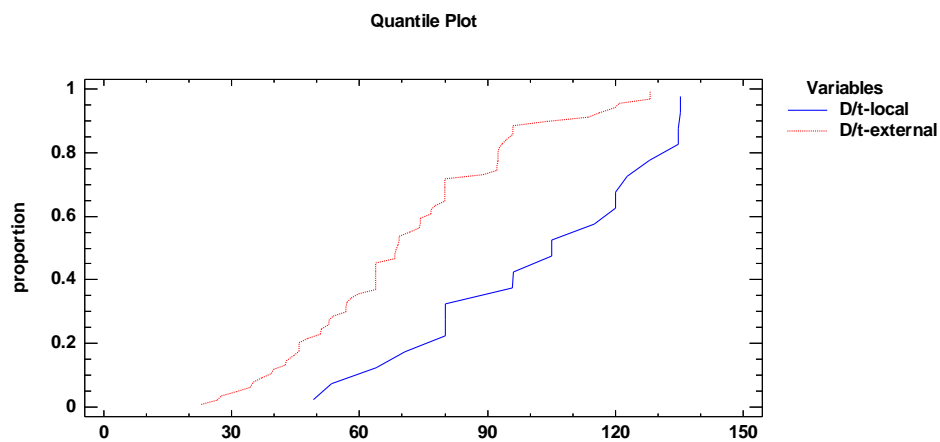
Figure 5.3 gives graphical comparison between the two samples of D/t of local vs. external companies in terms of frequency histogram, density traces, and quantile plot. The frequency histogram and the density traces show that the local company has distribution with higher D/t. The local company has the distribution skewed towards the high D/t of 110 to 140 while the external companies have distribution close to normal and centered on D/t of 60-80. The quantile plot illustrates that there is a significant difference



(a)



(b)



(c)

Figure 5.3 Comparison of two samples of D/t (local vs. external)
(a) frequency histogram (b) density traces (c) quantile plot

between the two distributions as the distance between them is significant. For quantitative assessment, table 5.1 gives the statistics of the comparison of the two samples of D/t as well as the other parameters under consideration. For D/t, the mean of the local company is 101.2 while the mean of external companies is only 71.0. The statistical test of difference of means indicates that there is a significant difference between the two means as the P-value is almost zero. For the standard deviation, the values are close (28.5 for local vs. 25.9 for external) and they can be assumed equal as the ratio test cannot reject the null hypothesis for the very high P-value (0.548). The K-S test illustrates that there is a significant difference between the distributions of the two samples as the P-value is almost zero.

The higher mean of D/t of the local company sample is a reflection of the total population of pipeline of the local company as they are mainly transporting large volumes of crude oil at relatively low pressure. Accordingly, the local company had more frequently extended the ranges of international pipeline specifications and standards to cover its special needs of large diameter pipelines of 1270 mm and above.

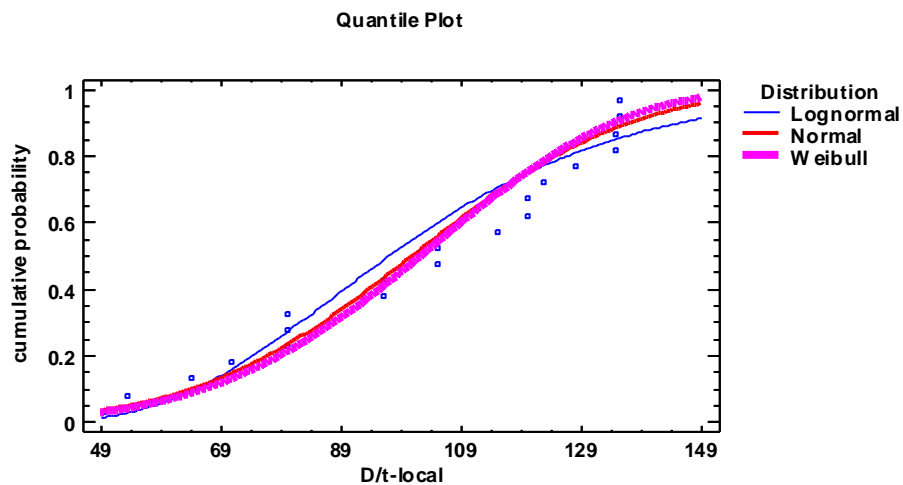
The distribution fitting of D/t data is given graphically in Fig. 5.4 in terms of the cumulative probability of the raw data as well three distribution functions: normal, lognormal, and Weibull. The graph suggests that the Weibull distribution is a good candidate to represent both the local and external data which is supported by the KS test parameters in Table 5.2 due to very high P-values. The table also gives numeric values of the shape and scale parameters for both samples.

The graphical comparison between the two samples of dent depth ($d/D\%$) is illustrated in Fig. 5.5. The histogram and density traces show that most of its dents are of

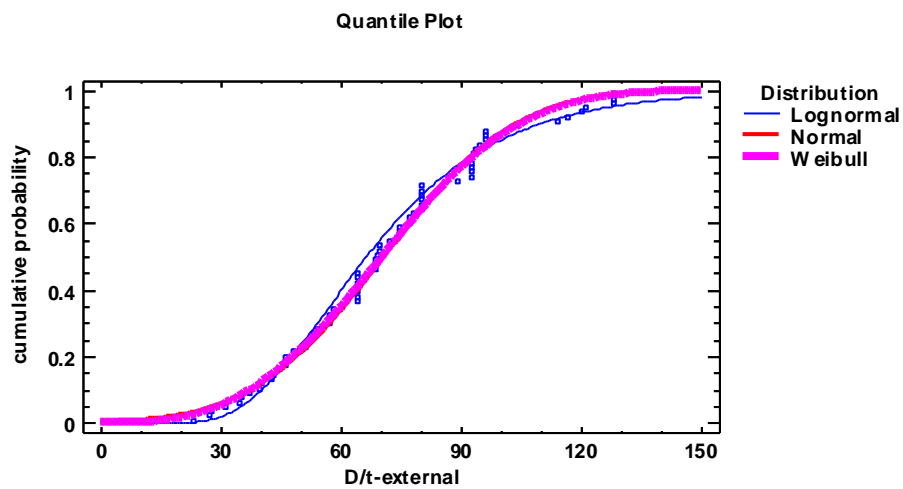
Table 5.1. Compare two samples of mechanical damage data (local vs. external)

		D/t	d/D%	l/d	SMYS	Age
General statistics (local/external)	n	20/72	127/78	95/68	9/51	9/25
	min	49.3/23.0	2.0/0.1	25/2.5	227.7/172.5	17/1.0
	max	135.2/128.1	8.5/9.4	236/91.2	414.0/448.5	55/75
	μ	101.2/71.0	3.7/3.6	124/19.2	349.6/332.2	36.2/39.6
	σ	28.5/25.9	1.2/2.1	47.2/19.2	70.1/72.8	10.6/17.8
	COV (%)	28.1/36.4	32.4/59.6	37.9/72.9	20.1/21.9	29.1/44.9
Ratio of standard deviation -null hypothesis test	CI	0.629, 2.725	0.204, 0.457	7.238, 17.68	0.377, 3.530	0.127, 1.392
	ν_1, ν_2	19, 71	126, 77	94, 67	8, 50	8, 24
	F-value	1.211	0.308	11.41	0.928	0.353
	P-value	0.548	4.469E-9	0.0	0.995	0.130
Difference of means- null hypothesis test	CI	17.0, 43.5	-0.44, 0.60*	93.8, 117*	-35.0, 69.9	-16.3, 9.5
	ν	90	108	125	85	31
	t-value	4.53	0.313	18.847	0.666	0.540
	P-value	1.804E-5	0.755	0.0	0.508	0.593
Difference of distributions- KS test	KSD	0.522	0.357	0.907	0.562	0.378
	K-S	2.07	2.48	5.71	1.55	0.972
	P-value	3.92E-4	8.73E-6	0.0	0.0159	0.303

* Not assuming equal variance



(a)

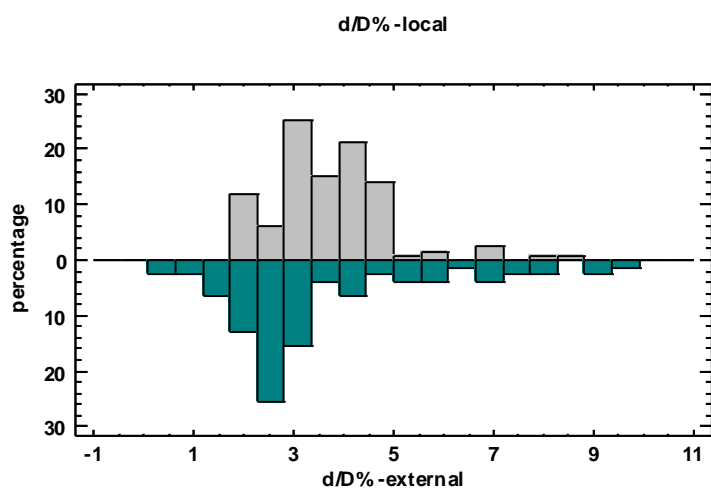


(b)

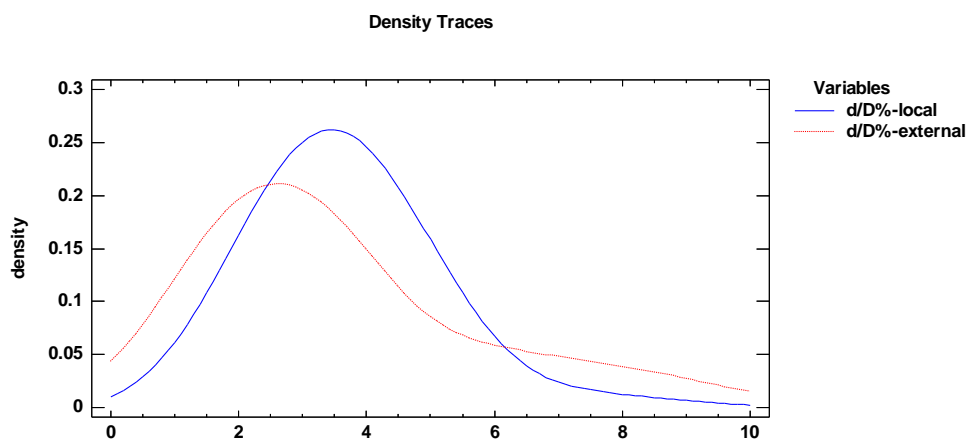
Figure 5.4 Cumulative probability of sample data and fitted distribution for D/t ratio
(a) local company (b) external companies

Table 5.2 Types and parameters of statistical distributions

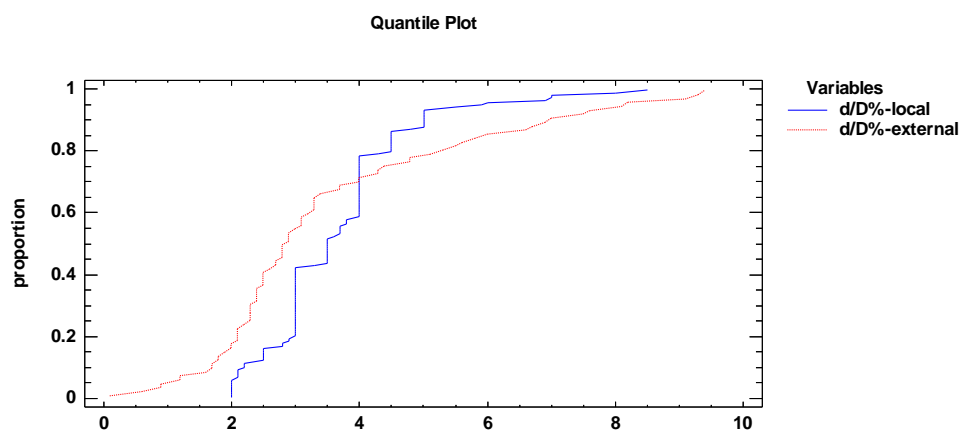
Variable	Distribution type	Distribution Parameters		KS Test Parameters	
		Local company	External companies	Local company	External companies
pipe D/t ratio	Weibull	$\beta=4.384$ $\delta=111.57$	$\beta=2.999$ $\delta=79.58$	KSD=0.1475 P=0.7772	KSD=0.0843 P=0.6860
dent depth d/D (%)	Log-normal	$\mu_1=3.654$ $\sigma_1=1.136$	$\mu_1=3.745$ $\sigma_1=2.882$	KSD=0.1158 P=0.0663	KSD=0.1275 P=0.1584
dent sharpness l/d	Weibull	$\beta=2.907$ $\delta=139.53$	$\beta=1.561$ $\delta=21.55$	KSD=0.0681 P=0.7704	KSD=0.1246 P=0.2418
pipe material SMYS	Weibull	$\beta=7.164$ $\delta=375.47$	$\beta=5.767$ $\delta=379.00$ $\gamma=-17.93$	KSD=0.2922 P=0.4324	KSD=0.2273 P=0.0103
dented pipe age	Weibull	$\beta=4.018$ $\delta=39.91$	$\beta=2.234$ $\delta=44.02$	KSD=0.2178 P=0.7866	KSD=0.1307 P=0.7862



(a)



(b)



(c)

Figure 5.5 Comparison of two samples of $d/D\%$ (local vs. external)
(a) frequency histogram (b) density traces (c) quantile plot

shallow type. The quantile plot shows that 62% of the dents of the local company and 70% of the dents of the external companies have depth less than 4% of the diameter. Table 5.1 indicates the means of the samples are very close (3.7% for local and 3.6% for external) and that this small difference is not statistically significant as the confidence interval of the difference $[-0.44, 0.60]$ contains the zero. However, there is a statistical significance difference between the two standard deviations as the F-test of the null hypothesis gives P-value almost zero. The external companies have higher dispersion in the data which is clear from the higher standard deviation value and higher coefficient of variation. Moreover, the distribution of the two samples is different according to the K-S test. The distribution fitting of $d/D\%$ data is given graphically in Fig. 5.6. The graph suggests that the lognormal distribution is a good candidate to represent both the local and external data which is supported by the KS test parameters in Table 5.2.

The fact that the center point of dent percent data is similar for two different sets of samples indicates that it is representative of the pipeline populations. Therefore, when selecting parameter ranges for characterization of pipeline dent, a single dent percent interval centered on this mean would serve majority of pipelines in the two sets under study. This optimization based on the statistical analysis will reduce the characterization cost.

The graphical comparison of the dent sharpness (l/d) shows that there is a significant difference between the local company and external companies (Fig. 5.7). The dents of the local company have smoother profiles as density traces show they have close to normal distribution centered on a ratio of 130 while the external companies have a distribution of significant skew towards very sharp dents. The quantile plot indicates that about 80% of

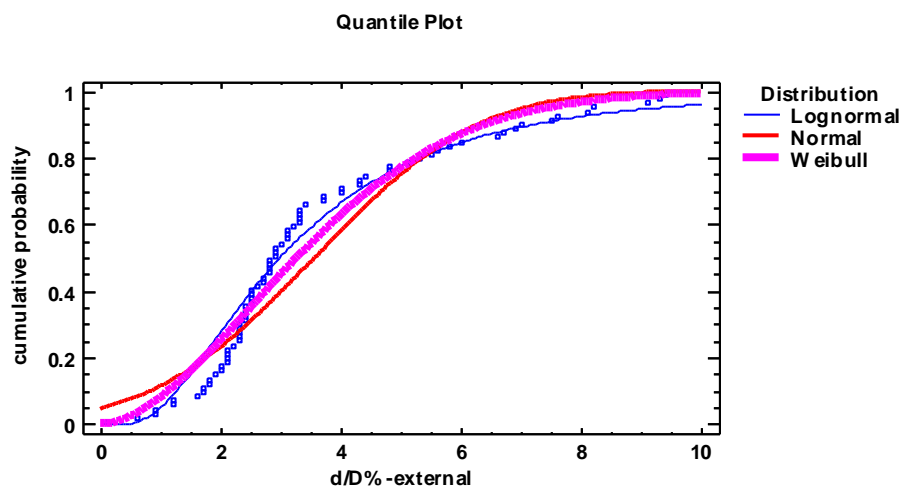
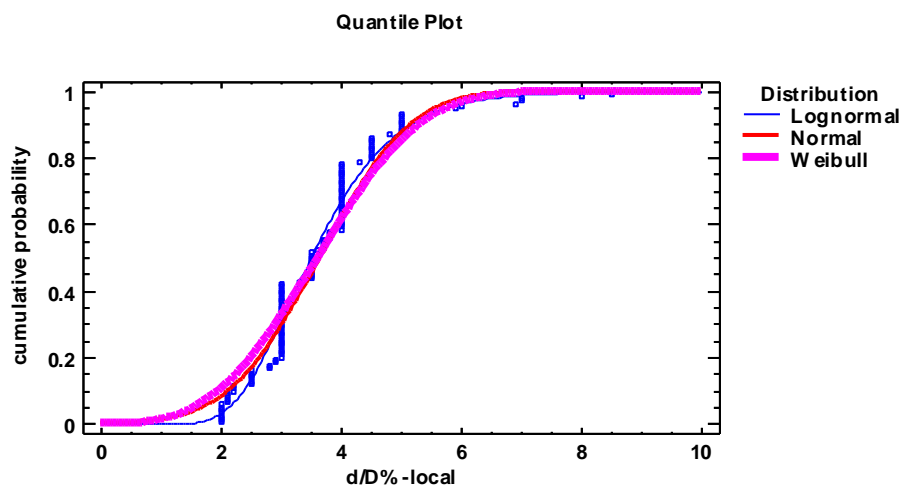
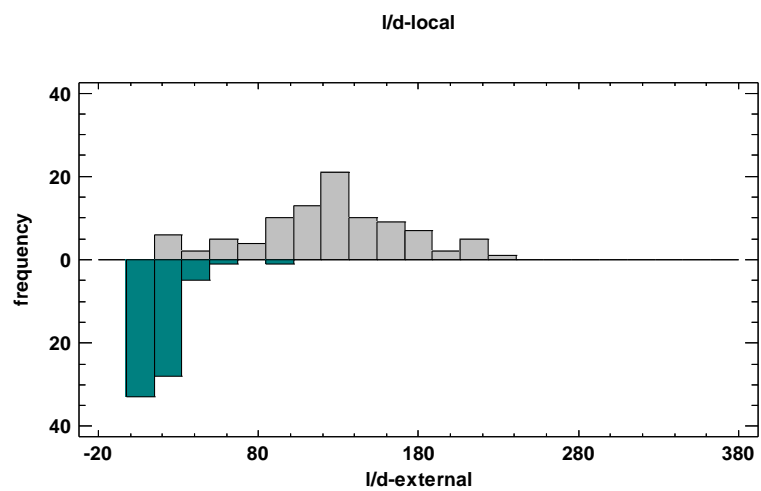
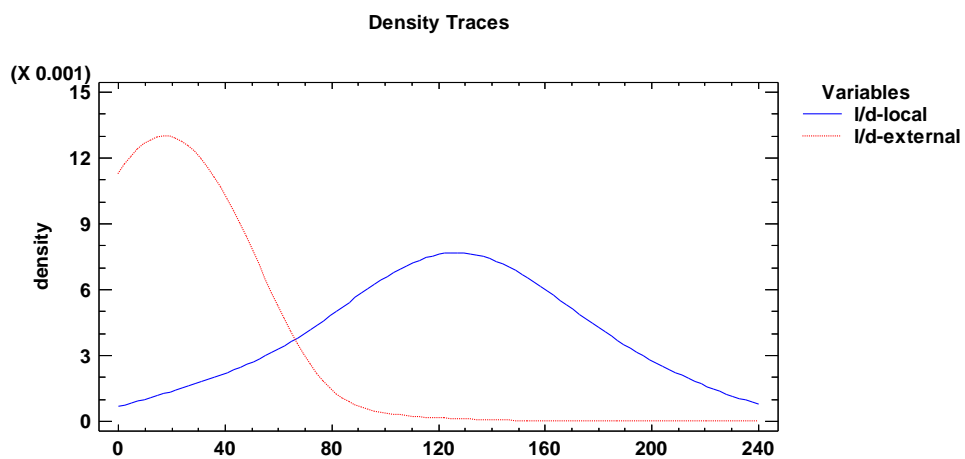


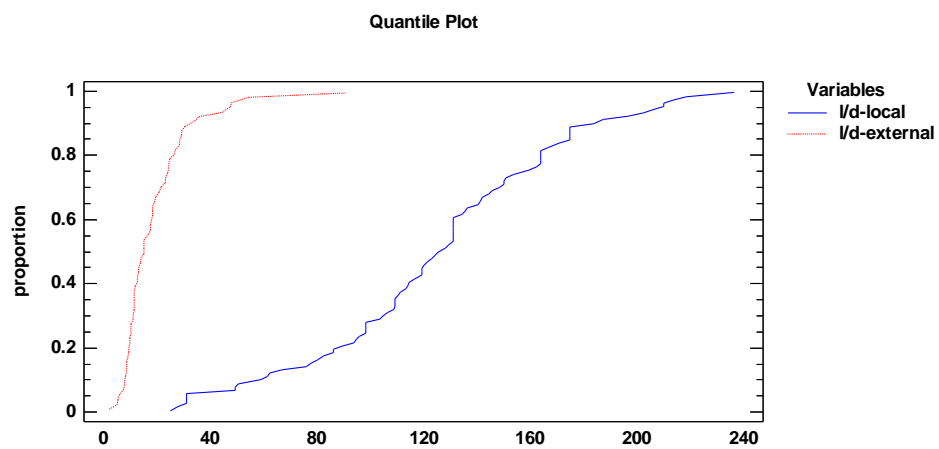
Figure 5.6 Cumulative probability of sample data and fitted distribution for $d/D\%$ ratio
(a) local company (b) external companies



(a)



(b)



(c)

Figure 5.7 Comparison of two samples of l/d (local vs. external)
(a) frequency histogram (b) density traces (c) quantile plot

the external dents have sharpness ratio less than 29. The statistical tests in Table 5.1 emphasize quantitatively that the mean, standard deviation and distribution all have significant difference between the two samples. The distribution fitting of l/D data is given graphically in Fig. 5.8. The KS test parameters in Table 5.2 show that the Weibull distribution is good candidate for both distributions although the distribution parameters, i.e. mean and deviation, are significantly different.

One factor that might be the reason of this significant difference in the dent sharpness between the local and external companies is the variance in the pipe D/t ratio discussed previously. The higher D/t ratio of the local company gives the pipe more flexibility to impact loading, and therefore, the final dent profile would be longer and smoother. The other factor could be the elimination of sharply rock dents in the case of the local company. All of the pipelines of the local company are installed in sand soil with back fill controlled by specification not have rocks larger than 12-mm diameter.

The local and external companies have similar distributions of pipe material SMYS as Fig. 5.9 suggests. The histogram and density traces show that the pipe material SMYS has two peaks at 242 and 359 MPa for both cases. The quantile plot shows wide steps of the SMYS intervals. This is because the SMYS can only have specific values governed by the pipe grade of API 5 L (2007) such as grade B (SMYS is 242 MPa), Grade X42 (290 MPa), grade X52 (SMYS is 359 MPa), etc. The quantitative tests given in Table 5.2 also show that the mean and standard deviation of pipe material SMYS is statistically similar. There is also no statistical difference between the two distributions at significance level of 0.01. The data of both samples can be fitted with Weibull distribution (Fig. 5.10) which passes the KS test with high P-value for the local (0.4324),

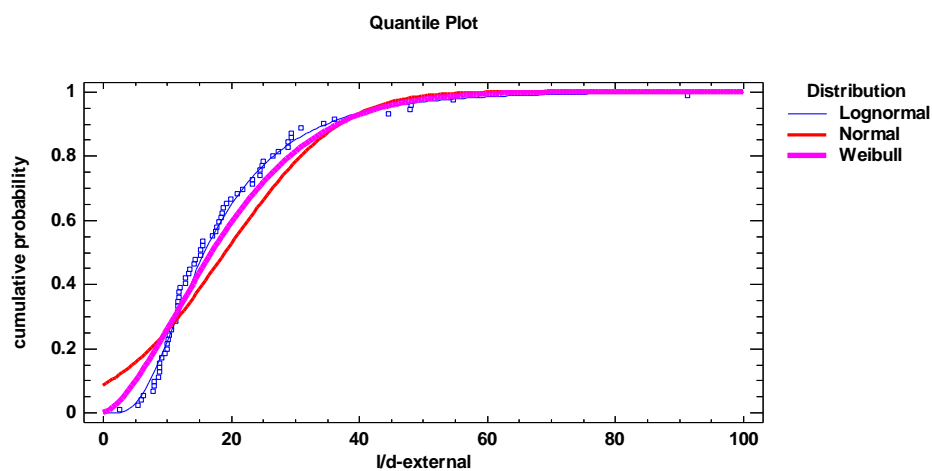
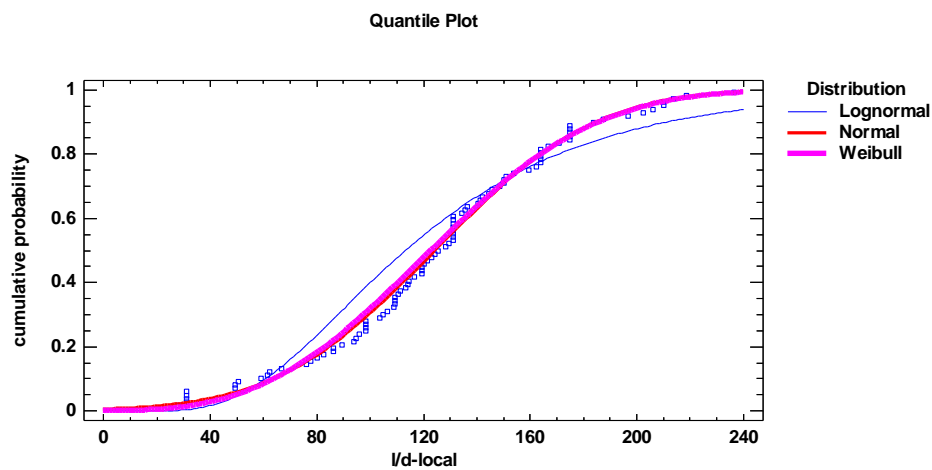
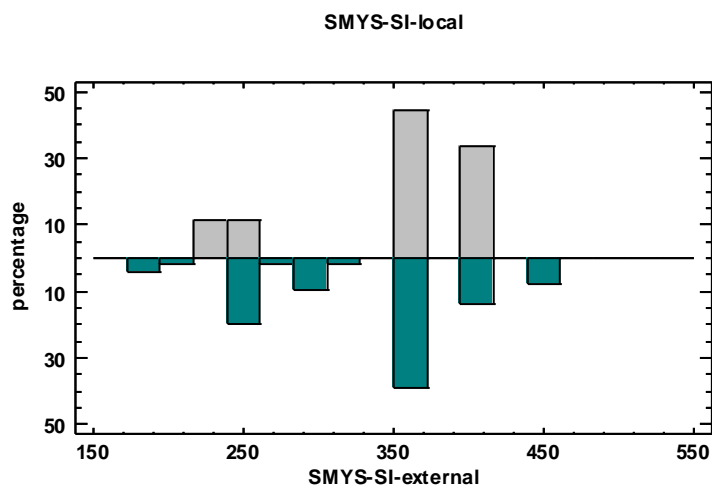
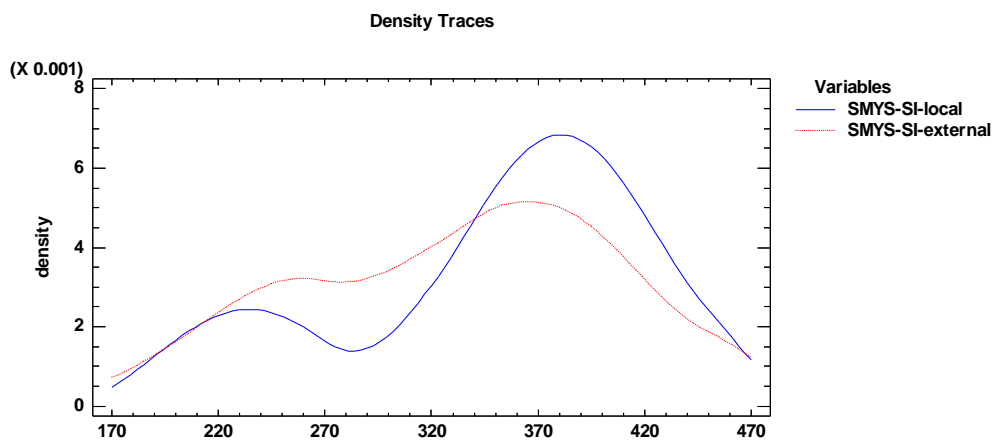


Figure 5.8 Cumulative probability of sample data and fitted distribution for l/d ratio
 (a) local company (b) external companies



(a)



(b)

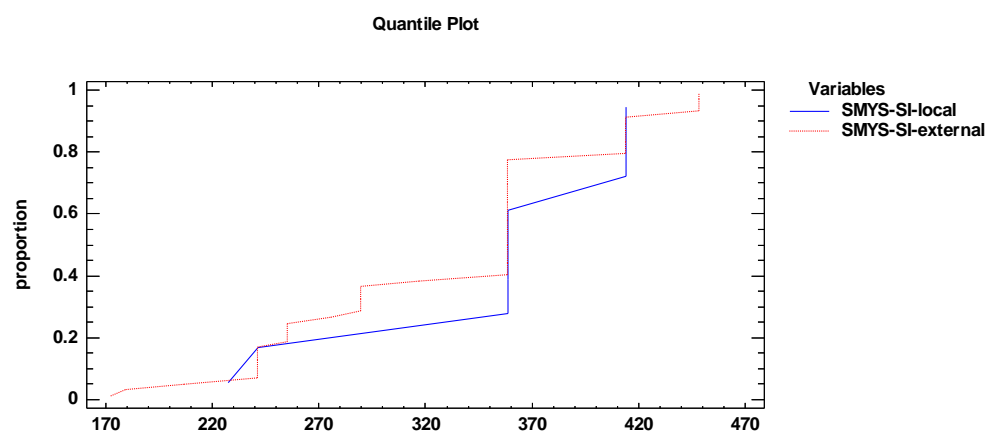


Figure 5.9 Comparison of two samples of SMYS (local vs. external)
(a) frequency histogram (b) density traces (c) quantile plot

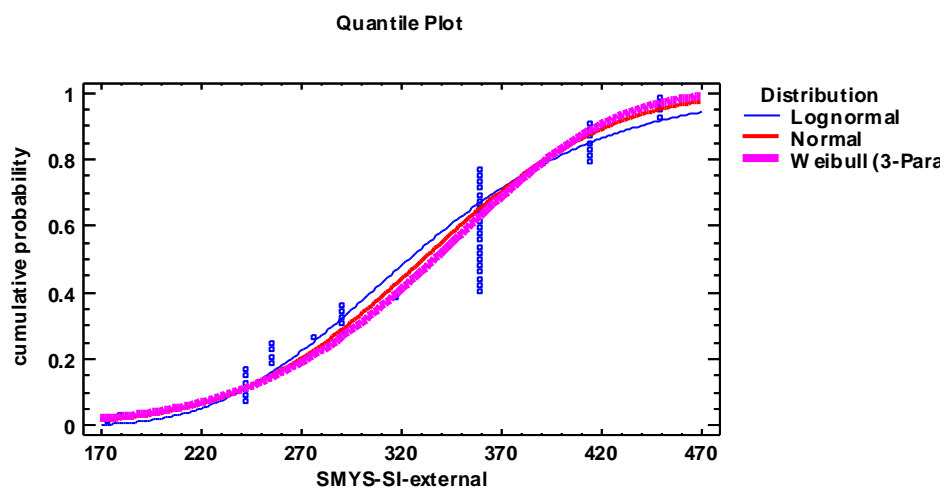
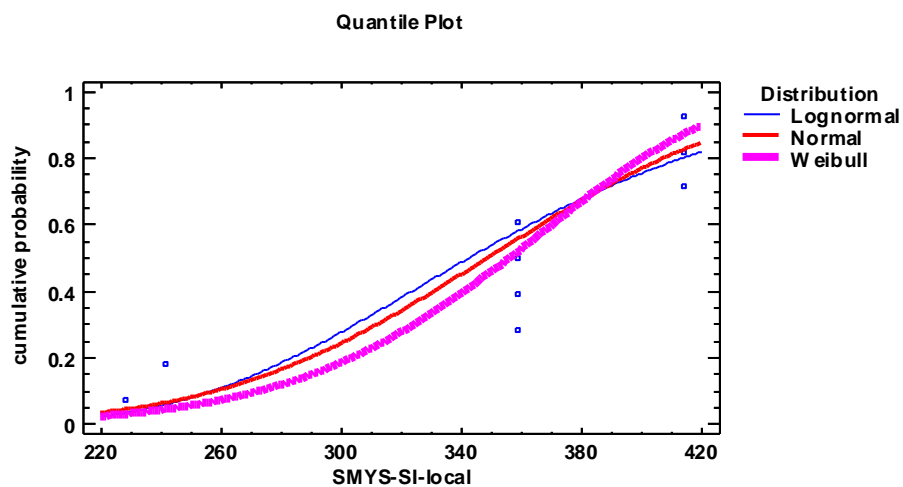
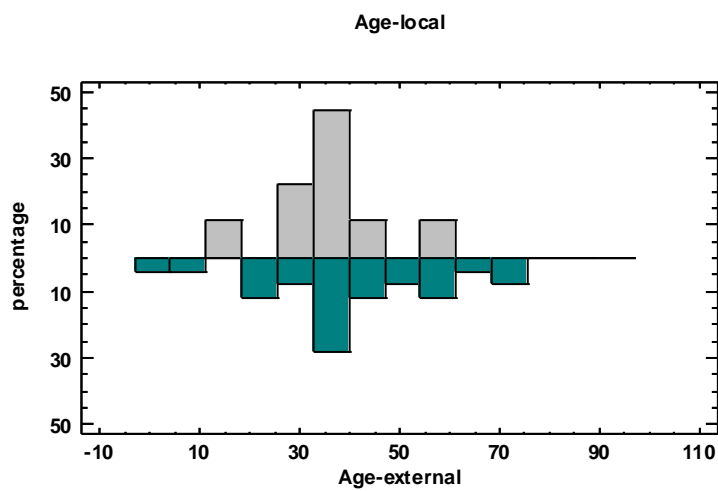


Figure 5.10 Cumulative probability of sample data and fitted distribution for SMYS
 (a) local company (b) external companies

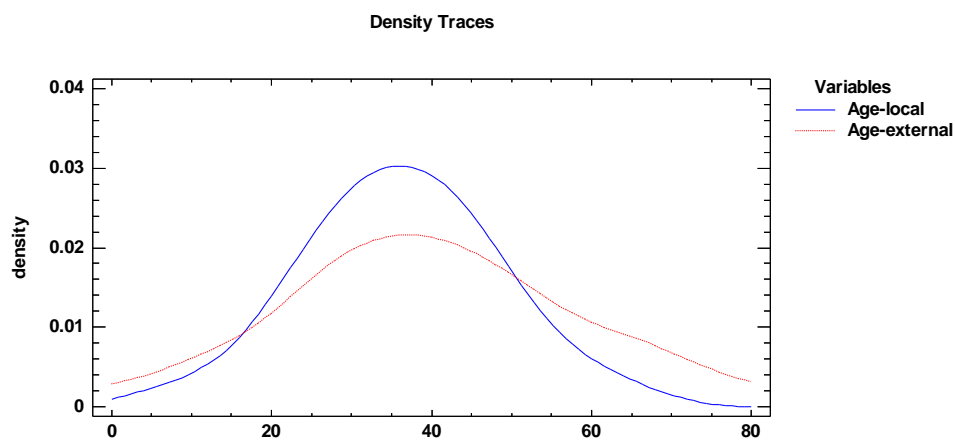
but with low P-value for the external (0.0103) as Table 5.2 illustrates. The standard significant level for goodness of fit test is 0.05, but other values have been used such as 0.005, 0.01, 0.1, 0.15, and 0.2. The lower significant value has been used in this fitting (which means lower goodness of fit) due to the fact that the SMYS is not a true distribution function, but can take only specific values. On the other hand, it cannot be modeled as discrete function as the specific values are not discrete events, but real values on scale with different interval widths.

The distribution of pipe material SMYS in damaged pipe data does not imply that this specific steel grade is subject to damage more than others. Rather, it is representative sample of the total pipeline population. Pipe grade B (SMYS is 242 MPa) and grade X52 (SMYS is 359 MPa) has been widely used previously due to its combined advantages of good strength and good weldability. However, recent trends has been towards using pipe grades X60 (equivalent to 414 MPa) and grades X65 (equivalent to 449 MPa), and therefore, the statistical distribution of future survey is expected to reflect this change.

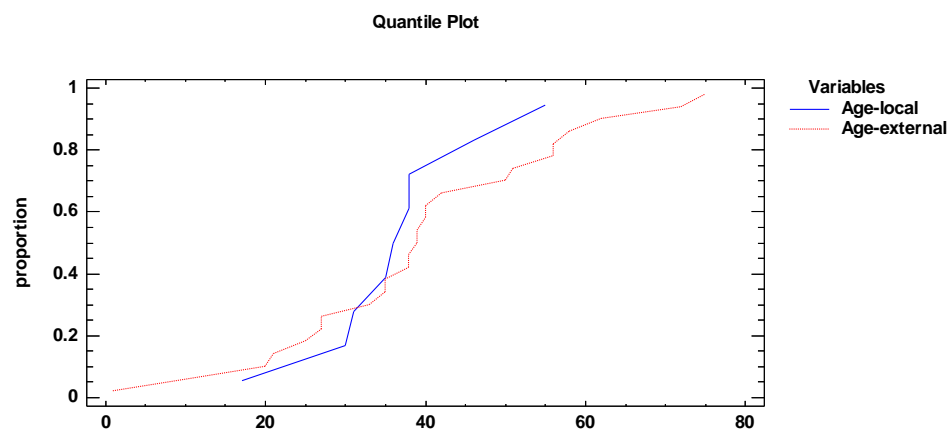
The graphical comparison of pipe age between the local and external companies is given in Fig. 5.11. Both the local company and the external companies have a mean pipe age close to 40 as the frequency histogram and density traces illustrate. However, the external companies have around 18% of their pipes of 70 years old. The maximum pipeline age of the local company is only 50 years old and only composes 8% of the pipeline population. The statistical values given in Table 5.1 show that the means of the two samples are very close (36.2 for local and 39.6 for external), but the deviations are not (10.6 for local and 17.8 for external). However, the F-test indicates that this difference between the deviations is not statistically significant. The data of both samples



(a)



(b)



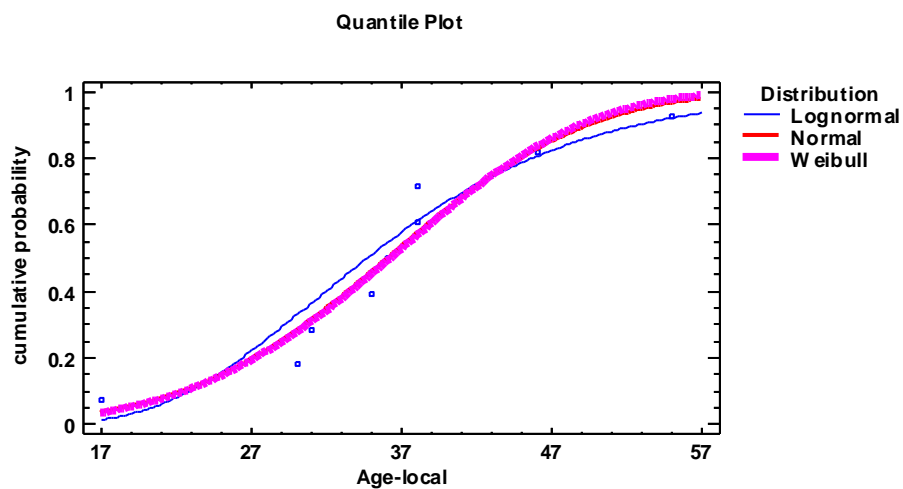
(c)

Figure 5.11 Comparison of two samples of age (local vs. external)
(a) frequency histogram (b) density traces (c) quantile plot

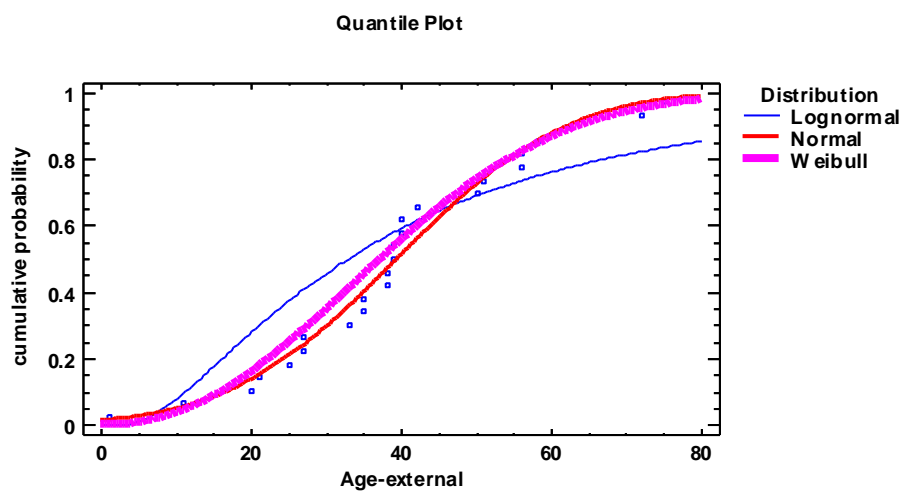
can be fitted with Weibull distribution (Fig. 5.12) which passes the KS test with high P-values for both samples as Table 5.2 indicates.

While the incident probability of mechanical damage itself is not a function of pipe age, the probability of failure of aged pipes due to damage is higher. This is because newer pipes have better resistance to damage due to improved material properties like fracture toughness as well as better manufacturing and construction controls. Therefore, it is less likely to have failures in the local company as compared to the external companies because of their relatively old-pipeline.

The interaction of dent with weld yields a more severe damage especially if the weld quality is low. Therefore, the statistical distribution of the pipe manufacturing seam is presented in Fig. 5.13. It is clearly shown the percentage of seamless pipes in both the local company and external companies are negligible. This is because of their limitation in size up to 610 mm, and higher cost compared to seamed-pipe. The figure also shows that both local and external companies have majority of the pipes of straight seam weld with percentage around 55%. However, there are differences in the other types of seams. The local company does not have any pipes classified as low welding quality (low-frequency electric resistance welding (LF ERW), lap welding, and electric fusion welding (EFW)). On the other hand, the local company has around 20% of the pipes of spiral weld compared to only around 3% for the external companies. The spiral weld pipe has been assumed to be of lower quality than straight steam, not because of the weld quality, but because of the manufacturing scheme that results in high residual stress of the pipe. The impact of interaction of dent with residual stresses is studied in Chapter 9.



(a)



(b)

Figure 5.12 Cumulative probability of sample data and fitted distribution for pipe age
(a) local company (b) external companies

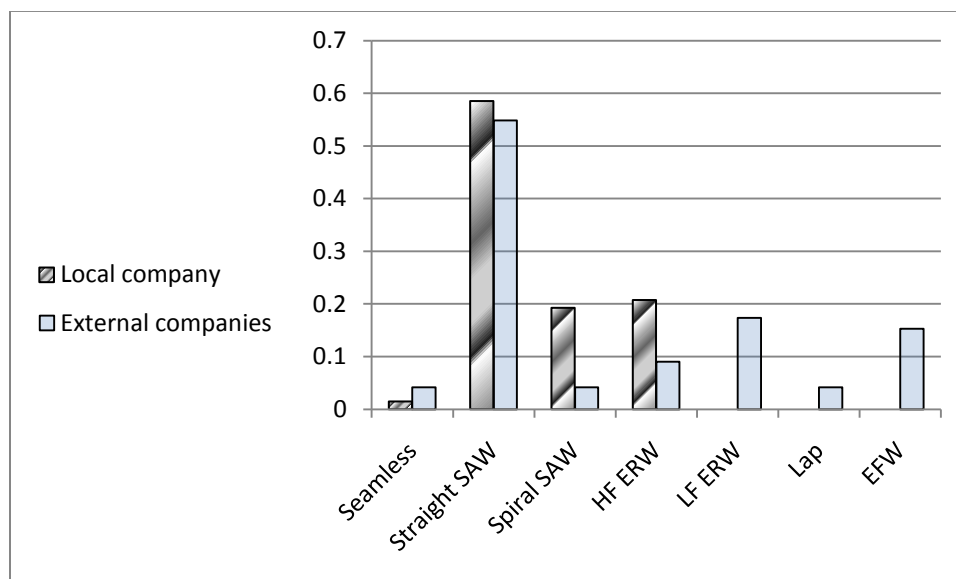


Figure 5.13 Statistical distributions of pipe manufacturing seam type

That statistical distribution of the product type is given in Fig. 5.14. The figure indicates that majority of the pipelines in the local company are liquid service while majority of the pipelines in the external companies are gas. This reflects the nature of operation of companies. The local company is in the business of producing and transporting crude oil while the external companies are distributing energy mainly gas. However, this population of the local company will change due to change in trend towards producing and distributing gas. The product type (whether gas or liquid) does not affect the incident rate, but it has effect on the probability of failure and failure mode. In liquid pipelines, the pressure cycles are more severe than gas pipelines due to the incompressibility nature of liquid (Veith et al. 2004). This makes liquid pipelines more subject to failure by pressure fatigue. However, the consequences of failure in gas pipelines are more severe. This is because the gas decompression energy extends the pipe defect in ductile fracture in the axial direction leading to rupture. In liquid lines, however, the decompressions is almost immediate and does not have enough energy to propagate the crack, and thus, results in leak. (Lyons et al. 2008)

5.4.1 Failure Rate

The failure rate is defined as the product of the probability of failure times the pipeline hit rate. The probability of failure is estimated using the statistical distribution of the damage data described in this chapter which is fed as input to the probabilistic analysis outlined in Chapter 6. Any case with maximum von Mises strain exceeding 20% is considered a failure. The 95% confidence interval of the probability of failure for the local company was found to range between 0.11% and 4.3% which is low and in line

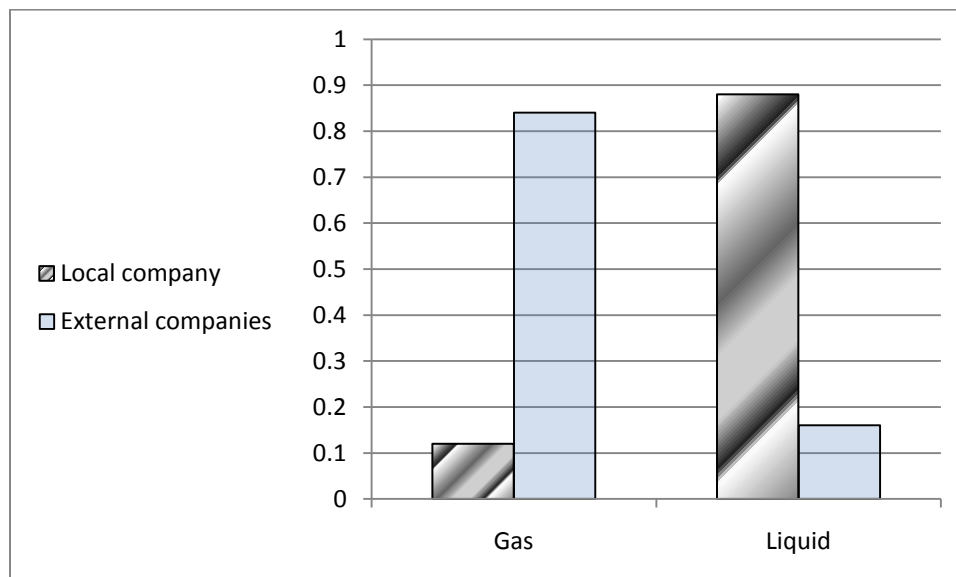


Figure 5.14 Statistical distributions of pipe product type

with the observations about the smooth dents nature of the local company. The 95% confidence interval of the probability of failure for the external company lies between 25.8% and 38.7% which is in agreement with the reported 28.7% probability of failure in the external sample pipelines (Semiga, 2007).

The statistical data of the local company can be used to establish trend of the hit rate defined as number of dents per km-yr of pipelines. The hit rate trend can be utilized to forecast number of dents in a certain population of pipeline depending on their exposure, i.e. total length times age. Table 3 lists the hit rate for the specific pipeline surveyed while Table 4 rearranges the data in terms of cumulative number of dents vs. cumulative exposure. Various regression models are tested to find correlation between the two variables and it was found that linear fit with zero intercept, presented in Eq. 32, is an excellent choice.

$$\text{number of dents} = (6.64 \pm 0.35) \times 10^{-3} \times \text{exposure} \quad (32)$$

Figure 15.a gives the fitted line along with the prediction interval lines for new observations. The R-squared value is 0.978 which indicates that this is a very good fit as the residual plot illustrates (Fig 15.b). The slope of the fitted line represents the hit rate which is equal to $(6.64 \pm 0.35) \times 10^{-3}$ dents/km.yr.

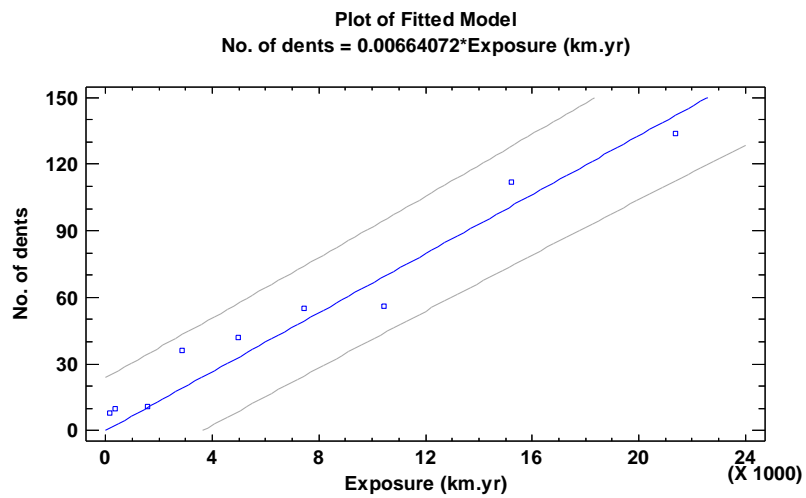
The hit rate (6.64×10^{-3}) is multiplied by the probability of failure interval [0.11%-4.3%] to define the failure rate interval $[0.73 \times 10^{-5}, 28.6 \times 10^{-5}]$. This is in good agreement with the historical failure rate of the local company which is 8.3×10^{-5} (Advantica, 2004).

Table 5.3. Hit rate for specific surveyed pipelines and generic pipeline population.

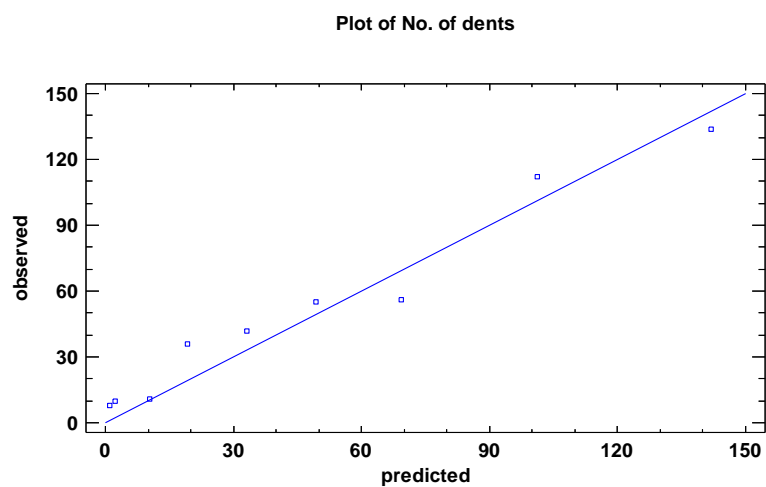
Pipeline #	No. of dents	Years of service	Length (km)	Exposure (km.yr)	Hit rate (dents/km.yr)
1	8	30	4.8	144	5.56E-02
2	1	35	86.0	3,010	3.32E-04
3	2	17	12.0	204	9.80E-03
4	6	36	58.3	2,099	2.86E-03
5	13	55	44.6	2,453	5.30E-03
6	22	31	197.7	6,130	3.59E-03
7	56	46	104.0	4,784	1.17E-02
8	1	35	34.7	1,213	8.24E-04
9	25	38	34.7	1,317	1.90E-02

Table 5.4. Cumulative number of dents vs. cumulative exposure.

Cumulative No. of dents	Cumulative Exposure (km.yr)
8	144
10	348
11	1,561
36	2,878
42	4,977
55	7,430
56	10,440
112	15,224
134	21,354



(a)



(b)

Figure 5.15. Linear regression fit of hit rate trend (a) fitted line and prediction intervals
(b) plot of residuals

5.5 SUMMARY

In this chapter, statistical analysis was conducted on mechanical damage inspection data of plain dents for a local company as well as external companies. Accordingly, the statistical distribution of dent parameters such as geometry of dented pipe, material of dented pipe, and geometry of the dent was derived to be used in the probabilistic design analysis. Also, based on comparison of the statistical data of the local and external companies, it was found that the local company has dents with smoother profiles. This could be explained by the flexibility of the local company pipes as they tend to be of larger D/t ratio compared to the external companies. Moreover, all of the installation of the local company are in sandy area which eliminate the sharply rock dents. Another difference was also observed in the pipeline service whereas majority of the local company are liquid while majority of the external companies are gas. The type of service is critical in the nature and consequences of failure. Finally, the failure rate interval for the local company was determined to be $[0.73 \times 10^{-5}, 28.6 \times 10^{-5}]$. This is in good agreement with the historical failure rate of the local company which is 8.3×10^{-5} .

CHAPTER 6

RELATIVE SIGNIFICANCE OF DENT PARAMETERS AND EFFECT OF THEIR VARIABILITIES

6.1 INTRODUCTION

It is impossible to cover all possible combination of input parameters of geometry, material, and operating conditions whether by full-scale tests or FEA. One approach to overcome this issue was by developing empirical formulas such as the one given in ASME B31.8 (2003) for calculating strain at the dent peak. Yet, this formula and other similar ones were subject to review and suggestion for improvements (Noronha et al. 2008, Gao et al. 2008). Another approach is to develop equations for strains/stresses based on curve fitting of the results of parametric FEA runs (Pinheiro et al. 2006, Pinheiro et al. 2008, Jandu et al. 2008, Francini et al. 2008).

The formulas developed for parametric FEA analyses are dependent on cases selected and analyzed. Those cases are pre-determined by the analyst by selecting discrete values of a certain parameter (such as pipe diameter-to-thickness ratio, indenter diameter, etc.) to cover its expected range. The analyst, then, selects a certain number of the larger number of possible combinations between those parameters to determine the FEA runs to be analyzed. In reality, the parameters values as well as their combination are random. Moreover, each nominal value of these parameters has its own variability due to

manufacturing tolerances, measurement uncertainties, etc. Therefore, the use of probabilistic design analysis offers an excellent way to study the problem and determine the sensitivity of the strain and stress fields to each of those input parameters.

The objective of this chapter is to identify and quantify the effect of geometry, material, and pressure variability on the strain and stress fields of dented pipe under static and cyclic pressure loading. The first part of the chapter uses deterministic analysis to present strain and stress contours at the end of indentation stage as well as the stress range and fatigue cycles at the end of pressure cycle stage. The second part uses probabilistic design analysis to determine the sensitivity of the strain, stress, and stress range to the input.

6.2 DESCRIPTION OF THE PROBLEM

The problem geometry, boundary conditions and loading are the same as that described in section 4.2 of the dissertation. This base case was already validated, and it is analyzed in details in the deterministic case of this chapter.

6.3 DESCRIPTION OF THE NUMERICAL MODEL

A quarter of the pipe is used due to the symmetry in geometry, loading and boundary conditions. Symmetry boundary conditions are applied in the two symmetry planes. The indentation process is modeled by a contact pair of rigid target with pilot node. A vertical load displacement is applied on the target in small load steps until it reaches the target depth. After that, two pressure cycles are applied.

The indentation process is modeled by a contact pair of rigid target with pilot node. A vertical load displacement is applied on the target in small load steps until it reaches the

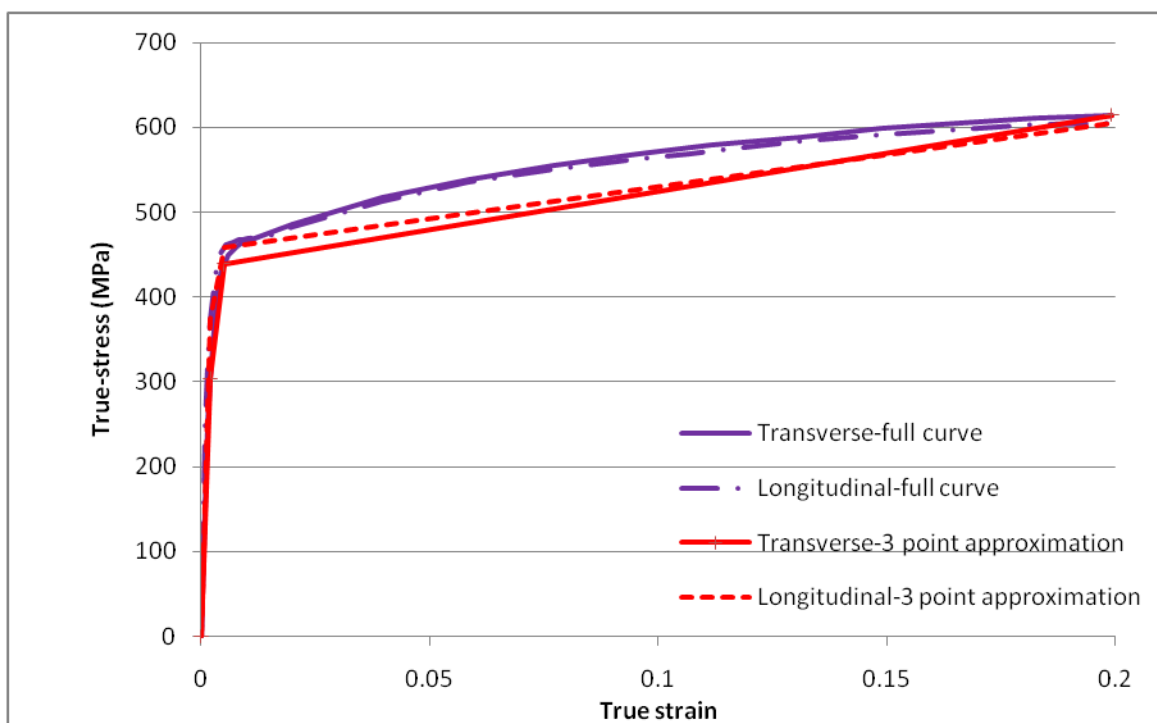
target depth. After that, the first hydrostatic pressure cycle is implemented in small load steps as well as small unloading steps to 0 gauge pressure. Subsequently, the second pressure cycle, the operating pressure, is simulated in two load steps of minimum and maximum pressure. One operating pressure cycle is enough to get the stress range in the as it was found in Chapter 4 to be of linear response.

6.3.1 FE Model

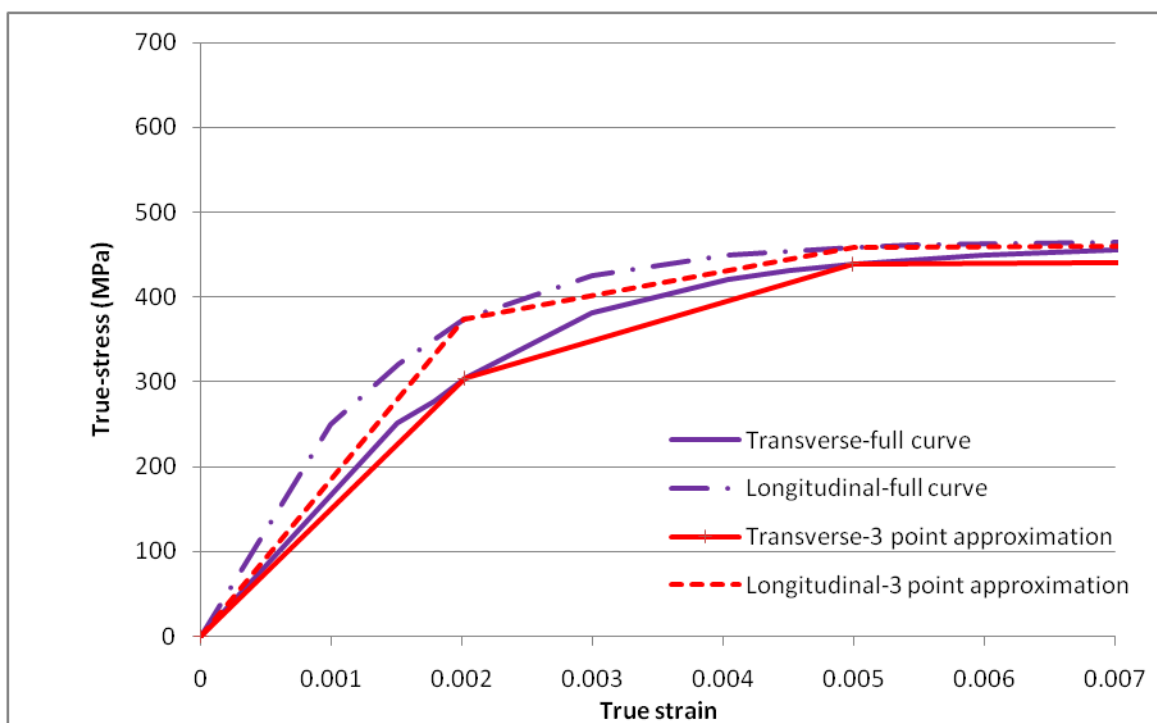
Elements used are shell element 181 (4-nodes). For the contact pair, the indenter is modeled with Target 170 while the contact areas are modeled with Contact 174. Similar mesh to that describe in section 4.3.1 is used.

6.3.2 Material Model

Detailed study on material modeling of indented pipe under static and cyclic loading using FEA was presented in the previous chapter. Based on the conclusions of that chapter, anisotropy in the pipe material should be included in the material model as it plays a decisive rule especially in the cyclic loading. For the plastic hardening rule, it was shown that kinematic hardening gave the closest result the experimental values of strain and fatigue cycles. Therefore, the material model in this chapter utilizes orthotropic linear anisotropy in the elastic part and multilinear kinematic hardening coupled with Hill's anisotropy in the plastic part. Three points are used to define the full stress-strain curve as these points can be easily acquired for the pipe material and they generate good approximation to the actual stress-strain curves as illustrated in Fig. 6.1. The first point is the end of proportional limit which has a strain value of 0.2% and a stress value



(a)



(b)

Figure 6.1. Full and 3-point approximation of stress-strain curves of the pipe material
(a) full range (b) zoom at elastic and initial plastic portion

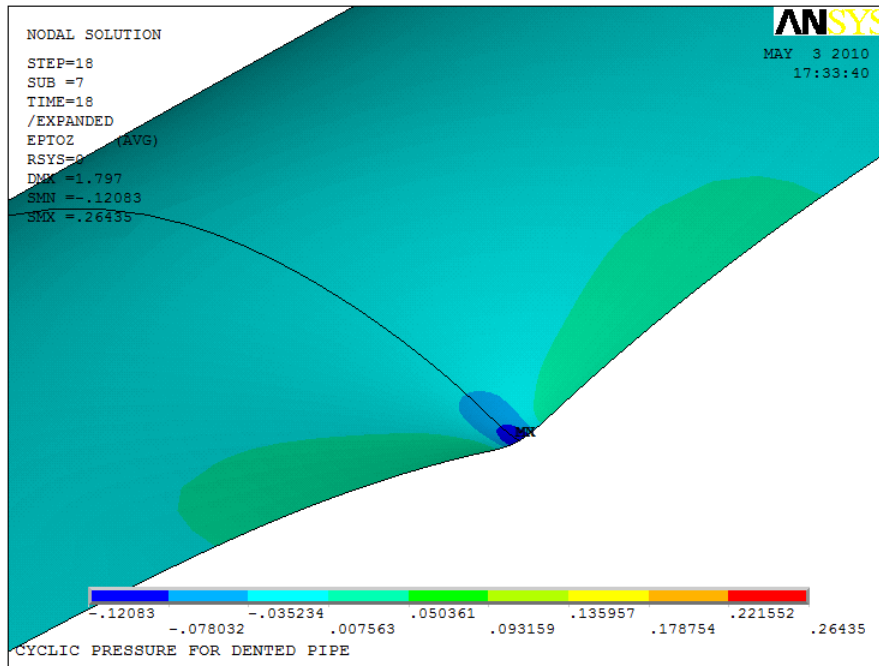
calculated based on the modulus of elasticity. The second point is the yield strength at 0.5% strain in accordance with the definition of API 5L (2007). The third point is the ultimate tensile strength at a true strain of 0.2 which is the minimum accepted for pipe material (API 5L, 2007).

6.4 DETERMINISTIC ANALYSIS OF THE BASE CASE

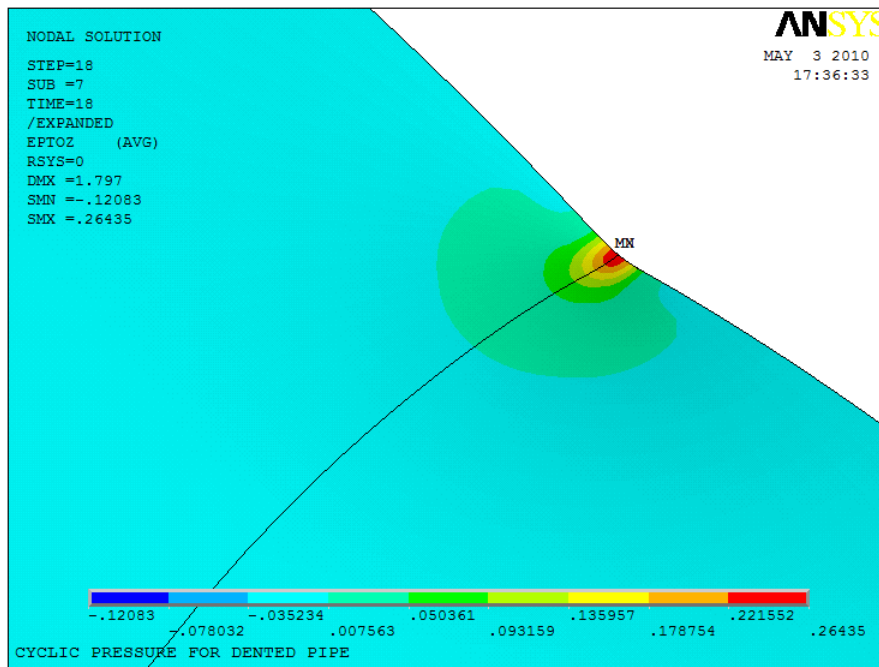
The strain and stress fields of the base case are first investigated to determine the output parameters that should be included in the probabilistic design as they must be defined prior to start of the FEA probabilistic loop analysis. The analysis is not limited to the dent peak, but is extended to the whole domain of the indentation area.

6.4.1 Strain Fields at End of Indentation Phase

The axial strain fields are shown in Fig. 6.2 for top and bottom of the pipe shell while the hoop strain fields are shown in Fig. 6.3. The figures emphasize that the dent peak, as expected, has the maximum magnitude of both axial and hoop strains on top and bottom shell. The axial and hoop strains are both compressive on the top shell and tensile on the bottom shell. This means that gouges and cracks at the dent might be less harmful than expected. However, the axial strains on the top shell switch from compressive to tensile along the longitudinal axis as illustrated further in Fig. 6.4. The switch point is close to the indenter periphery. The crack initiated at this location in the experimental part. Therefore, the magnitude of this strain and its location will be investigated in the probabilistic analysis in addition to the strains at the dent peak.

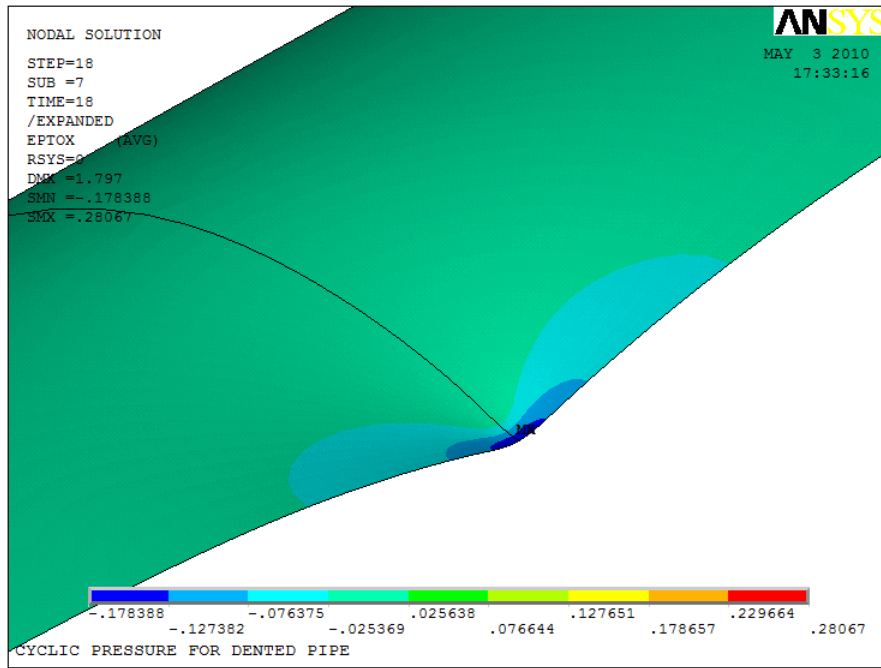


(a)

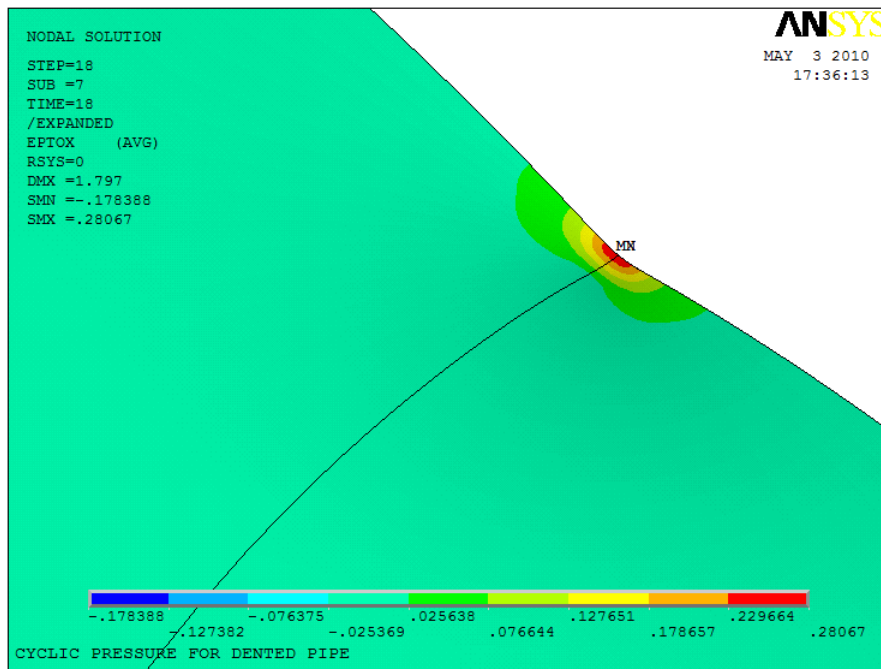


(b)

Figure 6.2. Axial strain profile at (a) top shell (b) bottom shell



(a)



(b)

Figure 6.3. Hoop strain profile at (a) top shell (b) bottom shell

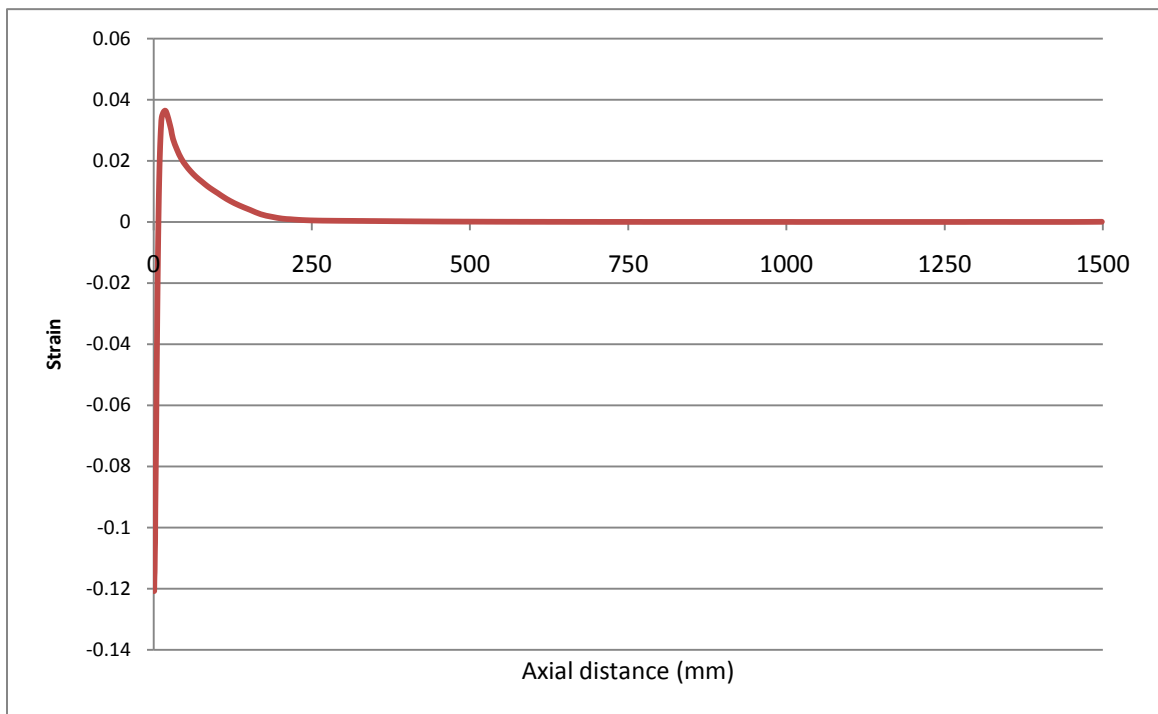


Figure 6.4. Axial strain profile along longitudinal axis from dent peak

6.4.2 Stress Fields at End of Indentation Phase

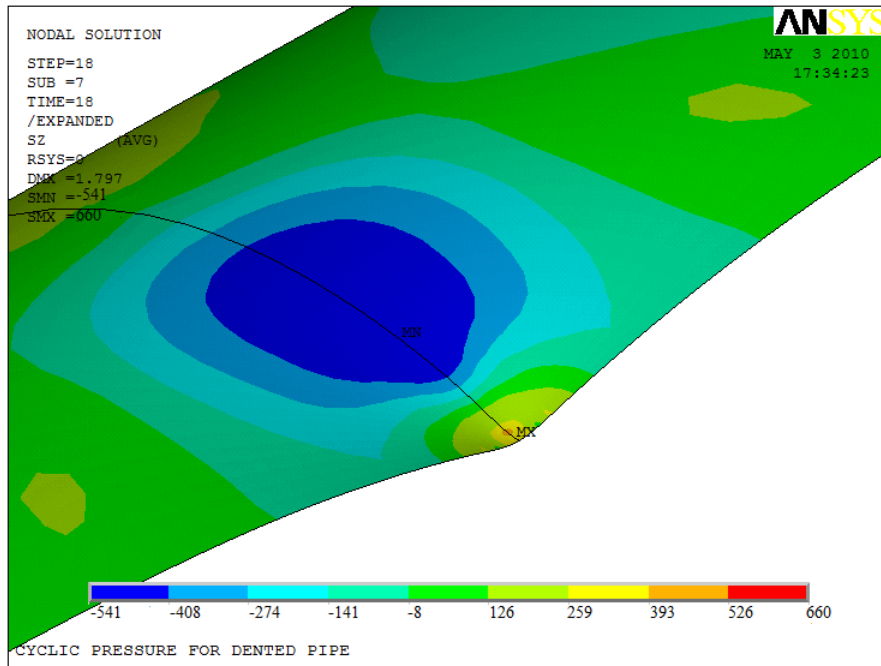
Unlike strain fields, the stress fields do not exhibit maximum magnitudes at the dent peak. The axial stress profile on the top shell (Fig. 6.5.a) has a maximum tensile value very close to the dent peak, but a maximum compressive value of magnitude of 538 MPa in the transverse direction from the dent peak. The axial stress field at the bottom shell (Fig. 6.5.b) shows similar trend of maximum tensile values very close to the dent peak and maximum compressive value in the transverse direction of the peak.

For the hoop stress field, Fig. 6.6.a indicates that the maximum tensile stress is very close to the dent while the maximum compressive stress is at a distance of around 35 mm in the longitudinal direction. This distance is almost at the indenter periphery. The hoop stress field (Fig. 6.6.b) has maximum tensile stresses at the dent peak and at a distance of around 30 mm axially while it has maximum compressive stresses are at transverse direction from the dent peak.

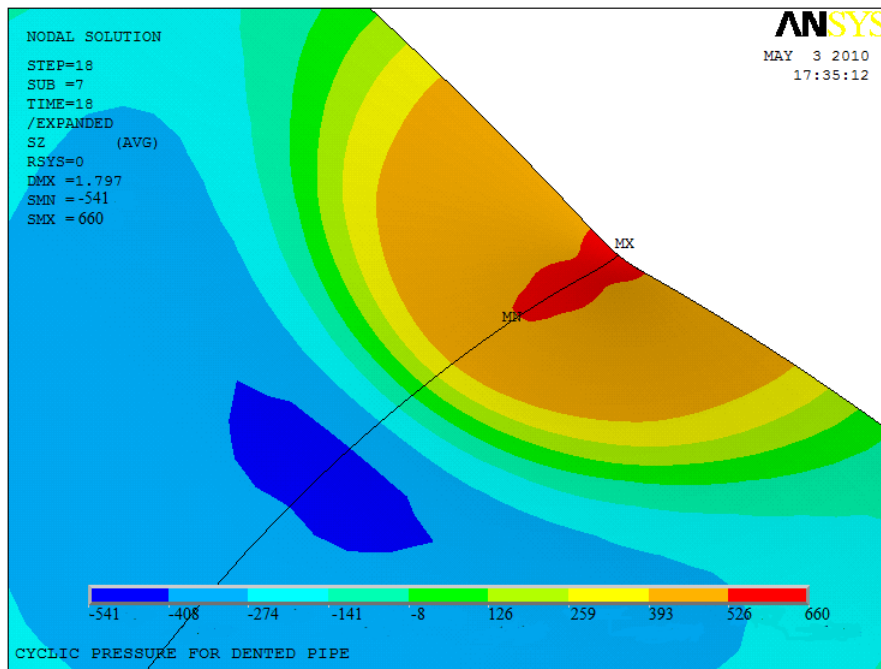
The above discussed observations clearly indicate that in order to assess the severity of damage based on stresses; it is not enough to study the stress field at the dent peak. Therefore, in the probabilistic analysis, maximum tensile and compressive stresses along both the axial and transverse direction of the dent peak are investigated in addition to the stresses at the dent peak.

6.4.3 Stress Range at End of Pressure Cycle and Fatigue Analysis

It was shown in Chapter 4 that pressure cycles after the first few ones follow linear response due to elastic shake-down. Therefore, the elastic stress range of second pressure cycle can be used for fatigue analysis to estimate the fatigue life based on Equation 4.8

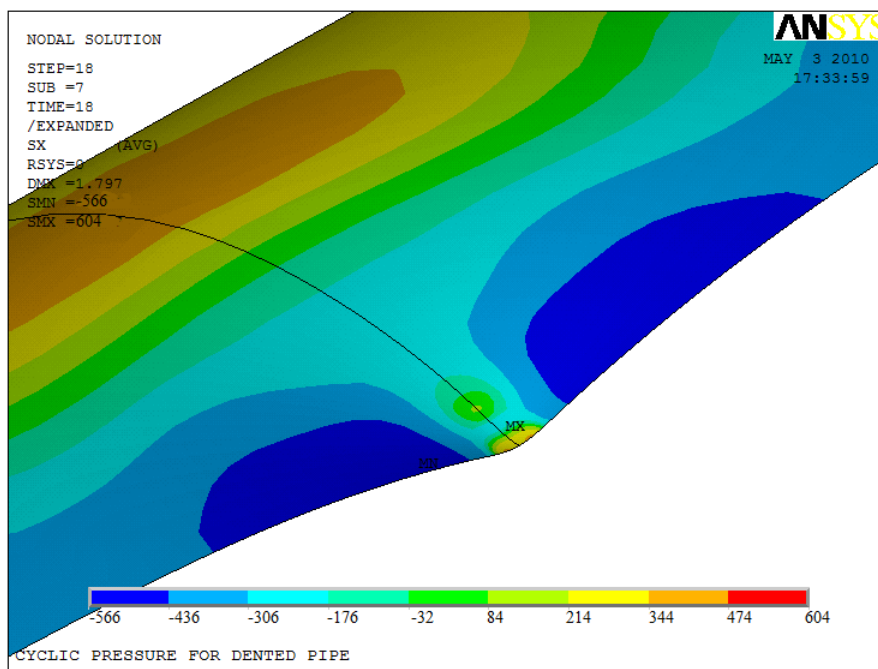


(a)

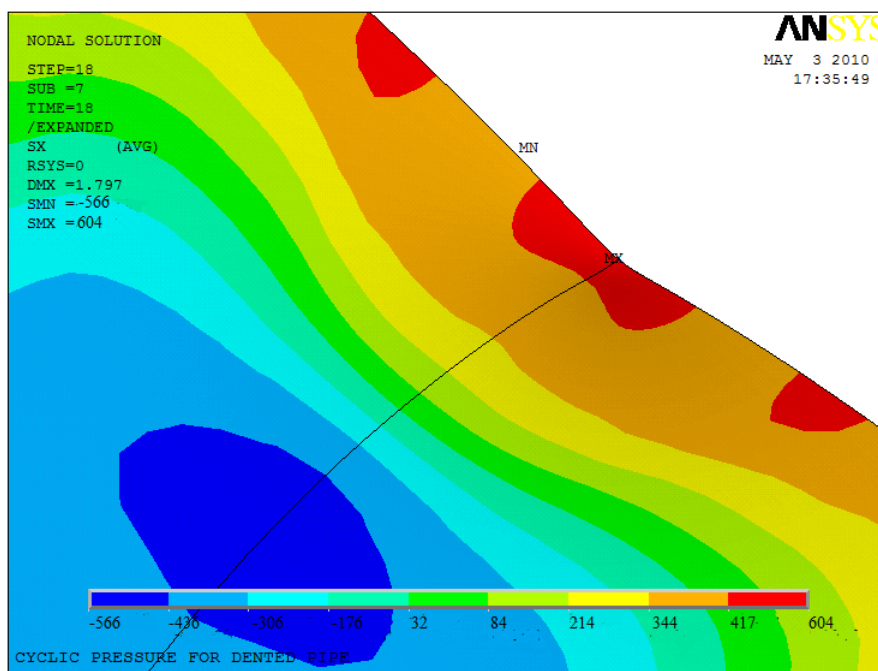


(b)

Figure 6.5. Axial stress profile at (a) top shell (b) bottom shell



(a)



(b)

Figure 6.6. Hoop stress profile at (a) top shell (b) bottom shell

Table 6.1 gives the stress range and fatigue cycles at different location of dent based on Von Mises stresses. As discussed in section 6.4.2, the maximum stresses are not always at the dent peak. This is why the locations and magnitudes of maximum Von Mises stress along the dent longitudinal direction as well as along the dent transverse direction are investigated in addition to the dent peak. The table emphasizes that the maximum stresses at the top shell are not at the dent peak although the maximum stress range in this specific case happened to be in the dent peak. This draws another important point that maximum stress and maximum stress range are not coincident. Therefore, probabilistic analysis will include determination of stress range and fatigue cycles of these four locations.

6.5 PROBABILISTIC ANALYSIS

The input parameters of the dent problem can be classified into three categories: material, geometry, and pressure loading. Each of these dent problem input parameters have a wide range of values. Moreover, each nominal value of these parameters has its own variability due to manufacturing tolerances, measurement uncertainties, etc. Therefore, in practice hundreds of random combinations of input parameters are possible. Therefore, the use of probabilistic design analysis offers an excellent way to study the problem and determine the sensitivity of the strain and stress fields to each of those input parameters.

6.5.1 Random Input Variables

The variability of input variables can be characterized in terms of probability measures such as statistical distribution functions. Table B.1.1 lists the random input variables,

Table 6.1. Stress range and fatigue cycles at different locations of dent (Note: $N_{\text{exp}} = 38,865$ (Semiga, Nov. 2007))

<i>Location</i>	σ_{max} (MPa)	σ_{min} (MPa)	σ_a (MPa)	<i>N</i>
Dent peak	370	98	136	77,024
24 mm dent longitudinal	479	357	61	300,401
25 mm dent transverse	470	344	63	404,136

their distribution, and distribution parameters. The input variables are grouped in three categories: material, geometry, and loading. In cases where statistical data of a certain parameter is available, the actual statistical histogram and distribution function fit are presented. For material properties, distribution fit is assumed normal with mean value and standard deviation estimated based on the properties range given by API 5L (2007). The distribution of hydrotest pressure (90% to 100% SMYS) and maximum operating pressure (72% to 80% SMYS) are selected in line design Code requirements (ASME 2003). The minimum operating pressure is limited to 30% SMYS as higher values will result in low pressure range, and thus, low stress range not to be significant in fatigue analysis.

The input variables are not totally uncorrelated. For example, the yield strength and ultimate tensile strength are correlated with the material SMYS. Another correlation also exists between the property, geometry, and load. The pressure load shall not produce a hoop stress value that is higher than a factor of SMYS. Those correlations are expressed in terms of mathematical relationships and are given in Table B.1.1.

6.5.2 Probability Analysis Loops

The probability analysis is conducted using ANSYS PDA module (ANSYS, 2007) with a total of 100 analysis loops to compute the random output parameters in terms of the random input variables. The values of the input variables are generated randomly using Monte Carlo simulation to find how the scatter in the input variables affect the output results and which input variable is the most significant. The number of analysis loops (samples) was selected to satisfy the requirements of multiple regressions of Eq.

6.1 which will be presented in section 6.5.4. The equation has 7 to 8 independent variables, and therefore, the minimum recommended sample size is 70 to 80 based on the rule of thumb of having 10 samples per independent variable (Halinsky and Feldt, 1970). A more recent work by Green (1991) suggested a sample size of 50+8 times the number of independent variables yielding sample size of 106 to 114. The intermediate sample size of 100 was eventually selected for this analysis.

6.5.3 Probability Analysis Results

The variation of axial strain at dent peak at the end of indentation phase due to variation in the input is shown in Fig. 6.7. The figure shows a great deal of scatter which proves the randomness nature of the problem. Table B.1.2 gives a summary of all output results (dent dimensions, strains, stresses, and stress range) along with their statistical distribution. The statistical distribution of the output can be useful to calculate a quick estimate of probability of failure without even measuring the dent dimensions to be used with risk assessment. For example, according to the analysis, the probability of the strain magnitude to exceed the 6% Code limit (ASME B31.8, 2003) is 48%. The probability of fatigue cycles to be less than 1000 is only 6.7%.

Sensitivity analysis is performed to find out which input variable(s) affect each of the output variables. Figure 6.8 shows that the axial strain at dent peak is sensitive only to three input variables: dent percent (loading), dent radius (indenter geometry) and modulus of elasticity (material). It is not affected by the material plastic properties such as yield stress or the diameter-to-thickness ratio. Table B.1.3 lists the results of sensitivity analysis of all output variables to input variables in terms of Spearman correlation factor.

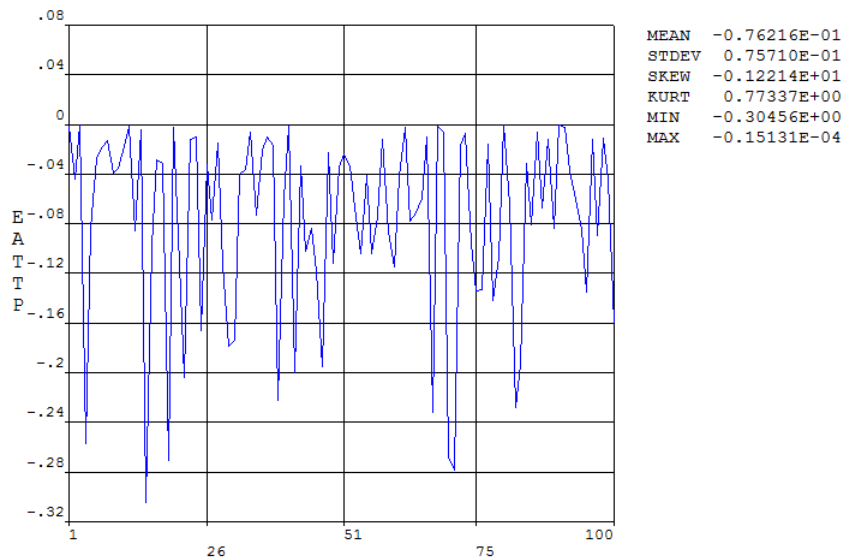


Figure 6.7. Sample history of axial strain at dent peak

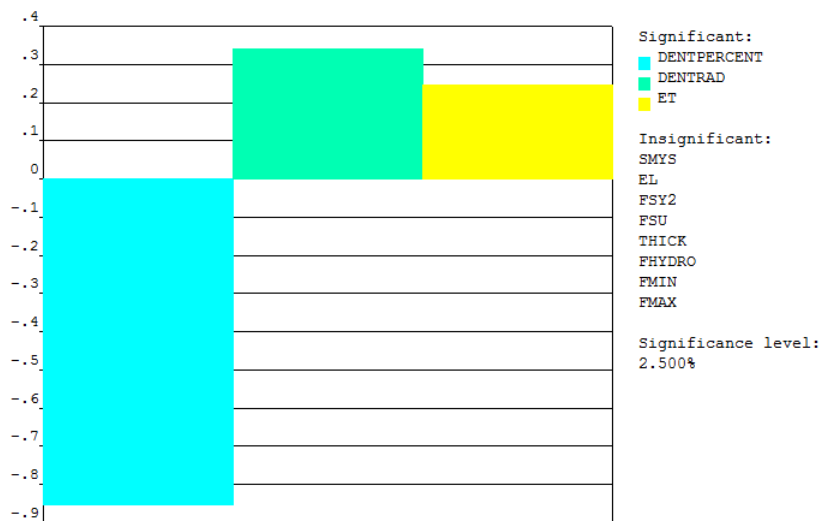


Figure 6.8. Sensitivity plot of axial strain at dent peak

Note: Legend top-to-bottom order matches left-to-right order in figure

The closer of the correlation factor magnitude to unity, the higher related the output variable to the input variable. Therefore, the correlation between the axial strain and dent percent is very strong (-0.853). Figure 6.9 is a scatter plot of liner fit between the two variable which further illustrate the strong relation.

Looking into the table for the other output variables, it is clear that the total and bending strains have similar sensitivity as the one discussed for the axial strain at dent peak. However, the membrane strains are different as they exhibit sensitivity with respect to the yield stress and diameter-to-thickness ratio. The stresses on the other hand, have less sensitivity to the dent percent and higher sensitivity to the yield stress. The stress range and fatigue life have sensitivity to the maximum operating pressure as well as material yield stress. They are not sensitive to the small variation in the hydrotest pressure.

6.5.4 Regression Analysis

In order to make the results of the probabilistic analysis to be easily applied in practical dent problems, regression analysis is conducted to derive mathematical formulas of the output variables in terms of practically measured variables. It was reported by Francini and Yoosef-Ghodsi (2008) that quadratic polynomial functions are the best fit for a similar problem. Therefore, the following general function (Equation 6.1) has been fit to all output variables where all output and input variables in dimensionless form. The two terms associate with pressure range are only applicable to output stress range and fatigue life.

ANSYS

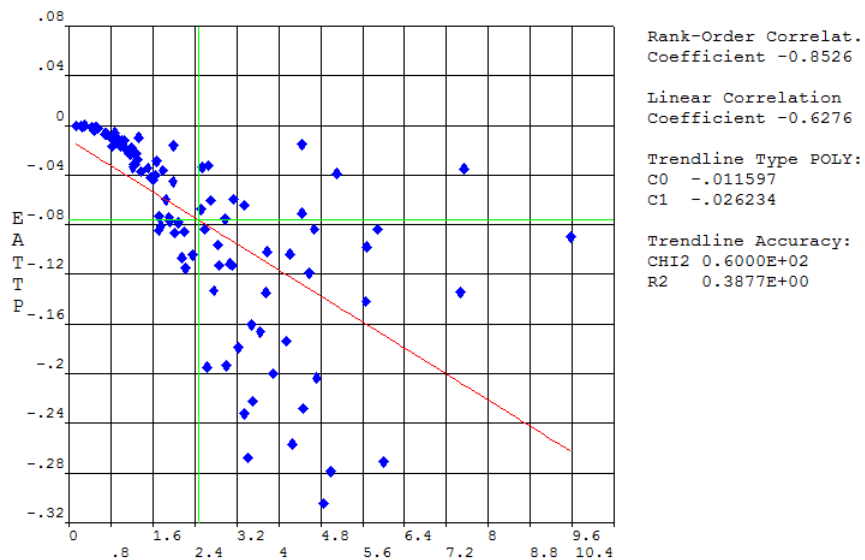


Figure 6.9. Scatter plot of axial strain at dent peak vs. percentage of dent-to-diameter ratio

$$\begin{aligned}
\text{Output variable} = & a_0 + b_1 \frac{D}{t} + b_2 \frac{d}{D} + b_3 \frac{l}{D} + b_4 \frac{w}{D} + b_5 \frac{ldw}{D^2 t} + b_6 \frac{\sigma_{flow}}{E_{avg}} + b_7 \frac{E_t}{E_l} + \\
& b_8 \frac{P_{max} - P_{min}}{P_{SMYS}} + c_1 \left(\frac{D}{t}\right)^2 + c_2 \left(\frac{d}{D}\right)^2 + c_3 \left(\frac{l}{D}\right)^2 + c_4 \left(\frac{w}{D}\right)^2 + c_5 \left(\frac{ldw}{D^2 t}\right)^2 + c_6 \left(\frac{\sigma_{flow}}{E_{avg}}\right)^2 + \\
& c_7 \left(\frac{E_t}{E_l}\right)^2 + c_8 \left(\frac{P_{max} - P_{min}}{P_{SMYS}}\right)^2
\end{aligned} \tag{6.1}$$

Table B.1.4 gives the constants values and R-squared value for the regression fit of all output variables of strain, stress, stress range, and fatigue life. The R-squared value is higher than 0.5 in 37 out of 45 output variables which indicate that the proposed general formula (6.1) is a good choice. The R-squared value is highest for the output strain variables as it reaches levels of 0.8 and 0.9. Figure 6.10 shows the regression curve for the axial strain at dent peak which is an excellent fit of R-squared 0.883. The regression fit for the output stress variables is also good as Fig. 6.11 illustrates where the R-squared values range between 0.6 and 0.8. For the stress range and fatigue life, the R-squared values are lower and range between 0.25 and 0.67, but they still show a reasonable fit as Fig. 6.12 shows.

6.6 SUMMARY

The effect of geometry, material and pressure variability on strain and stress fields in dented pipelines under static and cyclic pressure loading using probability design is evaluated. A total of 100 cases randomly generated using Monte Carlo simulations were analyzed. The statistical distribution of output parameters and correlation between output

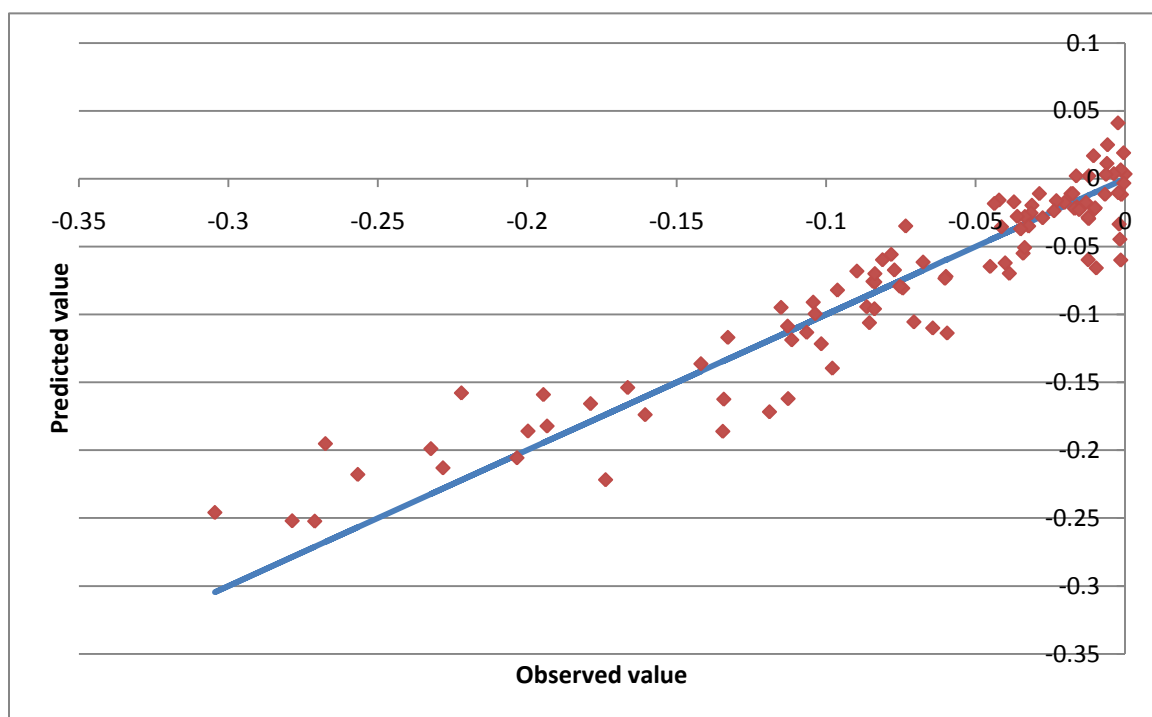


Figure 6.10. Regression fit curve for axial strain at dent peak

and input variables were presented. Accordingly, the sensitivity of strain and stress fields to the various input parameters was determined. Moreover, a general formula was proposed to relate the output variables in terms of practically measured variables. Regression analysis was conducted to derive the coefficients and the results showed the general formula was a good choice. The R-squared values were higher than 0.5 in most of the cases. The results can be used directly into strain based design approach. Moreover, they can be coupled with fracture mechanics to assess cracks, for which the state of stress must be known in the location of crack tip, not necessarily found in the dent peak. Furthermore, probabilities derived from the statistical distribution can be used in risk assessment.

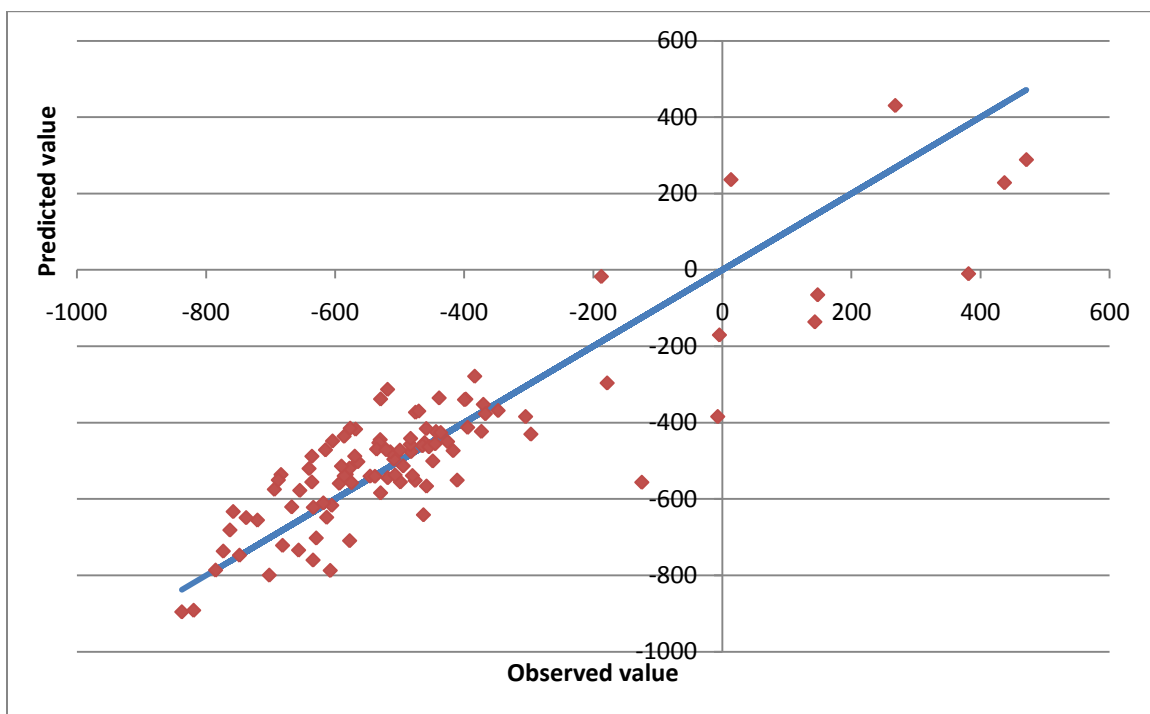


Figure 6.11. Regression fit curve for axial stress at dent peak

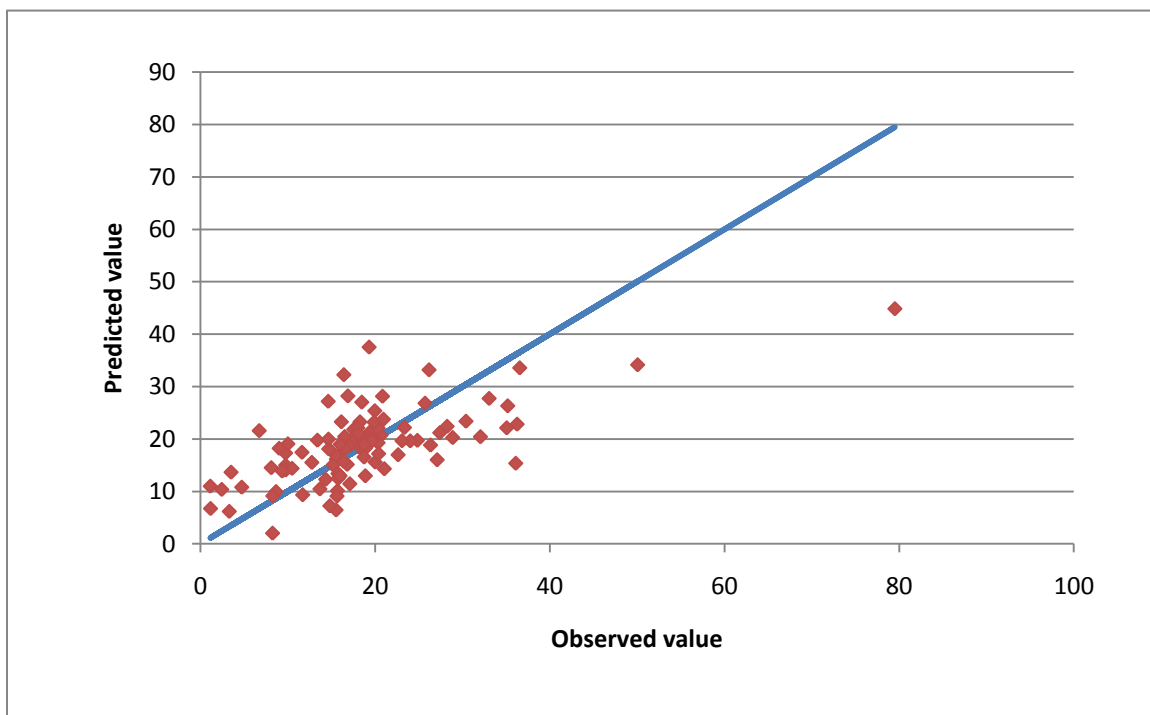


Figure 6.12. Regression fit curve for natural log of fatigue life

CHAPTER 7

IMPACT OF INTERACTION OF TWO DENTS

7.1 INTRODUCTION

It is possible that two or more dents be in close proximity such that they interact together to produce more severe damage in terms of strain, stress, and stress range values. An obvious example where this can happen is in the case of hit by an excavator of multiple teeth. It was also reported that some leaks in service pipelines were attributed to axial crack that developed between two axially-adjacent dents resulting from rocks in close proximity.

Experimental tests of two interacting dents subject to cyclic pressure were conducted by API 1156 (1999). A total of 10 tests were carried out on 324-mm diameter pipe with 100-mm and 200-mm spherical indenters. In each test, the indenter size was identical, and so was the final indentation depth. The center-to-center spacing between the indenters was varied at 1/2, 1, 2, or 3 times the indenter diameter. The results showed that the two dents interacted only when they are very close with 1/2 diameter spacing. The report defined the interaction when the curvature between the two dents is altered and flattened and recommended to remove all such dents as they present a threat to the structural integrity of the pipeline.

Dinovitzer et al. (2002) pointed out that the service life and failure location of interacting dents depend on the proximity of the dent peaks. They suggested a risk factor

that depends on a dimensionless parameter of two peaks separation divided by the dent depth. They considered interaction only if this parameter is less than one. A recent work by Francini and Yoosef-Ghodsi (2008) indicated that dents should be considered interacting if they are spaced closer than $2\sqrt{Rt}$, and in such cases, evaluation should be made by a subject-matter expert as no assessment method is available.

There are many parameters that affect the severity of the mechanical damage related to the pipe geometry and material properties, the defect geometry and boundary conditions, and the loading cycle. For two interacting dents, the separating distance and the orientation angle between them are two additional parameters. As it is impossible to run full-scale tests that cover the variation of all those parameters to understand their effect and not practical to run deterministic FEA analysis for all possible combinations, utilization of probabilistic design analysis would be the best approach. This is because in reality, the parameters values as well as their combination are random. Moreover, each nominal value of these parameters has its own variability due to manufacturing tolerances, measurement uncertainties, etc. Therefore, the use of probabilistic design analysis offers an excellent way to study the problem and determine the sensitivity of the strain and stress fields to each of those input parameters. This was proven successful for the case of a single dent (Chapter 6)

The objective of this chapter is to define when two dents should be considered interacting. Moreover, the chapter will investigate the impact on strain and stress fields as well as fatigue life of interacting dents in pipe under static and cyclic pressure. The first part of the chapter uses deterministic analysis to present strain and stress contours at the end of indentation stage as well as the stress range and fatigue cycles at the end of

pressure cycle stage. The second part uses probabilistic design analysis with variable geometry, material and pressure to determine the sensitivity of the strain, stress, and stress range to the input.

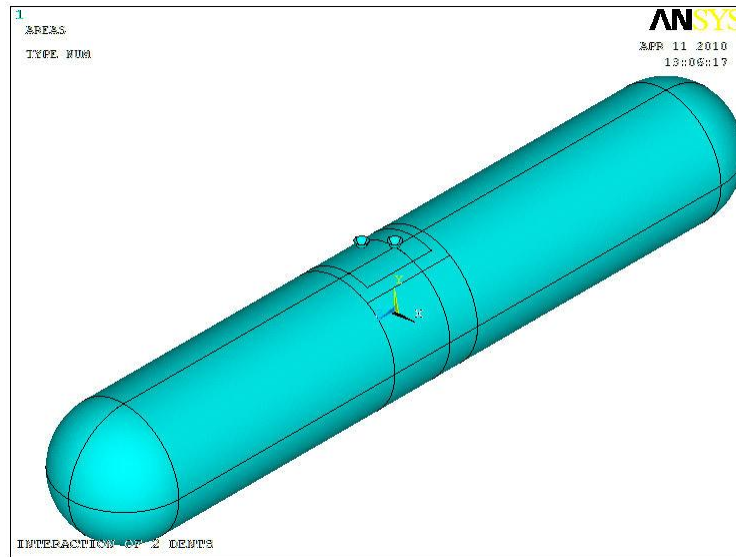
7.2 DESCRIPTION OF THE PROBLEM

The problem is similar to that described in section 6.2 of the dissertation with the addition of a second indenter as shown in Fig. 7.1. The second indenter is of the same diameter as the first indenter. The relative location between the two indenters is defined by the distance and orientation projected on the xz -plane as the figure illustrates.

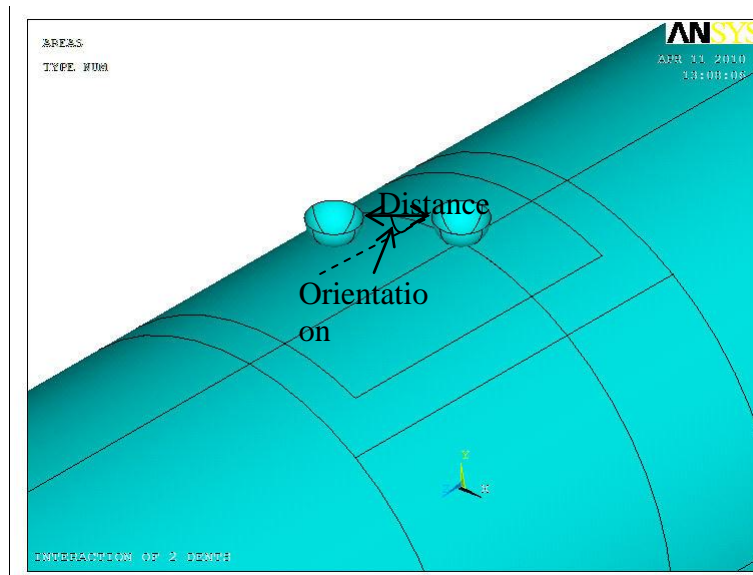
7.3 DESCRIPTION OF THE NUMERICAL MODEL

The full pipe must be modeled due to the unsymmetrical load caused by the second indenter. Therefore, additional boundary conditions are necessary to prevent rigid body motion as Fig. 7.2 illustrates. Two restraints of translation in the Z -direction are imposed on two opposite nodes along the X -axis whereas two restraints of translation in the X -direction are imposed on two opposite nodes along the Z -axis. These additional restraints act as guide only for the pipe to prevent rigid body motion while they do not prevent pipe expansion due to pressure load.

The indentation process is modeled by 2 contact pairs of rigid target with pilot node whereas each contact pair represents one indenter. The option for closing initial gap is selected for both contact pairs. The same amount vertical load displacement is applied simultaneously on the 2 targets in small load steps until it reached the final target depth.



(a)



(b)

Figure 7.1. Illustration of pipe with two indenters
(a) full pipe (b) zoom at indentation area.

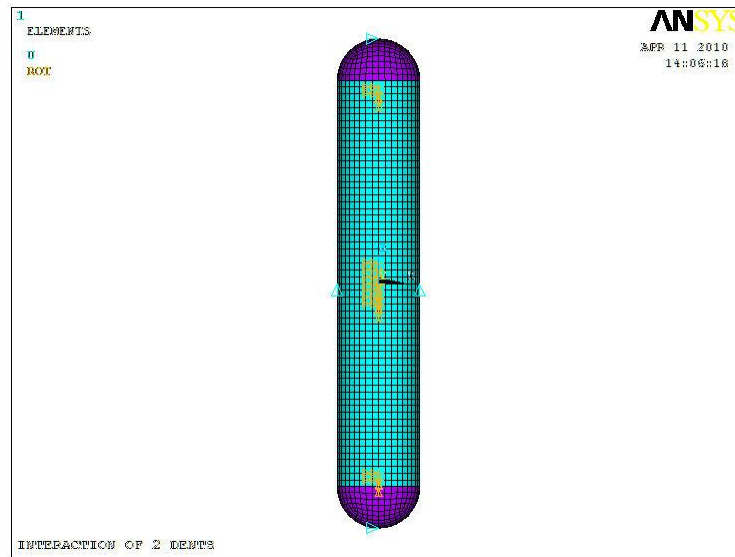


Figure 7.2. Boundary conditions for pipe with 2 indenters

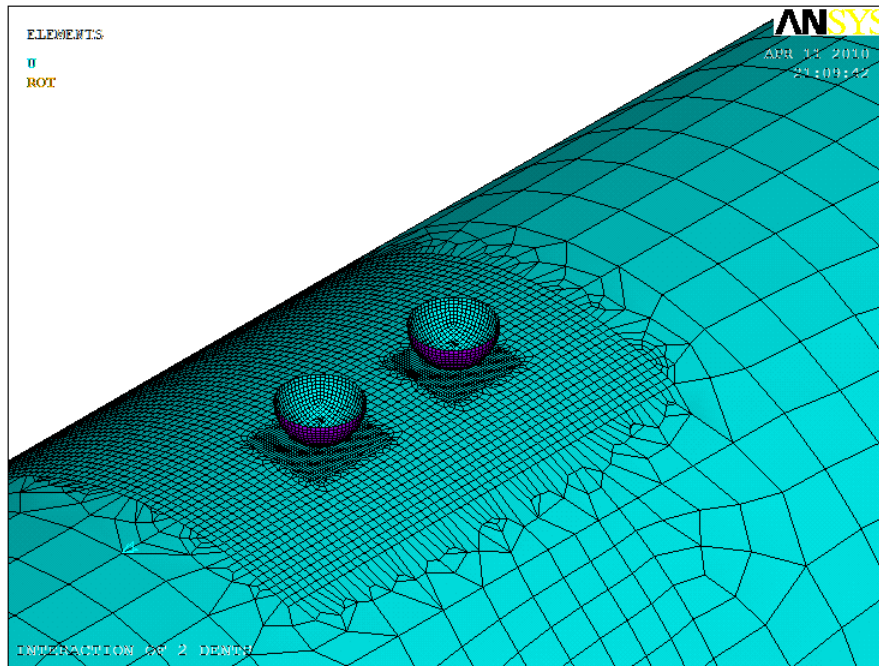
After that, two pressure cycles are applied. The first one is simulating the hydrostatic pressure test and the second cycle simulates the operating pressure range.

7.3.1 FE Model

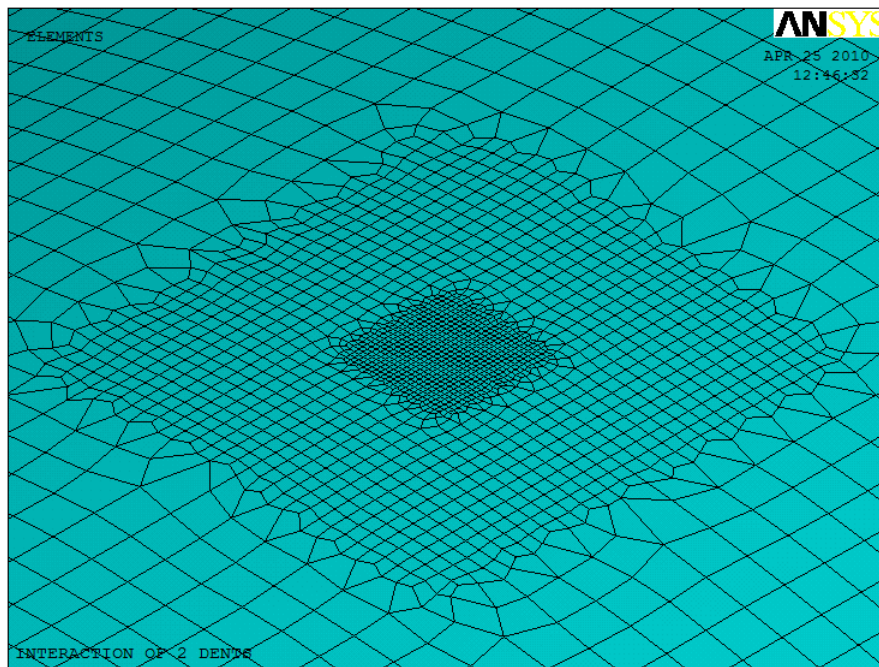
Elements used are shell element 181 (4-nodes). For the contact pair, the indenter is modeled with Target 170 while the contact areas are modeled with Contact 174. A fine square mapped mesh of 6 mm edge size is used in the indentation area. This mesh is refined in a square zone with an edge equal to the indenter diameter. A second mesh refinement is made at the indenter tip with an edge size of 0.7 mm as shown in Fig. 7.3. This refinement is necessary as the dent peak is expected to have high deformation as well as high strain and stresses. Moreover, the mesh at the remainder of the pipe should be kept coarser as it is not going under deformation loading and to optimize solution time. The selection of the appropriate element size was done through a series of convergence checks by increasing the number of elements in the indentation region and until convergence in maximum Von Mises strains and stresses are reached (Fig. 7.5).

7.3.2 Material Model

The material model is identical to the model described in section 6.3.2. The model is multi-linear kinematic hardening defined by three points. The first point is the end of proportional limit, the second point is the material yield stress at 0.5% strain, the third point is the true ultimate tensile strength.

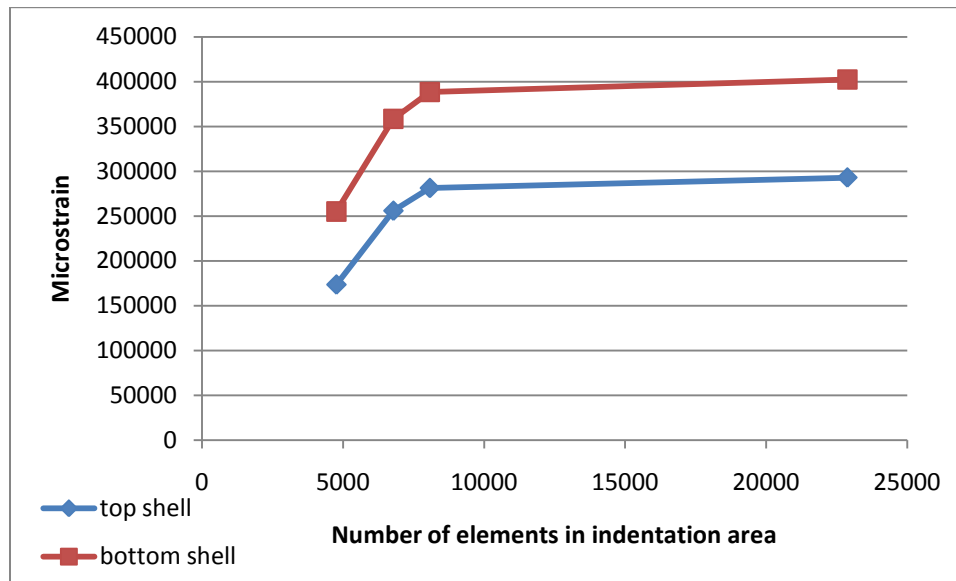


(a)

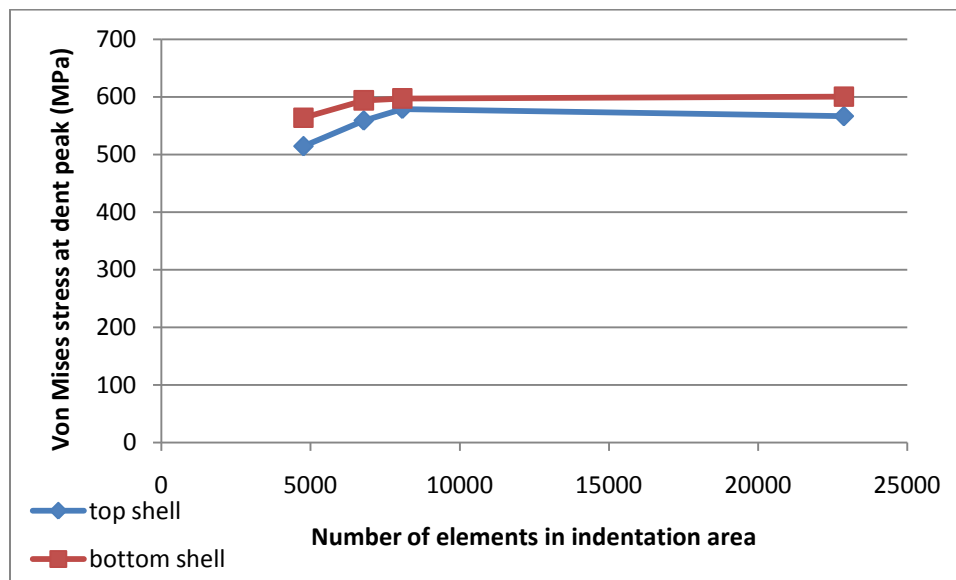


(b)

Figure 7.3. FE mesh at the indentation area for 2 indenters
(a) general (b) zoom at dent peak



(a)



(b)

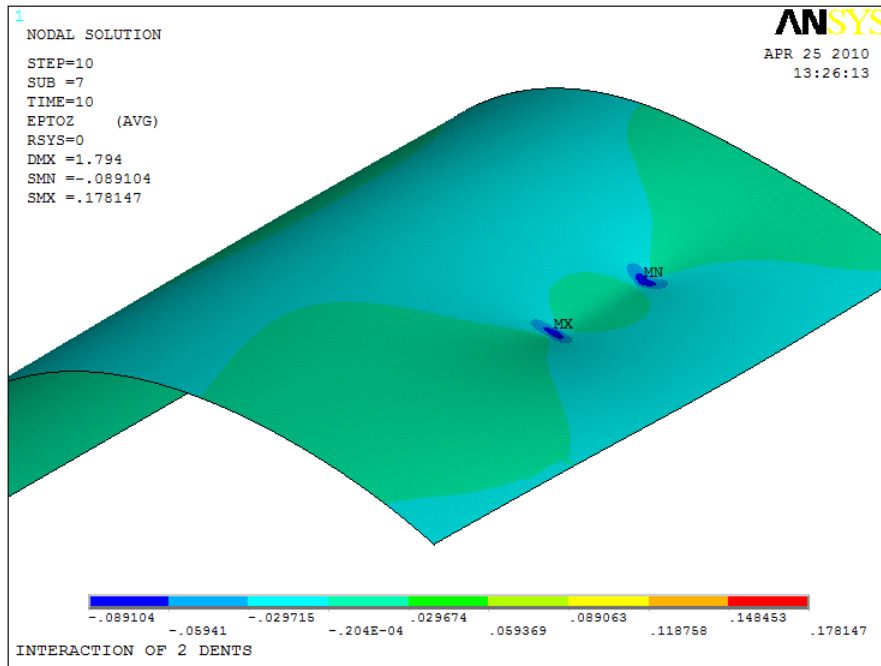
Figure 7.4. Convergence check of pipe with 2 indenters (a) Von Mises strains at dent peak (b) Von Mises stresses at dent peak

7.4 DETERMINISTIC ANALYSIS OF 2 INDENTERS

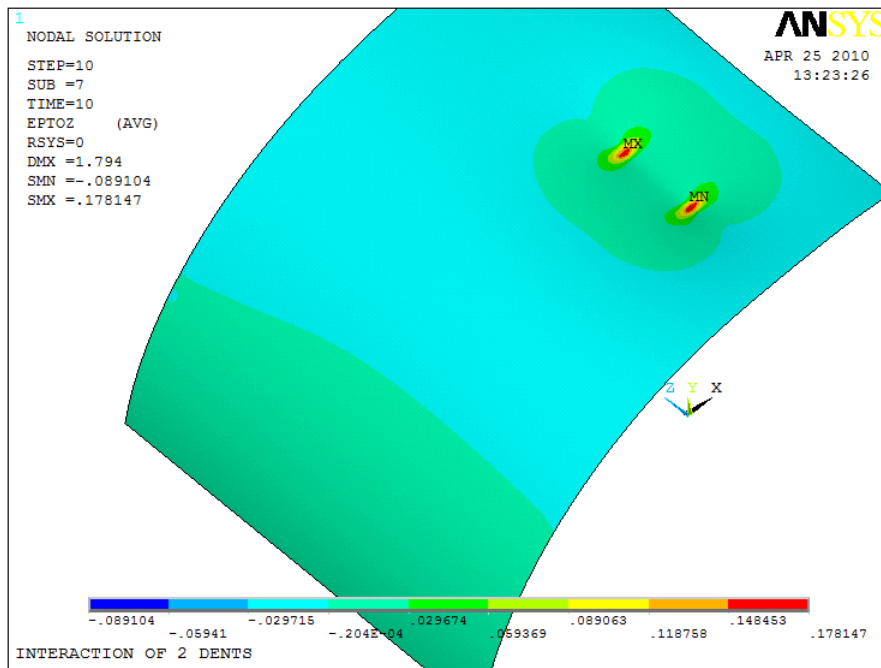
Two deterministic cases of 2 indenters are first investigated and compared with a single indenter case. Both cases are at 0 edge-to-edge distance, i.e. the two indenters are touching. Case I is for orientation 0° , i.e. the two indenters are aligned in pipe longitudinal axis; while Case II is for orientation 90° , i.e. the two indenters are aligned in pipe transverse axis.

7.4.1 Strain Fields at End of Indentation Phase

The axial strain fields are shown in Fig. 7.5 for top and bottom of the pipe shell while the hoop strain fields are shown in Fig. 7.6. The figures indicate that each of the indenters has its own maximum at its peak, and that the strains of the two dent peaks are of comparable profiles. The interaction region is characterized by steep strain gradients as Fig. 7.7.a illustrates. The axial strains on the top shell switch from compressive of value around 9% at the first dent peak to tensile of value around 2% at the interaction region, and then switch again to compressive at the second indenter. For the hoop strains, there are also steep strain gradients in the same interaction region, but the compressive type of strains is still maintained. The single dent case had only one switch point at the axial strains and no switch points in the hoop strains (Fig. 7.7.b). As discussed in Chapter 6, the switch point is close to the indenter periphery and that the crack initiated at this location in the experimental part. Therefore, the magnitude of this strain and its location will be investigated in the probabilistic analysis in addition to the strains at the dent peak.

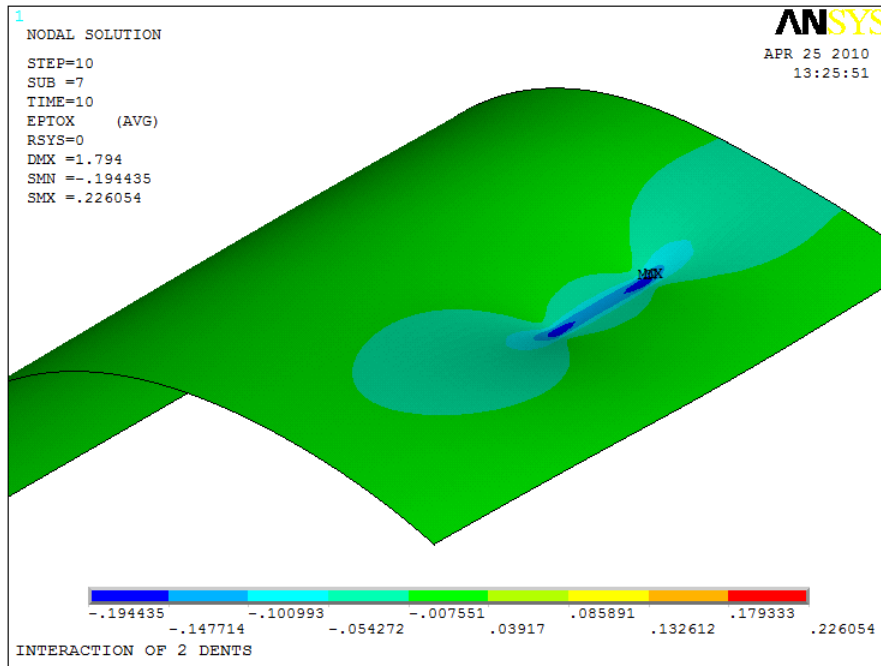


(a)

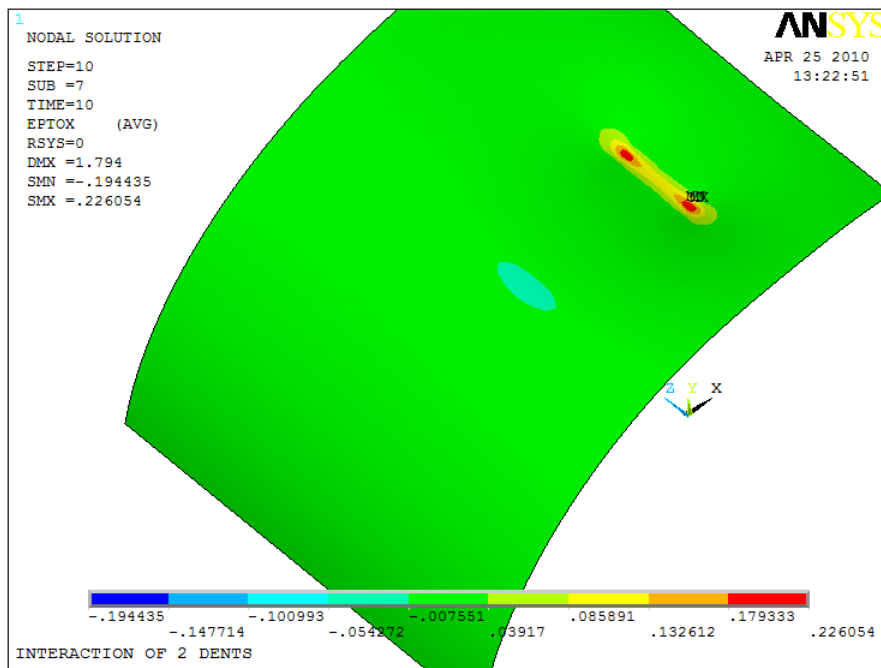


(b)

Figure 7.5. Axial strain profile for 2 dents at (a) top shell (b) bottom shell

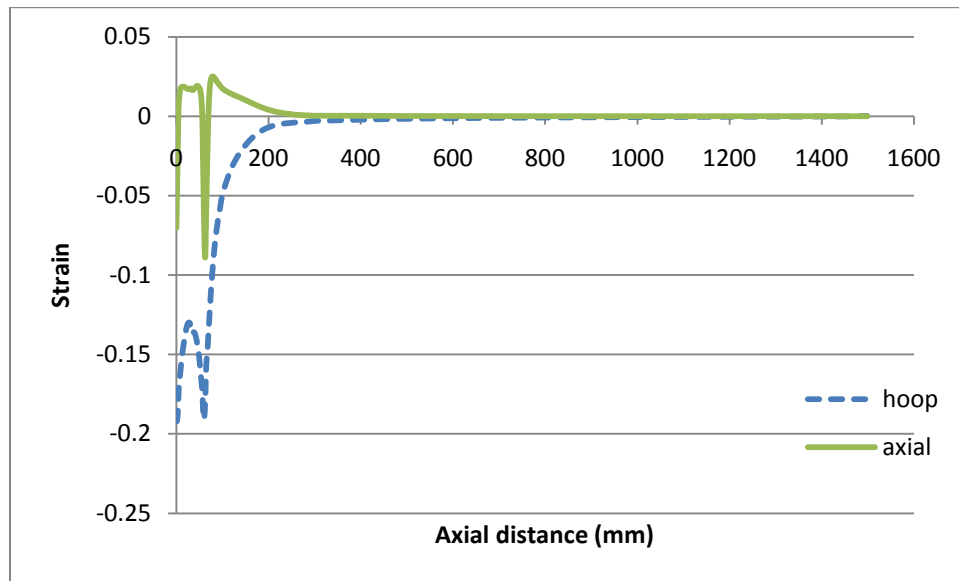


(a)

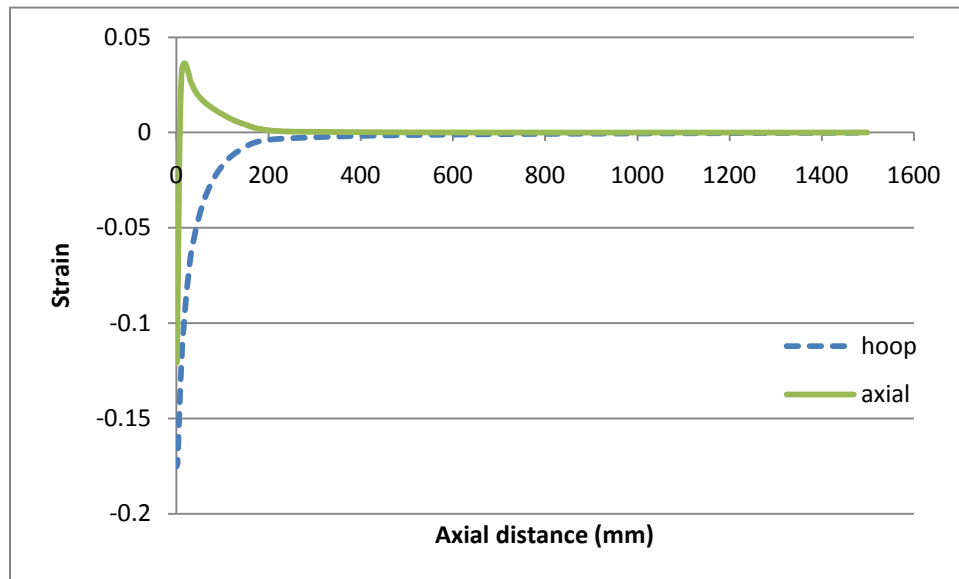


(b)

Figure 7.6. Hoop strain profile for 2 dents at (a) top shell (b) bottom shell



(a)



(b)

Figure 7.7. Strain profile along longitudinal axis from dent peak
(a) 2 dents (b) single dent

Table 7.1 compares the results of the single dent with the results of the interaction of 2 dents. The table indicates that the hoop strains in the top shell are 12.2% higher for the case of 2 dents aligned in the longitudinal direction. The other strains are lower by about 15 to 44%. On the other hand, the axial strains in the top shell are 25.4% higher for the case of 2 dents aligned in the transverse direction while the other strains are lower. Therefore, the strains increase in the direction perpendicular to the alignment of the 2 indenters and decrease in the direction parallel to the alignment. This could be explained by imagining the 2 indenters as one indenter with a larger diameter, and thus, produces smoother dents with less strain values. However, with only these two cases, no general conclusion can be derived on whether the interaction of 2 dents is more or less severe than a single indenter. The probabilistic analysis is expected to provide a better picture as more cases are analyzed.

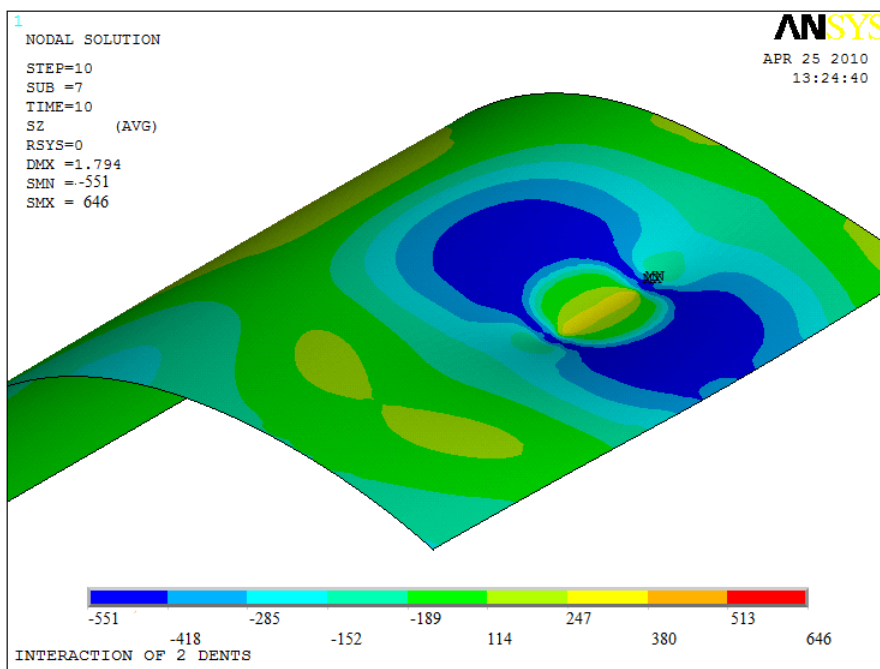
7.4.2 Stress Fields at End of Indentation Phase

The axial stresses are highly compressive (551 MPa) at the dent peaks on top shell side, but they switch to tensile values in the interaction region (Fig 7.8.a). On the bottom shell (Fig 7.8.b), the stresses are maximum tensile (646 MPa) at the dent peaks, but are maximum compressive in the transverse direction to the 2 dents alignment. Therefore, stress values at those locations should be captured in the probabilistic analysis as they present points of interest in the mechanical damage assessment.

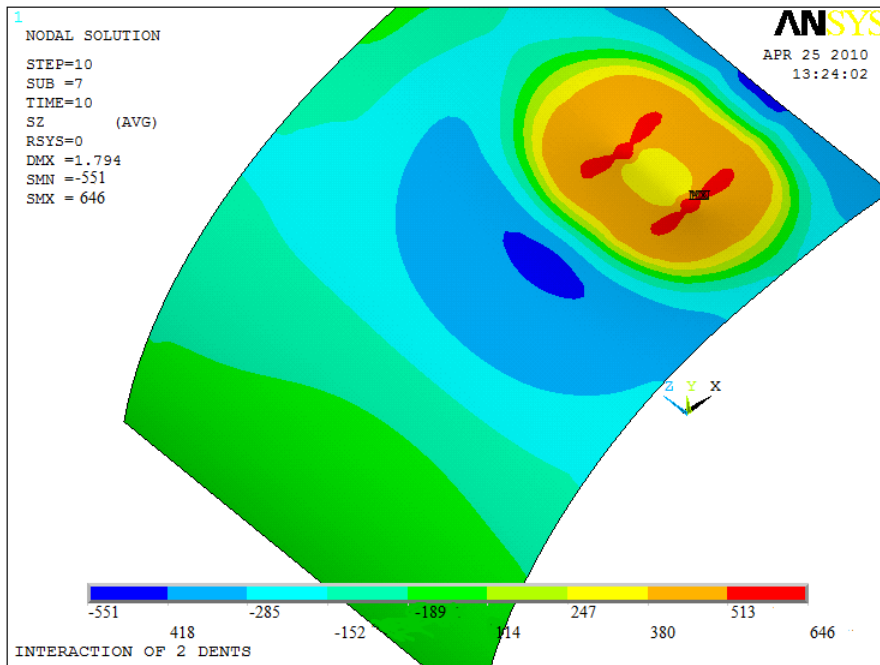
For the hoop stress field, Fig. 7.9.a indicates the existence of very high compressive stresses on top shell (383 to 672 MPa) at the dent peaks and in the region between them.

Table 7.1 Comparison of results between single dent and 2 dents

Parameter	Single dent	Case I: 2 dents along longitudinal axis		Case I: 2 dents along transverse axis	
	Value	Value	% difference	Value	% difference
Strains at end of indentation stage					
Axial, top shell	-0.114	-0.071	-38.1	-0.143	25.4
Axial, bottom shell	0.238	0.133	-44.3	0.197	-17.4
Hoop, top shell	-0.171	-0.192	12.2	-0.131	-23.6
Hoop, bottom shell	0.263	0.223	-15.0	0.149	-43.4
Stresses at end of indentation stage					
Axial, top shell	353	-335	-194.8	-28	-108.0
Axial, bottom shell	648	630	-2.8	577	-10.9
Hoop, top shell	313	-651	-307.9	-472	-250.7
Hoop, bottom shell	531	548	3.3	619	16.7
Stress range and fatigue life for cyclic pressure load					
Stress range	234	201	-14.0	163	-30.6
Mean stress	136	63	-53.5	121	-10.9
Fatigue life	78,262	1,926,141,765	2,461,059	2,518,871	3,118

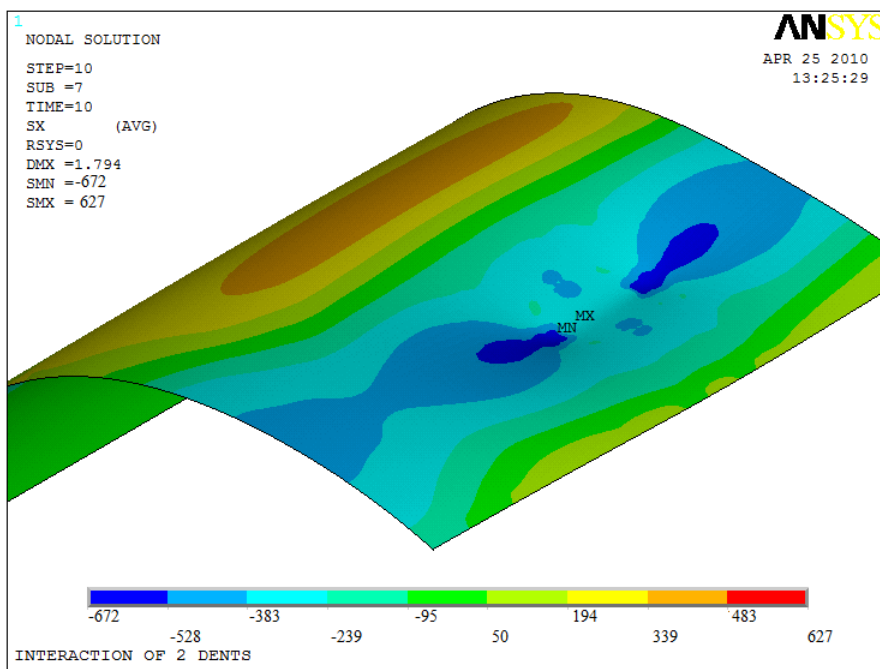


(a)

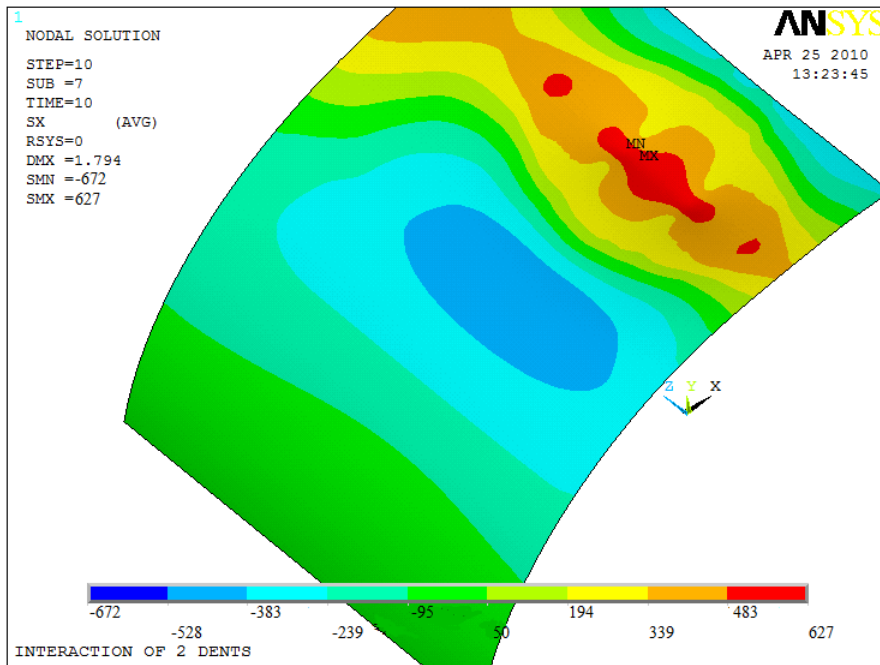


(b)

Figure 7.8. Axial stress profile for 2 dents at (a) top shell (b) bottom shell



(a)



(b)

Figure 7.9. Hoop stress profile for 2 dents at (a) top shell (b) bottom shell

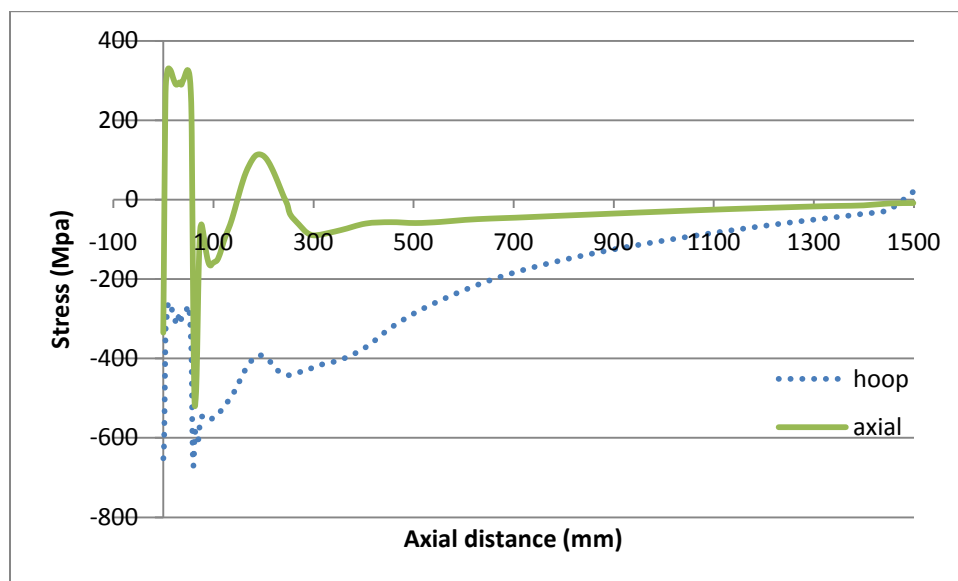
On the bottom shell (Fig. 7.9.b), there are three points of maximum tensile stress (627 MPa); at the dent peaks and at the midpoint between the 2 dents.

Figure 7.10 gives the stress profile along the pipe longitudinal direction for the case of single dent and 2 dents. The figure clearly shows the existence of steep stress gradients in the region between the 2 dents. API 1156 (1999) indicated that leak developed in the interaction area between the 2 dents in two of the ten experimental cases conducted. Therefore, the stresses at the midpoint between the two indenters must be considered in the probabilistic analysis.

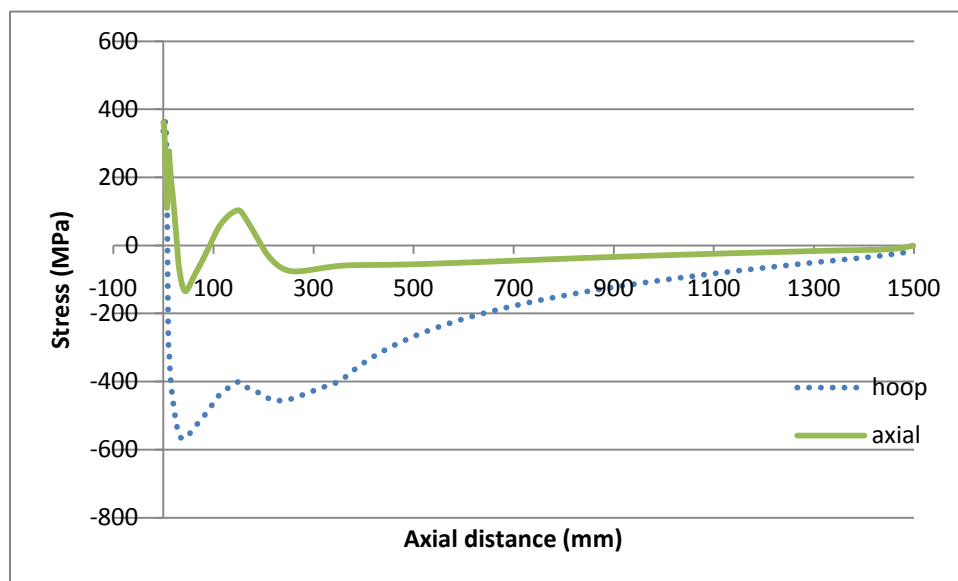
Table 7.1 lists the stress values at the dent peaks of single dent as well as the two cases of 2 dents. There is no clear trend in the change of stress values as some stress parameters increase, while other decrease. Moreover, some stress values switch their sign. This is attributed to the fact that the stress contours of the 2 dents change significantly from the single dent. Therefore, probabilistic analysis would be the best method to derive the right conclusions.

7.4.3 Stress Range at End of Pressure Cycle and Fatigue Analysis

Table 7.1 gives the stress range and fatigue cycles for the case of single dent and the two cases of 2 dents. The mean stress and stress range of the 2 dents decreases by 11 to 54% compared to the single dent, and accordingly, the fatigue life becomes infinite. The reason behind this is that the two dents act like a single larger dent which produces less severe dent profiles and stress ranges. However, this cannot be generalized to all 2 dent cases. Table 7.2 gives a comparison between single dent and 2 dents, but of shallow dent depth. In this circumstances, the stress range increases considerable by about 63%



(a)



(b)

Figure 7.10. Stress profile along longitudinal axis from dent peak
 (a) 2 dents (b) single dent

Table 7.2. Comparison of results between single dent and 2 dents for shallow dent depth (2% of pipe diameter)

Parameter	Single dent	2 dents	
	Value	Value	% difference
Strains at end of indentation stage			
Axial, top shell	-0.058	-0.023	-60.7
Axial, bottom shell	0.057	0.017	-70.4
Hoop, top shell	-0.083	-0.029	-65.4
Hoop, bottom shell	0.076	0.019	-74.8
Stresses at end of indentation stage			
Axial, top shell	-634	-564	-11.1
Axial, bottom shell	639	571	-10.6
Hoop, top shell	-701	577	-182.3
Hoop, bottom shell	685	-610	-189.0
Stress range and fatigue life for cyclic pressure load			
Stress range	346	329	-4.8
Mean stress	132	215	62.9
Fatigue life	661,195	3,182	-99.5

leading to drop in fatigue life to only 3,180 cycles vs. 661,000 for the single dent. Therefore, the impact of interaction of 2 dents could change the fatigue life from finite to infinite for deep dents, and from infinite to finite for shallow dents. The probabilistic analysis will be used to verify this conclusion.

7.5 PROBABILISTIC ANALYSIS

The input parameters of the dent problem can be classified into three categories: material, geometry, and pressure loading. Additional category is included for the case of 2 dents which includes the distance between the indenters and the orientation angle. Each of these input parameters have a wide range of values. Moreover, each nominal value of these parameters has its own variability due to manufacturing tolerances, measurement uncertainties, etc. Accordingly, hundreds of random combinations of input parameters are possible. Therefore, the use of probabilistic design analysis offers an excellent way to study the problem and determine the sensitivity of the strain and stress fields to each of those input parameters.

7.5.1 Random Input Variables

Table B.2.1 lists the random input variables, their distribution, and distribution parameters for the 2 interacting dents. The input variables are grouped in four categories: material, geometry, loading, and 2-dent interaction. The statistical distribution of the first three categories is the same as for the plain dent case. The statistical distribution of the distance between the two dents is varied uniformly from 0 to $2\sqrt{Rt}$, the onset distance of interaction as reported by Francini and Yoosef-Ghodsi (2008). The orientation angle is

varied between 0 and $\pi/2$ to cover the range between the terminal cases of 2 dents aligned in the longitudinal axis to 2 dents aligned along the transverse axis.

7.5.2 Probability Analysis Loops

The probability analysis is conducted using ANSYS PDA module (2007) with a total of 100 analysis loops to compute the random output parameters in terms of the random input variables. The values of the input variables are generated randomly using Monte Carlo simulation to find how the scatter in the input variables affect the output results and which input variable is the most significant.

7.5.3 Probability Analysis Results

Table B.2.2 gives a summary of all output results (dent dimensions, strains, stresses, and stress range) along with their statistical distribution for the case of interaction of 2 dents. Two output variables are of primary interest for discussion: the fatigue life as it was found from the deterministic case to be sensitive to the interaction, and the stress range at the midpoint between the two dents as it was reported by API 1156 (1999) to be the point of crack initiation in cyclic loading. The sample history of the fatigue life is given in Fig.7.11 which indicates a very random nature of the fatigue life as it ranges between few cycles to infinite life. However, the histogram presented in Figure 7.12 shows the majority of the cases have relatively low fatigue life. Around 44% of the cases have a fatigue life of only about 550 cycles. The reason behind the high percentage of the low fatigue life is that majority of the cases have low shallow dent as defined in the input parameters. It was found in section 7.4.3 that shallow dents pose a threat in case of interaction of 2 dents.

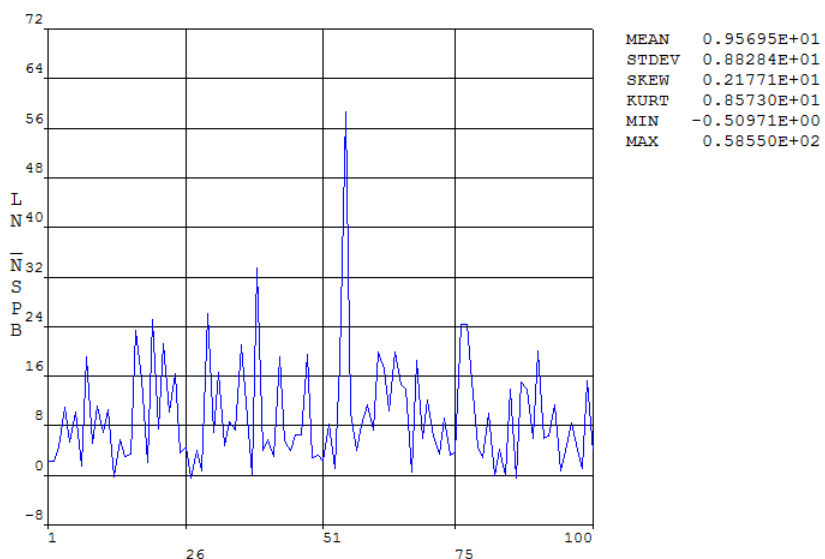


Figure 7.11. Sample history of natural log of fatigue life of pipe with 2 dents

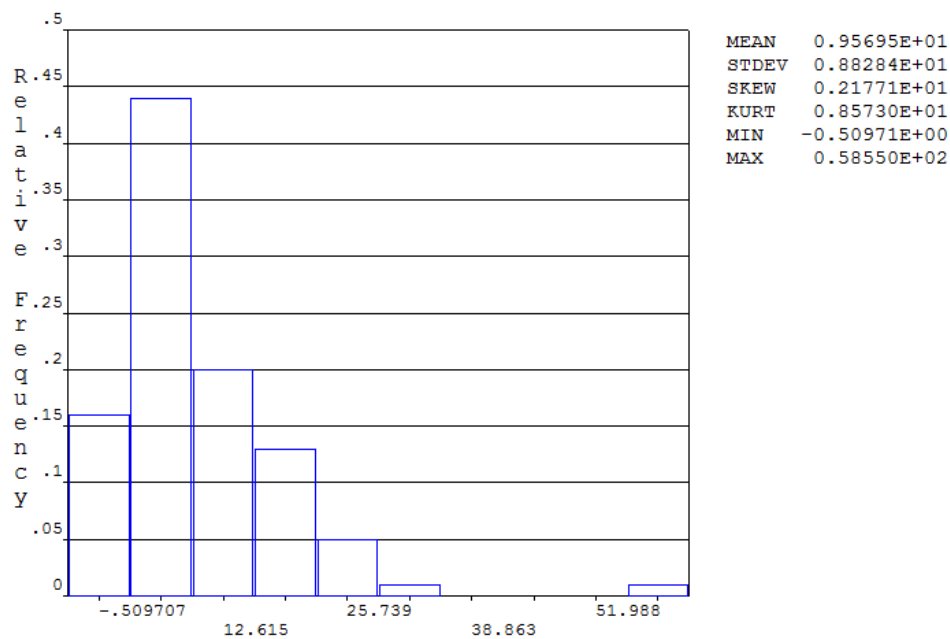


Figure 7.12. Histogram of natural log of fatigue life of pipe with 2 dents

The statistical distribution of the output can be useful to calculate a quick estimate of probability of failure without even measuring the dent dimensions to be used with risk assessment. Table 7.3 compares the probability of failure in terms of fatigue life for the case of single dent vs. the cases of 2 dents. The table shows that the probability of failure of the interaction of 2 dents is 3 to 7 times greater than that of a single dent. Accordingly, interaction of 2 dents poses a risk higher by 3 to 7 times of that of a single dent on the integrity of the pipeline under cyclic pressure.

Sensitivity analysis is performed to find out which input variable(s) affect each of the output variables. Figure 7.13 shows that the dentpercent is the primary parameter in determining the fatigue life in the case of the 2 dents with a strong positive correlation of 0.93. This means the shallower the dent depth, the less the fatigue life of pipe with 2 dents, which is in line with the conclusion of 7.4.3. The orientation angle between the 2 dents is the second most important parameters affecting the fatigue life of the pipe. There is a positive correlation between fatigue life and the orientation angle (Fig. 7.14), i.e. the 0 angle (2 dents aligned in the longitudinal direction) is more severe than the $\pi/2$ angle (2 dents aligned in the transverse direction). Figure 7.15 shows that there is a positive correlation between the distance between 2 indenters and the fatigue life, i.e. the farther separated the two indenters, the more the fatigue life. The correlation factor, only 0.0724, is quite weak. This could be explained by the original selection of distance values in the input variables as it was defined in a range that is known to have interact effect.

Table 7.3 Probability percentage of failure for pipe with 2 dents

Life	Single dent	2 dents
1,000	6.8	50.4
5,000	10.2	57.8
10,000	12.2	59.4
50,000	17.9	65.9
100,000	18.5	69.9
500,000	21.2	71.8
1,000,000	22.8	72.6

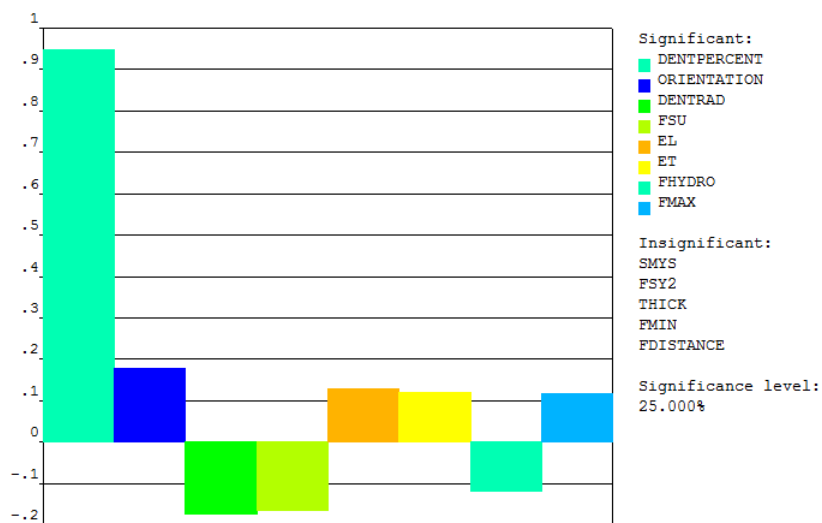


Figure 7.13. Sensitivity plot of natural log of fatigue life for pipe with 2 dents

Note: Legend top-to-bottom order matches left-to-right order in figure

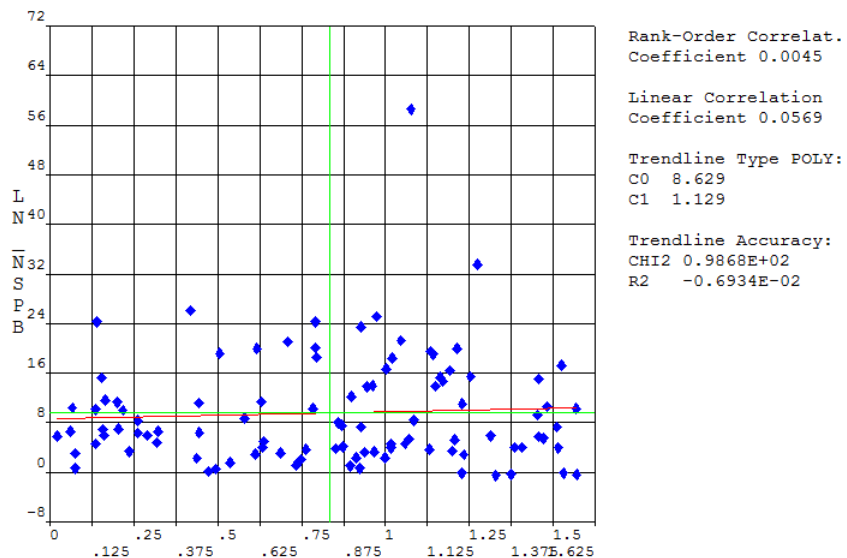


Figure 7.14. Scatter plot of fatigue life vs. orientation angle between 2 indenters

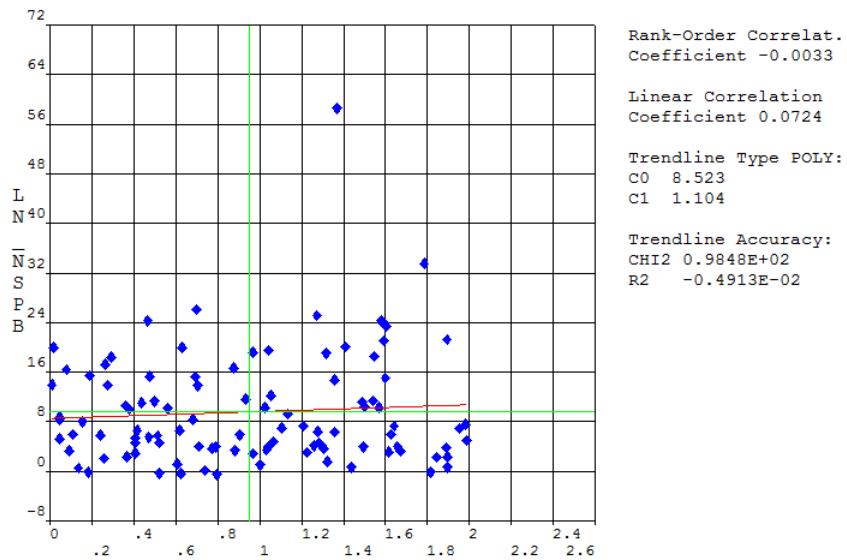


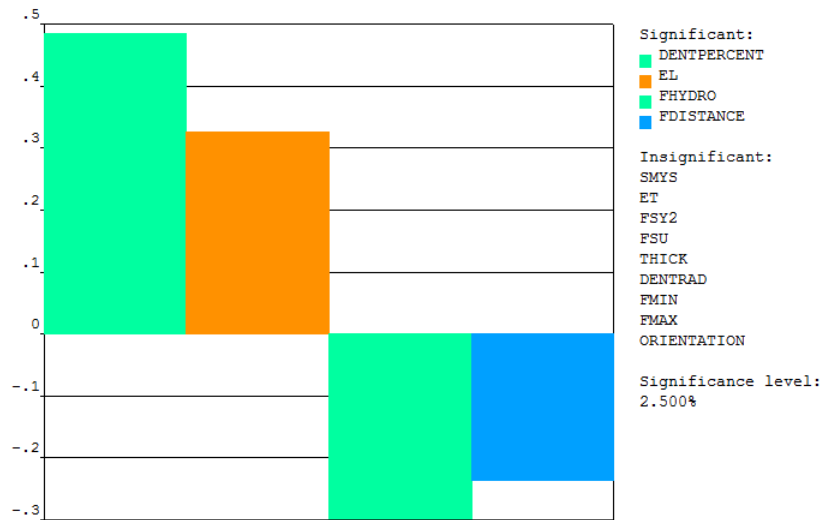
Figure 7.15. Scatter plot of fatigue life vs. distance between 2 indenters

For the stresses at the midpoint between the 2 indenters, Fig. 7.16.a shows the sensitivity plot of the mean stress while Fig. 7.16.b shows the stress range. The mean stress is sensitive to the dent percent, modulus of elasticity, hydrotest pressure, and the distance between the indenters. The mean stress has quite strong negative correlation of magnitude around 0.22 with the distance, i.e. the closer the 2 dents, the higher the mean stress value. On the other hand, the stress range is highly sensitive to the orientation with a very strong positive correlation of 0.65 meaning that the stress range is higher for 2 dents aligned in the transverse direction. The full correlations are listed in Table B.3.2.

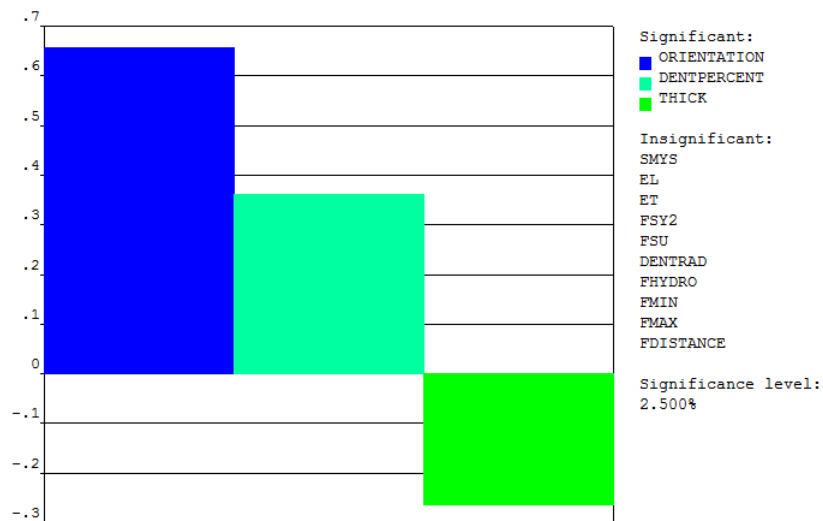
7.5.4 Regression Analysis

In order to make the results of the probabilistic analysis to be easily applied in practical 2 dents problems, regression analysis is conducted to derive mathematical formulas of the output variables in terms of practically measured variables. Quadratic polynomial functions are the best fit for a similar problem as stated in section 6.5.4. Therefore, the following general function (Equation 7.1) was fit to all output variables where all output and input variables in dimensionless form. The two terms associate with pressure range are only applicable to output stress range and fatigue life.

$$\begin{aligned}
 \text{Output variable} = & a_0 + b_1 \frac{D}{t} + b_2 \frac{d}{D} + b_3 \frac{l}{D} + b_4 \frac{w}{D} + b_5 \frac{ldw}{D^2t} + b_6 \frac{\sigma_{flow}}{E_{avg}} + b_7 \frac{E_t}{E_l} + \\
 & + b_8 \frac{d_{e-e}}{\sqrt{0.5 \times Dt}} + b_9 \emptyset + b_{10} \frac{P_{max} - P_{min}}{P_{SMYS}} + c_1 \left(\frac{D}{t}\right)^2 + c_2 \left(\frac{d}{D}\right)^2 + c_3 \left(\frac{l}{D}\right)^2 + c_4 \left(\frac{w}{D}\right)^2 + \\
 & c_5 \left(\frac{ldw}{D^2t}\right)^2 + c_6 \left(\frac{\sigma_{flow}}{E_{avg}}\right)^2 + c_7 \left(\frac{E_t}{E_l}\right)^2 + c_8 \frac{d_{e-e}}{\sqrt{0.5 \times Dt}}^2 + c_9 \emptyset^2 + c_{10} \left(\frac{P_{max} - P_{min}}{P_{SMYS}}\right)^2
 \end{aligned} \tag{7.1}$$



(a)



(b)

Figure 7.16. Sensitivity plot of stresses at the midpoint between 2 dents
(a) mean stress (b) stress range

Note: Legend top-to-bottom order matches left-to-right order in figure

Table B.2.4 gives the constants values and R-squared value for the regression fit of all output variables of strain, stress, stress range, and fatigue life for the case of 2 interacting dents. The R-squared value is higher than 0.5 in 40 out of 45 output variables which indicate that the proposed general formula (7.1) is a very good choice. Figure 7.17 shows the regression curve for the axial strain at dent peak which has a very good fit of R-squared 0.78. The regression fit for the output stress variables is also excellent as Fig. 7.18, regression fit curve for axial stress at dent peak for interaction of 2 dents, illustrates with R-squared of 0.90. The regression curve of the natural log of the fatigue life is given in Fig. 7.19 which shows very good correlation with R-squared value of 0.66. The regression fit of the mean stress and stress range at the midpoint between the 2 dents is also very good as Fig. 7.20 illustrates with an R-squared value of 0.67 and 0.83 respectively.

7.6 SUMMARY

In this chapter, the effect of interaction of 2 dents was investigated using both deterministic analysis and probabilistic analysis. In the deterministic analysis, two cases were analyzed; one for two dents aligned in the longitudinal direction and the second for the two dents aligned in the transverse direction. The results showed that the strains perpendicular to the dents alignment increase while the others decrease in comparison with the single dent. The stress values do not show a clear trend. For the fatigue cycle, the life shifted from finite in the case of single dent to infinite in the case of 2 dents as the 2 dents act like a combined larger dent with smoother profile. However, in the case of

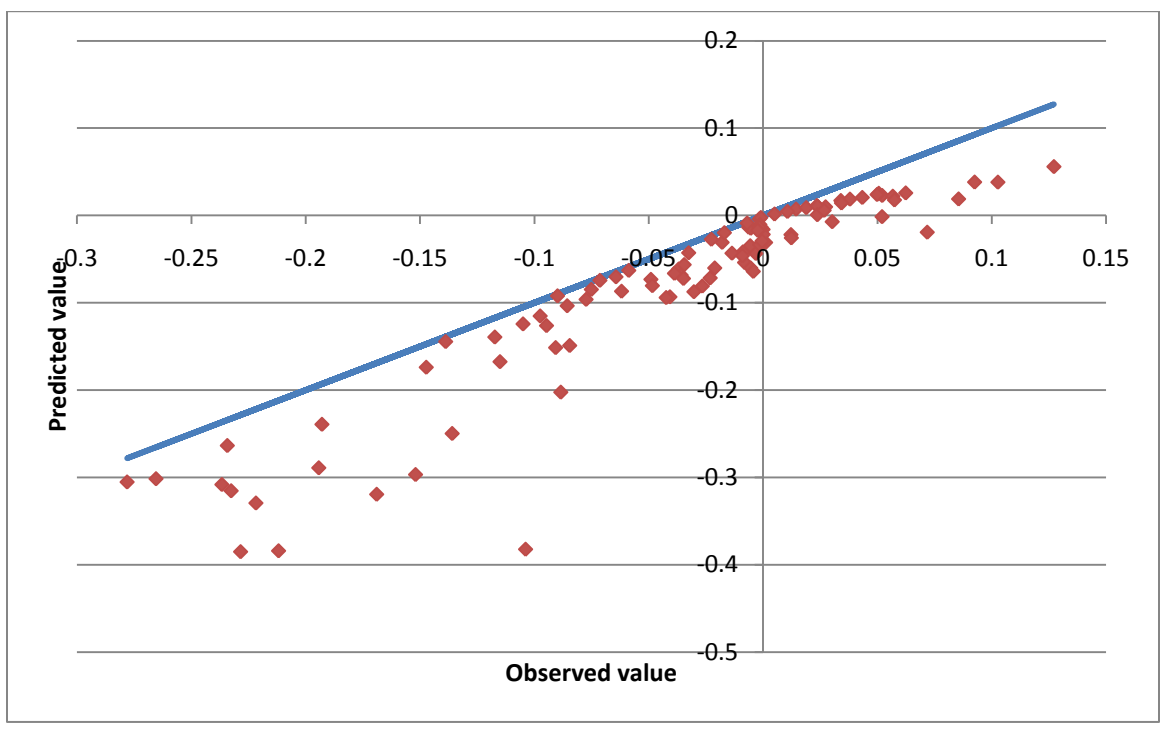


Figure 7.17. Regression fit curve for axial strain at dent peak for interaction of 2 dents

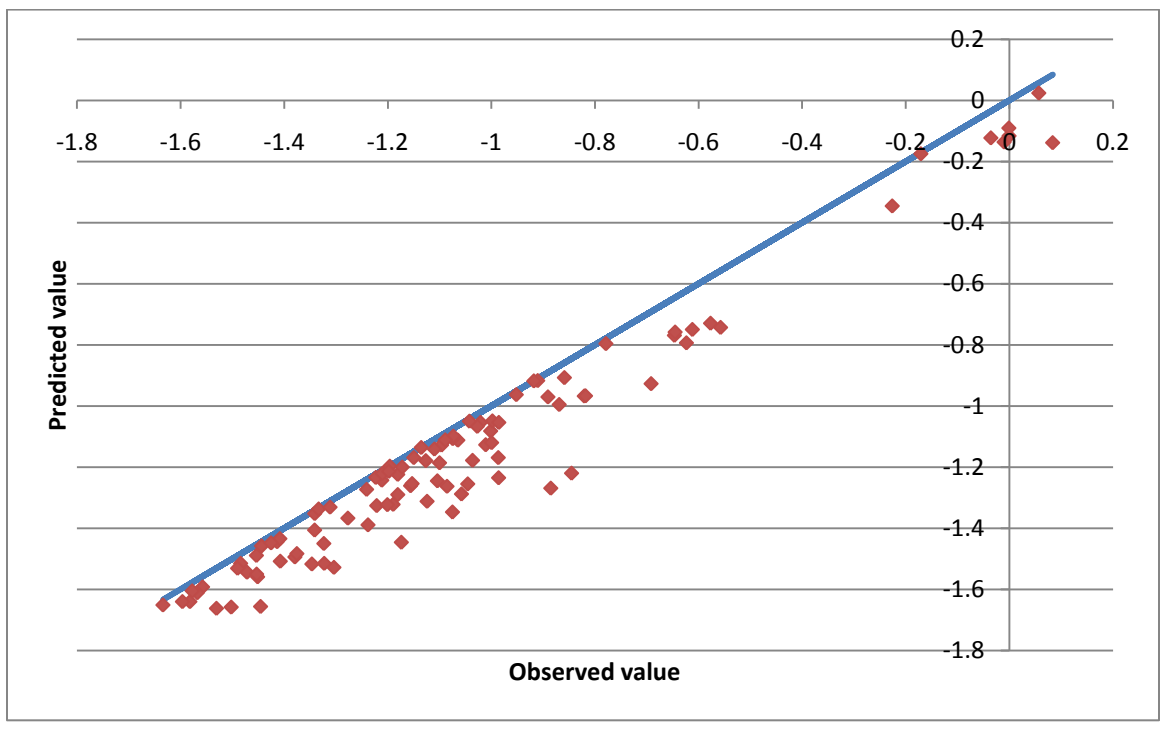


Figure 7.18. Regression fit curve for axial stress at dent peak for interaction of 2 dents

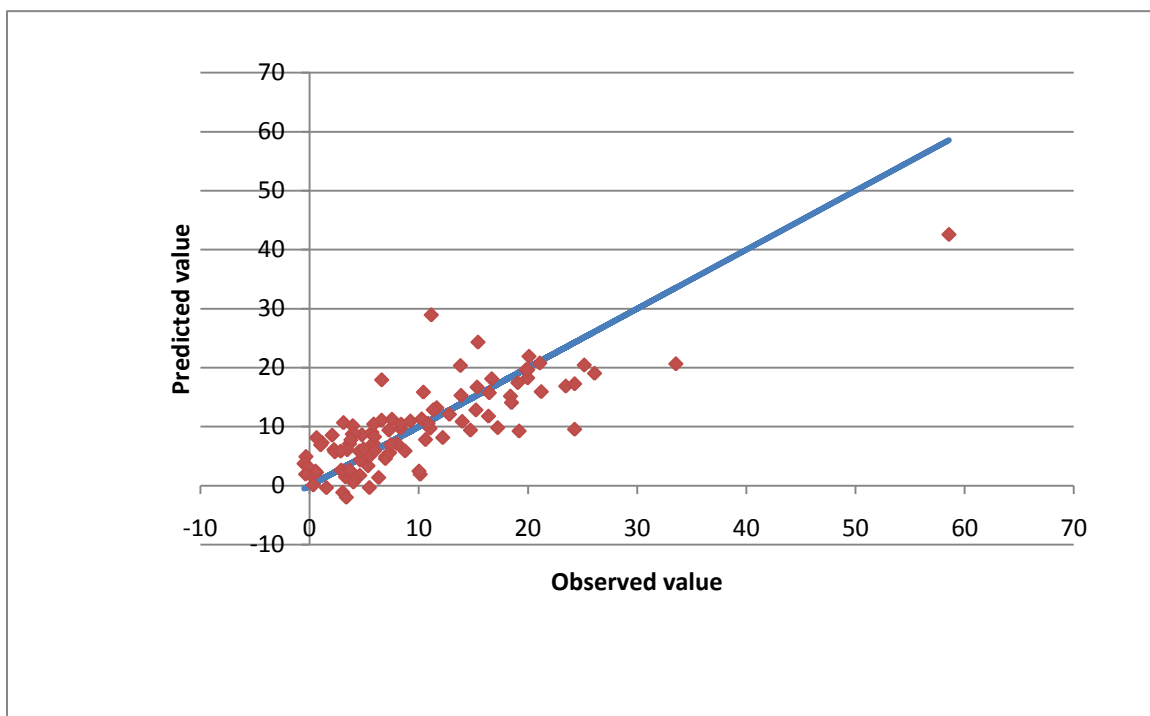
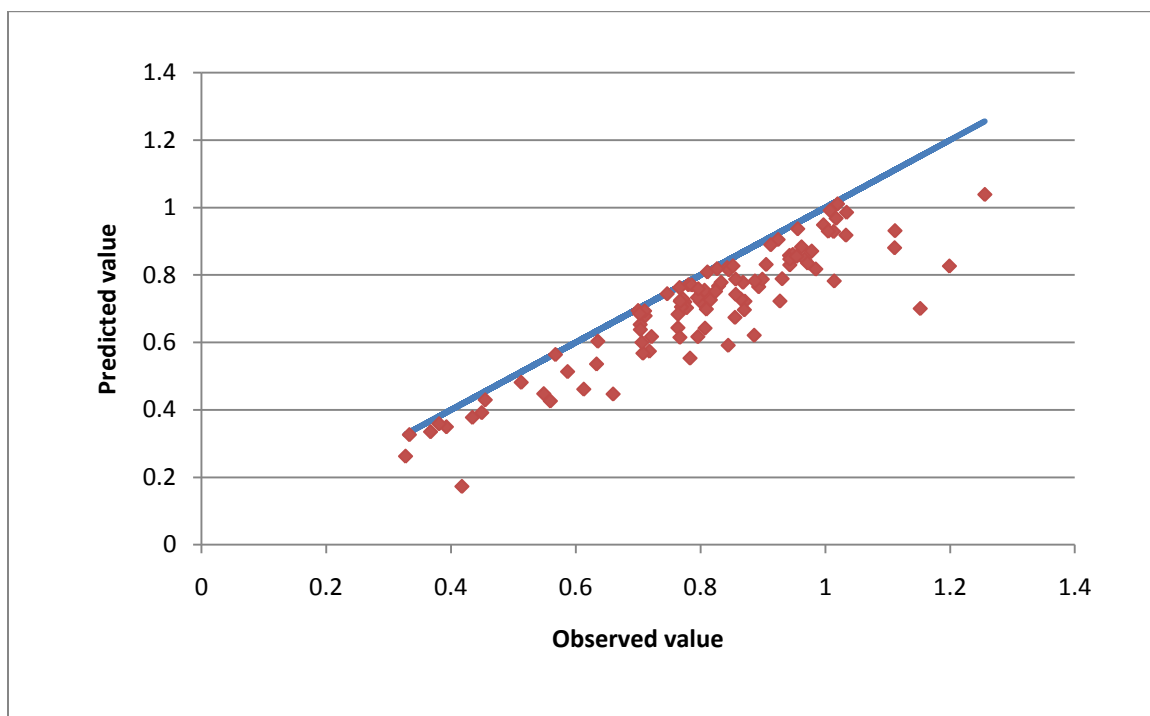
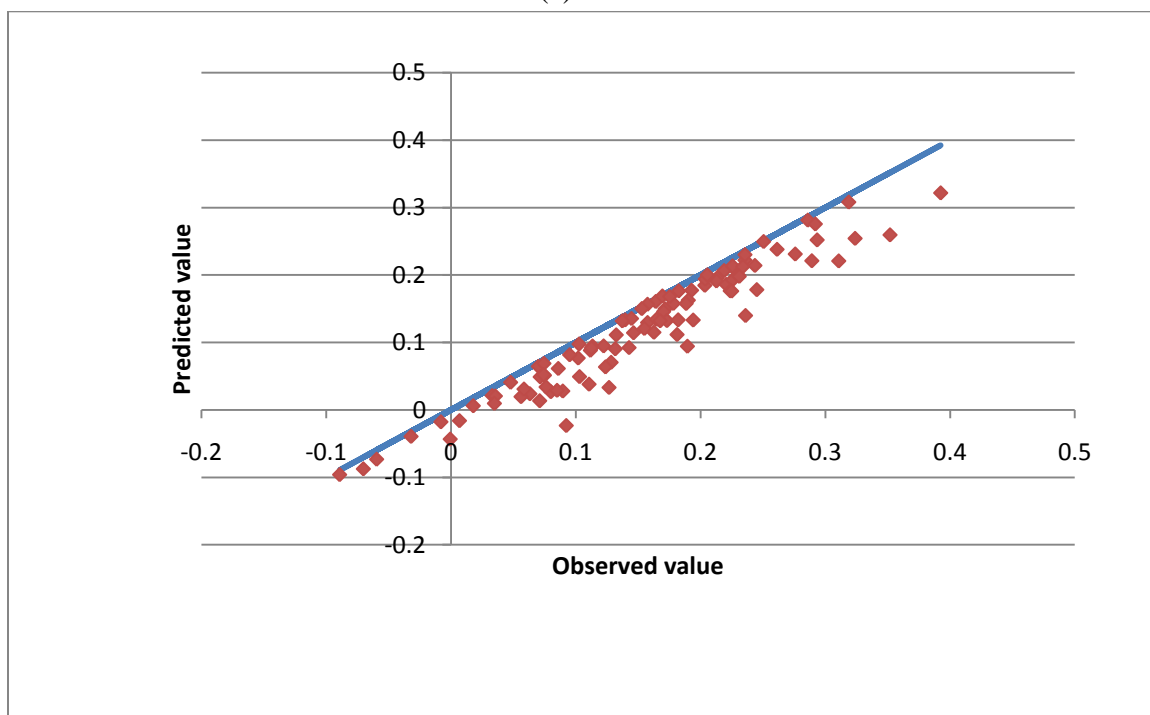


Figure 7.19. Regression fit curve for natural log of fatigue life for interaction of 2 dents



(a)



(b)

Figure 7.20. Regression fit curve for stresses at midpoint between the 2 indenters
(a) mean stress (b) stress range

shallow dents, it turned that the fatigue life of the 2 dents is very low and poses a threat to the pipeline. In the probabilistic analysis, a total of 100 cases of two interacting dents were randomly generated using Monte Carlo simulations were analyzed. The statistical distribution of output parameters and correlation between output and input variables were presented. The results showed that the probability of failure of 2 interacting dents is 3 to 7 times higher than that of plain dent which increases the failure risk proportionally. Additionally, the sensitivity of strain and stress fields as well as the fatigue life to the various input parameters was determined. There was a positive correlation between the fatigue life and both the distance on orientation angle between the two dents, i.e. the farther the dents are and the more offset in the transverse direction, the longer the fatigue life. Moreover, the fatigue life had a very strong positive correlation with the dent percent, which indicates that shallow 2 dents post higher risk to pipelines than deeper ones. Finally, a general formula was proposed to relate the output variables in terms of practically measured variables. Regression analysis was conducted to derive the coefficients and the results showed the general formula was a good choice. The R-squared values were higher than 0.5 in most of the cases and reaching values as high as 0.94 proving to be a very good choice.

CHAPTER 8

IMPACT OF INTERACTION OF DENT WITH METAL LOSS

8.1 INTRODUCTION

Metal loss can occur gradually in the dented pipe due to corrosion which is usually accelerated as the protective coating layer is also damaged. Semiga (December 2007) surveyed pipeline operators to collect data of damage reported by ILI as well field dig inspection. The survey showed that rock dents often tend to be associated with corrosion. This is due to the fact that the rock will also damage the protective coating layer.

Metal loss can also happen intentionally as gouges associated with dents are normally removed by grinding. The current codes and practice conduct separate assessments for dents with metal loss, i.e. the dent is assessed based on the maximum depth or maximum strain criteria while the metal loss is assessed based on the metal loss depth and length. ASME B31.8 (2007) states that dents with metal loss are injurious if they exceed 6% depth or the corrosion exceeds the code criteria given in Appendix L of the Code. It allows removal of gouge associate with dent such that it is limited 10% of the wall thickness or up to 40% of the wall thickness with restrictions on the grinding length. CSA Z662 (2003) requires engineering assessment of dents with metal loss more than 40% of

the thickness or as low as 10% if corrosion defect length exceed the maximum allowable by the code. ASME B31.4 (2006) limits the acceptable maximum metal loss associated with dent to only 12.5% of the original thickness. In all the reviewed literature, there are no assessment procedures that consider the dent with metal loss as a combined damage.

In this chapter, a combined damage of dent with metal loss will be analyzed to determine the strain and stress fields as well as fatigue life of pipe under static and cyclic pressure. The first part of the chapter uses deterministic analysis to present strain and stress contours at the end of indentation stage as well as the stress range and fatigue cycles at the end of pressure cycle stage for metal loss of 12.5% as well as 50% of the original wall thickness. The second part uses probabilistic design analysis with variable geometry, material and pressure in addition to the metal loss percentage to determine the sensitivity of the strain, stress, and stress range to the input.

8.2 DESCRIPTION OF THE PROBLEM

The problem is similar to that described in section 4.2 of the dissertation, but with having a localized metal loss area that is concentric with the indenter and of 100 mm radius. The layout of the problem is shown in Fig. 8.1.

8.3 DESCRIPTION OF THE NUMERICAL MODEL

A quarter of the pipe is used due to the symmetry in geometry, loading and boundary conditions. Symmetry boundary conditions are applied in the two symmetry planes. The metal loss is modeled by defining a second set of real constant thickness of the shell element in the metal loss area with a value that is a factor of the pipe original wall

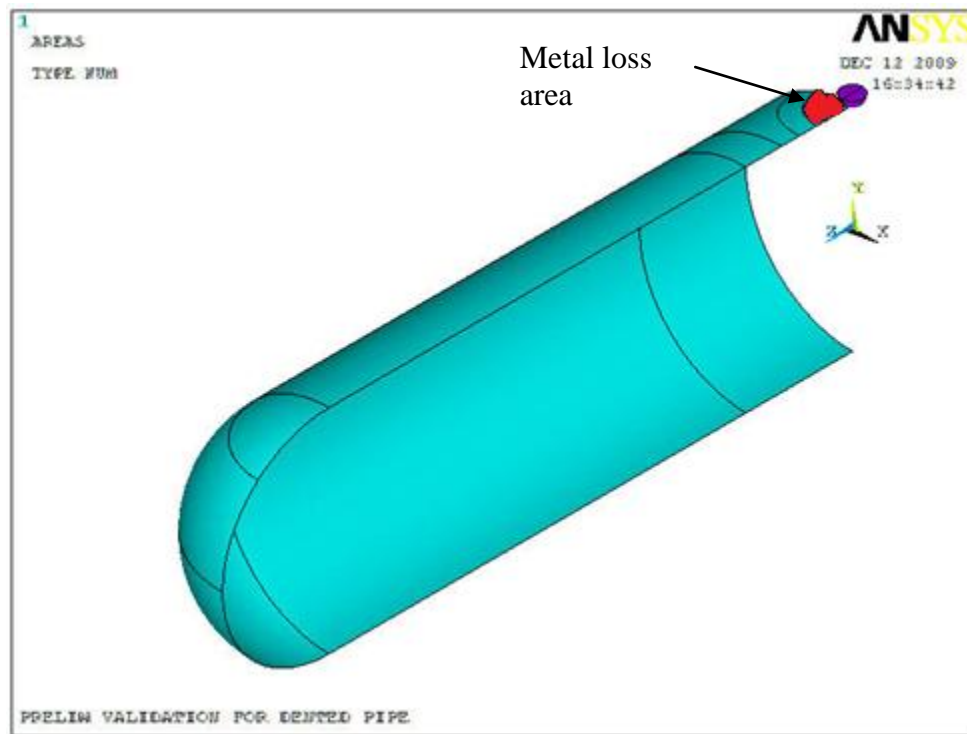


Figure 8.1. Illustration of pipe with combined damage of dent with metal loss.

thickness. The indentation process is modeled by a contact pair of rigid target with pilot node. A vertical load displacement is applied on the target in small load steps until it reaches the target depth. After that, two pressure cycles are applied. The first one is simulating the hydrostatic pressure test and the second cycle simulates the operating pressure range.

8.3.1 FE Model

Elements used are shell element 181 (4-nodes). For the contact pair, the indenter is modeled with Target 170 while the contact areas are modeled with Contact 174. Similar mesh to that describe in section 4.3.1 is used.

8.3.2 Material Model

The material model is identical to the model described in section 4.3.2. The model is multi-linear kinematic hardening defined by three points. The first point is the end of proportional limit, the second point is the material yield stress at 0.5% strain, and the third point is the true ultimate tensile strength.

8.4 DETERMINISTIC ANALYSIS OF DENT WITH METAL LOSS

Two deterministic cases of metal loss of 12.5% and 50% are first investigated and compared with no-metal loss indenter case. The strain and stress fields as well as the stress range and fatigue life are evaluated.

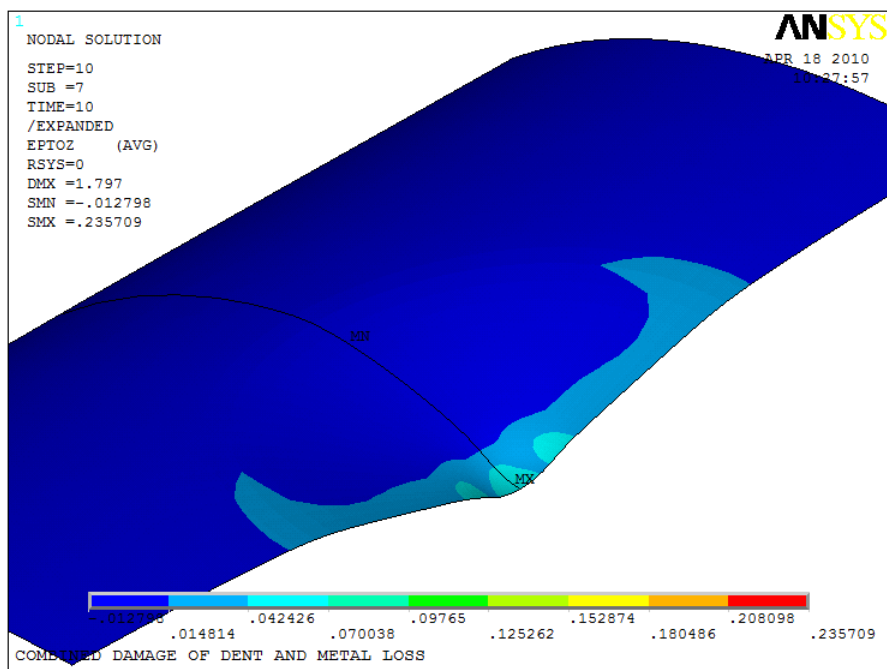
8.4.1 Strain Fields at End of Indentation Phase

The axial strain fields are shown in Fig. 8.2 for top and bottom of the pipe shell while the hoop strain fields are shown in Fig. 8.3. The figures show that the strains on the top shell are lower in the dent peak, which is coincident with the metal loss, than they are in the surrounding pipe area that does not have metal loss. This is attributed to the flexibility in the metal loss area because of less wall thickness. At the bottom shell, the strains are maximum at the peak similar to the case of no metal loss, but they are of lower magnitudes.

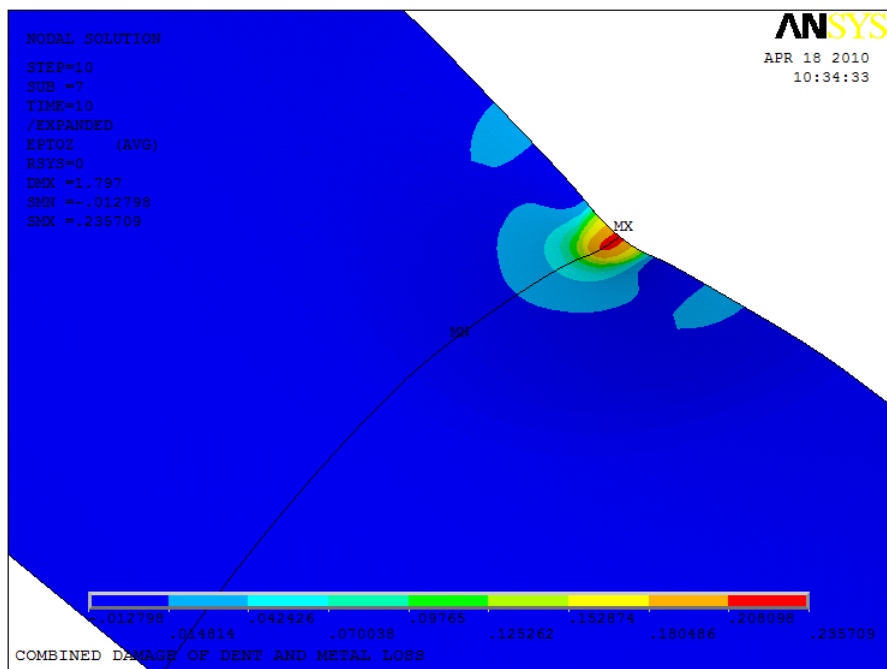
Table 8.1 compares the values of the strains the two metal loss cases with reference to the no metal loss case. The table shows that the strains decrease in the case of 12.5% metal loss at a percentage of 11.7 to 28.5% of the base case with no metal loss. The decrease is even higher for the 50% metal loss and it ranges between 32% and 153%. This is attributed to the fact that the thinner section has lower stiffness and thus more flexible to deform. This also agrees with the formula given in ASME B31.8 (2007) where the strains are directly proportional to the thickness.

8.4.2 Stress Fields at End of Indentation Phase

The stresses are very high in the dent peak both at top and bottom shell as shown in Fig 8.4 and 8.5. The axial stresses reach a value of 659 MPa which exceeds the tensile strength of the pipe indicating that this case of 7.5% dent and 50% corrosion is a severe one and might fail under the static loading of denting without even pressure application. The hoop stresses are also high and reach a maximum value of 589 MPa but they are lower than the axial stresses.

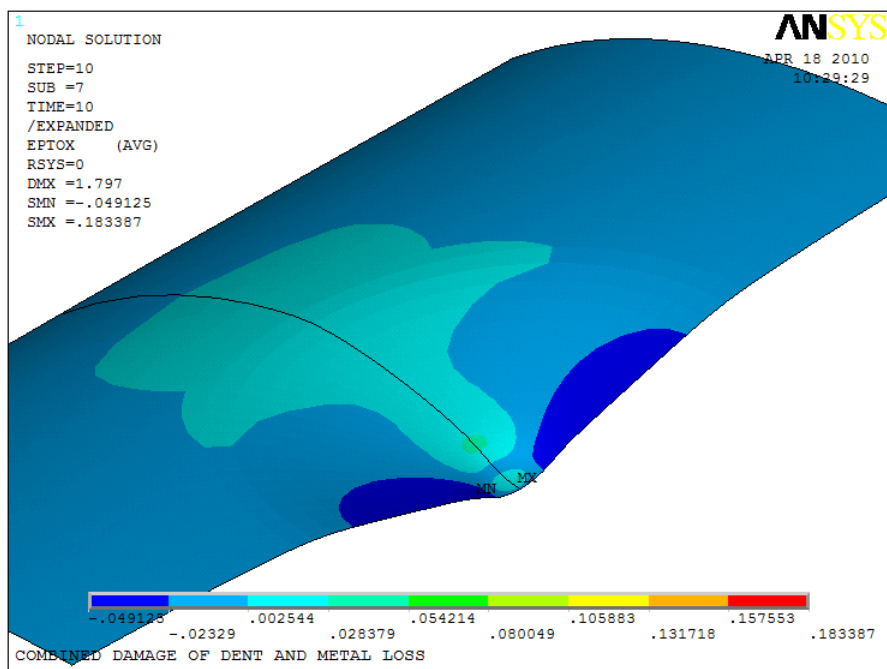


(a)

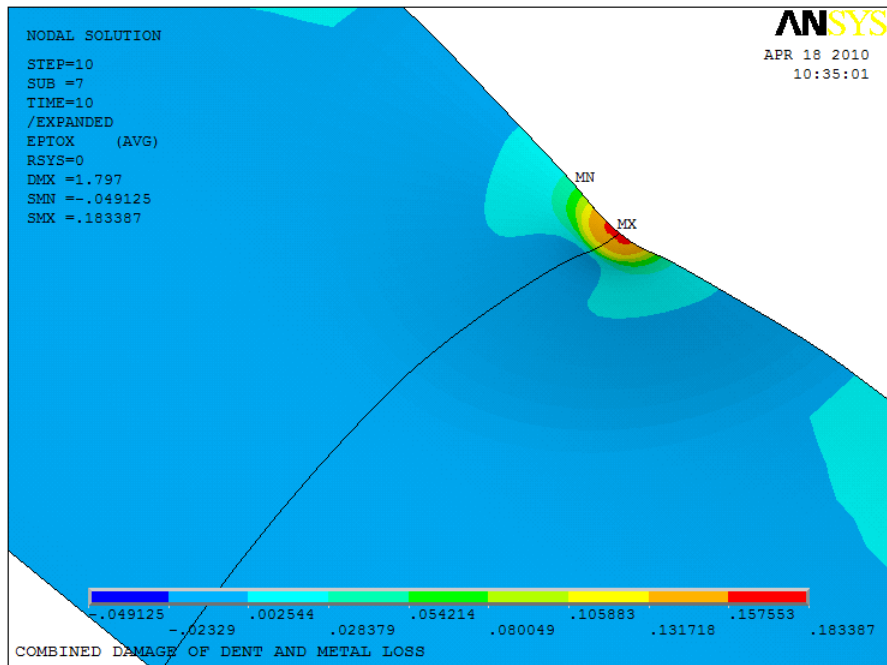


(b)

Figure 8.2. Axial strain profile for dent with metal loss at (a) top shell (b) bottom shell



(a)

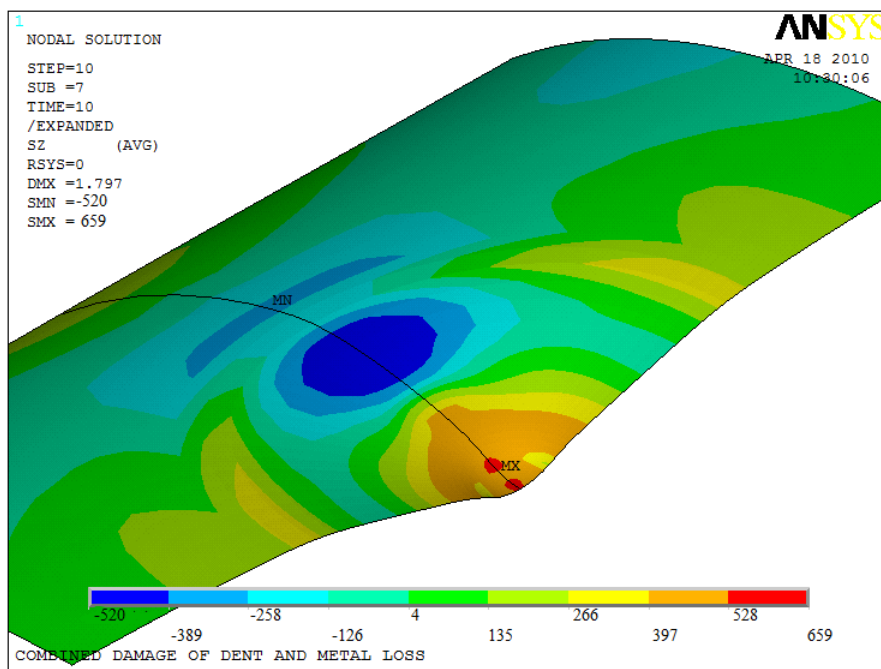


(b)

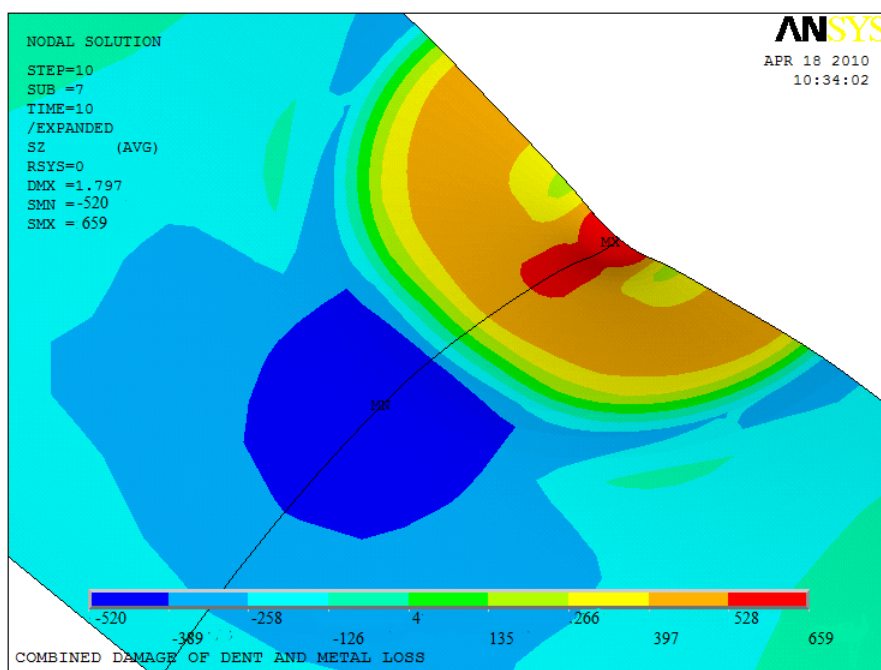
Figure 8.3. Hoop strain profile for dent with metal loss at (a) top shell (b) bottom shell

Table 8.1 Comparison of results between no-metal loss case with 12.5% and 50% metal loss cases

Parameter	No-metal loss	Metal loss (12.5%)		Metal loss (50%)	
	Value	Value	% difference	Value	% difference
Strains at end of indentation stage					
Axial, top shell	-0.114	-0.081	-28.5	0.061	-153.2
Axial, bottom shell	0.238	0.212	-10.8	0.206	-13.5
Hoop, top shell	-0.171	-0.131	-23.5	0.001	-100.4
Hoop, bottom shell	0.263	0.232	-11.7	0.177	-32.5
Stresses at end of indentation stage					
Axial, top shell	353	356	0.7	523	48.0
Axial, bottom shell	648	660	2.0	628	-3.0
Hoop, top shell	313	348	11.1	430	37.4
Hoop, bottom shell	531	386	-27.2	576	8.6
Stress range and fatigue life for cyclic pressure load					
Stress range	234	252	7.7	455	94.4
Mean stress	136	147	8.0	131	-3.9
Fatigue life	78,262	17,248	-78.0	3	-100.0

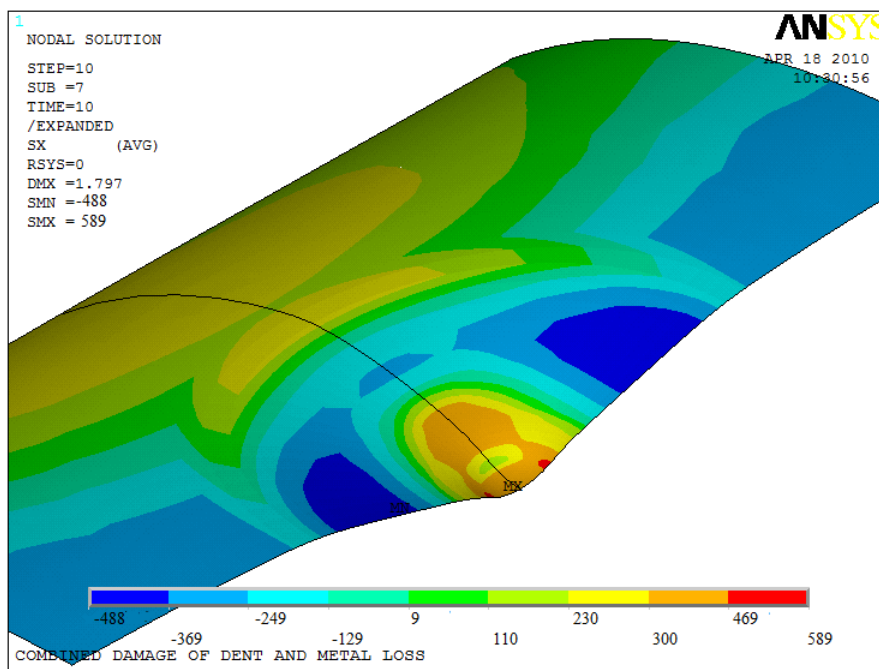


(a)

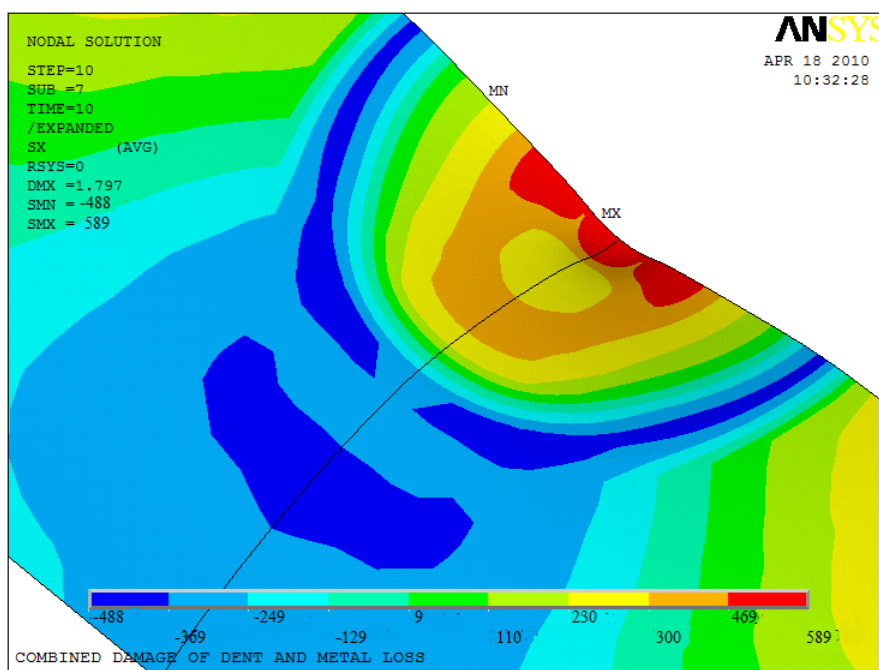


(b)

Figure 8.4. Axial stress profile for dent with metal loss at (a) top shell (b) bottom shell



(a)



(b)

Figure 8.5. Hoop stress profile for dent with metal loss at (a) top shell (b) bottom shell

The comparison of stresses given in Table 8.1 shows that the stresses of the 12.5% metal loss are close to that of the no-metal loss. The decrease in stress is offset by the decrease in pipe wall thickness which resists the indentation load. However, in the 50% metal loss case, the stress increase is up to 48%. The results are in line with Code guidelines to accept dents with mild metal loss up to 12.5%, in case there is no cyclic pressure, while higher metal loss must be evaluated.

8.4.3 Stress Range at End of Pressure Cycle and Fatigue Analysis

Table 8.1 gives the stress range and fatigue cycles for no-metal loss case and the two cases of metal loss. In the case of the 12.5% metal loss, the mean stress and stress range increase by about 7%, but the fatigue life drops to around 25% of the no-metal loss case. In the case of the 50% metal loss, the estimated life is only few cycles which practically means that this combined damage is a threat and must be removed. Therefore, the impact of the combined damage of dent and metal loss is more severe in the case of cyclic loading than in the case of static loading.

8.5 PROBABILISTIC ANALYSIS

The input parameters of the dent problem can be classified into three categories: material, geometry, and pressure loading. Additional category is included for the case of the combined dent with metal loss, which includes the metal loss input parameters. Each of these input parameters have a wide range of values. Moreover, each nominal value of these parameters has its own variability due to manufacturing tolerances, measurement uncertainties, etc. Therefore, in practice hundreds of random combinations of input parameters are possible. Therefore, the use of probabilistic design analysis offers an

excellent way to study the problem and determine the sensitivity of the strain and stress fields to each of those input parameters.

8.5.1 Random Input Variables

Table B.3.1 lists the random input variables, their distribution, and distribution parameters for the combined damage of dent with metal loss. The input variables are grouped in four categories: material, geometry, loading, and metal loss. The statistical distribution of the first three categories is the same as for the no-metal loss case. The statistical distribution of the percentage metal loss is based on a distribution function fit of field-collected statistical data (Semiga, December 2007).

8.5.2 Probability Analysis Loops

The probability analysis is conducted using ANSYS PDA module (ANSYS 2007) with a total of 100 analysis loops to compute the random output parameters in terms of the random input variables. The values of the input variables are generated randomly using Monte Carlo simulation to find how the scatter in the input variables affect the output results and which input variable is the most significant.

8.5.3 Probability Analysis Results

Table B.3.2 gives a summary of all output results (dent dimensions, strains, stresses, and stress range) along with their statistical distribution. The discussion in this section will be focused on the fatigue life as it was found from the deterministic case to be the most sensitive parameter to the combined damage of dent with metal loss. The sample history of the fatigue life is given in Fig.8.6 which indicates a very random nature of the fatigue

life as it ranges between few cycles to infinite life. The histogram presented in Fig. 8.7 shows that around 38% of the cases have a fatigue life of about than 230,000 cycles. However, about 8% of the cases cannot withstand cyclic pressure as they have a fatigue life less than 12 cycles. The statistical distribution of the output can be useful to calculate a quick estimate of probability of failure without even measuring the dent dimensions to be used with risk assessment. Table 8.2 compares the probability of failure in terms of fatigue life for the case of plain dent without metal loss vs. the case of combined damage of dent with metal loss. The table shows that the probability of failure of the combined damage is almost double that of the plain dent. Accordingly, combined damage of dent with metal loss poses a higher risk on the integrity of the pipeline under cyclic pressure.

Sensitivity analysis is performed to find out which input variable(s) affect each of the output variables. Figure 8.8 shows the sensitivity of the fatigue life to three variables: maximum applied pressure, dent percent, and modulus of elasticity. Both applied pressure and dent percent have negative correlation with the fatigue life, i.e. the fatigue life decrease as they increase which is expected. Table B.3.3 lists the results of sensitivity analysis of all output variables to input variables in terms of Spearman correlation factor. The percentage of metal loss has also a negative correlation with the fatigue life, but of low value of -0.0135. This is also illustrated in Fig 8.9 which gives scatter plot of the fatigue life vs. the percentage of metal loss. Although, there is no good fit between the two variables, few trends can be observed. For metal loss percentage up to 25%, a wide scatter exists in the fatigue life indicating that metal loss is not deterministic in this case.

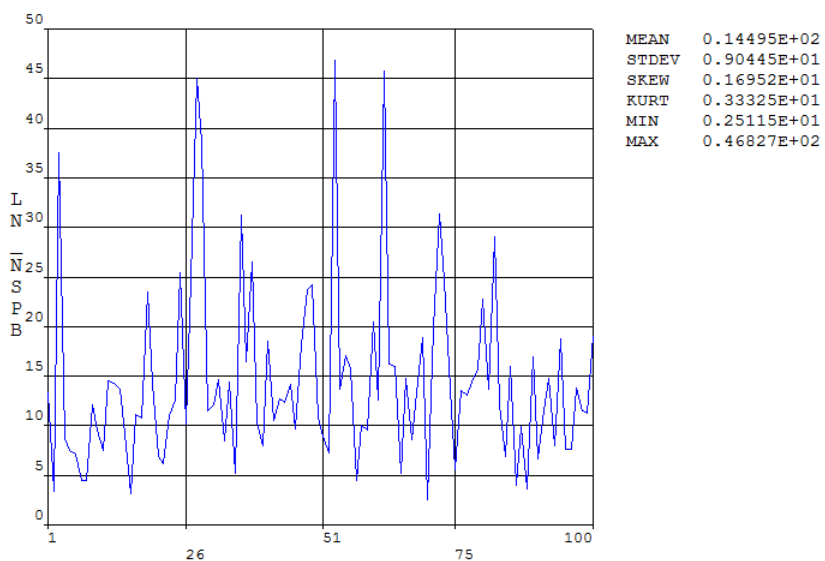


Figure 8.6. Sample history of natural log of fatigue life for dent with metal loss

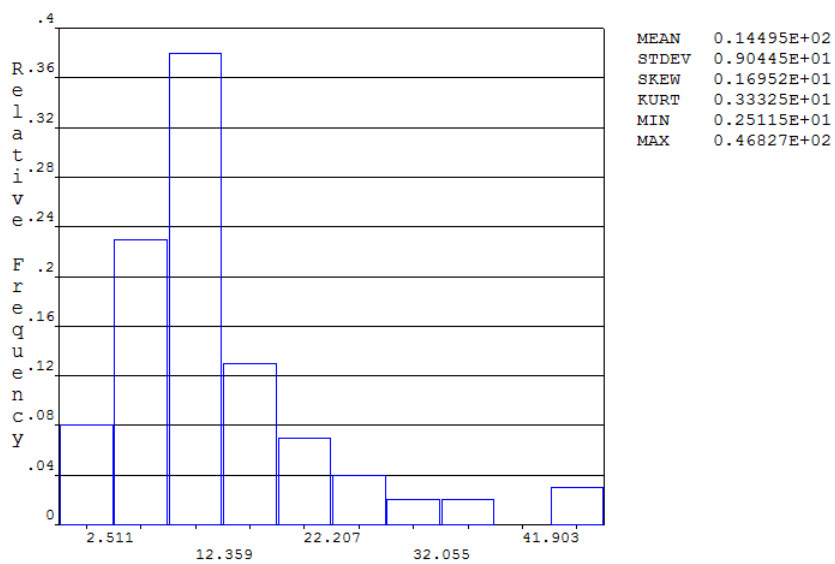


Figure 8.7. Histogram natural log of fatigue life for dent with metal loss

Table 8.2 Probability percentage of failure for combined damage of dent and metal loss

Life	Single dent	Dent with metal loss
1,000	6.8	14.3
5,000	10.2	24.3
10,000	12.2	27.6
50,000	17.9	37.7
100,000	18.5	43.2
500,000	21.2	51.8
1,000,000	22.8	59.6

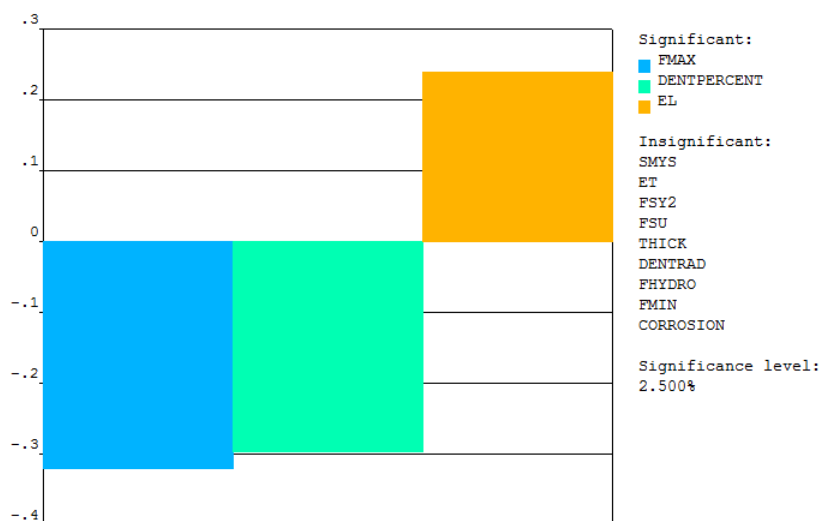


Figure 8.8. Sensitivity plot of fatigue life for dent with metal loss
 Note: Legend top-to-bottom order matches left-to-right order in figure

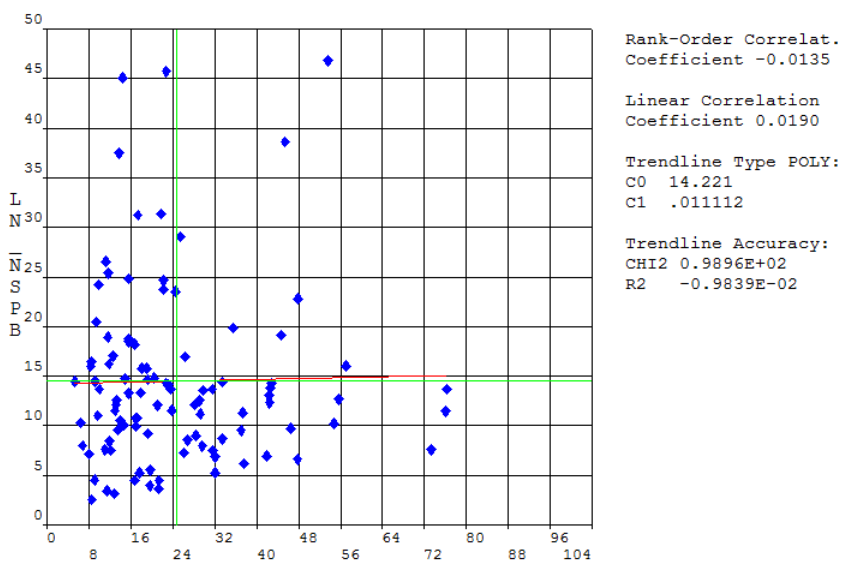


Figure 8.9. Scatter plot of fatigue life vs. percentage of metal loss

For percentage of metal loss exceeding 50%, the fatigue life is very low and this case should be considered a threat to the pipe line and must be removed. Between 25% and 50% metal loss, more data points are clustered in the low fatigue life range, and therefore, these incidents must be evaluated on a case by case for the combined damage of dent and metal loss.

8.5.4 Regression Analysis

In order to make the results of the probabilistic analysis to be easily applied in practical dent with metal loss problems, regression analysis is conducted to derive mathematical formulas of the output variables in terms of practically measured variables. Quadratic polynomial functions are the best fit for a similar problem as stated in section 6.5.4. Therefore, the following general function (Equation 8.1) was fit to all output variables where all output and input variables in dimensionless form. The two terms associate with pressure range are only applicable to output stress range and fatigue life.

$$\begin{aligned}
 \text{Output variable} = & a_0 + b_1 \frac{D}{t} + b_2 \frac{d}{D} + b_3 \frac{l}{D} + b_4 \frac{w}{D} + b_5 \frac{ldw}{D^2 t} + b_6 \frac{\sigma_{flow}}{E_{avg}} + b_7 \frac{E_t}{E_l} + \\
 & b_8 \frac{d_m}{t_m} + b_9 \frac{P_{max} - P_{min}}{P_{SMYS}} + c_1 \left(\frac{D}{t}\right)^2 + c_2 \left(\frac{d}{D}\right)^2 + c_3 \left(\frac{l}{D}\right)^2 + c_4 \left(\frac{w}{D}\right)^2 + c_5 \left(\frac{ldw}{D^2 t}\right)^2 + \\
 & c_6 \left(\frac{\sigma_{flow}}{E_{avg}}\right)^2 + c_7 \left(\frac{E_t}{E_l}\right)^2 + c_8 \left(\frac{d_m}{t_m}\right)^2 + c_9 \left(\frac{P_{max} - P_{min}}{P_{SMYS}}\right)^2
 \end{aligned} \tag{8.1}$$

Table B.3.4 gives the constants values and R-squared value for the regression fit of all output variables of strain, stress, stress range, and fatigue life. The R-squared value is

higher than 0.5 in 40 out of 45 output variables which indicate that the proposed general formula (8.1) is a very good choice. Figure 8.10 shows the regression curve for the axial strain at dent peak which has a very good fit of R-squared 0.68. The regression fit for the output stress variables is also good as Fig. 8.11 illustrates where the R-squared values range between 0.6 and 0.9. For the stress range and fatigue life, the R-squared values are lower and range between 0.31 and 0.64. The regression curve of the natural log of the fatigue life is given in Fig. 8.12 which shows good correlation at low values up to natural log of 20 (equivalent to 5×10^7 fatigue cycles) which exceeds the endurance level, and therefore, it is considered a good fit in the practical range of use.

8.6 SUMMARY

In this chapter, the effect of combined mechanical damage of dent with metal loss was investigated using both determinist analysis and probabilistic analysis. In the deterministic analysis, two cases of metal loss one of 12.5% and the other of 50% were studied and compared with the case of no-metal loss. The results showed that the strains decrease as the metal loss increase at the end of the indentation stage. However, the stresses increase slightly for the 12.5% metal loss and significantly for the 50% case. The fatigue life in the cyclic pressure is reduced by 75% in the case of 12.5% metal loss while the 50% metal loss case cannot take any cyclic load. In the probabilistic analysis, a total of 100 cases randomly generated using Monte Carlo simulations were analyzed. The statistical distribution of output parameters and correlation between output and input variables were presented. The results showed that the probability of failure of a pipe with combined mechanical damage of dent with metal loss is twice that of pipe with plain dent

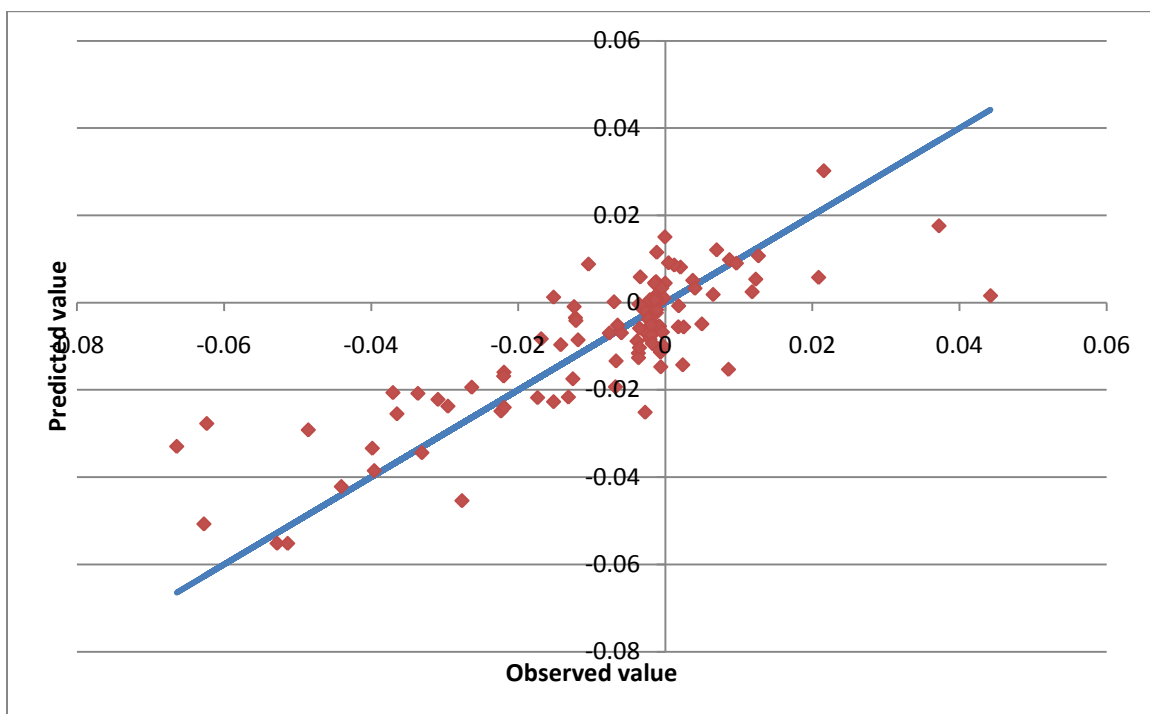


Figure 8.10. Regression fit curve for axial strain at dent peak for dent with metal loss

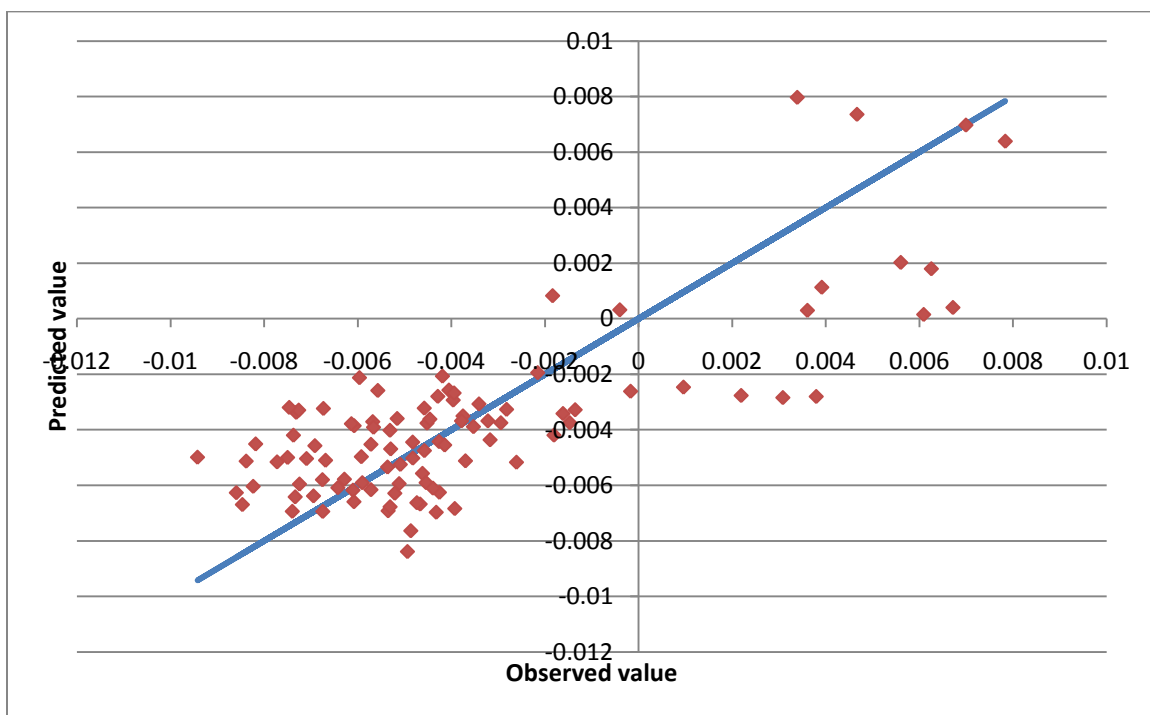


Figure 8.11. Regression fit curve for axial stress at dent peak for dent with metal loss

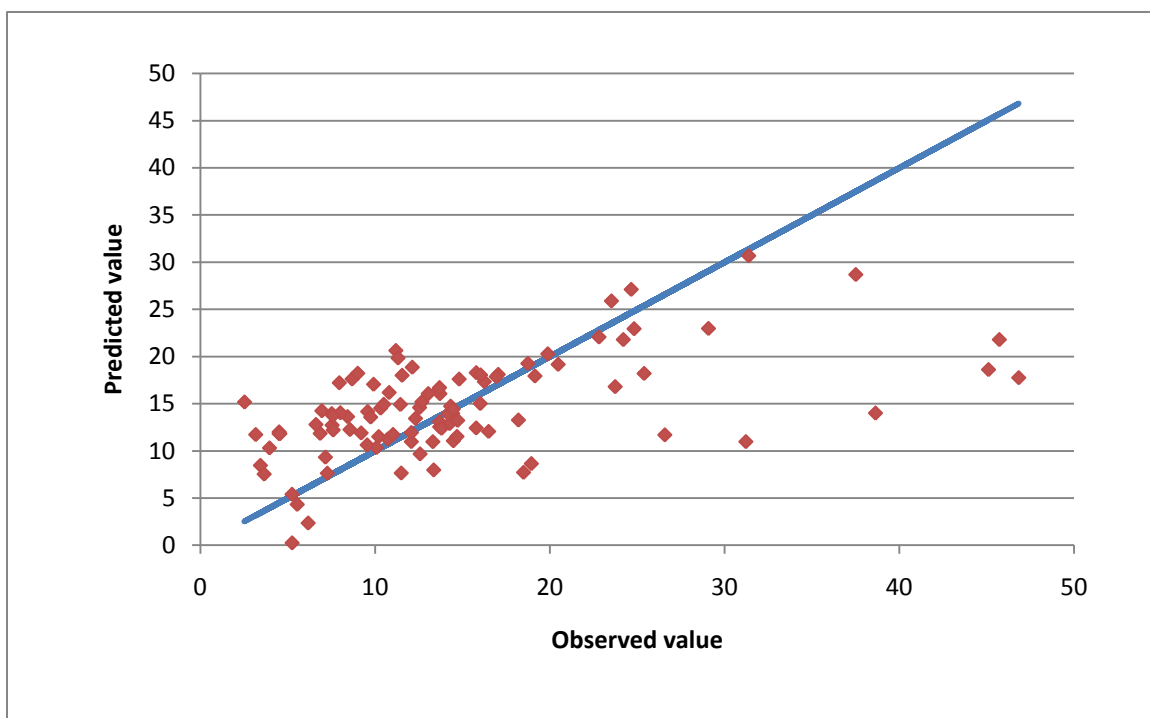


Figure 8.12. Regression fit curve for natural log of fatigue life for dent with metal loss

without metal loss. Accordingly, the sensitivity of strain and stress fields as well as the fatigue life to the various input parameters was determined. Moreover, a general formula was proposed to relate the output variables in terms of practically measured variables. Regression analysis was conducted to derive the coefficients and the results showed the general formula was a good choice. The R-squared values were higher than 0.5 in most of the cases.

CHAPTER 9

IMPACT OF INTERACTION OF DENT WITH RESIDUAL STRESSES OF WELDS

9.1 INTRODUCTION

Welding is necessary during the pipe manufacturing process in the form of longitudinal or spiral weld. It is also needed during the pipeline installation to joint pipe section together in the form of transverse weld known as girth weld. The interaction of dent with the weld has always been considered a threat to the pipeline. ASME B31.8 (2007) considers dents deeper than 2% and interacting with welds to be injurious and requires an engineering assessment if they are to be left without repair. It mandates removal of dents interacting with welds if they are deeper than 4%.

Fowler et al. (1994) conducted full scale experiments for damaged pipes under cyclic. Some pipes had plain dents while other pipes had dents on longitudinal welds and girth welds. They found that the fatigue life of the dented pipe on girth weld is only 9.4% of that of plain dent. The dented pipe with longitudinal weld had a slightly higher life of 13.6% of that of plain dent. Accordingly, the authors recommended repair of dents regardless of their depth if they are interacting with girth weld. For dents interacting with longitudinal welds, the authors recommended repair if the dent exceeded 5% depth.

Rosenfeld (1999) proposed an analytical method to evaluate dents interacting welds. The first step is to estimate the stress concentration factor of plain dent using available literature or engineering analysis. The second step is to find the operating cycle range to calculate the stress range. Then, the S-N curve of the affect weld is used to calculate the fatigue life. Based on this methodology, Rosenfeld concluded that interaction of dents with girth welds can be left without repair for certain conditions including, the dent is shallow, the weld is of high quality, and the pressure cycle is not severe.

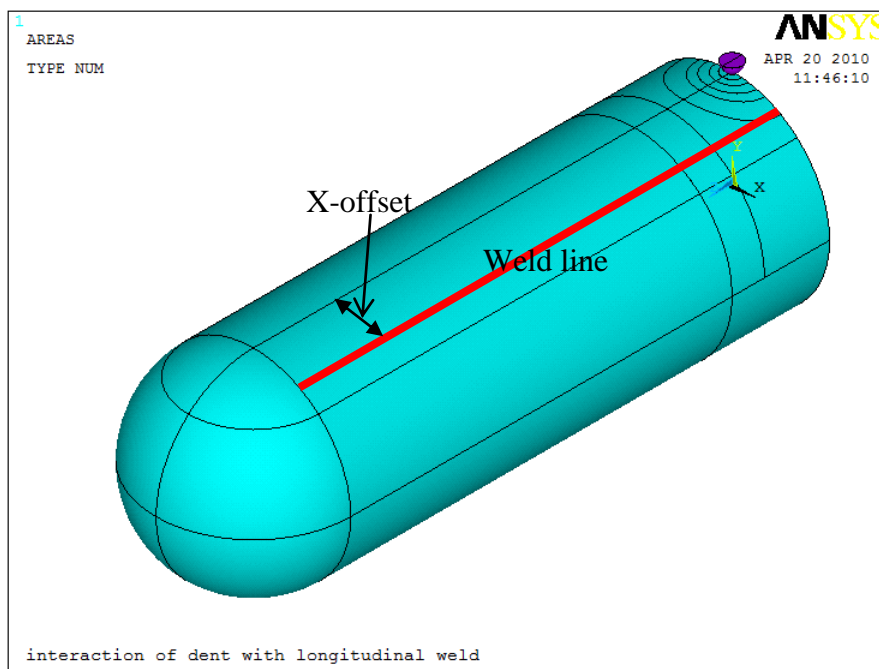
Dinovitzer et al. (2007) studied the acceptable distance between the dent peak and a longitudinal or girth weld for pipes under cycling pressure using numerical FEA. Their approach was not to model the weld explicitly in the numerical model, but to multiply the resulting stress range for the plain dent model with a stress concentration factor of 3 to account for the stress riser of the weld geometry. They limited the dent depth in their study to 6%. They concluded that the longitudinal weld is not interacting with the dent as long as it is outside the dent deformed region. However, for the girth weld, no straight forward criterion was possible. The authors developed a regression formula to estimate the acceptable distance between a dent peak and girth weld.

All of the reviewed literature did not combine the dent and weld features in one numerical model. Moreover, none of the reviewed literature has considered the effect of interaction of dent with the residual stresses of welds. High residual stresses exist in the vicinity of the weld line reaching values up to the yield stress of the pipe. Even after post weld heat treatment, which is done only for very thick pipes exceeding 32 mm, residual stresses will not in general reduce to zero. There are estimated to be at a level of 30% of the pipe yield stress. (BS 7910, 2005)

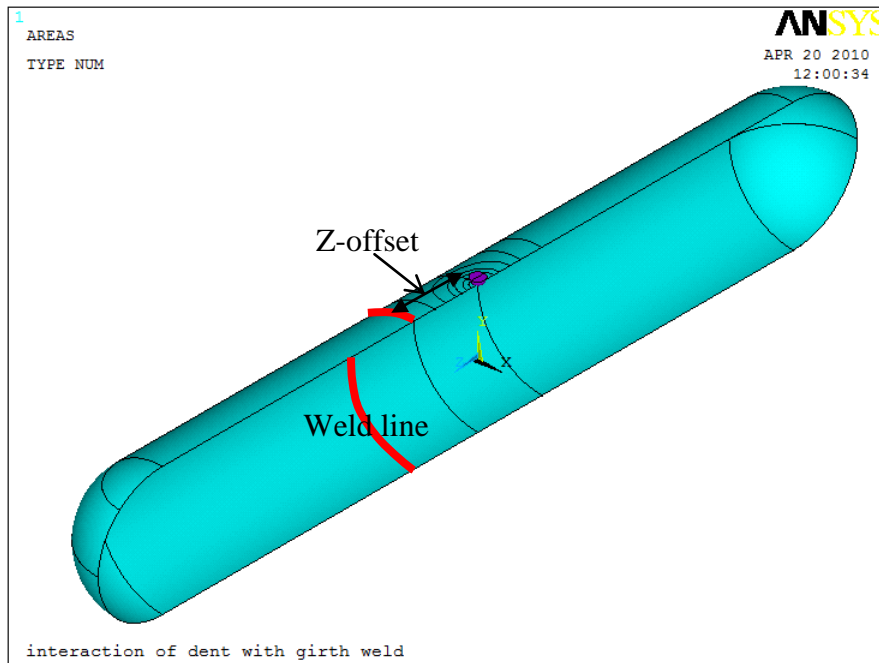
In this chapter, the impact of interaction of dent with longitudinal welds and girth welds will be under static and cyclic pressure conditions will be evaluated. The combined effect are included in a single FEA model and the welds will be simulated by imposing initial residual stresses along the weld line. The first part of the chapter uses deterministic analysis to present strain and stress contours at the end of indentation stage as well as the stress range and fatigue cycles at the end of pressure cycle stage for a longitudinal weld case as well as girth weld case. The second part uses probabilistic design analysis with variable geometry, material and pressure in addition to the weld location and residual stress value to determine the sensitivity of the strain, stress, and stress range to the input. Two probabilistic design analyses are conducted: one for the interaction of dent with longitudinal welds, the other for the interaction of dent with girth welds.

9.2 DESCRIPTION OF THE PROBLEM

The problem is configuration is shown in Fig. 9.1 (a) for longitudinal weld and (b) for girth weld. The weld geometry is defined by the weld location offset from the dent peak and the weld width. The weld width as assumed to equal $\frac{1}{2}$ the thickness as double V-groove is considered. The weld residual stress is defined by the magnitude of the residual stresses and the affected width. The magnitude of the residual stress ranges between 30% SMYS for heat-treated pipes and 100% SMYS for as-welded pipe (BS 7910, 2005). The residual stress affected width is estimated based Fig. 9.2 which is adopted from API 579 (2005) with the assumption that the residual stress distribution of girth weld is similar as that of the longitudinal one.

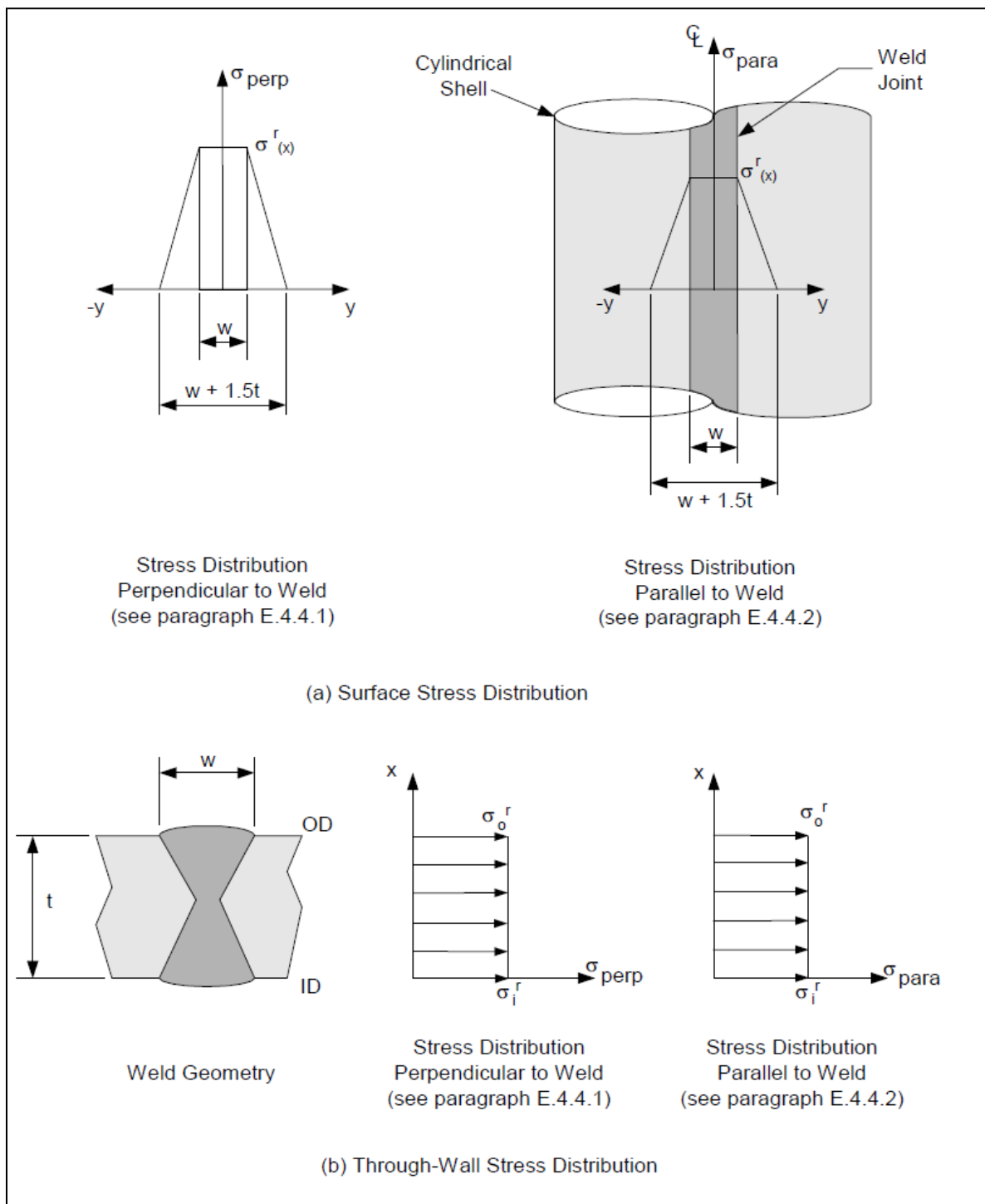


(a)

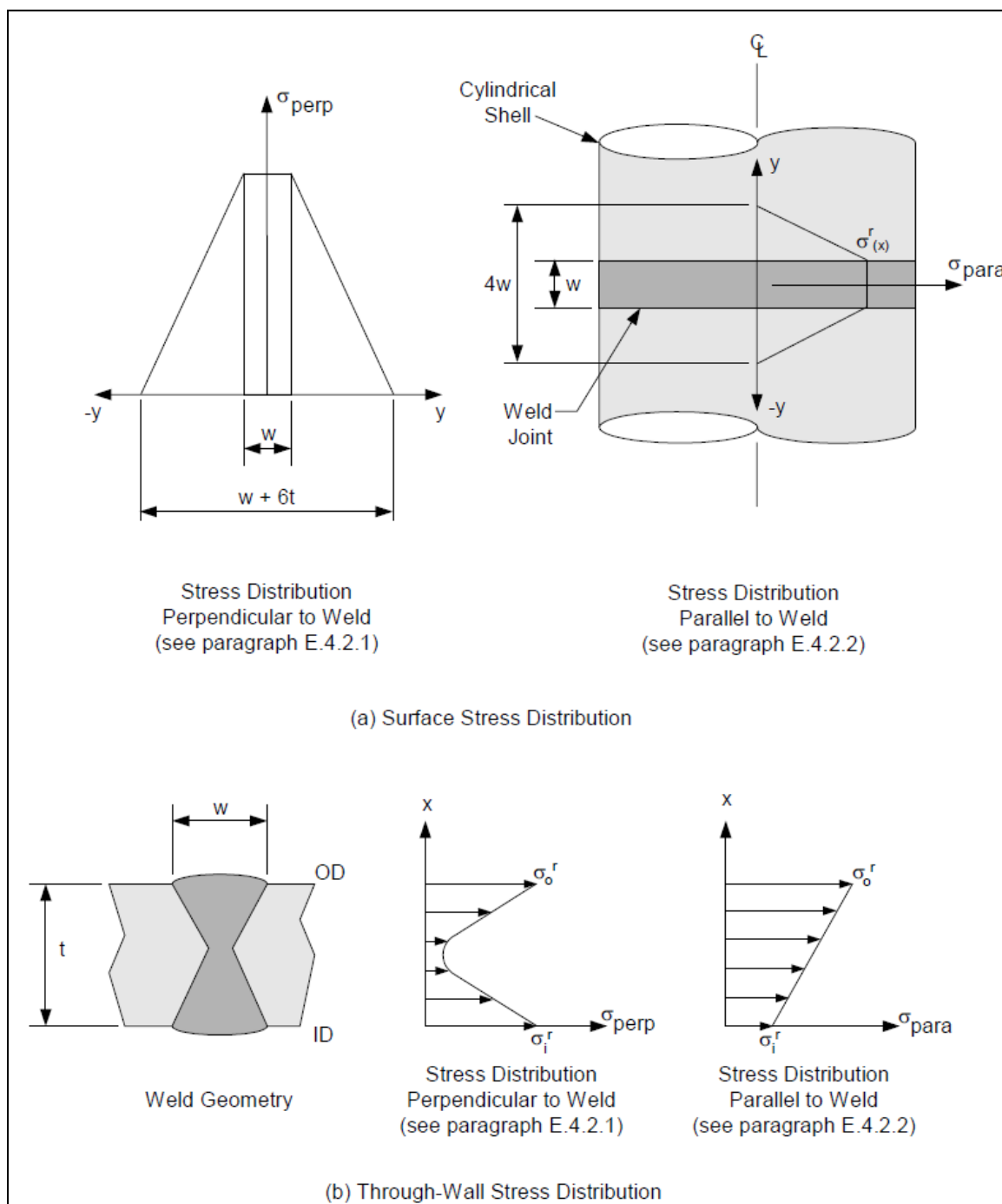


(b)

Figure 9.1. Illustration of interaction of dent with (a) longitudinal weld (b) girth weld



(a)



(b)

Figure 9.2. Residual stress distribution for double-groove weld in pipes (a) longitudinal welds (b) girth welds

9.3 DESCRIPTION OF THE NUMERICAL MODEL

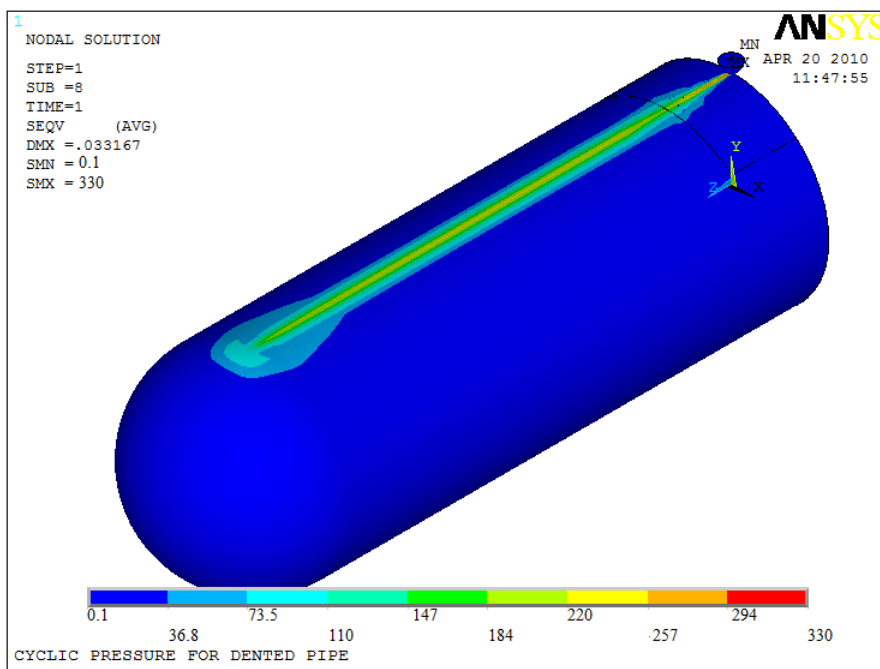
Half symmetry of the pipe about the x-z plan is used for the case of dent with longitudinal weld, while symmetry about the x-y plane is used in the case of dent with girth weld. Symmetry boundary conditions are applied in the symmetry planes. The residual stress is applied by using the initial stress command available in ANSYS to selected elements along the weld line and covering width described in section 9. Initial stresses are applied in two directions along the line weld and perpendicular to the line weld. The indentation process is modeled by a contact pair of rigid target with pilot node. The first load step in the problem is solved without additional loads to generate the effect of the residual stresses (Fig. 9.3). Then, a vertical load displacement is applied on the target in small load steps until it reaches the target depth. After that, two pressure cycles are applied. The first one is simulating the hydrostatic pressure test and the second cycle simulates the operating pressure range.

9.3.1 FE Model

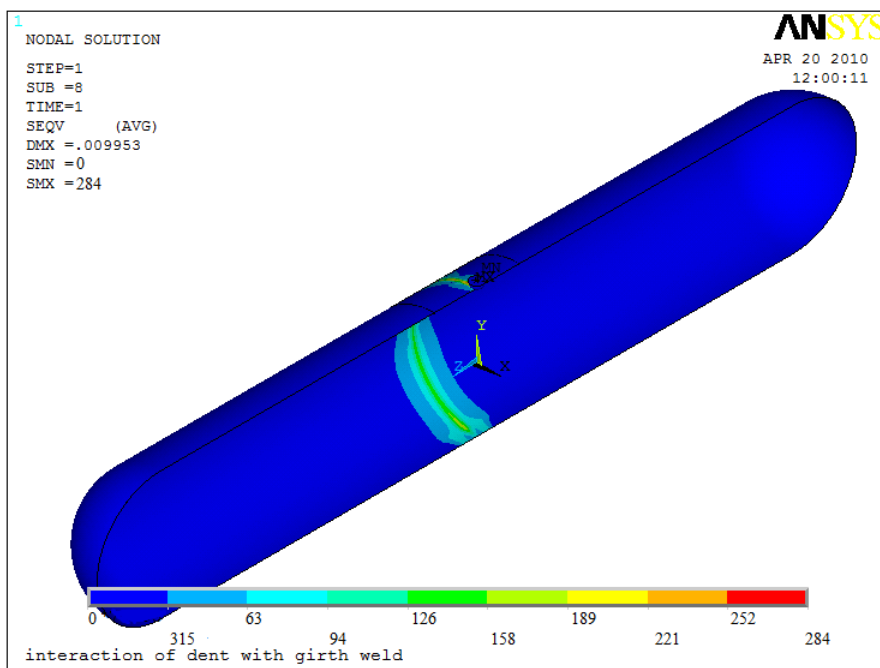
Elements used are shell element 181 (4-nodes). For the contact pair, the indenter is modeled with Target 170 while the contact areas are modeled with Contact 174. Similar mesh to that described in section 4.3.1 is used.

9.3.2 Material Model

The material model is identical to the model described in section 4.3.2. The model is multi-linear kinematic hardening defined by three points. The first point is the end of



(a)



(b)

Figure 9.3. Residual stress distribution along weld lines before dent and pressure loading
 (a) longitudinal weld (b) girth weld

proportional limit, the second point is the material yield stress at 0.5% strain, and the third point is the true ultimate tensile strength.

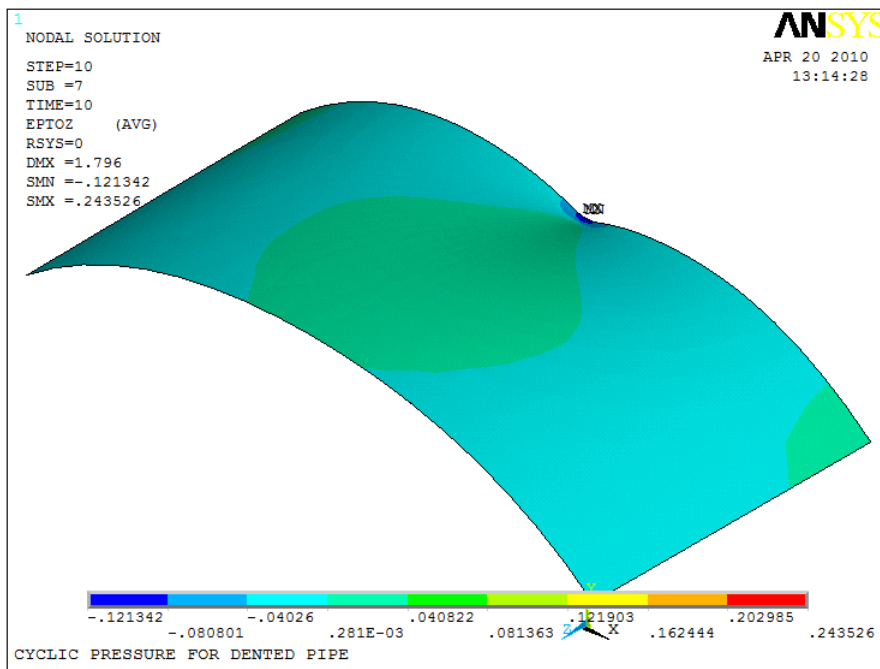
9.4 DETERMINISTIC ANALYSIS OF DENT WITH WELD RESIDUAL STRESS

Two deterministic cases of metal loss of 12.5% and 50% are first investigated and compared with no-metal loss indenter case. The strain and stress fields as well as the stress range and fatigue life are evaluated.

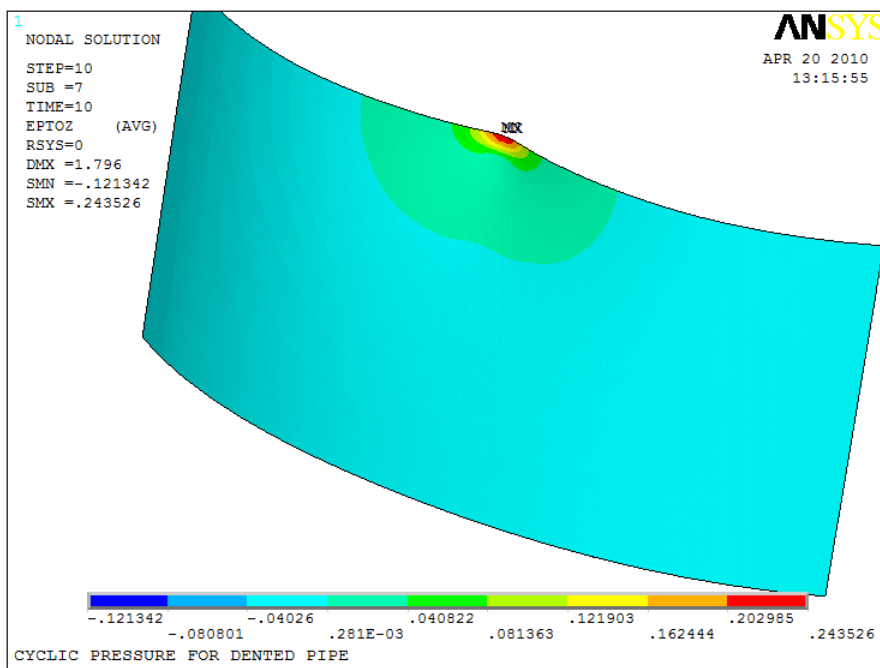
9.4.1 Strain Fields at End of Indentation Phase

The axial strain fields for dent interacting with longitudinal weld are shown in Fig. 9.4 for top and bottom of the pipe shell while the hoop strain fields are shown in Fig. 9.5. The figures show that the maximum strain values are at the dent peak and that they are compressive at the top shell and tensile at the bottom shell. Similar strain profiles also exist for the case of dent interacting with girth weld as Fig. 9.6 and Fig 9.7 illustrate. Therefore, the pre-existence of weld residual stresses does not affect the strain fields at the end of the indentation phase.

Table 9.1 compares the values of the strains no weld case to the longitudinal and girth weld cases. The table shows that the strains are almost the same as the difference in strain values does not exceed 5%. This is expected in this case due to the high plastic strain resulting from the denting process compared to the low strains resulting from the welding residual stress. In cases of shallower indentation depth, and thus lower indentation strains, the interaction might be more significant. This will be evaluated further in the probabilistic design analysis.

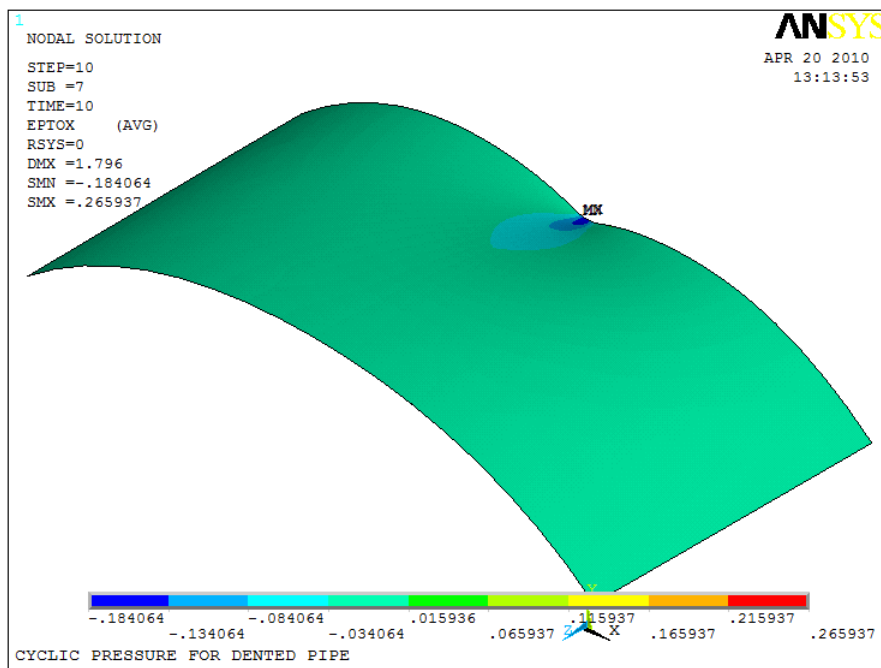


(a)

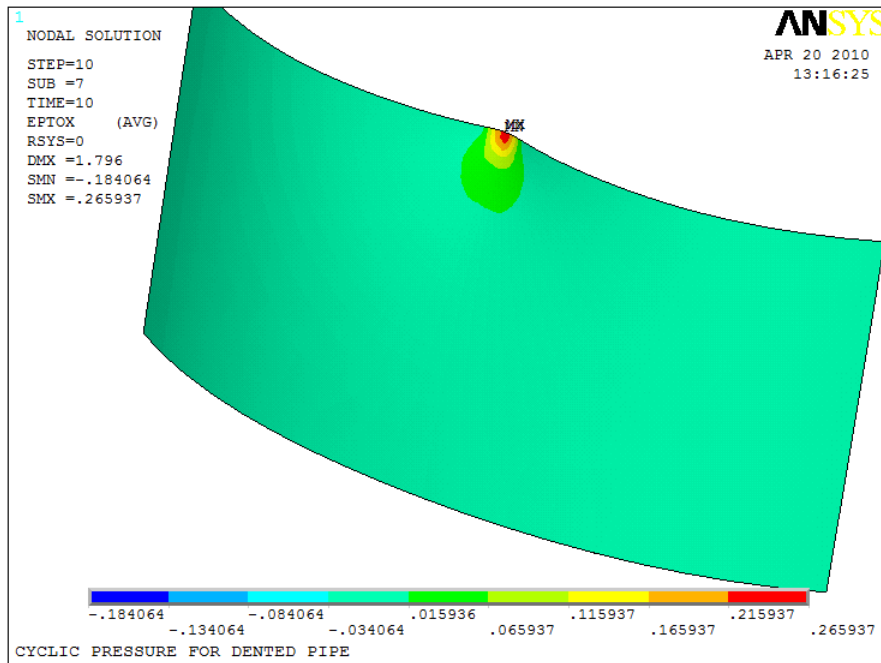


(b)

Figure 9.4. Axial strain profile for dent with longitudinal weld at (a) top shell (b) bottom shell

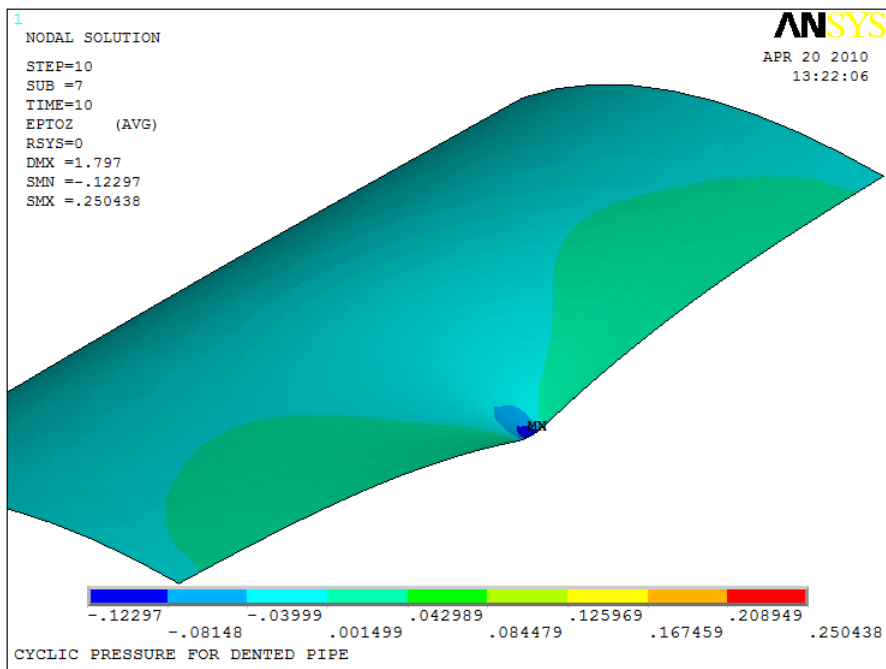


(a)

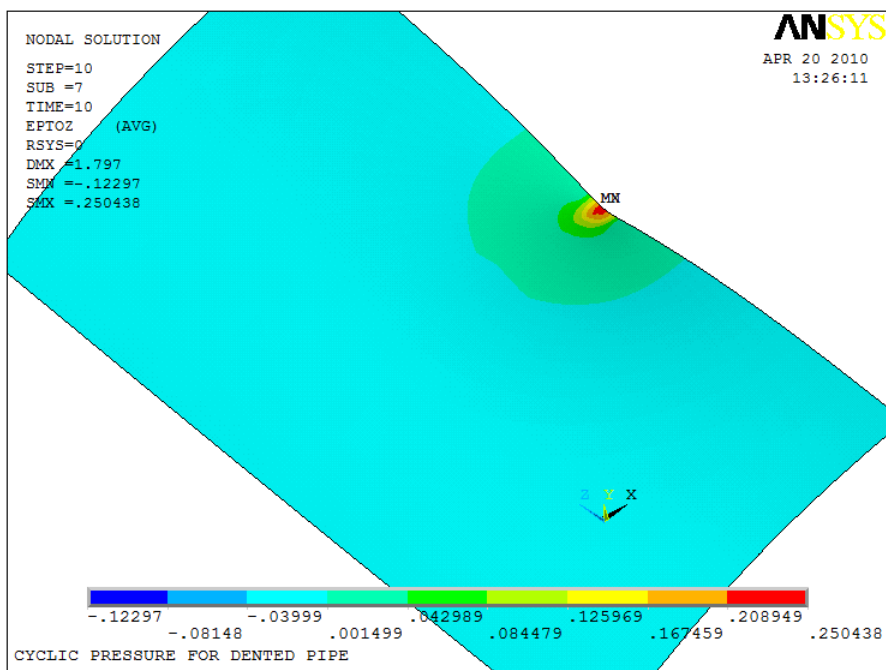


(b)

Figure 9.5. Hoop strain profile for dent with longitudinal weld at (a) top shell (b) bottom shell

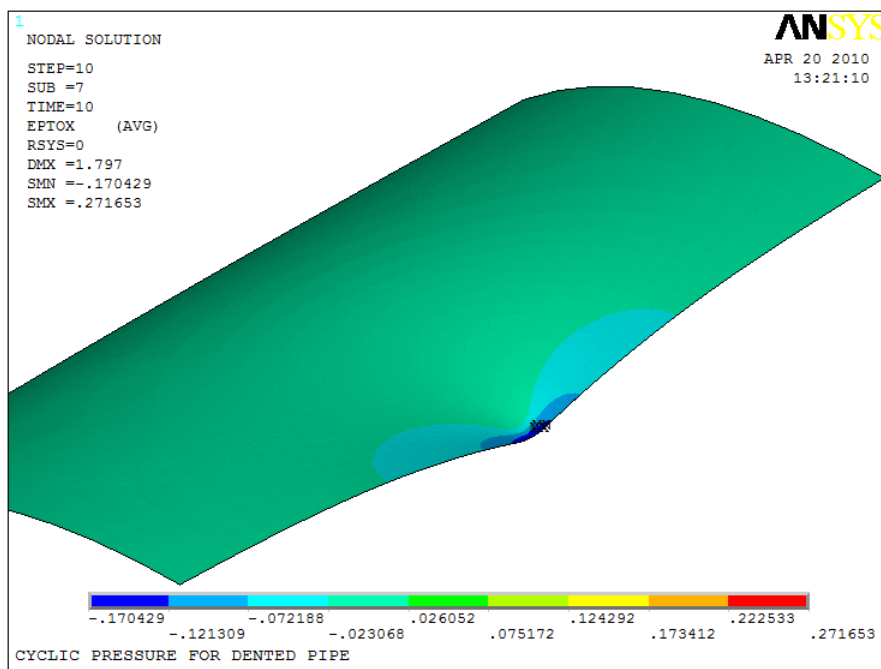


(a)

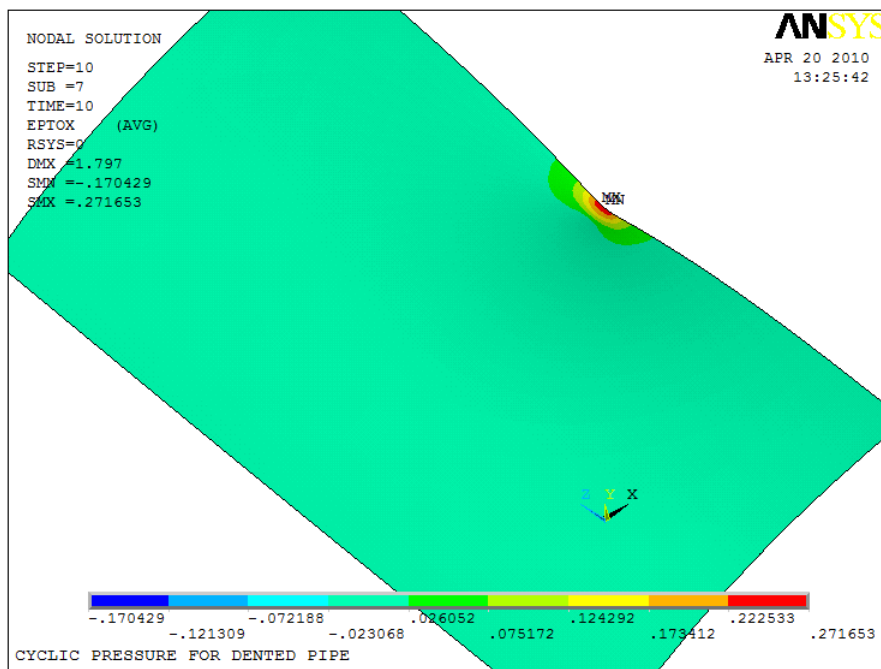


(b)

Figure 9.6. Axial strain profile for dent with girth weld at (a) top shell (b) bottom shell



(a)



(b)

Figure 9.7. Hoop strain profile for dent with girth weld at (a) top shell (b) bottom shell

Table 9.1 Comparison of results between no-weld case and longitudinal and girth weld cases

Parameter	No-weld	Longitudinal weld		Girth weld	
	Value	Value	% difference	Value	% difference
Strains at end of indentation stage					
Axial, top shell	-0.114	-0.114	0.2	-0.112	-1.3
Axial, bottom shell	0.238	0.229	-3.7	0.227	-4.5
Hoop, top shell	-0.171	-0.175	2.4	-0.164	-4.0
Hoop, bottom shell	0.263	0.254	-3.4	0.263	0.0
Stresses at end of indentation stage					
Axial, top shell	353	340	-3.7	329	-6.8
Axial, bottom shell	648	603	-6.9	639	-1.3
Hoop, top shell	313	319	2.0	326	4.0
Hoop, bottom shell	531	499	-6.0	559	5.3
Stress range and fatigue life for cyclic pressure load					
Stress range	234	225	-4.1	226	-3.6
Mean stress	136	168	23.6	151	11.2
Fatigue life	78,262	8,464	-89.2	28,998	-62.9

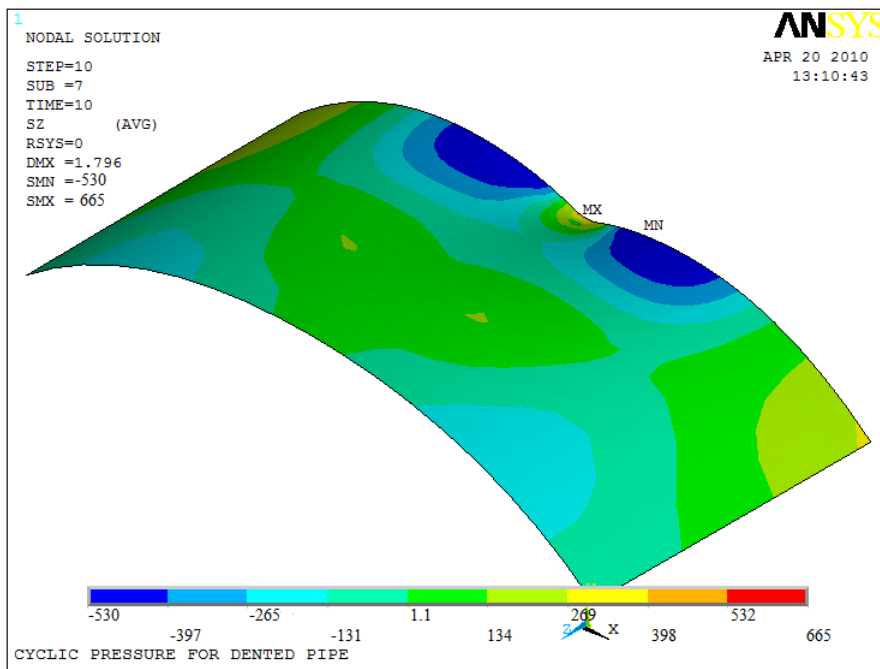
9.4.2 Stress Fields at End of Indentation Phase

The axial stresses are maximum tensile at the dent peak bottom shell as shown in Fig. 9.8 for the case of dent with longitudinal weld. However, the maximum axial compressive stresses are not at the dent peak, rather they are at the periphery of the dented area along the transverse pipe direction. Similarly, for the hoop stresses (Fig. 9.9), the maximum tensile stresses are at the bottom shell of the dent peak, but the maximum compressive stresses are at the periphery of the dented area, in this case, along the axial pipe direction. Therefore, it is not enough only to determine the stresses at the dent peak, but stresses around the dent periphery must be evaluated as well. Similar trends are also observed in the case of dent interaction of girth welds (Fig. 9.10 and Fig. 9.11), and accordingly, not only stresses at the dent peak must be evaluated, but also stresses along the pipe axial and transverse directions should be checked.

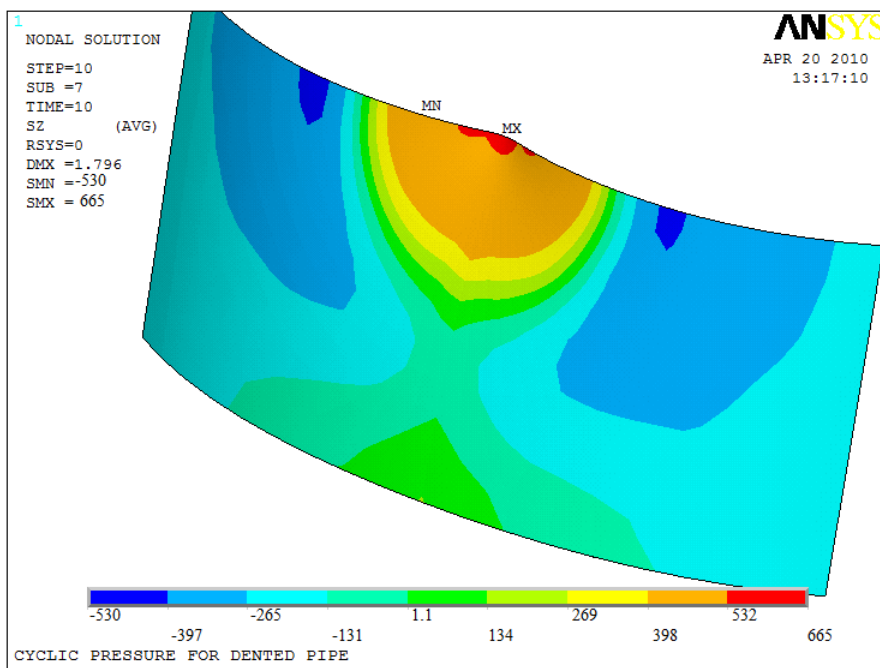
The comparison of stresses given in Table 9.1 shows that the stresses of the cases of dent interacting with longitudinal welds or girth welds are of comparable magnitude to the stresses of the plain dent. This is due to the fact that the stresses of the plain dent are already exceeding the yield point. Therefore, additional stresses cannot change the resulting stress significantly, as the material will follow the plastic tangent modulus which is of low slope. Therefore, it can be concluded that the pre-existence of weld residual stresses does not affect the pipe integrity in the case of static loading only.

9.4.3 Stress Range at End of Pressure Cycle and Fatigue Analysis

Table 9.1 gives the stress range and fatigue cycles for no-metal loss case and the two cases of metal loss. The mean stress does not change much for the cases with welds.

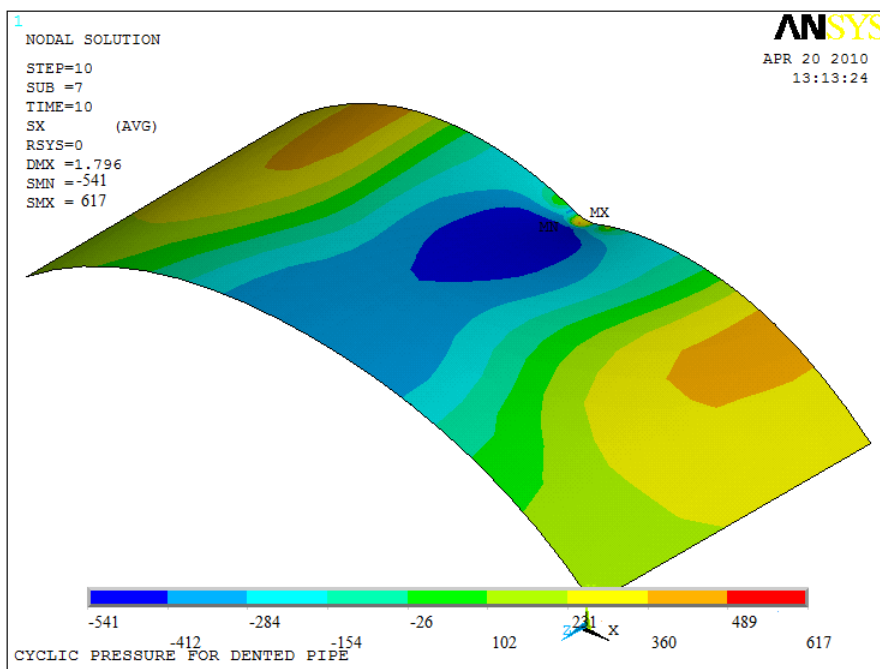


(a)

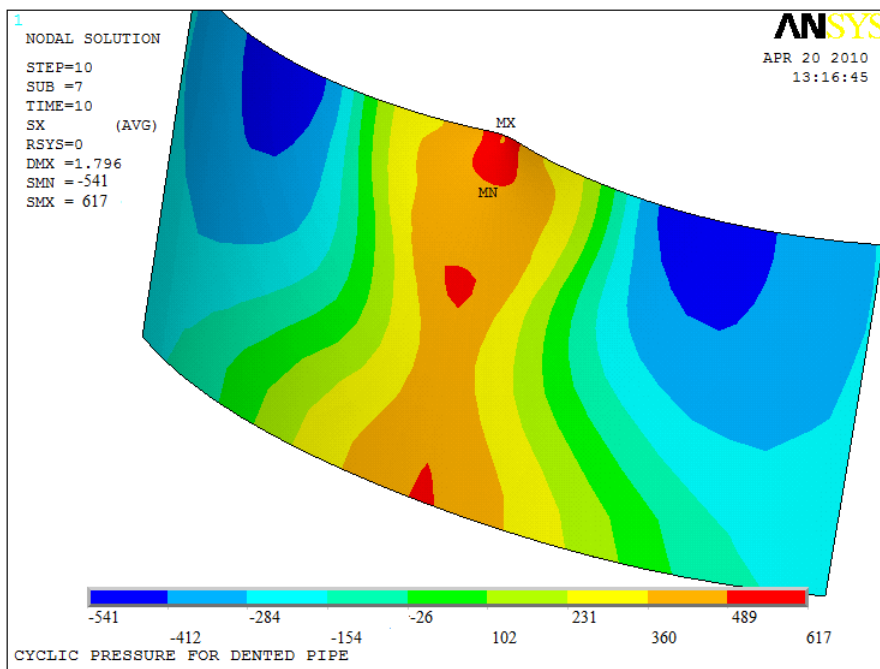


(b)

Figure 9.8. Axial stress profile for dent with longitudinal weld at (a) top shell (b) bottom shell

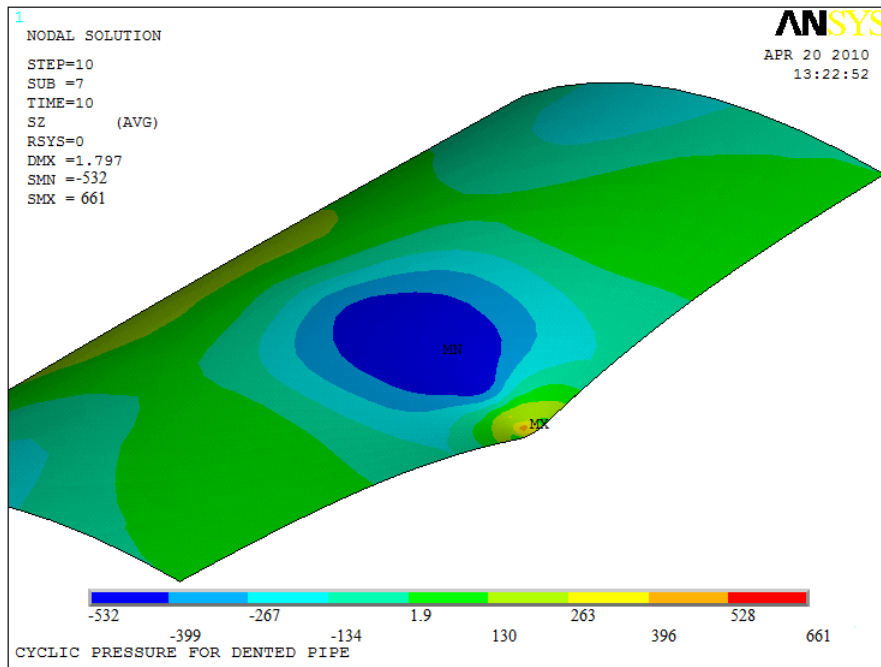


(a)

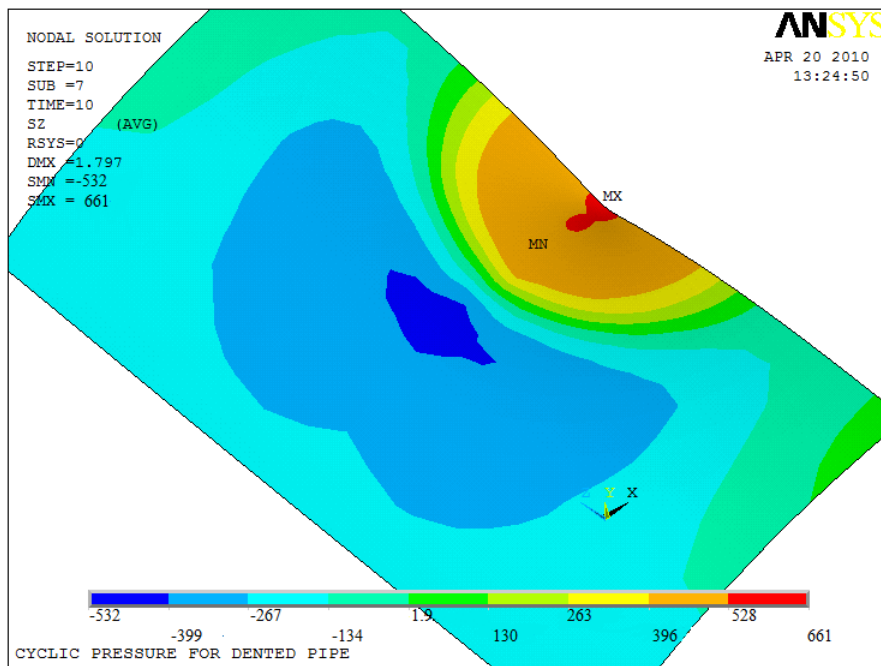


(b)

Figure 9.9. Hoop stress profile for dent with longitudinal weld at (a) top shell (b) bottom shell

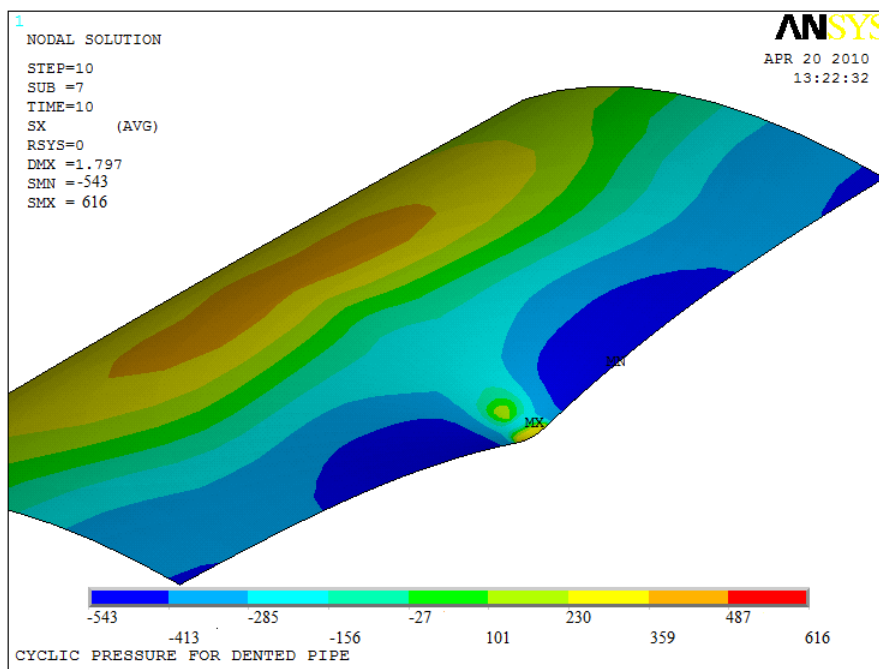


(a)

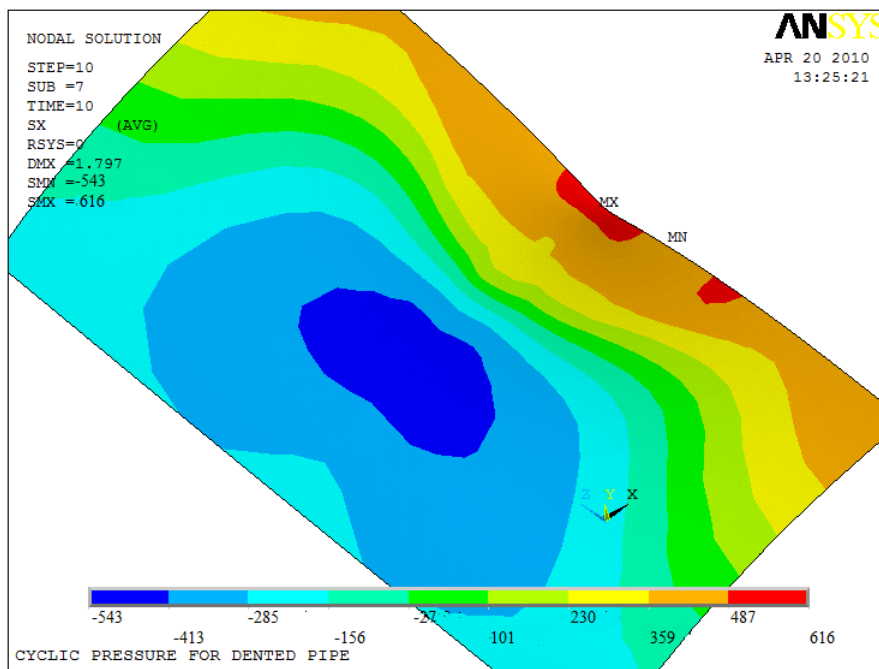


(b)

Figure 9.10. Axial stress profile for dent with girth weld at (a) top shell (b) bottom shell



(a)



(b)

Figure 9.11. Hoop stress profile for dent with girth weld at (a) top shell (b) bottom shell

However, the stress range increases by 23.6% for the case of longitudinal weld and by 11.2% for the case of girth weld. Accordingly, the fatigue life drops significantly for dents interacting with welds. The fatigue life of dent with longitudinal weld is only 10.8% of that of plain dent while it is 37.1% for the case of dent with girth weld. Therefore, the impact of the interaction of dent with residual stresses of welds whether longitudinal or girth is severe in the case of cyclic pressure loading and such cases must be evaluated if to be left in the pipeline without repair.

9.5 PROBABILISTIC ANALYSIS

The input parameters of the dent problem can be classified into three categories: material, geometry, and pressure loading. Additional category is included for the case of dent with weld is the weld residual stresses, which includes the residual stress level and the offset from dent peak. Each of these input parameters have a wide range of values. Moreover, each nominal value of these parameters has its own variability due to manufacturing tolerances, measurement uncertainties, etc. Therefore, in practice hundreds of random combinations of input parameters are possible. Therefore, the use of probabilistic design analysis offers an excellent way to study the problem and determine the sensitivity of the strain and stress fields to each of those input parameters. Two probabilistic design analyses will be conducted: one for the dent interacting with longitudinal welds and the other for dent interacting with girth welds.

9.5.1 Random Input Variables

Table B.4.1 lists the random input variables, their distribution, and distribution parameters for the dent interacting with longitudinal weld while Table B.5.1 lists the

random input variables for the dent interacting with girth weld. The input variables are grouped in four categories: material, geometry, loading, and weld residual stress. The statistical distribution of the first three categories is the same as for the plain dent case. The statistical distribution of the residual stress is varied uniformly between 30% of the yield stress, for the case of the heat treated pipe, and 100% of the yield stress, for the case of as-welded pipe (BS 7910, 2005). For the case of longitudinal weld, the x-offset is defined to vary uniformly between 0 and 150 mm from the dent peak. This is based on Dinovitzer et al. (2007) conclusion that the longitudinal weld interacts with the dent only if it is with its deforming region. The work of this dissertation (Chapter 6) showed that the mean of the dent width of the problem geometry under consideration is 78 mm, and therefore, it was selected to be the mean of the x-offset variation. For the case of girth weld, the z-offset is defined to vary uniformly between 0 and 686 mm which is selected based on the interaction distance between dent and girth weld estimated by Dinovitzer et al. (2007) for the case of pipe of 610 mm diameter.

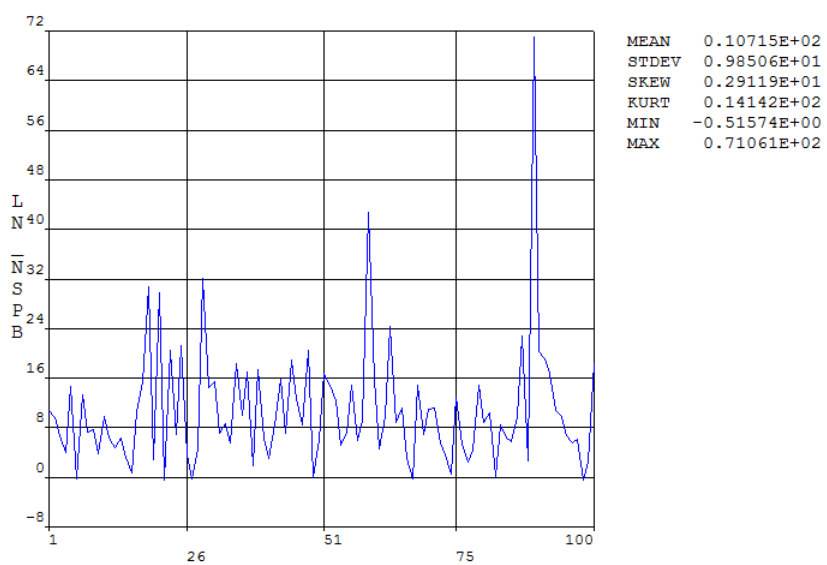
9.5.2 Probability Analysis Loops

The probability analysis is conducted using ANSYS PDA module (ANSYS 2007) with a total of 100 analysis loops for the interaction of dent with longitudinal weld, and another 100 analysis loops for the interaction of dent with girth weld. The analyses will compute the random output parameters in terms of the random input variables. The values of the input variables are generated randomly using Monte Carlo simulation to find how the scatter in the input variables affect the output results and which input variable is the most significant.

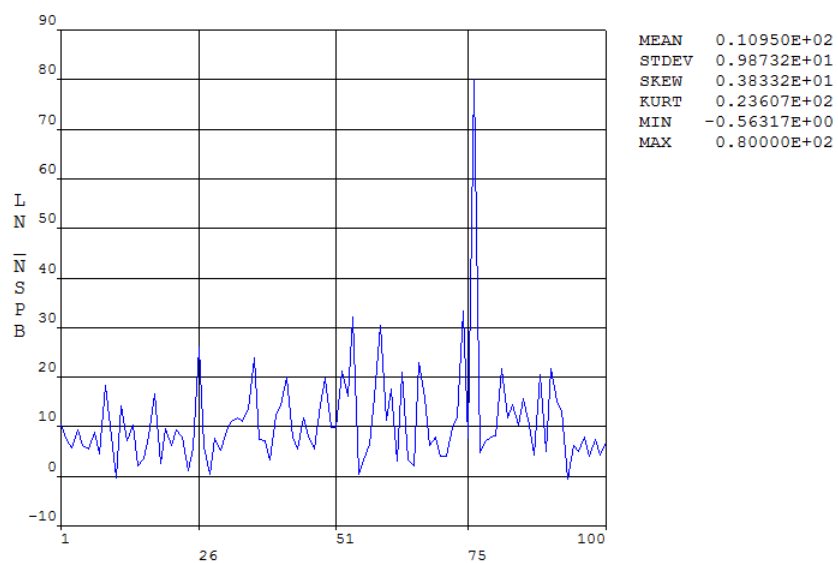
9.5.3 Probability Analysis Results

Table B.4.2 gives a summary of all output results (dent dimensions, strains, stresses, and stress range) along with their statistical distribution for the case of interaction of dent with longitudinal weld, while Table B.5.2 gives the output results of the case of interaction of dent with girth weld. The discussion in this section will be focused on the fatigue life as it was found from the deterministic case to be the most sensitive parameter to the interaction dent with residual stresses of welds. The sample history of the fatigue life is given in Fig.9.12 which indicates a very random nature of the fatigue life as it ranges between few cycles to infinite life. However, the histogram presented in Figure 9.13 shows the majority of the cases have relatively low fatigue life. For the case of dent interacting with longitudinal weld, around 50% of the cases have a fatigue life of only about 1,800 cycles. For the case of dent interacting with girth weld, around 58% of the cases have a fatigue life of only about 5,800 cycles.

The statistical distribution of the output can be useful to calculate a quick estimate of probability of failure without even measuring the dent dimensions to be used with risk assessment. Table 9.2 compares the probability of failure in terms of fatigue life for the case of plain dent vs. the cases of dent interacting with residual stresses of welds. The table shows that the probability of failure of the interaction of dent with welds is 3 to 8 times greater than that of plain dents. Accordingly, a dent interacting with residual stresses of welds poses a risk higher by 3 to 8 times of that of plain on the integrity of the pipeline under cyclic pressure. It is interesting to note that the probability of failure for both cases of longitudinal and girth welds are of comparable levels with slight increase for the case of girth weld. This could be attributed to the fact that the weld produces

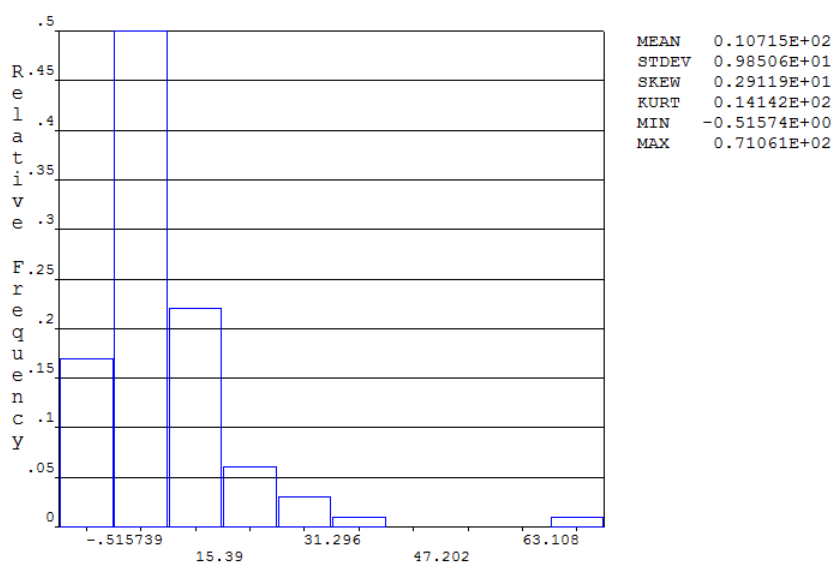


(a)

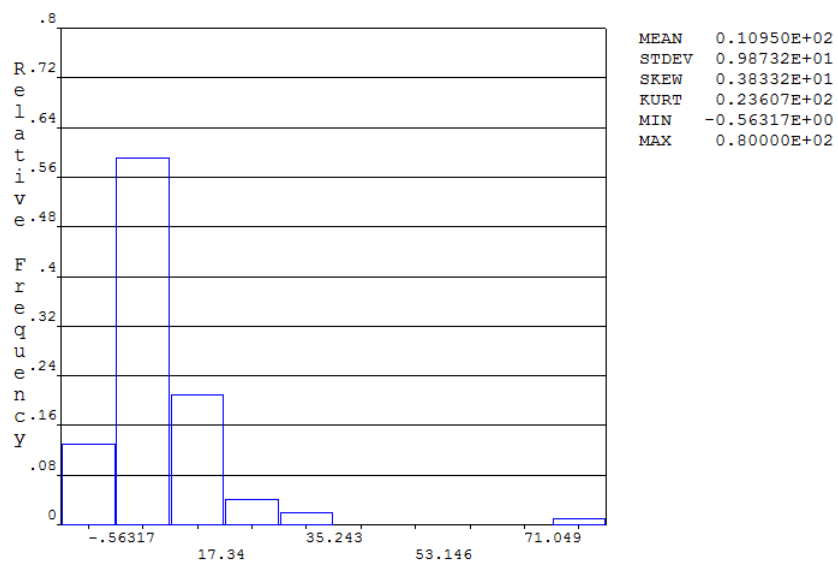


(b)

Figure 9.12. Sample history of natural log of fatigue life of interaction of dent with
 (a) longitudinal weld (b) girth weld



(a)



(b)

Figure 9.13. Histogram natural log of fatigue life of interaction of dent with
 (a) longitudinal weld (b) girth weld

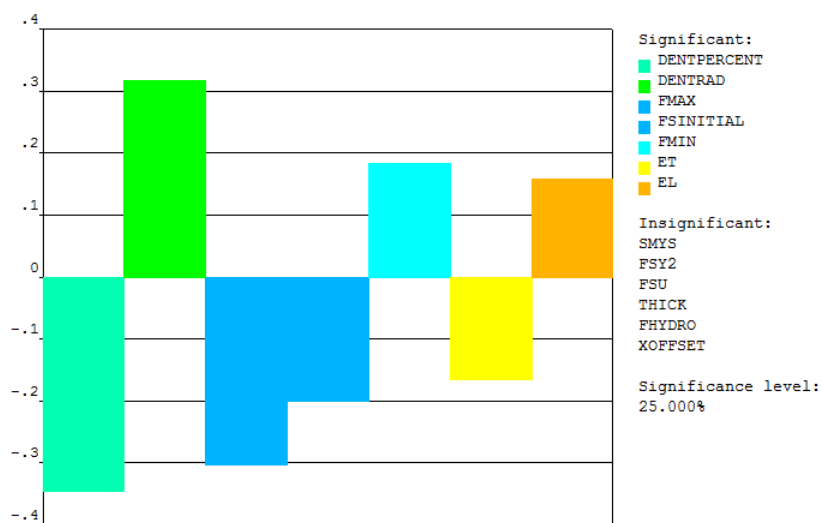
Table 9.2 Probability percentage of failure for dents interacting with welds

Life	Single dent	Dent with long weld	Dent with girth weld
1,000	6.8	41.8	35.4
5,000	10.2	49.6	50.8
10,000	12.2	53.3	53.1
50,000	17.9	63.3	64.2
100,000	18.5	66.6	66.8
500,000	21.2	70.1	72.4
1,000,000	22.8	70.7	73.8

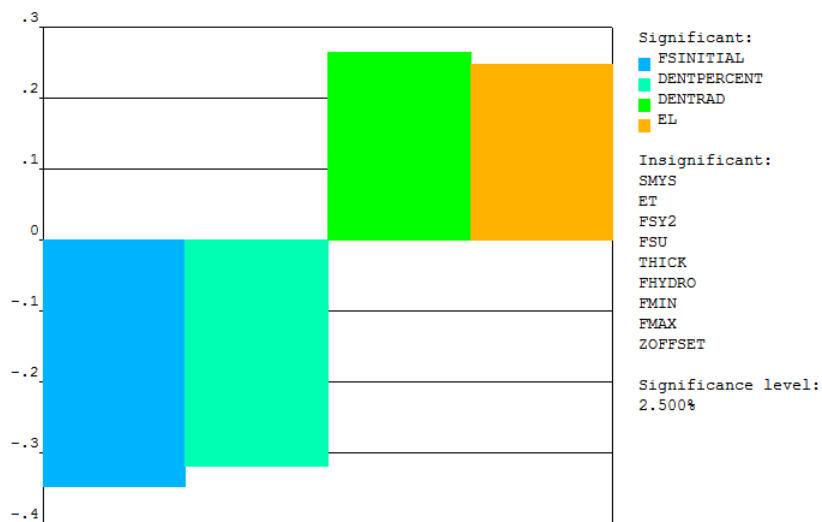
residual stresses in longitudinal and transverse directions. Moreover, in this dissertation work, the distribution of the residual stresses was assumed to be equal and uniform in both directions to simplify the problem, while the width of the affected residual stress was simulated longer in the case of girth weld in accordance with API 579 (2000). Therefore, the residual stresses effect of both cases would be similar.

Sensitivity analysis is performed to find out which input variable(s) affect each of the output variables. Figure 9.14.a shows the residual stress value is the fourth parameter affecting the fatigue life of dent interacting with longitudinal weld. The other three parameters preceding it in significance are the dent percent, dent radius and maximum applied pressure. In the case of dent interacting with girth weld, the residual stress value is the most significant parameter followed by the dent percent and the dent radius. Therefore, it can be concluded that the impact of interaction of weld with girth weld is more significant than the interaction of weld with longitudinal weld. It is noted that in both cases, the offset between the dent peak and the weld is not significant. This could be explained by the original selection of offset values in the input variables as it was defined in a range that is known to have interact effect.

The scatter plot of the natural log of fatigue life vs. the residual stress level is shown in Fig. 9.15. For the case of dent interacting with longitudinal weld, there is a negative correlation between the residual stress level and fatigue life, i.e. as the residual stress level increases, the fatigue life decreases. The same trend of negative correlation also exists for the case of dent interacting with girth weld. However, for the case of longitudinal weld, the magnitude of correlation is 0.20, while it is higher for the case of girth weld with a value of 0.35. Table B.4.3 lists the results of sensitivity analysis of all



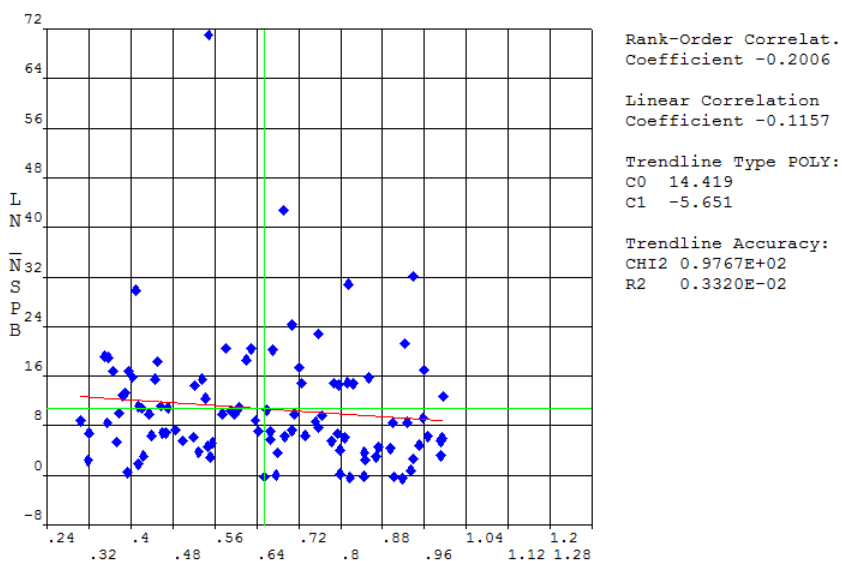
(a)



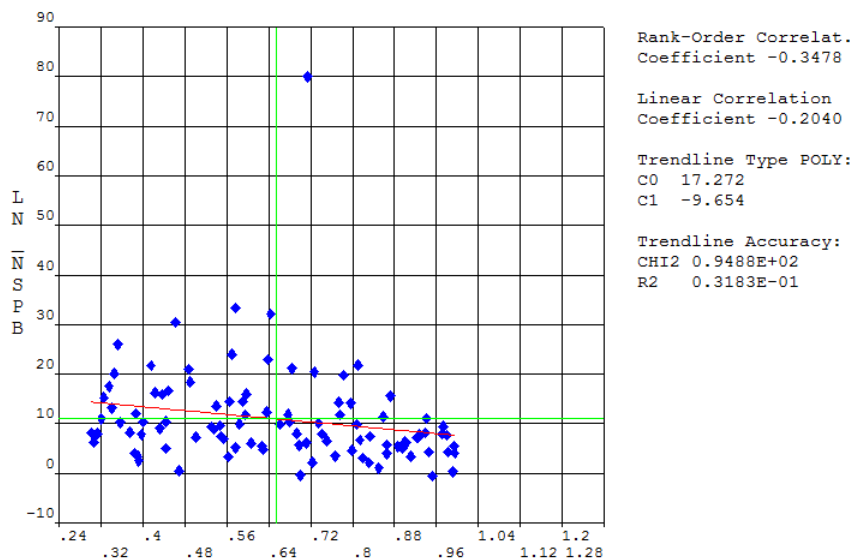
(b)

Figure 9.14. Sensitivity plot of fatigue life for interaction of dent with
 (a) longitudinal weld (b) girth weld

Note: Legend top-to-bottom order matches left-to-right order in figure



(a)



(b)

Figure 9.15. Scatter plot of fatigue life vs. residual stress value for dent interacting with
(a) longitudinal weld (b) girth weld

output variables to input variables in terms of Spearman correlation factor for the case of dent interacting with longitudinal welds while Table B.5.3 lists the sensitivity results for the case of dent interacting with girth welds.

9.5.4 Regression Analysis

In order to make the results of the probabilistic analysis to be easily applied in practical dent with metal loss problems, regression analysis is conducted to derive mathematical formulas of the output variables in terms of practically measured variables. Quadratic polynomial functions are the best fit for a similar problem as stated in section 6.5.4. Therefore, the following general function (Equation 9.1) was fit to all output variables where all output and input variables in dimensionless form. The two terms associate with pressure range are only applicable to output stress range and fatigue life.

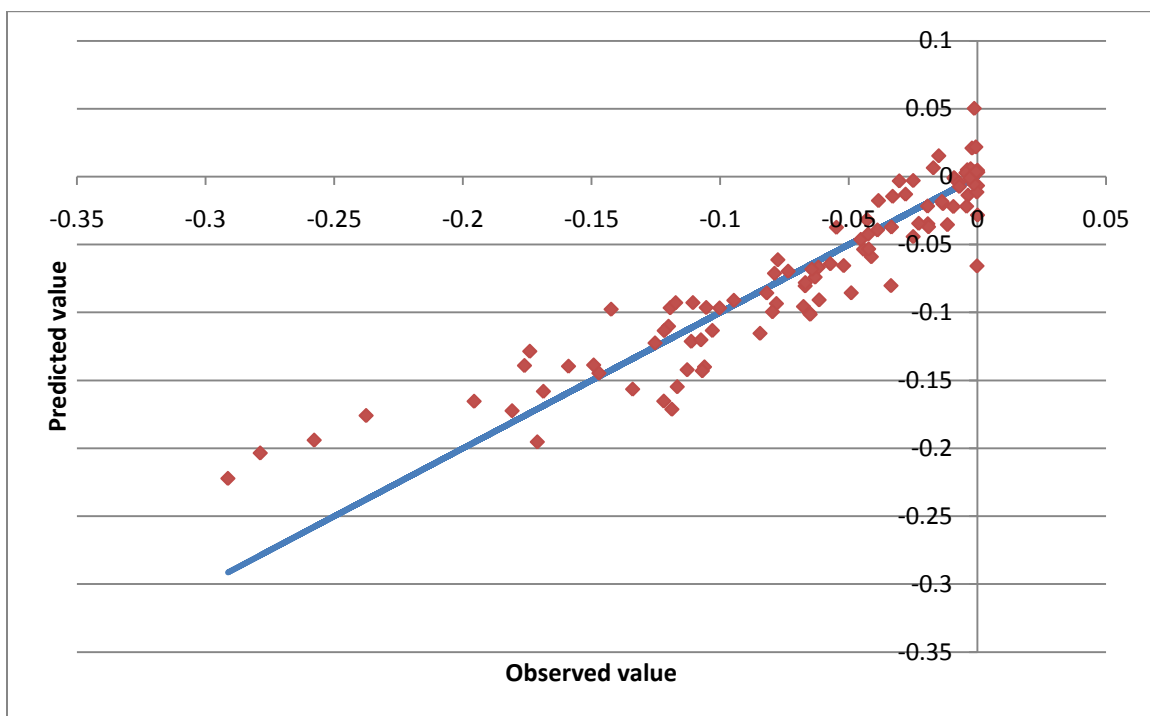
$$\begin{aligned}
 \text{Output variable} = & a_0 + b_1 \frac{D}{t} + b_2 \frac{d}{D} + b_3 \frac{l}{D} + b_4 \frac{w}{D} + b_5 \frac{ldw}{D^2 t} + b_6 \frac{\sigma_{flow}}{E_{avg}} + b_7 \frac{E_t}{E_l} + \\
 & b_8 \frac{\sigma_{residual}}{\sigma_y} + b_9 \frac{offset}{D} + b_{10} \frac{P_{max} - P_{min}}{P_{SMYS}} + c_1 \left(\frac{D}{t}\right)^2 + c_2 \left(\frac{d}{D}\right)^2 + c_3 \left(\frac{l}{D}\right)^2 + c_4 \left(\frac{w}{D}\right)^2 + \\
 & c_5 \left(\frac{ldw}{D^2 t}\right)^2 + c_6 \left(\frac{\sigma_{flow}}{E_{avg}}\right)^2 + c_7 \left(\frac{E_t}{E_l}\right)^2 + c_8 \left(\frac{\sigma_{residual}}{\sigma_y}\right)^2 + c_9 \left(\frac{offset}{D}\right)^2 + c_{10} \left(\frac{P_{max} - P_{min}}{P_{SMYS}}\right)^2 \quad (9.1)
 \end{aligned}$$

Table B.4.4 gives the constants values and R-squared value for the regression fit of all output variables of strain, stress, stress range, and fatigue life for the case of interaction of

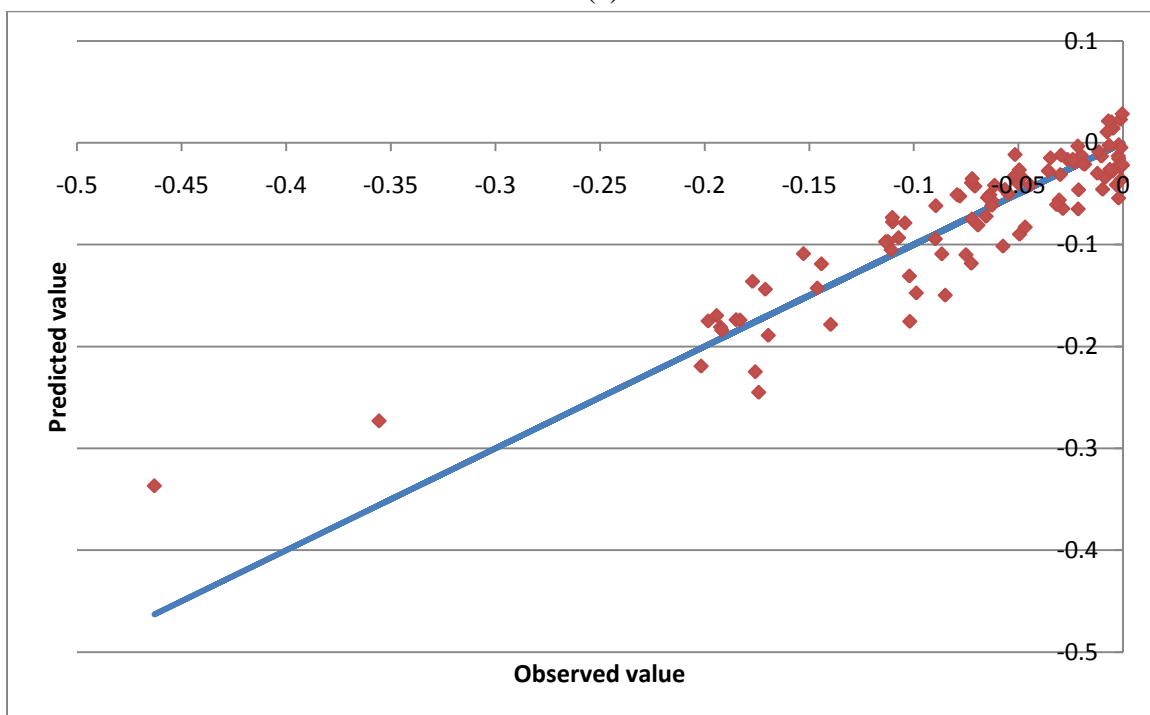
dent with longitudinal weld. The R-squared value is higher than 0.5 in 41 out of 45 output variables which indicate that the proposed general formula (9.1) is a very good choice. For the case of dent interacting with girth weld, the regressions coefficients are given in Table B.5.4. Once again, the R-squared value is more than 0.5 in 39 out of 45 variables which means also that the proposed general formula is good for girth weld case. Figure 9.16 shows the regression curve for the axial strain at dent peak which has an excellent fit of R-squared 0.85 for the case of longitudinal weld and 0.84 for the case of girth weld. The regression fit for the output stress variables is also very good for the case of denting interacting with longitudinal weld as Fig. 9.17.a illustrates with R-squared of 0.77. The fit is not as good for output stress variable for dent interacting with girth weld as the R-squared is 0.5 (Fig. 9.17.b). The regression curve of the natural log of the fatigue life is given in Fig. 9.18 which shows very good correlation at values up to natural log of 20 (equivalent to 5×10^7 fatigue cycles) which exceeds the endurance level, and therefore, it is considered an acceptable fit in the practical range of use.

9.6 SUMMARY

In this chapter, the effect of interaction of dent with residual stresses of longitudinal as well as girth welds was investigated using both deterministic analysis and probabilistic analysis. In the deterministic analysis, two cases one for the dent interaction with longitudinal weld and the other for dent interacting with girth weld were studied and compared with the plain dent case. The results showed that the values of strains and stresses are not affected much at the end of indentation phase, and therefore, the effect of weld is not significant for the case of pipes under static loading. However, the fatigue life

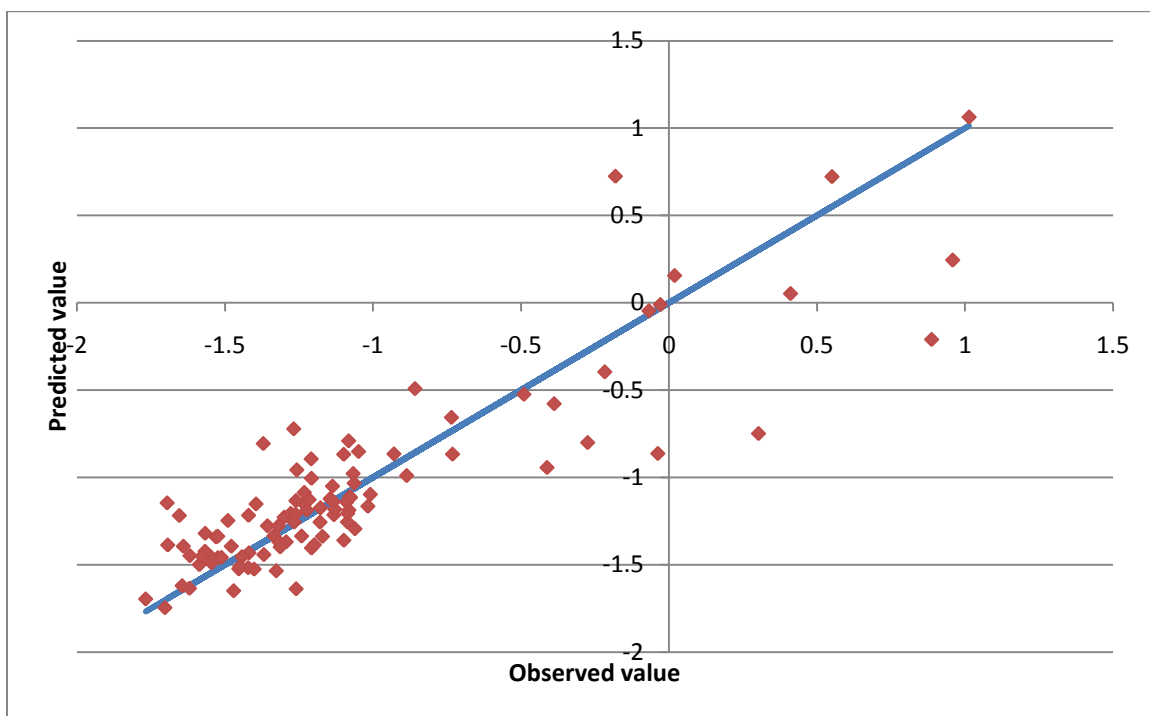


(a)

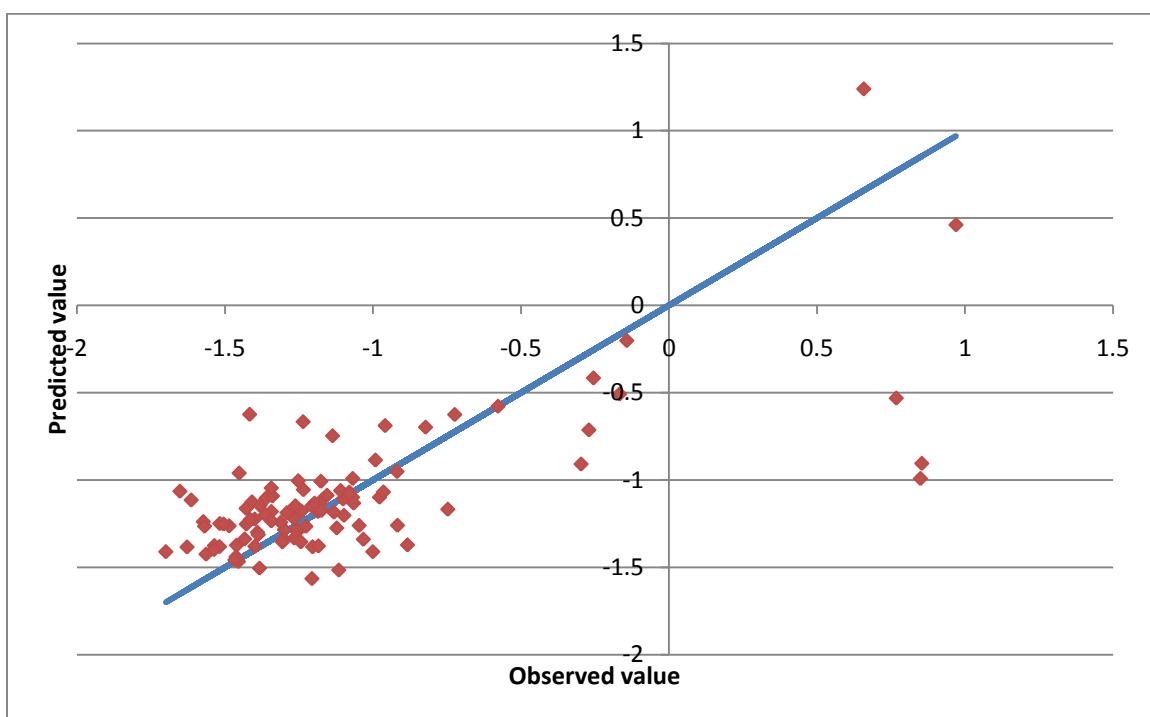


(b)

Figure 9.16. Regression fit curve for axial strain at dent peak for dent interacting with (a) longitudinal weld (b) girth weld

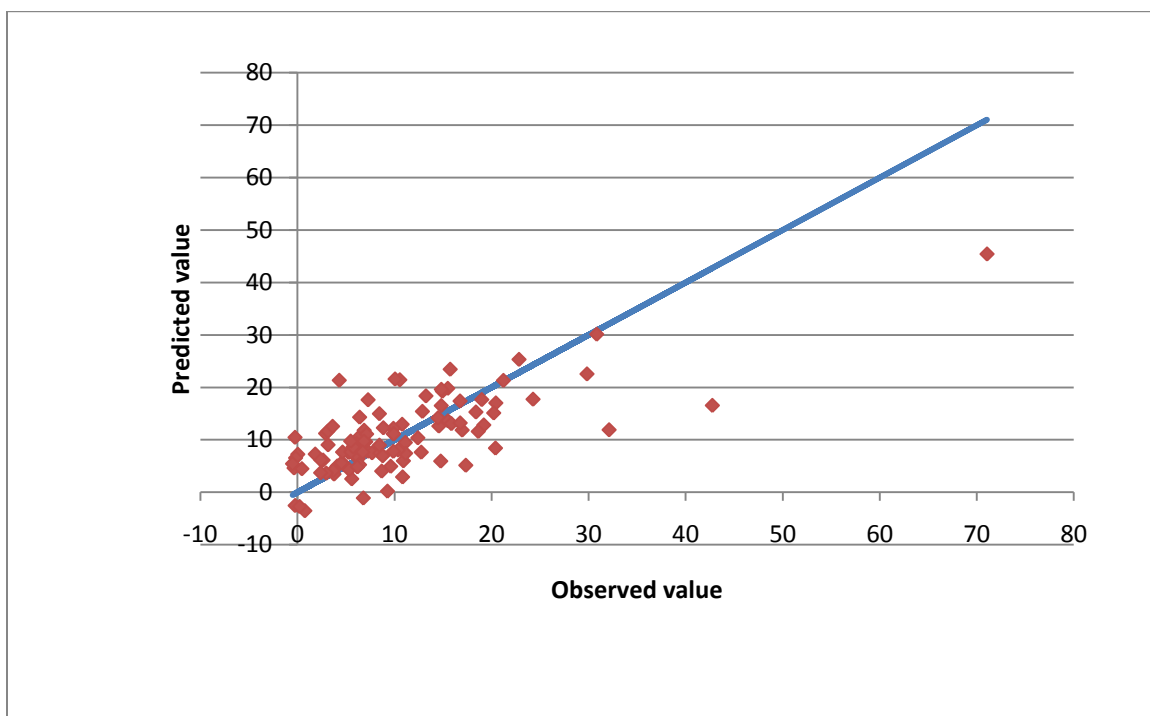


(a)

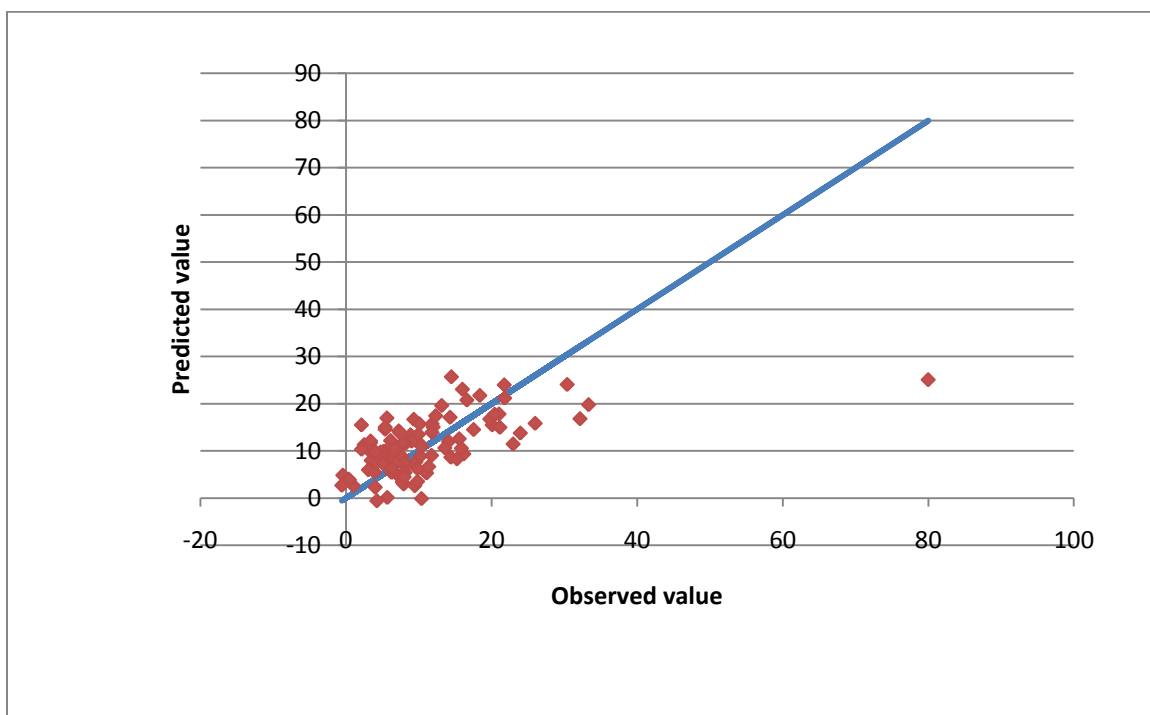


(b)

Figure 9.17. Regression fit curve for axial stress at dent peak for dent interacting with
(a) longitudinal weld (b) girth weld



(a)



(b)

Figure 9.18. Regression fit curve for natural log of fatigue life for dent interacting with (a) longitudinal weld (b) girth weld

in the cyclic pressure is reduced by 89% in the case of dent interacting with longitudinal weld and by 63% in the case of dent interacting with girth weld. Therefore, dents interacting with welds are considered a serious threat to the integrity of pipelines under cyclic pressure conditions. In the probabilistic analysis, a total of 200 cases, two sets of 100 cases for each weld configuration, randomly generated using Monte Carlo simulations were analyzed. The statistical distribution of output parameters and correlation between output and input variables were presented. The results showed that the probability of failure of a dent interacting with weld is 3 to 8 times higher than that of plain dent which increases the failure risk proportionally. Additionally, the sensitivity of strain and stress fields as well as the fatigue life to the various input parameters was determined. There was a negative correlation between the level of the residual stresses and the fatigue life, and therefore, the higher the level of the weld residual stress, the lower the fatigue life. Finally, a general formula was proposed to relate the output variables in terms of practically measured variables. Regression analysis was conducted to derive the coefficients and the results showed the general formula was a good choice. The R-squared values were higher than 0.5 in most of the cases and reaching values as high as 0.96 proving to be a very good choice.

CHAPTER 10

CONCLUSIONS AND RECOMMENDATIONS

In this research, an approach of combined probabilistic and numerical FEA analyses was developed and utilized for the first time in the assessment of mechanical damage of transportation pipelines under static and cyclic pressure loading. The probabilistic model was developed based on real-life inspection data collected from many local and external pipeline companies. The base case of the FEA numerical model was validated against published full-scale tests that had comprehensive instrumentations in various location and direction. Several cases were analyzed using this approach including plain dent, 2 interacting dents, dent interacting with metal loss, and dent interacting with residual stresses of longitudinal and girth weld. A Comprehensive set of regression formulas for strains, stresses, and fatigue life was derived and can be programmed into a spreadsheet for use by the pipeline operators to determine severity of mechanical damage. Moreover, probabilities of failure were also estimated for two different sets of pipelines inspection data and for different cases of combined damage. The probability of failure can be used in risk assessment of new pipelines.

10.1 CONCLUSIONS

- The material model plays decisive rule on the accuracy of the FEA results especially in the case of cyclic pressure loading. Therefore, detailed material properties are

needed to conduct appropriate integrity assessment of dented pipes under such cyclic conditions to calculate the expected cycles to failure. If those material properties are not available, appropriate safety factor must be included.

- The conditions of pipeline installations affect the probability of failure. It was found that the local company which has installation mostly in sandy areas have smoother dent profiles, and thus, less probability of failure compared to external companies which have installation in rocky areas.
- The probability of failure of two interacting dents is 3 to 7 times higher than that of plain dent which increases the failure risk proportionally.
- The fatigue life had a very strong positive correlation with the dent percent, which indicates that shallow 2 dents post higher risk to pipelines than deeper ones.
- The probability of failure of a pipe with combined mechanical damage of dent with metal loss is twice that of pipe with plain dent without metal loss.
- The fatigue life in the cyclic pressure is reduced by 89% in the case of dent interacting with longitudinal weld and by 63% in the case of dent interacting with girth weld.
- The probability of failure of a dent interacting with weld is 3 to 8 times higher than that of plain dent which increases the failure risk proportionally.

10.2 RECOMMENDATIONS

- Develop software of integrity assessment of mechanical damage based on the regression formulas in this paper to be used in real life situations of mechanical damage. Evaluate the need of calibration and modification.

- Append the inspection data of mechanical damage of the local company in Saudi Arabia on yearly basis. Any significant change in the distribution of the input parameters would mean a change in the probability of failure.
- Evaluate the sensitivity of the regression formulas to different range and distribution of the input parameters by repeating the approach several times for different distributions.
- Increase the sample size in the probability analysis from 100 to other sizes such as 200, 500, 1000, etc. and investigate the effect on the mean and confidence interval of probability of failure.
- Utilize the approach and results of this paper in a formal uncertainty analysis to determine the effects of pipe manufacturing tolerances and dent measurement errors on the expected error of the calculated strains, stresses, and fatigue life.

NOMENCLATURE

Material modeling (Ch # 4):

C	translation multiplier
C_i, γ_i	special material parameters for Chaboche model
E	modulus of elasticity
F	yield criterion
R	yield stress
R_0, R_∞	special material parameters for non-linear isotropic hardening model
r_{ij}	Stress-to-reference stress ratios in Hill's anisotropy model
{S}	deviatoric stress
{ α }	yield surface translation
$\hat{\epsilon}^{pl}$	equivalent plastic strain
ν	poisson's ratio
{ σ }	stresses
σ_y	material yield parameter

Statistical terms (Chapter # 5)

C	constant
CI	Confidence Interval
COV	Coefficient of Variation
f	probability density function
F	probability value of the statistical F-distribution

F_0	theoretical cumulative distribution function
F_n	empirical cumulative distribution function
KSD	Kolmogorov-Smirnov distance test parameter
P-value	probability associated with null hypothesis test
S	variance
x	random variable
\hat{t}	probability value of the statistical t-distribution
α	significance level
β	shape parameter of the Weibull distribution
Δ	difference operator
δ	scale parameter of the Weibull distribution
γ	location parameter of the Weibull distribution
ν	degrees of freedom
μ	arithmetic mean
μ_1	arithmetic mean of logarithm of random variable x
σ	standard deviation of random variable x
σ_1	standard deviation of logarithm of random variable x
ω	ratio of variances

Fatigue analysis:

b	fatigue exponent
N	Fatigue cycles to failure
σ_a	stress amplitude

σ_{ar}	equivalent completely reversed stress amplitude
σ_m	mean stress
σ_f	fatigue strength
S_e	endurance limit
S_{ut}	ultimate tensile strength

Damage parameters for probabilistic analysis and regression formulas:

E_l	modulus of elasticity in longitudinal direction
E_t	modulus of elasticity in transverse direction
D	pipe diameter
d	depth of dent
d_m	depth of metal loss
d_{e-e}	edge-to-edge distance of 2 dents
l	length
P	pressure
r	indenter radius
SMYS	specified minimum yield strength
t	pipe thickness
t_m	thickness of metal loss area
w	width
ϕ	orientation angle between two dents, radians
σ_{flow}	average of actual yield and tensile strengths
σ_u	true tensile strength
$\sigma_{residual}$	weld residual stress

σ_y yield strength

APPENDIX A

INSPECTION DATA OF MECHANICAL DAMAGE

Table A.1. Inspection data of dents from local company

No.	D (mm)	t (mm)	Const date	Survey date	SMYS (MPa)	P (MPa)	Design factor	Depth (mm)	d/D (%)	Length (mm)	l/d	Service	Seam type
1	610	6.4	1978	2008	359	3.7	50	24.4	4	1950.7	79.9	gas	ERW
2	610	6.4	1978	2008	359	3.7	50	21.3	3.5	3401.1	159.7	gas	ERW
3	610	6.4	1978	2008	359	3.7	50	18.3	3	2199.6	120.2	gas	ERW
4	610	6.4	1978	2008	359	3.7	50	15.2	2.5	1999.0	131.5	gas	ERW
5	610	6.4	1978	2008	359	3.7	50	12.2	2	1999.0	163.9	gas	ERW
6	610	6.4	1978	2008	359	3.7	50	27.4	4.5	2601.0	94.9	gas	ERW
7	610	6.4	1978	2008	359	3.7	50	12.2	2	1999.0	163.9	gas	ERW
8	610	6.4	1978	2008	359	3.7	50	18.3	3	1999.0	109.2	gas	ERW
9	1168	9.5	1973	2008	359	4.0	72	58.4	5			liquid	SAW
10	254	5.2	1988	2005	359	5.0	50	17.8	7			gas	seamless
11	254	5.2	1988	2005	359	5.0	50	5.1	2			gas	seamless
12	406	6.4	1971	2007	242	3.0	40	20.3	5	20.3	1.0	gas	ERW
13	406	6.4	1971	2007	242	3.0	50	16.3	4	20.3	1.2	gas	ERW
14	406	6.4	1971	2007	242	3.0	40	18.3	4.5	20.3	1.1	gas	ERW
15	406	6.4	1971	2007	242	3.0	50	16.3	4	20.3	1.2	gas	ERW
16	406	6.4	1971	2007	242	3.0	50	16.3	4	20.3	1.2	gas	ERW
17	406	6.4	1971	2007	242	3.0	50	16.3	4	20.3	1.2	gas	ERW
18	559	7.9	1952	2007	228	2.9	60	22.4	4	2999.7	133.9	liquid	ERW
19	559	7.9	1952	2007	228	2.9	60	16.8	3	1999.0	119.0	liquid	ERW
20	559	7.9	1952	2007	228	2.9	72	16.8	3	1999.0	119.0	liquid	ERW
21	559	7.9	1952	2007	228	2.9	72	16.8	3	1999.0	119.0	liquid	ERW
22	559	7.9	1952	2007	228	2.9	72	16.8	3	1501.1	89.4	liquid	ERW
23	559	7.9	1952	2007	228	2.9	72	22.4	4	2799.1	125.0	liquid	ERW
24	508	6.4	1952	2007	228	2.8	50	20.3	4	2301.2	113.4	liquid	ERW
25	508	6.4	1952	2007	228	2.8	50	15.2	3	2499.4	164.4	liquid	ERW
26	508	6.4	1952	2007	228	2.8	50	30.5	6	4000.5	131.2	liquid	ERW
27	508	9.5	1952	2007	359	2.8	40	15.2	3	2301.2	151.4	liquid	ERW
28	508	9.5	1952	2007	359	2.8	40	25.4	5	2900.7	114.2	liquid	ERW
29	508	9.5	1952	2007	359	2.8	40	40.6	8			liquid	ERW
30	508	9.5	1952	2007	359	2.8	40	55.9	11			liquid	ERW
31	1168	11.1	1977	2008	414	4.4	72	81.8	7			liquid	SAW
32	1168	11.1	1977	2008	414	4.4	72	46.7	4			liquid	SAW
33	1168	11.1	1977	2008	414	4.4	72	80.6	6.9			liquid	SAW
34	1219	10.2	1977	2008	414	4.4	72	36.6	3			liquid	SAW

No.	D (mm)	t (mm)	Const date	Survey date	SMYS (MPa)	P (MPa)	Design factor	Depth (mm)	d/D (%)	Length (mm)	l/d	Service	Seam type
35	1219	10.2	1977	2008	414	4.4	72	24.4	2			liquid	SAW
36	1219	10.2	1977	2008	414	4.4	72	103.6	8.5			liquid	SAW
37	1219	9.5	1977	2008	414	4.4	72	36.6	3			liquid	SAW
38	1219	9.5	1977	2008	414	4.4	72	36.6	3			liquid	SAW
39	1219	9.5	1977	2008	414	4.4	72	36.6	3			liquid	SAW
40	1219	9.5	1977	2008	414	4.4	72	36.6	3			liquid	SAW
41	1219	9.5	1977	2008	414	4.4	72	36.6	3			liquid	SAW
42	1219	9.5	1977	2008	414	4.4	72	36.6	3			liquid	SAW
43	1219	9.5	1977	2008	414	4.4	72	61.0	5			liquid	SAW
44	1168	11.1	1977	2008	414	4.4	72	23.4	2			liquid	SAW
45	1168	11.1	1977	2008	414	4.4	72	35.1	3			liquid	SAW
46	1168	10.2	1977	2008	414	4.4	72	23.4	2			liquid	SAW
47	1168	10.2	1977	2008	414	4.4	72	40.9	3.5			liquid	SAW
48	1168	10.2	1977	2008	414	4.4	72	23.4	2			liquid	SAW
49	1168	10.2	1977	2008	414	4.4	72	23.4	2			liquid	SAW
50	1168	10.2	1977	2008	414	4.4	72	23.4	2			liquid	SAW
51	1168	10.2	1977	2008	414	4.4	72	23.4	2			liquid	SAW
52	1168	10.2	1977	2008	414	4.4	72	23.4	2			liquid	SAW
53	762	9.5	1960	2006	359	4.3	50	21.3	2.8	1999.0	93.8	liquid	SAW
54	762	9.5	1960	2006	359	4.3	50	34.3	4.5	4000.5	116.6	liquid	SAW
55	762	9.5	1960	2006	359	4.3	50	26.7	3.5	3500.1	131.1	liquid	SAW
56	762	9.5	1960	2006	359	4.3	50	19.1	2.5	2601.0	136.2	liquid	SAW
57	762	9.5	1960	2006	359	4.3	50	22.9	3	3401.1	148.5	liquid	SAW
58	762	9.5	1960	2006	359	4.3	50	22.9	3	4000.5	174.7	liquid	SAW
59	762	8.0	1960	2006	359	4.3	60	22.9	3	4000.5	174.7	liquid	SAW
60	762	8.0	1960	2006	359	4.3	60	22.9	3	2999.7	131.0	liquid	SAW
61	762	8.0	1960	2006	359	4.3	60	15.2	2			liquid	SAW
62	762	9.5	1960	2006	359	4.3	50	19.1	2.5	4000.5	209.5	liquid	SAW
63	762	9.5	1960	2006	359	4.3	50	34.3	4.5	5001.3	145.8	liquid	SAW
64	762	6.4	1960	2006	359	4.3	72	30.5	4	3700.8	121.3	liquid	SAW
65	762	6.4	1960	2006	359	4.3	72	15.2	2	2999.7	197.3	liquid	SAW
66	762	6.4	1960	2006	359	4.3	72	22.1	2.9	2999.7	135.7	liquid	SAW
67	762	6.4	1960	2006	359	4.3	72	21.3	2.8	2799.1	131.4	liquid	SAW
68	762	6.4	1960	2006	359	4.3	72	22.9	3	4000.5	174.7	liquid	SAW
69	762	6.4	1960	2006	359	4.3	72	45.0	5.9	5001.3	111.1	liquid	SAW

No.	D (mm)	t (mm)	Const date	Survey date	SMYS (MPa)	P (MPa)	Design factor	Depth (mm)	d/D (%)	Length (mm)	l/d	Service	Seam type
70	762	6.4	1960	2006	359	4.3	72	83.8	11			liquid	SAW
71	762	6.4	1960	2006	359	4.3	72	30.5	4	5001.3	164.0	liquid	SAW
72	762	6.4	1960	2006	359	4.3	72	26.7	3.5	4000.5	149.8	liquid	SAW
73	762	6.4	1960	2006	359	4.3	72	106.7	14			liquid	SAW
74	762	6.4	1960	2006	359	4.3	72	91.4	12			liquid	SAW
75	762	6.4	1960	2006	359	4.3	72	114.3	15			liquid	SAW
76	762	6.4	1960	2006	359	4.3	72	28.2	3.7	2999.7	106.4	liquid	SAW
77	762	6.4	1960	2006	359	4.3	72	22.9	3	5001.3	218.4	liquid	SAW
78	762	6.4	1960	2006	359	4.3	72	30.5	4	4000.5	131.2	liquid	SAW
79	762	6.4	1960	2006	359	4.3	72	19.1	2.5	4000.5	209.5	liquid	SAW
80	762	6.4	1960	2006	359	4.3	72	19.1	2.5	4500.9	235.6	liquid	SAW
81	762	6.4	1960	2006	359	4.3	72	22.9	3	2999.7	131.0	liquid	SAW
82	762	6.4	1960	2006	359	4.3	72	38.1	5	4000.5	105.0	liquid	SAW
83	762	6.4	1960	2006	359	4.3	72	30.5	4	4399.3	144.2	liquid	SAW
84	762	6.4	1960	2006	359	4.3	72	22.9	3	4000.5	174.7	liquid	SAW
85	762	6.4	1960	2006	359	4.3	72	76.2	10			liquid	SAW
86	762	6.4	1960	2006	359	4.3	72	29.0	3.8	4699.0	162.0	liquid	SAW
87	762	6.4	1960	2006	359	4.3	72	26.7	3.5	5001.3	187.3	liquid	SAW
88	762	6.4	1960	2006	359	4.3	72	26.7	3.5	5499.1	206.0	liquid	SAW
89	762	6.4	1960	2006	359	4.3	72	26.7	3.5	5400.0	202.2	liquid	SAW
90	762	6.4	1960	2006	359	4.3	72	30.5	4	4000.5	131.2	liquid	SAW
91	762	6.4	1960	2006	359	4.3	72	41.9	5.5	4800.6	114.6	liquid	SAW
92	762	6.4	1960	2006	359	4.3	72	29.0	3.8	3200.4	110.4	liquid	SAW
93	762	6.4	1960	2006	359	4.3	72	28.2	3.7	4000.5	141.9	liquid	SAW
94	762	6.4	1960	2006	359	4.3	72	26.7	3.5	5699.8	213.5	liquid	SAW
95	762	6.4	1960	2006	359	4.3	72	34.3	4.5	5999.5	174.9	liquid	SAW
96	762	6.4	1960	2006	359	4.3	72	36.6	4.8	6101.1	166.7	liquid	SAW
97	762	6.4	1960	2006	359	4.3	72	28.2	3.7	2700.0	95.7	liquid	SAW
98	762	6.4	1960	2006	359	4.3	72	26.7	3.5	2900.7	108.6	liquid	SAW
99	762	6.4	1960	2006	359	4.3	72	22.9	3	4201.2	183.5	liquid	SAW
100	762	6.4	1960	2006	359	4.3	72	34.3	4.5	4399.3	128.3	liquid	SAW
101	762	6.4	1960	2006	359	4.3	72	22.1	2.9	3401.1	153.9	liquid	SAW
102	762	6.4	1960	2006	359	4.3	72	34.3	4.5			liquid	SAW
103	762	6.4	1960	2006	359	4.3	72	32.8	4.3	2700.0	82.3	liquid	SAW
104	762	6.4	1960	2006	359	4.3	72	27.4	3.6	2999.7	109.5	liquid	SAW

No.	D (mm)	t (mm)	Const date	Survey date	SMYS (MPa)	P (MPa)	Design factor	Depth (mm)	d/D (%)	Length (mm)	l/d	Service	Seam type
105	762	6.4	1960	2006	359	4.3	72	26.7	3.5	4000.5	149.8	liquid	SAW
106	762	6.4	1960	2006	359	4.3	72	25.1	3.3	4300.2	171.3	liquid	SAW
107	762	6.4	1960	2006	359	4.3	72	30.5	4	4300.2	141.0	liquid	SAW
108	762	6.4	1960	2006	359	4.3	72	15.2	2			liquid	SAW
109	965	7.1	1971	2006	414	3.1	50	154.4	16			liquid	Spiral SAW
110	965	7.1	1971	2009	414	4.3	72	48.3	5	2999.7	62.1	liquid	Spiral SAW
111	1016	7.5	1971	2009	414	4.3	72	40.6	4	2499.4	61.6	liquid	Spiral SAW
112	1016	7.5	1971	2009	414	4.3	72	25.4	2.5	1699.3	66.9	liquid	Spiral SAW
113	1016	7.5	1971	2009	414	4.3	72	50.8	5	2999.7	59.0	liquid	Spiral SAW
114	1016	7.5	1971	2009	414	4.3	72	40.6	4	5001.3	123.2	liquid	Spiral SAW
115	1016	7.5	1971	2009	414	4.3	72	30.5	3	5001.3	164.0	liquid	Spiral SAW
116	1016	7.5	1971	2009	414	4.3	72	35.6	3.5	5001.3	140.5	liquid	Spiral SAW
117	1016	7.5	1971	2009	414	4.3	72	40.6	4	4000.5	98.5	liquid	Spiral SAW
118	1016	7.5	1971	2009	414	4.3	72	20.3	2			liquid	Spiral SAW
119	1016	7.5	1971	2009	414	4.3	72	40.6	4	4000.5	98.5	liquid	Spiral SAW
120	1016	7.5	1971	2009	414	4.3	72	40.6	4	3500.1	86.2	liquid	Spiral SAW
121	1016	7.5	1971	2009	414	4.3	72	38.6	3.8	5001.3	129.6	liquid	Spiral SAW
122	1016	7.5	1971	2009	414	4.3	72	40.6	4	1999.0	49.2	liquid	Spiral SAW
123	1016	7.5	1971	2009	414	3.1	50	30.5	3	2999.7	98.4	liquid	Spiral SAW
124	1016	7.5	1971	2009	414	3.1	50	40.6	4	1999.0	49.2	liquid	Spiral SAW
125	965	7.1	1971	2009	414	3.1	50	38.6	4	2999.7	77.7	liquid	Spiral SAW
126	965	7.1	1971	2009	414	3.1	50	48.3	5	5999.5	124.2	liquid	Spiral SAW
127	965	7.1	1971	2009	414	3.1	50	35.7	3.7	1800.9	50.4	liquid	Spiral SAW
128	965	7.1	1971	2009	414	3.1	50	29.0	3	2499.4	86.2	liquid	Spiral SAW
129	965	7.1	1971	2009	414	3.1	50	29.0	3	2199.6	75.8	liquid	Spiral SAW
130	965	7.1	1971	2009	414	3.1	50	38.6	4			liquid	Spiral SAW
131	965	7.1	1971	2009	414	3.1	50	38.6	4	4000.5	103.6	liquid	Spiral SAW
132	965	7.1	1971	2009	414	3.1	50	43.4	4.5			liquid	Spiral SAW
133	1016	7.5	1971	2009	414	2.5	40	40.6	4	4000.5	98.5	liquid	Spiral SAW
134	1016	7.5	1971	2009	414	2.5	40	45.7	4.5	5001.3	109.4	liquid	Spiral SAW

Table A.2. Sample of mechanical damage survey data by PRCI (Semiga, December 2007)

No.	Type	Corrosion	D (mm)	t (mm)	Const date	Survey date	SMYS (MPa)	P (MPa)	DF	Multiple dents
1	Gouge and dent	No	914	7.1	1968	2001	359	4.0	0.72	No
2	Gouge and dent	d <10%	168	4.8	1963	2001	290	9.9	0.72	No
3	Gouge and dent	No	219	4.8	1963	2005	290	9.1	0.72	No
4	Gouge and dent	No	406	6.4	1979	2006	414	9.3	0.72	No
5	Gouge and dent	No	406	6.4	1978	2005	414	9.3	0.72	No
6	Dent	d <10%	813	7.1	1963	2003	359	4.5	0.72	No
7	Buckle	No	914	7.1	1963	2002	359	4.0	0.72	Yes
8	Dent	No	762	12.7	1963	2001	290	7.1	0.72	No
9	Dent	No	914	7.1	1963	2002	359	4.0	0.72	No
10	Dent	No	1016	8.7	1978	2003	359	4.0	0.72	No

No.	ILI data					dent	metal los	depth	location
	Depth (mm)	d/D	length (mm)	l/d	w (mm)				
1	17.4	1.9	152.4	8.8		Yes	Yes	d <10%	
2	11.9	7	152.4	12.8		Yes	Yes	10%<d>20%	
3	9.4	4.3	1513.8	161.0		Yes	Yes	No	
4	2.5	0.6	73.7	29.5		Yes	No	No	
5	6.9	1.7	61.0	8.8		Yes	Yes	Pass B31G	
6	14.6	1.8	304.8	20.9		Unknown	Unknown	Unknown	
7	68.6	7.5	1219.2	17.8		Yes	No	No	
8	19.1	2.5	464.8	24.3		Yes	No	No	
9	86.0	9.4	736.6	8.6		Yes	No	No	
10	12.2	1.2	30.5	2.5		Yes	No	No	

Digging data							
No.	depth (mm)	d/D	length (mm)	l/d	w (mm)	corros depth (mm)	corros length (mm)
1	15.9	1.7	50.8	3.2	50.8		
2	25.4	15	127.0	5.0	127.0		
3	18.0	8.2	381.0	21.2	101.6		
4	2.0	0.5	72.9	36.5	76.2		
5	10.8	2.6	355.6	32.9	228.6		
6	15.9	2	609.6	38.3	584.2		
7	34.9	3.8	914.4	26.2	1600.2		
8	15.9	2.1	457.2	28.8	355.6		
9	11.1	1.2	609.6	54.9	431.8		
10	18.5	1.8	965.2	52.2	1676.4		

APPENDIX B

DETAILED INPUT AND RESULTS OF PROBABILISTIC DESIGN ANALYSIS

Table B.1.1. List of random input variables and their statistical distribution (μ = mean value, σ = standard deviation) for single dent

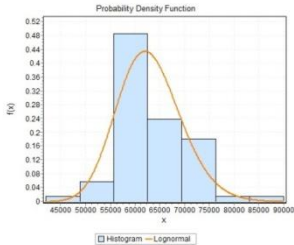
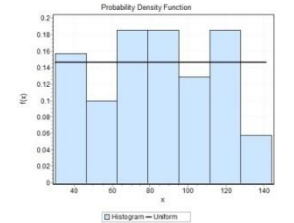
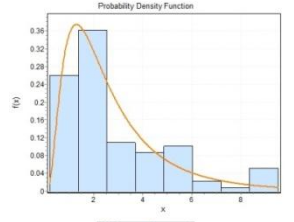
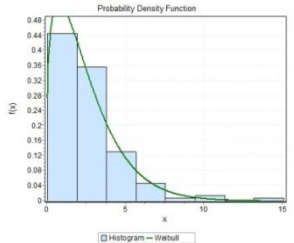
Variable	Distribution	μ	σ	Density function
MATERIAL INPUT PARAMETERS				
SMYS (MPa), SMYS (data collected from a local source for a list of pipeline purchase orders)	Lognormal	434	44	
E_l (MPa), EL	Normal	1.90×10^5	2.6×10^4	
E_t (MPa), ET	Normal	1.90×10^5	2.6×10^4	
$\sigma_v @ \varepsilon = 0.002$ (MPa), SY1=0.002*EI				
FSY2	Normal	1.15	0.075	
$\sigma_v @ \varepsilon = 0.005$ (MPa), SY2=FSY2*SMYS				
FSU	Normal	1.65	0.12	
σ_u (MPa), SU=FSU*SMYS				
GEOMETRY INPUT PARAMETERS				
D (mm), PIPEDIA=610				
D/t, DTRATIO (data collected from a local source for a list of pipeline purchase orders)	Uniform	85	± 55	
t (mm), THICK=DTRATIO*PIPEDIA				
r (mm), DENTRAD	Lognormal	73	61	
INDENTATION AND PRESSURE LOADING INPUT PARAMETERS				
d/D (%), DENTPERCENT	Weibul		$\gamma=1.2689$ $\text{Char}=2.6618$ $\text{Offset}=0$	
d (mm), d=DENTPERCENT/100*PIPEDIA				
P_{SMYS} (MPa), PSMYS=SMYS*2*THICK/PIPDIA				
FHYDRO	Normal	0.95	0.025	
FMIN	Uniform	0.2	± 0.1	
FMAX	Triangular	0.72	0.6-0.8	
P_{hydro} (MPa), PHYDRO=FHYDRO*PSMYS				
P_{min} (MPa), PMIN=FMIN*PSMYS				
P_{max} (MPa), PMAX=FMAX*PSMYS				

Table B.1.2. Output parameters and their statistical distribution for single dent (μ = mean value, σ = standard deviation)

NAME	DESCRIPTION			μ	σ
	Direction	Component	Location		
LENGTH	Dent length			216	144
WIDTH	Dent width			78	21
Strains at end of indentation phase					
EATP	Axial	Total	dent peak	-7.62E-02	7.57E-02
EAMP	Axial	Membrane	dent peak	5.54E-03	1.27E-02
EABP	Axial	Bending	dent peak	8.18E-02	8.40E-02
EATXA_Z	Location of maximum tensile value along dent longitudinal			10.34	21.13
EATXA	Axial	Total	maximum tensile in dent longitudinal	1.12E-02	1.39E-02
EAMXA	Axial	Membrane	maximum tensile in dent longitudinal	3.32E-03	5.35E-03
EABXA	Axial	Bending	maximum tensile in dent longitudinal	7.90E-03	9.32E-03
EHTP	Hoop	Total	dent peak	-1.03E-01	9.26E-02
EHMP	Hoop	Membrane	dent peak	-5.53E-04	9.89E-03
EHBP	Hoop	Bending	dent peak	1.03E-01	9.56E-02
Strains at end of indentation phase					
SATP	Axial	Total	dent peak	-470	256
SAMP	Axial	Membrane	dent peak	75	226
SABP	Axial	Bending	dent peak	515	172
SATNA_Z	Location of maximum compressive value along dent longitudinal			4	11
SATNA	Axial	Total	maximum tensile in dent longitudinal	-529	150
SAMNA	Axial	Membrane	maximum tensile in dent longitudinal	56	200
SABNA	Axial	Bending	maximum tensile in dent longitudinal	544	148
SATNH_X	Location of maximum compressive value along dent transverse			13	14
SATNH	Axial	Total	maximum tensile in dent transverse	-588	137
SAMNH	Axial	Membrane	maximum tensile in dent transverse	-13	189
SABNH	Axial	Bending	maximum tensile in dent transverse	581	149
SHTP	Hoop	Total	dent peak	-563	237
SHMP	Hoop	Membrane	dent peak	-29	222
SHBP	Hoop	Bending	dent peak	577	174
SHTNA_Z	Location of maximum compressive value along dent longitudinal			9	11
SHTNA	Hoop	Total	maximum tensile in dent longitudinal	-635	150
SHMNA	Hoop	Membrane	maximum tensile in dent longitudinal	-74	172
SHBNA	Hoop	Bending	maximum tensile in dent longitudinal	615	149
SHTXH_X	Location of maximum tensile value along dent transverse			137	29
SHTXH	Hoop	Total	maximum tensile in dent transverse	241	172
SHMXH	Hoop	Membrane	maximum tensile in dent transverse	-76	61
SHBXH	Hoop	Bending	maximum tensile in dent transverse	276	183
SHTNH_X	Location of maximum compressive value along dent transverse			2	6
SHTNH	Hoop	Total	maximum tensile in dent transverse	-612	150
SHMNH	Hoop	Membrane	maximum tensile in dent transverse	-38	208
SHBNH	Hoop	Bending	maximum tensile in dent transverse	604	145
Stress range and fatigue life at end of pressure cycle phase					
SRP	Von Mises	Range	dent peak	58	47
SMP	Von Mises	Mean	dent peak	334	158
SRA_Z	Location of maximum stress range in dent longitudinal direction			1.314	5.34
SRA	Von Mises	Range	maximum in dent longitudinal	33	43
SMA	Von Mises	Mean	maximum in dent longitudinal	476	121
SRH_X	Location of maximum stress range in dent transverse direction			0.8546	1.394
SRH	Von Mises	Range	maximum in dent transverse direction	57	45
SMH	Von Mises	Mean	maximum in dent transverse direction	426	136
N_log	fatigye cycles to failure (in natural log)			18.75	10.26

Table B.1.3. Rank order Spearman Correlation factors between output and input parameters for single dent

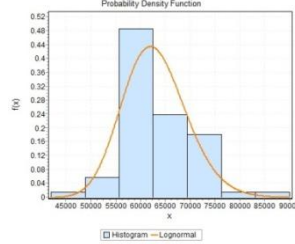
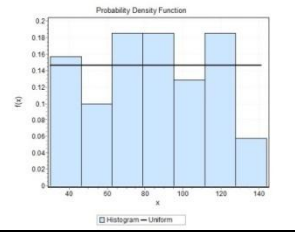
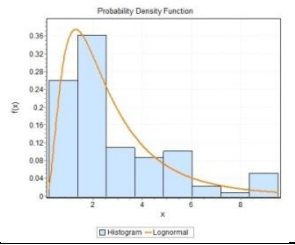
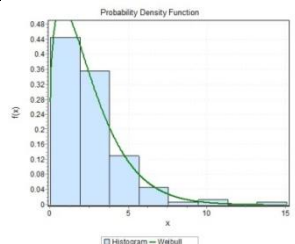
Out\Inp	SMY S	EL	ET	FSY2	FSU	THIC K	DENT- RAD	DENT- PERCEN T	FHYDR O	FMIN	FMA X
LENGT H	0.002	-0.142	0.051	-0.025	0.124	-0.443	0.401	-0.612	0.083	-0.061	-0.01
WIDTH	0.056	-0.123	0.044	0.069	0.135	-0.117	0.528	-0.469	0.01	-0.109	small
EATP	-0.129	-0.08	0.247	-0.068	0.095	-0.13	0.34	-0.853	0.019	-0.006	0.087
EAMP	0.226	-0.043	-0.135	0.143	0.014	-0.324	-0.233	0.733	-0.036	-0.067	-0.11
EABP	0.148	0.086	-0.243	0.069	-0.088	0.078	-0.347	0.884	-0.017	-0.005	-0.096
EATXA_ Z	-0.086	-0.058	0.268	0.045	0.058	0.296	0.444	-0.649	0.022	-0.037	0.111
EATXA	0.111	0.115	-0.206	0.093	-0.058	0.055	-0.204	0.938	-0.021	-0.045	-0.074
EAMXA	0.109	0.095	-0.151	0.112	0.024	-0.102	-0.182	0.818	-0.042	-0.064	-0.088
EABXA	0.104	0.094	-0.217	0.066	-0.105	0.146	-0.212	0.895	0.003	-0.025	-0.082
EHTP	-0.135	-0.074	0.234	-0.076	0.104	-0.13	0.292	-0.88	0.024	0.02	0.087
EHMP	0.176	0.004	0.086	0.08	0.065	-0.458	-0.259	0.081	0.099	-0.058	0.012
EHBP	0.153	0.073	-0.228	0.075	-0.104	0.089	-0.305	0.896	-0.019	-0.026	-0.087
SATP	-0.388	0.084	0.149	-0.188	0.057	-0.228	0.365	-0.293	0.037	-0.08	0.014
SAMP	0.169	-0.025	-0.199	0.116	0.054	-0.293	-0.14	0.798	-0.023	-0.085	-0.095
SABP	0.4	-0.084	-0.197	0.18	-0.056	0.177	-0.353	0.394	-0.056	0.068	-0.036
SATNA_ Z	0.025	0.285	-0.256	0.125	0.069	-0.156	0.209	0.473	-0.053	-0.13	-0.038
SATNA	-0.436	0.06	0.183	-0.235	0.042	-0.192	0.321	-0.516	0.051	-0.04	0.069
SAMNA	0.191	-0.038	-0.244	0.117	0.036	-0.226	-0.168	0.768	-0.022	-0.077	-0.107
SABNA	0.43	-0.036	-0.208	0.229	-0.037	0.135	-0.302	0.625	-0.029	0.017	-0.075
SATNH_ X	-0.07	0.087	0.112	0.083	-0.171	0.072	0.479	0.22	0.034	-0.06	-0.071
SATNH	-0.584	-0.019	0.136	-0.333	0.06	-0.134	0.35	-0.583	0.103	0.028	0.076
SAMNH	0.13	0.043	-0.233	0.011	-0.019	-0.027	-0.479	0.362	-0.091	-0.031	-0.022
SABNH	0.544	0.06	-0.171	0.266	-0.067	0.134	-0.374	0.612	-0.105	-0.037	-0.056
SHTP	-0.437	0.04	0.233	-0.186	0.045	-0.156	0.222	-0.389	0.083	-0.013	0.02
SHMP	0.143	0.023	-0.15	0.076	0.078	-0.326	-0.226	0.619	-0.043	-0.081	-0.129
SHBP	0.47	-0.037	-0.242	0.19	-0.06	0.144	-0.249	0.435	-0.093	0.011	-0.024
SHTNA _Z	0.074	0.084	0.261	0.113	-0.058	0.291	0.048	0.052	0.011	-0.019	-0.048
SHTNA	-0.563	-0.023	0.19	-0.277	0.031	-0.109	0.28	-0.669	0.094	0.059	0.072
SHMNA	0.115	0.077	-0.223	0.005	0.066	-0.311	-0.242	0.37	-0.029	-0.058	-0.111
SHBNA	0.543	0.009	-0.199	0.258	-0.059	0.139	-0.319	0.573	-0.094	-0.04	-0.05
SHTXH _X	-0.024	0.04	0.246	0.143	0.006	0.52	0.04	-0.547	-0.035	0.007	0.096
SHTXH	0.197	0.142	-0.237	0.123	-0.039	-0.08	-0.068	0.976	-0.026	-0.049	-0.11
SHMXH	-0.151	-0.11	0.242	-0.066	0.091	-0.123	0.074	-0.922	0.056	0.044	0.074

SHBXH	0.221	0.128	-0.261	0.15	-0.039	-0.047	-0.088	0.967	-0.043	-0.053	-0.105
SHTNH _X	-0.008	-0.279	0.33	0.028	-0.01	-0.083	0.064	0.182	-0.042	0.07	0.106
SHTNH	-0.519	0.027	0.238	-0.231	0.015	-0.096	0.217	-0.584	0.096	0.035	0.056
SHMNH	0.145	0.032	-0.166	0.08	0.081	-0.321	-0.235	0.616	-0.048	-0.081	-0.126
SHBNH	0.538	-0.016	-0.234	0.246	-0.019	0.077	-0.253	0.637	-0.096	-0.054	-0.048
SRP	0.05	0.06	0.069	0.178	0.022	-0.22	-0.051	-0.088	-0.108	0.02	0.329
SMP	0.155	0.036	-0.134	0.189	0.038	0.357	small	0.218	-0.163	-0.024	0.139
SRA	-0.048	0.015	0.085	0.068	-0.067	small	0.284	-0.061	0.072	0.004	-0.182
SMA	0.142	-0.129	-0.007	0.222	0.08	-0.148	-0.056	0.037	-0.155	-0.162	0.35
SRA_Z	0.446	0.2	-0.207	0.286	-0.035	0.16	-0.128	0.622	-0.168	-0.016	-0.116
SRH	-0.008	-0.013	0.124	-0.063	-0.098	0.062	0.085	-0.137	0.112	-0.014	-0.223
SMH	0.124	-0.013	0.115	0.087	-0.026	0.077	-0.126	-0.528	-0.117	-0.121	0.263
SRH_X	0.366	0.071	-0.21	0.224	0.039	0.042	-0.038	0.728	-0.093	-0.017	-0.047
N_log	-0.163	0.004	0.11	-0.336	0.013	-0.179	0.232	-0.115	0.088	0.1	-0.352

Table B.1.4. Regression analysis- Coefficients and R² value for single dent

	a ₀	b ₁	b ₂	b ₃	b ₄	b ₅	b ₆	b ₇	b ₈	c ₁	c ₂	c ₃	c ₄	c ₅	c ₆	c ₇	c ₈	R ²
EATP	-9.61E-02	2.13E-03	-1.04E+01	-1.84E-01	-2.02E-01	3.68E-01	8.22E+00	2.09E-01	-	-1.14E-05	7.54E+01	6.55E-03	2.09E+00	-1.35E-01	-3.66E+03	-1.04E-01	-	0.883
EAMP	2.64E-02	3.60E-04	1.21E+00	1.69E-02	-1.61E-01	-5.68E-02	-2.45E+01	-5.32E-03	-	-7.77E-07	-5.66E+00	-4.03E-03	3.23E-01	1.58E-02	3.75E-03	1.67E-03	-	0.592
EABP	1.23E-01	-1.77E-03	1.16E+01	2.01E-01	4.14E-02	-4.25E-01	-3.27E+01	-2.14E-01	-	1.07E-05	-8.10E+01	-1.06E-02	-1.77E+00	1.51E-01	7.40E+03	1.06E-01	-	0.880
EATXA_Z/D	6.10E+00	5.24E-02	-6.37E+01	-2.70E+00	-1.05E+01	-3.65E+00	-2.73E+03	-1.34E+00	-	-2.11E-04	6.65E+02	1.02E+00	3.43E+01	1.41E+00	4.20E+05	8.27E-01	-	0.754
EATXA	5.76E-02	-2.01E-04	1.71E+00	3.18E-02	-5.55E-02	-6.10E-02	-2.43E+01	-3.78E-02	-	1.18E-06	-8.28E+00	-1.73E-03	-1.10E-01	1.81E-02	3.37E+03	1.86E-02	-	0.928
EAMXA	2.16E-02	8.77E-05	4.24E-01	5.20E-03	-4.16E-02	-1.78E-02	-1.19E+01	-7.75E-03	-	-2.97E-07	-3.79E-01	-1.07E-04	6.53E-02	4.31E-03	1.56E+03	3.26E-03	-	0.905
EABXA	3.60E-02	-2.88E-04	1.29E+00	2.67E-02	-1.41E-02	-4.33E-02	-1.24E+01	-2.99E-02	-	1.47E-06	-7.89E+00	-1.62E-03	-1.75E-01	1.37E-02	1.81E+03	1.53E-02	-	0.909
EHTP	-7.24E-02	2.63E-03	-1.26E+01	-2.17E-01	-2.64E-01	3.83E-01	-6.48E+00	2.20E-01	-	-1.36E-05	9.01E+01	1.20E-02	2.46E+00	-1.31E-01	-1.61E+03	-1.14E-01	-	0.912
EHMP	9.41E-03	5.23E-04	5.56E-01	8.75E-03	-1.73E-01	-4.00E-02	-2.11E+01	1.58E-02	-	-1.61E-06	-1.83E+00	-4.05E-03	4.13E-01	1.08E-02	3.15E+03	-7.43E-03	-	0.363
EHBP	8.18E-02	-2.10E-03	1.32E+01	2.26E-01	9.05E-02	-4.23E-01	-1.46E+01	-2.04E-01	-	1.20E-05	-9.19E+01	-1.61E-02	-2.05E+00	1.41E-01	4.76E+03	1.07E-01	-	0.904
SATP/SMYS	3.58E-01	2.58E-02	-4.02E+01	-1.11E+00	-7.75E+00	9.23E-01	-4.85E+02	-1.42E-01	-	-1.12E-04	5.96E+02	4.20E-02	2.68E+01	-1.98E-01	2.90E+04	-1.13E-02	-	0.691
SAMP/SMYS	-4.40E-01	2.76E-02	3.40E+01	-7.40E-01	-2.36E+00	-1.67E+00	-3.18E+01	-1.45E+00	-	-9.29E-05	-1.34E+02	1.73E-01	8.68E+00	5.56E-01	1.41E+04	7.31E-01	-	0.933
SABP/SMYS	-4.63E-01	-1.65E-02	3.49E+01	4.17E-01	6.65E+00	-3.65E-01	3.33E+02	7.72E-01	-	7.21E-05	-4.38E+02	6.60E-02	-1.94E+01	2.69E-02	-2.26E+04	-3.24E-01	-	0.691
SATNA_Z/D	-2.11E-02	3.82E-04	-6.31E-01	-3.06E-02	-1.46E-02	4.10E-02	6.67E+00	2.78E-02	-	-2.40E-06	1.23E+01	5.53E-03	2.23E-01	3.27E-03	-1.92E+03	-1.35E-02	-	0.854
SATNA/SMYS	-7.01E-02	1.59E-02	-2.61E+01	-1.46E-01	-6.95E+00	1.98E-02	-2.41E+02	-3.44E-01	-	-6.57E-05	2.76E+02	-1.56E-01	1.86E+01	7.25E-02	2.60E+04	1.31E-01	-	0.614
SAMNA/SMYS	4.97E-03	2.28E-02	3.69E+01	-3.77E-01	-1.87E+00	-1.87E+00	-9.96E+01	-2.04E+00	-	-7.14E-05	-1.95E+02	1.01E-01	5.08E+00	5.07E-01	3.03E+04	1.03E+00	-	0.885
SABNA/SMYS	-1.01E-01	-1.31E-02	2.80E+01	1.91E-02	6.40E+00	6.58E-02	2.35E+02	5.77E-01	-	5.53E-05	-2.81E+02	1.46E-01	-1.60E+01	-8.69E-02	-2.17E+04	-2.54E-01	-	0.686
SATNH_X/D	4.35E-02	-4.43E-04	-2.39E-01	5.50E-03	-1.81E-01	8.30E-02	-2.13E+01	7.08E-02	-	1.39E-06	9.76E+00	-1.14E-02	6.78E-01	-1.29E-02	1.22E+03	-3.36E-02	-	0.837
SATNH/SMYS	-2.85E-01	1.71E-02	-2.81E+01	-2.15E-01	-5.70E+00	-3.65E-01	-1.28E+02	-7.77E-01	-	-6.86E-05	2.79E+02	-9.68E-02	1.47E+01	7.50E-02	1.47E+04	3.74E-01	-	0.744
SAMNH/SMYS	1.56E+00	1.79E-02	3.42E+01	-6.45E-02	-1.34E+00	-2.90E+00	-6.04E+02	-3.09E+00	-	-4.28E-05	-2.21E+02	1.11E-01	1.72E+00	7.13E-01	1.15E+05	1.43E+00	-	0.708
SABNH/SMYS	3.60E-01	-1.79E-02	2.97E+01	2.24E-01	5.95E+00	6.55E-01	1.18E+02	6.08E-01	-	7.30E-05	-2.98E+02	8.85E-02	-1.60E+01	-4.61E-01	-1.28E+04	-2.86E-01	-	0.772
SHTP/SMYS	-6.54E-01	2.52E-02	-3.89E+01	-8.55E-01	-7.45E+00	2.18E-02	-2.33E+02	5.55E-01	-	-1.06E-04	5.50E+02	2.53E-02	2.33E+01	2.64E-01	4.96E+03	-2.83E-01	-	0.626
SHMP/SMYS	7.26E-02	3.79E-02	2.79E+01	-8.20E-01	-5.45E+00	-2.70E+00	-4.04E+02	-1.69E+00	-	-1.27E-04	-3.66E+01	1.95E-01	1.75E+01	8.81E-01	7.19E+04	8.04E-01	-	0.876
SHBP/SMYS	3.10E-01	-1.78E-02	3.27E+01	3.39E-01	6.65E+00	1.66E-01	2.12E+02	1.14E-01	-	7.37E-05	-4.29E+02	6.20E-02	-1.80E+01	-1.68E-01	-1.01E+04	-7.34E-02	-	0.628
SHTNA_Z/D	8.35E-02	-4.41E-04	-1.09E+00	-3.40E-02	3.95E-02	6.05E-02	-3.32E+01	1.30E-02	-	1.83E-06	1.71E+01	5.83E-03	2.10E-01	-1.39E-02	3.82E+03	-3.81E-03	-	0.740
SHTNA/SMYS	-2.90E-01	1.53E-02	-3.17E+01	-7.90E-02	-6.05E+00	-1.60E-01	-1.25E+02	-7.09E-01	-	-6.28E-05	3.02E+02	-1.58E-01	1.49E+01	3.06E-02	1.21E+04	3.60E-01	-	0.765
SHMNA/SMYS	7.67E-01	3.60E-02	2.00E+01	-3.63E-01	-5.25E+00	-2.88E+00	9.28E+02	-1.04E+00	-	-1.22E-04	-6.02E+01	2.78E-02	1.54E+01	8.19E-01	1.60E+05	3.82E-01	-	0.687
SHBNA/SMYS	1.07E-01	-1.71E-02	3.32E+01	2.62E-01	5.85E+00	1.37E-01	2.31E+02	7.48E-01	-	7.17E-05	-3.41E+02	9.80E-02	-1.54E+01	-2.19E-02	-2.57E+04	-3.75E-01	-	0.737
SHTXH_X/D	4.13E-01	-1.48E-05	-4.22E+00	-2.96E-02	-4.95E-01	-4.95E-02	-5.15E+01	1.10E-02	-	-2.39E-06	4.52E+01	-1.00E-02	1.77E+00	3.66E-02	7.46E+03	4.71E-04	-	0.785
SHTXH/SMYS	8.46E-01	3.03E-03	4.01E+01	-2.25E-01	6.55E-01	-2.90E-01	-2.03E+02	-1.19E+00	-	-1.02E-05	-2.98E+02	8.70E-02	-5.28E-01	1.25E-01	1.69E+04	5.32E-01	-	0.949
SHMXH/SMYS	-4.90E-02	3.56E-03	-1.51E+01	-4.19E-04	-7.75E-01	9.18E-02	-7.57E+01	2.38E-01	-	-1.57E-05	1.12E+02	-5.50E-02	2.63E+00	1.86E-04	1.41E+04	-1.09E-01	-	0.879
SHBXH/SMYS	6.01E-01	-4.06E-04	4.22E+01	-2.20E-01	1.60E+00	-5.18E-02	-8.39E+01	-9.87E-01	-	5.06E-06	-3.36E+02	8.18E-02	-3.00E+00	2.34E-02	2.66E+03	4.35E-01	-	0.940
SHTNH_X/D	9.90E-03	1.15E-06	-7.91E-01	-2.82E-02	4.61E-02	4.83E-02	3.04E+00	-1.40E-02	-	-1.49E-07	1.21E+01	6.23E-03	2.75E-02	-2.29E-02	-9.23E+02	8.73E-03	-	0.821
SHTNH/SMYS	-1.56E-01	1.54E-02	-2.87E+01	-1.65E-02	-6.70E+00	-3.68E-01	-2.64E+02	-3.65E-01	-	-6.34E-05	3.20E+02	-1.53E-01	1.60E+01	1.50E-01	2.72E+04	1.98E-01	-	0.682
SHMNH/SMYS	3.18E-01	1.02E-02	-6.50E+00	3.20E-01	-2.20E+00	-8.98E-01	-2.21E+01	-7.57E-01	-	-4.21E-05	9.43E+01	-1.92E-01	4.23E+00	3.51E-01	1.12E+04	3.97E-01	-	0.451
SHBNH/SMYS	1.51E-01	-1.37E-02	2.82E+01	-7.75E-03	6.15E+00	4.15E-01	1.73E+02	6.43E-01	-	5.45E-05	-3.02E+02	1.37E-01	-1.45E+01	-1.45E-01	-1.65E+04	-3.33E-01	-	0.729
SRP/SMYS	5.06E-01	4.95E-03	1.05E+00	1.04E-01	-4.35E-01	-1.72E-01	-2.90E+02	-5.26E-01	3.12E-01	-2.40E-05	1.08E+00	-4.73E-02	2.05E+00	8.13E-02	3.89E+04	2.53E-01	-2.28E-02	0.250
SMP/SMYS	5.22E+00	-2.19E-02	4.07E+01	1.02E+00	1.18E-01	-6.20E-01	-1.21E+03	-9.07E-01	-7.27E+00	8.71E-05	-3.93E+02	-2.26E-02	-9.25E+00	4.69E-01	1.83E+05	3.97E-01	7.60E+00	0.523
SRA_Z/D	1.93E+00	3.61E-03	-1.45E+01	-5.10E-01	-3.03E+00	5.75E-01	-9.74E+01	5.87E-01	-6.09E+00	-2.66E-05	1.14E+02	1.15E-01	6.25E+00	-1.86E-01	2.54E+04	-3.45E-01	6.43E+00	0.444
SMA/SMYS	8.00E-01	7.23E-04	-2.49E+00	1.97E-01	4.75E-01	2.60E-01	-2.43E+02	-2.91E-01	-1.16E+00	-1.44E-05	2.25E+01	-1.55E-02	-4.10E+00	-3.29E-02	3.61E+04	1.64E-01	1.62E+00	0.352
SRA/SMYS	3.37E+00	-9.39E-03	3.00E+01	1.48E-01	4.58E-01	-6.88E-01	-7.13E+02	-1.06E+00	-2.76E+00	5.65E-05	-2.50E+02	4.58E-02	-5.20E-01	1.99E-01	1.07E+05	4.26E-01	2.47E+00	0.670
SRH_X/D	1.81E-01	1.00E-03	-4.35E+00	-1.01E-01	-9.00E-01	8.18E-02	6.78E+01	-3.23E-01	2.38E-01	-6.01E-06	3.95E+01	-2.63E-03	2.32E+00	-2.91E-02	-9.89E+03	1.73E-01	-2.80E-01	0.457
SMH/SMYS	-4.47E-01	-1.57E-04	-4.22E+00	1.25E-01	6.35E-01	2.00E-02	1.90E+02	-2.18E-01	1.19E+00	-5.73E-06	2.50E+01	-1.31E-02	-2.29E+00	3.87E-02	-2.73E+04	1.02E-01	-8.09E-01	0.399
SRH/SMYS	4.75E+00	-1.03E-02	3.31E+01	4.08E-01	9.65E-03	-2.13E-01	-9.50E+02	-1.31E+00	-6.95E+00	5.13E-05	-2.73E+02	-1.77E-02	-3.28E+00	8.44E-02	1.45E+05	6.12E-01	6.83E+00	0.660
N_log	-8.16E+01	1.26E-01	-8.57E+01	1.09E+01	-2.82E+02	-9.85E+00	3.53E+04	6.62E+01	1.70E+02	5.10E-04	1.96E+03	-1.06E+01	6.65E+02	-3.90E+00	-5.49E+06	-3.27E+01	-2.12E+02	0.453

Table B.2.1. List of random input variables and their statistical distribution for interaction of 2 dents (μ = mean value, σ = standard deviation)

Variable	Distribution	μ	σ	Density function
MATERIAL INPUT PARAMETERS				
SMYS (MPa), SMYS (data collected from a local source for a list of pipeline purchase orders)	Lognormal	434	44	
E_l (MPa), EL	Normal	1.90×10^5	2.6×10^4	
E_t (MPa), ET	Normal	1.90×10^5	2.6×10^4	
σ_v @ $\varepsilon = 0.002$ (MPa), SY1=0.002*E1				
FSY2	Normal	1.15	0.075	
σ_v @ $\varepsilon = 0.005$ (MPa), SY2=FSY2*SMYS				
FSU	Normal	1.65	0.12	
σ_u (MPa), SU=FSU*SMYS				
GEOMETRY INPUT PARAMETERS				
D (mm), PIPEDIA=610				
D/t, DTRATIO (data collected from a local source for a list of pipeline purchase orders)	Uniform	85	± 55	
t (mm), THICK=DTRATIO*PIPEDIA				
r (mm), DENTRAD	Lognormal	73	61	
INDENTATION AND PRESSURE LOADING INPUT PARAMETERS				
d/D (%), DENTPERCENT	Weibul		$\gamma=1.2689$ Char=2.661 8 Offset=0	
d (mm), d=DENTPERCENT/100*PIPEDIA				
P_{SMYS} PSMYS=SMYS*2*THICK/PIPDIA (MPa),				
FHYDRO	Normal	0.95	0.025	
FMIN	Uniform	0.2	± 0.1	

FMAX	Triangular	0.72	0.6-0.8	
P_{hydro} (MPa), PHYDRO=FHYDRO*PSMYS				
P_{min} (MPa), PMIN=FMIN*PSMYS				
P_{max} (MPa), PMAX=FMAX*PSMYS				
2 DENTS PARAMETERS				
FIDSTANCE	Uniform	1.0	±1.0	
DISTANCE=FDISTANCE*(PIPERAD*THICK) ^0.5				
ORIENTATION	Uniform	0.785	±0.785	

Table B.2.2. Output parameters and their statistical distribution for interaction of 2 dents (μ = mean value, σ = standard deviation)

NAME	DESCRIPTION			μ	σ
	Direction	Component	Location		
LENGTH	Dent length			434	236
WIDTH	Dent width			81	31
Strains at end of indentation phase					
EATP	Axial	Total	dent peak	-7.93E-02	1.23E-01
EAMP	Axial	Membrane	dent peak	-6.20E-04	7.08E-03
EABP	Axial	Bending	dent peak	7.87E-02	1.25E-01
EATXA_Z	Location of maximum tensile value along dent longitudinal			72	77
EATXA	Axial	Total	maximum tensile in dent longitudinal	4.38E-03	8.02E-03
EAMXA	Axial	Membrane	maximum tensile in dent longitudinal	7.84E-04	2.85E-03
EABXA	Axial	Bending	maximum tensile in dent longitudinal	-2.81E-03	3.11E-03
EHTP	Hoop	Total	dent peak	-8.14E-02	9.95E-02
EHMP	Hoop	Membrane	dent peak	-3.88E-03	8.97E-03
EHBP	Hoop	Bending	dent peak	7.37E-02	9.36E-02
Stresses at end of indentation phase					
SATP	Axial	Total	dent peak	-506	181
SAMP	Axial	Membrane	dent peak	-95	309
SABP	Axial	Bending	dent peak	501	199
SATNA_Z	Location of maximum compressive value along dent longitudinal			40	210
SATNA	Axial	Total	maximum tensile in dent longitudinal	-513	182
SAMNA	Axial	Membrane	maximum tensile in dent longitudinal	492	207
SABNA	Axial	Bending	maximum tensile in dent longitudinal	-97	290
SATNH_X	Location of maximum compressive value along dent transverse			18	18
SATNH	Axial	Total	maximum tensile in dent transverse	-542	191
SAMNH	Axial	Membrane	maximum tensile in dent transverse	-120	297
SABNH	Axial	Bending	maximum tensile in dent transverse	513	209
SHTP	Hoop	Total	dent peak	-550	187
SHMP	Hoop	Membrane	dent peak	-222	297
SHBP	Hoop	Bending	dent peak	532	188
SHTNA_Z	Location of maximum compressive value along dent longitudinal			12	17
SHTNA	Hoop	Total	maximum tensile in dent longitudinal	-569	193
SHMNA	Hoop	Membrane	maximum tensile in dent longitudinal	-224	283
SHBNA	Hoop	Bending	maximum tensile in dent longitudinal	535	193
SHTXH_X	Location of maximum tensile value along dent transverse			99	30
SHTXH	Hoop	Total	maximum tensile in dent transverse	150	135
SHMXH	Hoop	Membrane	maximum tensile in dent transverse	-54	95
SHBXH	Hoop	Bending	maximum tensile in dent transverse	-167	143
SHTNH_X	Location of maximum compressive value along dent transverse			6	12
SHTNH	Hoop	Total	maximum tensile in dent transverse	-558	191
SHMNH	Hoop	Membrane	maximum tensile in dent transverse	-200	304
SHBNH	Hoop	Bending	maximum tensile in dent transverse	538	192
Stress range and fatigue life at end of pressure cycle phase					
SRP	Von Mises	Range	dent peak	184	72
SMP	Von Mises	Mean	dent peak	316	96
SRA_Z	Location of maximum stress range in dent longitudinal direction			30	37
SRA	Von Mises	Range	maximum in dent longitudinal	452	124
SMA	Von Mises	Mean	maximum in dent longitudinal	19	55
SRH_X	Location of maximum stress range in dent transverse direction			19	23
SRH	Von Mises	Range	maximum in dent transverse direction	412	126
SMH	Von Mises	Mean	maximum in dent transverse direction	24	61
N_log	fatigye cycles to failure (in natural log)			9.57	8.828
SRH	Von Mises	Range	mid distance between two dent peaks	53	44
SMH	Von Mises	Mean	mid distance between two dent peaks	309	94

Table B.2.3. Rank order Spearman Correlation factors between output and input parameters for interaction of 2 dents

Out\Inp	SMYS	EL	ET	FSY2	FSU	THICK	DENTRAD	DENTPER CENT	FHYDRO	FMIN	FMAX	FDISTAN CE	ORIENT ATION
LENGTH	0.015	-0.15	-0.082	-0.019	0.107	-0.571	0.223	-0.323	0.07	-0.116	-0.136	0.012	-0.073
WIDTH	0.01	-0.144	-0.099	0.042	0.132	-0.159	0.238	-0.319	0.1	-0.077	-0.029	-0.012	-0.493
EATP	-0.078	-0.136	-0.119	0.07	0.163	-0.116	0.181	-0.943	0.122	-0.081	-0.114	0.059	-0.184
EAMP	0.21	-0.102	-0.095	0.134	0.135	-0.334	0.014	-0.104	0.014	-0.13	-0.154	0.203	-0.16
EABP	0.086	0.128	0.12	-0.068	-0.164	0.108	-0.175	0.947	-0.118	0.072	0.117	-0.059	0.178
EATXA_Z	-0.071	-0.102	-0.136	0.095	0.105	0.274	0.141	-0.783	0.045	-0.011	-0.017	-0.085	-0.25
EATXA	0.123	0.152	0.118	-0.085	-0.183	0.04	-0.088	0.862	-0.031	0.088	0.125	0.051	0.214
EAMXA	-0.085	-0.056	0.031	-0.002	-0.091	0.029	-0.112	0.346	0.029	-0.03	0.018	0.058	0.465
EABXA	-0.123	-0.164	-0.088	0.079	0.075	-0.053	0.054	-0.891	0.121	-0.101	-0.065	-0.03	-0.031
EHTP	-0.084	-0.141	-0.125	0.059	0.135	-0.114	0.162	-0.944	0.124	-0.082	-0.119	0.07	-0.129
EHMP	0.14	-0.088	-0.225	0.161	0.189	-0.201	-0.007	-0.382	0.025	-0.18	-0.137	0.237	-0.324
EHBP	0.099	0.142	0.121	-0.05	-0.127	0.094	-0.162	0.944	-0.125	0.074	0.114	-0.058	0.09
SATP	-0.276	-0.062	-0.186	-0.009	0.078	-0.052	0.106	-0.857	0.162	-0.077	-0.057	-0.008	-0.149
SAMP	0.087	-0.064	-0.067	0.035	0.051	-0.163	-0.079	0.314	-0.018	small	-0.039	0.065	0.14
SABP	0.295	0.068	0.158	0.011	-0.125	0.01	-0.092	0.918	-0.141	0.055	0.088	-0.012	0.162
SATNA_Z	0.119	0.017	-0.051	-0.005	-0.098	0.038	0.116	0.177	0.237	-0.036	0.144	0.008	-0.194
SATNA	-0.297	-0.075	-0.17	-0.017	0.1	-0.052	0.091	-0.885	0.135	-0.037	-0.085	small	-0.111
SAMNA	0.244	0.062	0.135	0.009	-0.11	0.004	-0.132	0.91	-0.14	0.054	0.058	-0.014	0.208
SABNA	0.087	-0.021	-0.026	0.073	0.063	-0.101	-0.049	0.268	-0.004	0.029	-0.02	0.015	0.122
SATNH_X	0.011	0.038	0.037	0.004	-0.354	0.067	0.205	0.157	0.138	0.02	0.15	0.023	0.069
SATNH	-0.307	-0.072	-0.158	-0.076	0.125	-0.051	0.054	-0.875	0.12	-0.075	-0.089	0.012	-0.124
SAMNH	0.053	-0.089	-0.077	0.071	0.164	-0.088	-0.049	0.069	-0.006	0.014	-0.082	0.06	0.007
SABNH	0.256	0.082	0.171	-0.002	-0.099	0.003	-0.091	0.929	-0.098	0.032	0.092	-0.009	0.149
SHTP	-0.37	-0.067	-0.115	-0.076	0.043	0.051	0.021	-0.856	0.145	-0.077	-0.058	-0.004	0.024
SHMP	0.044	-0.149	-0.16	0.071	0.184	-0.252	0.026	-0.121	0.06	-0.081	-0.065	0.137	-0.174
SHBP	0.373	0.078	0.078	0.112	-0.046	-0.07	-0.013	0.847	-0.14	0.08	0.059	0.012	-0.091
SHTNA_Z	-0.036	0.04	-0.067	0.084	-0.25	0.137	0.064	0.033	0.05	-0.034	0.113	0.023	0.025
SHTNA	-0.372	-0.09	-0.092	-0.11	0.095	-0.033	0.032	-0.86	0.147	-0.079	-0.059	0.004	-0.03
SHMNA	-0.025	-0.117	-0.174	0.031	0.233	-0.161	0.036	-0.233	0.027	-0.067	-0.107	0.169	-0.179
SHBNA	0.366	0.105	0.112	0.093	-0.033	-0.028	-0.022	0.85	-0.135	0.019	0.072	0.006	-0.09
SHTXH_X	-0.019	0.008	-0.114	0.025	-0.219	0.364	0.127	-0.547	-0.02	-0.023	-0.045	0.358	0.295
SHTXH	0.159	0.153	0.134	-0.037	-0.134	0.02	-0.124	0.957	-0.102	0.061	0.088	-0.188	0.15
SHMXH	-0.072	-0.081	-0.163	-0.006	0.026	-0.169	0.266	-0.63	-0.093	0.011	-0.054	0.289	-0.344
SHBXH	-0.153	-0.146	-0.153	0.033	0.12	-0.038	0.136	-0.932	0.087	-0.05	-0.087	0.225	-0.186
SHTNH_X	0.087	0.138	0.009	-0.051	-0.313	0.048	-0.29	0.324	-0.106	-0.059	0.054	0.249	0.403
SHTNH	-0.376	-0.075	-0.114	-0.071	0.071	0.028	0.058	-0.87	0.151	-0.05	-0.068	-0.014	-0.003
SHMNH	0.012	-0.098	-0.152	0.072	0.204	-0.17	-0.056	-0.089	0.045	-0.056	-0.117	0.188	-0.121
SHBNH	0.365	0.093	0.074	0.095	-0.059	-0.035	-0.055	0.843	-0.156	0.062	0.069	0.064	-0.084
SRP	0.221	small	0.021	-0.02	0.113	-0.084	-0.122	0.487	-0.067	-0.104	0.212	0.088	-0.175

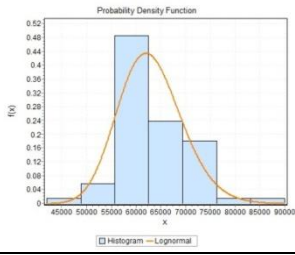
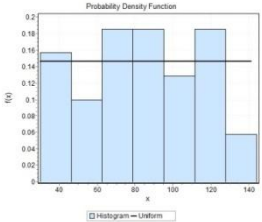
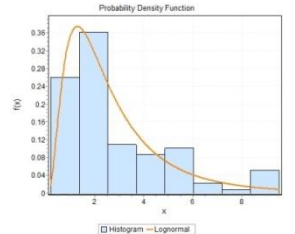
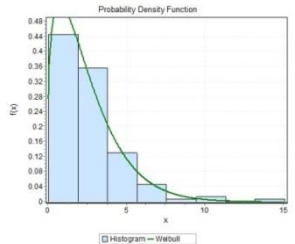
SMP	0.187	0.032	0.031	-0.043	0.11	-0.138	-0.07	0.719	-0.188	0.079	0.215	-0.051	-0.043
SRA	0.149	-0.148	0.053	-0.077	0.191	-0.246	-0.242	0.111	0.034	-0.067	0.062	0.028	0.179
SMA	0.227	0.234	0.117	0.267	-0.098	0.138	-0.037	0.686	-0.224	0.134	0.078	-0.049	-0.074
SRA_Z	0.076	-0.065	-0.18	0.12	-0.09	-0.042	0.234	-0.232	-0.011	-0.075	-0.115	0.132	-0.14
SRH	0.113	-0.273	-0.136	-0.003	0.117	-0.237	-0.126	-0.064	0.045	-0.126	0.141	0.083	-0.002
SMH	0.206	0.28	0.217	0.119	-0.059	0.17	-0.149	0.749	-0.213	0.149	0.095	-0.116	0.094
SRH_X	0.094	-0.112	0.102	0.005	-0.074	-0.026	0.079	-0.186	-0.07	-0.12	-0.146	0.184	0.037
N_log	0.059	-0.061	-0.051	0.05	0.014	-0.033	0.226	-0.667	0.153	-0.061	-0.205	-0.003	0.005
SRMID	0.207	-0.069	-0.059	-0.018	-0.183	-0.264	-0.129	0.36	0.052	-0.093	0.123	0.126	0.655
SMMID	0.181	0.325	0.182	0.095	-0.119	0.192	-0.003	0.485	-0.299	0.128	0.148	-0.236	-0.182

Table B.2.4. Regression analysis- Coefficients and R² value for interaction of 2 dents

	a ₀	b ₁	b ₂	b ₃	b ₄	b ₅	b ₆	b ₇	b ₈	b ₉	b ₁₀	c ₁	c ₂	c ₃	c ₄	c ₅	c ₆	c ₇	c ₈	c ₉	c ₁₀	R ²
EATP	-3.90E-01	-1.70E-03	1.06E+01	1.63E-01	-5.65E-01	3.88E-01	1.74E+02	2.79E-01	1.70E-03	-1.44E-02	-	6.80E-06	7.34E+01	-4.55E-02	5.08E-02	-1.88E-01	2.08E+04	-9.48E-02	-1.43E-02	-2.58E-02	-	0.78
EAMP	-2.09E-02	5.38E-05	-9.01E-01	8.35E-03	-1.84E-02	1.12E-02	9.68E+00	1.30E-02	1.40E-03	-1.60E-03	-	-3.22E-07	1.78E+01	-2.28E-03	-2.15E-03	-4.79E-03	1.48E+03	-6.70E-03	2.80E-05	-1.20E-03	-	0.75
EABP	3.69E-01	1.80E-03	9.68E+00	-1.55E-01	5.45E-01	-3.78E-01	1.64E+02	-2.66E-01	-3.89E-04	1.28E-02	-	-7.12E-06	5.56E+01	4.30E-02	-5.28E-02	1.83E-01	1.93E+04	8.81E-02	1.43E-02	2.46E-02	-	0.78
EATXA_Z/D	4.52E-01	-2.60E-03	6.94E+00	2.10E-01	-9.75E-01	-2.02E-01	2.88E+02	-6.59E-01	-1.23E-01	-1.62E-01	-	7.70E-06	7.47E+01	-4.03E-02	2.16E-01	7.88E-02	3.57E+04	2.76E-01	3.16E-02	3.26E-02	-	0.61
EATXA	2.34E-02	1.19E-04	4.52E-01	6.55E-03	-5.65E-02	-2.43E-02	4.67E+00	-2.90E-02	3.00E-03	-6.20E-03	-	-5.75E-07	2.05E+00	-6.25E-04	9.43E-02	1.08E-02	3.80E+02	1.18E-02	-8.60E-04	4.30E-03	-	0.87
EAMXA	-2.09E-02	5.38E-05	-9.01E-01	8.35E-03	-1.84E-02	1.12E-02	9.68E+00	1.30E-02	1.40E-03	-1.60E-03	-	-3.22E-07	1.78E+01	-2.28E-03	-2.15E-03	-4.79E-03	1.48E+03	-6.70E-03	2.80E-05	-1.20E-03	-	0.75
EABXA	1.14E-02	6.98E-05	3.59E-01	2.25E-03	-2.10E-02	-1.34E-02	1.47E+00	-1.59E-02	2.50E-03	-4.20E-03	-	-3.87E-07	5.59E-02	8.23E-05	2.95E-02	5.78E-03	3.28E+01	6.00E-03	-6.94E-04	2.40E-03	-	0.85
EHTP	-5.09E-02	-3.10E-03	1.25E+01	2.34E-01	1.02E+00	2.83E-01	1.03E+02	-3.34E-02	-3.34E-02	7.80E-03	-	1.38E-05	1.36E+02	-5.73E-02	9.78E-01	-1.21E-01	1.18E+04	3.76E-02	5.20E-03	-1.62E-02	-	0.89
EHP	0.00E+00	-2.63E-02	-1.45E-04	-8.40E-01	7.35E-03	1.39E-02	1.50E-01	1.46E+01	1.76E-02	2.60E-03	-	4.50E-03	6.54E-07	6.10E+00	-2.73E-03	-2.60E-02	-2.53E-01	2.03E+03	-9.90E-03	-1.94E-04	-	0.75
EHP	2.45E-02	2.90E-03	1.09E+01	-2.27E-01	1.05E+00	-2.46E-01	8.85E+01	5.12E-02	3.60E-02	-3.20E-03	-	-1.32E-05	1.12E+02	5.45E-02	1.08E+00	1.05E-01	9.75E+03	-4.76E-02	-5.40E-03	8.90E-03	-	0.88
SATP/SMYS	2.61E-01	-3.60E-03	4.45E+01	3.29E-01	5.40E+00	2.21E-01	7.35E+01	3.31E-01	-1.11E-01	-2.84E-01	-	2.45E-05	5.16E+02	-7.10E-02	6.53E+00	-1.31E-01	1.86E+04	-2.12E-01	2.10E-02	1.02E-01	-	0.90
SAMP/SMYS	1.05E+00	2.00E-02	1.19E+01	-5.90E-02	1.18E+00	-6.68E-01	8.25E+01	6.12E-01	2.00E-01	-2.27E-01	-	-6.67E-05	6.83E+01	-6.08E-03	1.04E+00	1.13E-01	2.56E+04	-2.47E-01	-9.42E-02	8.42E-02	-	0.81
SABP/SMYS	-1.74E-01	2.20E-03	4.22E+01	-4.05E-01	5.60E+00	3.90E-02	4.48E+01	-9.44E-02	8.24E-02	3.37E-01	-	-1.70E-05	4.69E+02	7.80E-02	6.55E+00	2.88E-02	3.29E+03	1.09E-01	-5.70E-03	-1.17E-01	-	0.92
SATNA_Z/D	4.65E-01	-1.40E-03	1.22E+00	-1.58E-02	2.42E-01	-3.68E-03	9.17E+01	-1.50E-01	-1.95E-02	-2.53E-01	-	7.11E-06	1.56E+01	9.00E-04	-3.28E-01	4.27E-02	9.14E+03	5.56E-02	1.18E-02	1.18E-01	-	0.39
SATNA/SMYS	-1.92E-01	-1.90E-03	3.97E+01	3.09E-01	5.40E+00	8.55E-02	4.50E+01	5.02E-01	-6.87E-02	-1.93E-01	-	1.56E-05	4.35E+02	-5.88E-02	6.28E+00	-8.56E-02	4.14E+03	-2.83E-01	6.20E-03	5.21E-02	-	0.91
SAMNA/SMYS	-8.97E-01	2.17E-02	6.72E+00	-9.70E-02	-9.70E-01	-3.53E-01	2.26E+02	6.01E-01	2.20E-01	-1.21E-01	-	-8.37E-05	1.05E+02	-1.01E-02	8.98E-01	-7.00E-02	4.73E+04	-2.24E-01	-1.20E-01	4.75E-02	-	0.80
SABNA/SMYS	-1.90E-01	6.40E-04	4.35E+01	-3.12E-01	4.73E+00	3.13E-02	7.86E+00	-1.50E-01	5.38E-02	3.54E-01	-	-5.75E-06	4.55E+02	6.53E-02	5.28E+00	3.50E-03	1.05E+04	1.38E-01	4.40E-03	-1.25E-01	-	0.91
SATNH_X/D	9.58E-02	3.37E-05	-5.21E-01	-3.93E-02	2.59E-01	1.53E-02	4.46E+01	-2.91E-02	6.20E-03	-3.30E-03	-	-1.19E-06	2.57E+00	5.90E-03	-1.71E-01	7.25E-03	5.40E+03	7.90E-03	-1.90E-03	1.39E-02	-	0.27
SATNH/SMYS	-4.48E-01	-2.20E-03	3.75E+01	4.77E-01	6.00E+00	1.40E-01	1.52E+02	6.54E-01	-9.96E-02	-2.82E-01	-	2.33E-05	3.88E+02	-1.02E-01	5.90E+00	-2.17E-01	4.18E+03	-3.54E-01	2.01E-02	5.70E-02	-	0.91
SAMNH/SMYS	-2.96E-01	1.78E-02	-2.83E-01	-4.70E-02	1.25E+01	-5.38E-01	4.52E+02	-7.87E-02	1.32E-01	-5.63E-01	-	-7.89E-05	2.62E+02	3.63E-02	1.04E-01	5.63E-02	1.31E+04	1.01E-01	-8.15E-02	1.95E-01	-	0.78

SRH_X/D	5.27E-01	-1.90E-03	5.39E+00	5.40E-02	1.74E+00	1.44E-01	2.71E+01	7.26E-01	3.50E-03	1.00E-02	2.19E+00	1.00E-05	7.51E+01	-1.67E-02	2.46E+00	-6.38E-02	4.44E+03	-3.05E-01	2.20E-03	5.30E-03	2.06E+00	0.58
SMH/SMYS	-7.45E-01	2.10E-03	1.92E+00	-2.36E-01	5.15E-01	5.28E-01	2.64E+02	-6.32E-01	-5.74E-02	-2.12E-02	2.30E+00	-2.63E-05	8.53E+01	7.90E-02	-8.63E-01	-2.62E-01	3.48E+04	3.38E-01	3.26E-02	1.84E-02	1.87E+00	0.54
SRH/SMYS	1.83E+00	6.90E-03	1.33E+01	-6.20E-01	7.40E+00	-1.69E-01	8.15E+02	4.41E-01	9.41E-02	-2.70E-03	1.03E+00	-4.87E-05	2.10E+02	7.80E-02	1.12E+01	2.68E-01	1.08E+05	-3.00E-01	-1.62E-02	4.95E-02	5.84E-01	0.76
N_log	9.39E+01	3.78E-02	4.95E+02	2.02E+01	1.13E+02	2.58E+01	5.08E+04	4.67E+01	1.05E+00	4.67E+00	6.99E+01	3.91E-05	9.78E+03	2.93E+00	1.18E+02	9.00E+00	8.02E+06	2.00E+01	-3.11E-01	1.70E+00	6.30E+01	0.66
SMMID/SMYS	4.24E-01	-6.20E-03	1.02E+01	-3.49E-01	3.84E+00	3.20E-01	2.00E+02	1.11E+00	-1.47E-01	7.43E-02	8.62E-01	1.17E-05	1.77E+02	7.60E-02	6.00E+00	-5.88E-03	1.55E+04	-5.98E-01	5.33E-02	-9.05E-02	-8.28E-01	0.67
SRHMID/SMYS	-6.97E-02	1.90E-03	2.00E+00	5.05E-02	-8.70E-01	8.55E-02	9.97E+01	-9.08E-02	3.70E-03	1.25E-01	8.61E-01	-8.81E-06	1.24E+01	-1.75E-03	5.78E-01	-5.31E-02	1.59E+04	5.42E-02	5.10E-03	-1.69E-02	-7.10E-01	0.83

Table B.3.1. List of random input variables and their statistical distribution for interaction of dent with metal loss (μ = mean value, σ = standard deviation)

Variable	Distribution	μ	σ	Density function
MATERIAL INPUT PARAMETERS				
SMYS (MPa), SMYS (data collected from a local source for a list of pipeline purchase orders)	Lognormal	434	44	
E_l (MPa), EL	Normal	1.90×10^5	2.6×10^4	
E_t (MPa), ET	Normal	1.90×10^5	2.6×10^4	
σ_y @ $\varepsilon = 0.002$ (MPa), SY1=0.002*EI				
FSY2	Normal	1.15	0.075	
σ_y @ $\varepsilon = 0.005$ (MPa), SY2=FSY2*SMYS				
FSU	Normal	1.65	0.12	
σ_u (MPa), SU=FSU*SMYS				
GEOMETRY INPUT PARAMETERS				
D (mm), PIPEDIA=610				
D/t, DTRATIO (data collected from a local source for a list of pipeline purchase orders)	Uniform	85	± 55	
t (mm), THICK=DTRATIO*PIPEDIA				
r (mm), DENTRAD	Lognormal	73	61	
INDENTATION AND PRESSURE LOADING INPUT PARAMETERS				
d/D (%), DENTPERCENT	Weibul		$\gamma=1.2689$ $\text{Char}=2.6618$ $\text{Offset}=0$	
d (mm), d=DENTPERCENT/100*PIPEDIA				
P_{SMYS} (MPa), PSMYS=SMYS*2*THICK/PIPDIA				
FHYDRO	Normal	0.95	0.025	
FMIN	Uniform	0.2	± 0.1	
FMAX	Triangular	0.72	0.6-0.8	
P_{hydro} (MPa),				

PHYDRO=FHYDRO*PSMYS				
P _{min} (MPa), PMIN=FMIN*PSMYS				
P _{max} (MPa), PMAX=FMAX*PSMYS				
METAL LOSS INPUT PARAMETERS				
d _m /t (%), CORROSION	Lognormal	22	21	
T _m (mm), THICK2=(1-CORROSION/100)*THICK				

Table B.3.2. Output parameters and their statistical distribution for interaction of dent with metal loss (μ = mean value, σ = standard deviation)

NAME	DESCRIPTION			μ	σ
	Direction	Component	Location		
LENGTH	Dent length			63	33
WIDTH	Dent width			45	13
Strains at end of indentation phase					
EATP	Axial	Total	dent peak	-8.57E-03	1.90E-02
EAMP	Axial	Membrane	dent peak	1.00E-02	1.35E-02
EABP	Axial	Bending	dent peak	1.96E-02	2.42E-02
EATXA_Z	Location of maximum tensile value along dent longitudinal			31	21
EATXA	Axial	Total	maximum tensile in dent longitudinal	2.10E-02	1.95E-02
EAMXA	Axial	Membrane	maximum tensile in dent longitudinal	8.62E-03	8.90E-03
EABXA	Axial	Bending	maximum tensile in dent longitudinal	-3.74E-03	8.73E-03
EHTP	Hoop	Total	dent peak	-6.03E-02	4.90E-02
EHMP	Hoop	Membrane	dent peak	-3.20E-03	6.97E-03
EHBP	Hoop	Bending	dent peak	5.39E-02	4.83E-02
Stresses at end of indentation phase					
SATP	Axial	Total	dent peak	-239	250
SAMP	Axial	Membrane	dent peak	237	301
SABP	Axial	Bending	dent peak	441	167
SATNA_Z	Location of maximum compressive value along dent longitudinal			40	210
SATNA	Axial	Total	maximum tensile in dent longitudinal	-495	174
SAMNA	Axial	Membrane	maximum tensile in dent longitudinal	578	155
SABNA	Axial	Bending	maximum tensile in dent longitudinal	303	313
SATNH_X	Location of maximum compressive value along dent transverse			18	18
SATNH	Axial	Total	maximum tensile in dent transverse	-585	118
SAMNH	Axial	Membrane	maximum tensile in dent transverse	156	332
SABNH	Axial	Bending	maximum tensile in dent transverse	579	160
SHTP	Hoop	Total	dent peak	-482	252
SHMP	Hoop	Membrane	dent peak	-5	357
SHBP	Hoop	Bending	dent peak	520	136
SHTNA_Z	Location of maximum compressive value along dent longitudinal			12	17
SHTNA	Hoop	Total	maximum tensile in dent longitudinal	-651	135
SHMNA	Hoop	Membrane	maximum tensile in dent longitudinal	22	324
SHBNA	Hoop	Bending	maximum tensile in dent longitudinal	582	158
SHTXH_X	Location of maximum tensile value along dent transverse			99	30
SHTXH	Hoop	Total	maximum tensile in dent transverse	363	184
SHMXH	Hoop	Membrane	maximum tensile in dent transverse	-209	187
SHBXH	Hoop	Bending	maximum tensile in dent transverse	-406	225
SHTNH_X	Location of maximum compressive value along dent transverse			6	12
SHTNH	Hoop	Total	maximum tensile in dent transverse	-599	164
SHMNH	Hoop	Membrane	maximum tensile in dent transverse	140	367

SHBNH	Hoop	Bending	maximum tensile in dent transverse	616	132
Stress range and fatigue life at end of pressure cycle phase					
SRP	Von Mises	Range	dent peak	131	63
SMP	Von Mises	Mean	dent peak	310	82
SRA_Z	Location of maximum stress range in dent longitudinal direction			30	37
SRA	Von Mises	Range	maximum in dent longitudinal	32	55
SMA	Von Mises	Mean	maximum in dent longitudinal	460	112
SRH_X	Location of maximum stress range in dent transverse direction			19	23
SRH	Von Mises	Range	maximum in dent transverse direction	51	49
SMH	Von Mises	Mean	maximum in dent transverse direction	434	102
N_log	fatigye cycles to failure (in natural log)			14.49	9.044

Table B.3.3. Rank order Spearman Correlation factors between output and input parameters for interaction of dents with metal loss

Out\Inp	SMYS	EL	ET	FSY2	FSU	THICK	DENTRAD	DENTPERCENT	FHYDRO	FMIN	FMAX	CORROSION
LENGTH	-0.013	-0.09	-0.106	0.007	0.135	0.501	0.353	0.736	0.021	0.056	0.048	0.312
WIDTH	-0.052	-0.048	-0.152	-0.072	0.071	0.43	-0.057	0.758	-0.067	0.102	0.01	0.178
EATP	0.022	-0.058	-0.152	-0.1	0.117	0.189	-0.256	0.774	0.026	0.122	-0.038	0.114
EAMP	0.036	-0.047	-0.111	-0.151	0.096	0.1	-0.02	0.881	0.014	0.068	-0.065	0.42
EABP	-0.029	-0.012	-0.118	-0.173	0.106	0.18	-0.03	0.908	0.032	0.093	-0.048	0.367
EATXA_Z	-0.035	-0.046	-0.098	-0.133	0.026	0.268	-0.242	0.642	-0.097	0.099	-0.051	0.173
EATXA	-0.029	-0.074	-0.079	-0.019	0.159	0.41	0.343	0.77	0.07	0.07	0.041	0.375
EAMXA	0.016	-0.031	0.064	-0.122	0.047	-0.496	0.024	-0.107	0.149	-0.069	-0.003	0.183
EABXA	-0.062	-0.1	-0.09	-0.15	-0.017	0.281	-0.35	0.404	-0.19	0.021	-0.015	0.058
EHTP	0.037	-0.047	-0.111	-0.151	0.095	0.099	-0.021	0.881	0.014	0.067	-0.065	0.42
EHMP	-0.03	-0.012	-0.117	-0.173	0.105	0.177	-0.034	0.908	0.033	0.092	-0.05	0.367
EHBP	-0.019	-0.023	0.017	-0.142	-0.164	-0.091	-0.474	-0.052	-0.198	0.043	-0.039	-0.098
SATP	0.088	0.098	0.054	-0.151	-0.08	-0.631	-0.559	-0.141	-0.029	-0.008	-0.146	-0.025
SAMP	-0.041	-0.031	-0.149	-0.116	0.101	0.328	-0.06	0.871	-0.019	0.094	-0.009	0.256
SABP	-0.023	-0.11	-0.037	0.232	-0.018	0.387	0.466	-0.26	-0.124	-0.017	0.04	-0.049
SATNA_Z	-0.031	-0.013	-0.163	-0.092	0.115	0.356	-0.026	0.847	-0.023	0.135	-0.015	0.265
SATNA	-0.007	0.046	-0.026	-0.246	-0.034	-0.054	-0.404	0.234	-0.002	0.046	-0.088	0.138
SAMNA	-0.016	-0.054	-0.169	-0.001	0.067	0.469	0.039	0.787	-0.021	0.087	0.031	0.182
SABNA	0.08	-0.12	0.002	-0.034	0.036	-0.526	-0.341	0.029	-0.051	-0.143	-0.108	-0.179
SATNH_X	0.003	0.067	0.169	0.007	-0.079	-0.414	-0.02	-0.832	0.006	-0.073	-0.031	-0.183
SATNH	0.078	-0.121	0.001	-0.034	0.035	-0.524	-0.342	0.031	-0.05	-0.144	-0.109	-0.178
SAMNH	0.019	0.037	0.165	-0.01	-0.063	-0.518	-0.067	-0.727	0.036	-0.106	-0.041	-0.174
SABNH	0.015	-0.057	-0.181	-0.129	0.094	0.192	-0.073	0.863	0.074	0.096	0.047	0.301
SHTP	-0.047	-0.088	-0.184	-0.002	0.048	0.467	0.028	0.715	-0.046	0.101	0.038	0.124
SHMP	0.011	-0.055	-0.182	-0.132	0.096	0.195	-0.071	0.864	0.075	0.094	0.046	0.303
SHBP	-0.046	-0.088	-0.186	0.001	0.05	0.467	0.03	0.713	-0.047	0.1	0.038	0.119
SHTNA_Z	0.01	0.017	-0.148	-0.008	0.001	0.42	-0.159	0.582	-0.066	0.081	0.027	0.016
SHTNA	0.074	-0.315	-0.017	-0.104	0.079	0.283	0.197	0.129	-0.036	-0.145	-0.026	-0.061
SHMNA	0.01	0.017	-0.144	-0.005	small	0.419	-0.161	0.582	-0.062	0.083	0.027	0.017

SHBNA	0.098	0.591	-0.328	-0.06	0.118	-0.107	-0.118	0.105	-0.033	0.036	0.036	0.082
SHTXH_X	-0.089	0.099	0.115	-0.168	-0.033	0.545	-0.174	-0.101	-0.124	0.044	0.011	0.338
SHTXH	-0.275	0.339	0.117	0.001	-0.082	0.175	0.024	-0.103	-0.01	small	-0.33	0.127
SHMXH	-0.052	0.074	-0.005	0.078	-0.063	0.115	-0.015	-0.285	-0.123	0.071	-0.002	-0.31
SHBXH	-0.128	0.164	0.025	0.069	-0.029	0.021	0.086	-0.146	-0.231	0.083	-0.124	-0.135
SHTNH_X	0.015	-0.152	-0.107	0.105	-0.142	-0.271	-0.282	-0.048	-0.078	-0.062	0.275	-0.174
SHTNH	-0.129	0.24	0.028	0.051	-0.031	0.141	0.098	-0.297	-0.009	-0.073	-0.321	-0.013
SHMNH	0.034	-0.012	-0.058	-0.033	0.092	0.047	0.144	-0.192	-0.053	0.015	-0.064	-0.175
SHBNH	0.413	-0.065	-0.071	0.186	0.108	0.236	-0.109	0.104	-0.084	0.123	0.071	-0.139
SRP	0.563	-0.06	-0.081	0.377	0.006	0.153	-0.171	0.196	-0.06	0.101	0.019	-0.179
SMP	0.223	-0.067	-0.035	0.166	0.027	0.422	0.353	0.169	-0.06	0.08	0.112	0.135
SRA	0.101	0.106	-0.015	-0.117	0.023	0.506	0.264	0.488	0.104	0.103	-0.036	0.552
SMA	0.083	-0.157	-0.055	-0.012	0.053	0.398	0.163	0.48	-0.114	-0.003	0.065	0.016
SRA_Z	0.196	-0.053	-0.07	-0.064	0.072	0.061	0.07	0.723	0.025	0.087	0.01	0.337
SRH	0.062	0.062	0.003	-0.152	-0.11	0.268	-0.146	0.312	-0.134	0.114	-0.027	0.188
SMH	0.09	-0.014	-0.118	-0.098	0.108	-0.024	0.1	0.865	0.059	0.075	-0.059	0.472
SRH_X	0.044	0.021	0.13	0.095	-0.111	0.027	-0.089	-0.67	-0.003	-0.051	0.073	-0.475
N_log	0.103	-0.053	-0.163	0.157	0.151	0.075	-0.147	0.752	0.041	0.099	0.007	-0.099

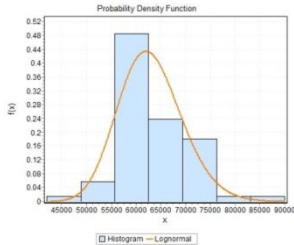
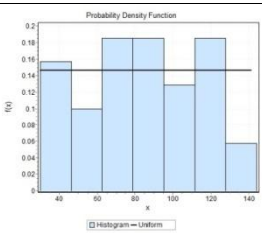
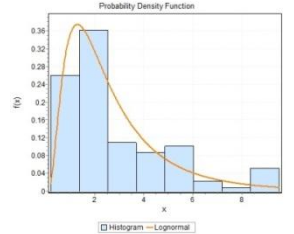
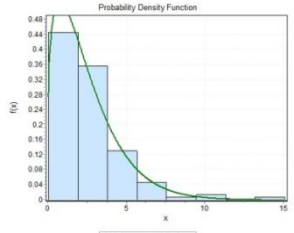
Table B.3.4. Regression analysis- Coefficients and R² value for interaction of dent with metal loss

	a ₀	b ₁	b ₂	b ₃	b ₄	b ₅	b ₆	b ₇	b ₈	b ₉	c ₁	c ₂	c ₃	c ₄	c ₅	c ₆	c ₇	c ₈	c ₉	R ²
EATP	-1.02E-01	1.62E-03	-4.86E-01	-1.45E-03	2.83E-01	2.55E-01	4.65E+01	-2.91E-02	-5.05E-02	-	-9.75E-06	4.95E+00	9.38E-02	2.80E+00	-1.08E-01	6.92E+03	1.14E-02	5.94E-02	-	0.68
EAMP	6.03E-03	2.67E-04	3.66E-01	3.15E-03	1.92E-01	-2.78E-02	7.03E+00	-2.41E-02	2.65E-02	-	-1.57E-06	9.01E+00	4.33E-02	1.29E+00	9.19E-03	9.48E+02	1.10E-02	-2.64E-02	-	0.78
EABP	9.84E-02	-1.32E-03	9.39E-01	1.90E-02	-4.68E-02	-2.46E-01	4.53E+01	-4.96E-04	7.38E-02	-	7.90E-06	4.25E+00	-4.83E-02	9.98E-01	9.75E-02	6.57E+03	1.23E-03	-8.85E-02	-	0.77
EATXA_Z/D	2.54E-01	-1.11E-03	1.29E+00	3.06E-01	1.45E+00	-4.48E-02	4.04E+01	-9.96E-02	9.07E-02	-	3.62E-06	8.69E+00	-2.93E-01	5.25E+00	-2.13E-02	7.33E+03	5.29E-02	-1.08E-01	-	0.45
EATXA	-2.56E-02	-2.73E-04	1.11E+00	-9.00E-02	3.83E-01	-9.50E-02	2.09E+01	6.32E-04	9.28E-03	-	1.93E-06	3.70E+00	1.31E-01	1.67E+00	4.47E-02	3.64E+03	-3.43E-03	-3.33E-02	-	0.83
EAMXA	6.03E-03	2.67E-04	3.66E-01	3.15E-03	1.92E-01	-2.78E-02	7.03E+00	-2.41E-02	2.65E-02	-	-1.57E-06	9.01E+00	4.33E-02	1.29E+00	9.19E-03	9.48E+02	1.10E-02	-2.64E-02	-	0.78
EABXA	-2.51E-02	-3.04E-04	7.83E-01	-5.60E-02	2.45E-01	-8.60E-02	1.85E+01	1.56E-02	-1.23E-02	-	2.05E-06	1.05E-01	7.95E-02	1.07E+00	4.54E-02	3.03E+03	-9.77E-03	-9.28E-03	-	0.70
EHTP	5.83E-02	2.24E-03	3.23E+00	3.64E-01	-9.70E-01	5.38E-01	3.50E+01	-1.36E-01	1.98E-02	-	-1.48E-05	6.09E+00	-3.20E-01	1.92E+00	-2.68E-01	5.49E+03	7.29E-02	4.94E-02	-	0.83
EHMP	-8.58E-04	4.05E-04	-2.21E-01	7.00E-02	-1.30E-02	4.13E-02	6.11E+00	-1.42E-02	-3.93E-03	-	-2.42E-06	8.04E+00	-3.55E-02	-7.03E-01	-2.06E-02	1.10E+03	8.48E-03	3.58E-03	-	0.71
EHP	-5.91E-02	-1.83E-03	3.01E+00	-2.93E-01	9.55E-01	-4.95E-01	2.88E+01	1.22E-01	-2.37E-02	-	1.24E-05	1.94E+00	2.83E-01	2.63E+00	2.48E-01	4.40E+03	-6.44E-02	-4.58E-02	-	0.84
SATP/SMYS	-8.48E-01	2.03E-02	-3.58E-01	1.57E+00	1.02E+01	3.78E+00	4.73E+02	1.28E+00	1.19E+00	-	-1.17E-04	1.55E+02	-7.85E-01	2.60E+01	2.19E+00	1.00E+05	5.02E-01	-9.45E-01	-	0.61
SAMP/SMYS	-6.81E-02	6.54E-03	3.34E+01	2.85E+00	5.25E-01	1.72E+00	1.92E+02	-7.57E-01	1.96E+00	-	-8.36E-06	1.65E+02	2.08E+00	1.33E+01	6.81E-01	2.99E+04	3.09E-01	1.25E+00	-	0.91
SABP/SMYS	5.53E-01	-1.50E-02	9.14E+00	2.24E+00	1.02E+01	1.67E+00	2.37E+02	6.75E-01	-3.21E-01	-	8.52E-05	1.33E+02	1.35E+00	2.36E+01	9.63E-01	5.25E+04	-2.50E-01	4.91E-01	-	0.49
SATNA_Z/D	-5.47E-01	7.79E-03	1.06E+01	2.16E+00	3.78E-01	-8.93E-01	2.96E+02	-2.93E-01	3.00E-01	-	-5.01E-05	7.62E+01	-4.00E-01	2.55E+01	6.19E-01	4.89E+04	4.24E-02	-4.24E-01	-	0.19
SATNA/SMYS	-2.21E-01	1.33E-02	6.52E+00	4.40E+00	1.23E+01	3.35E+00	1.31E+02	1.36E+00	1.63E+00	-	-8.64E-05	1.81E+02	3.25E+00	1.70E+01	2.13E+00	9.20E+03	5.69E-01	1.32E+00	-	0.61
SAMNA/SMYS	1.89E+00	-1.55E-03	3.11E+01	5.75E+00	5.85E+00	3.05E+00	3.39E+02	1.64E+00	4.40E-01	-	6.24E-05	2.43E+02	3.70E+00	7.98E+00	1.37E+00	3.96E+04	-7.29E-01	8.89E-02	-	0.74
SABNA/SMYS	3.72E-01	-1.05E-02	9.26E+00	4.53E+00	1.28E+01	1.62E+00	4.16E+01	1.05E+00	1.44E+00	-	6.75E-05	2.05E+02	3.28E+00	1.94E+01	1.10E+00	3.80E+03	-4.24E-01	1.35E+00	-	0.50
SATNH_X/D	1.42E-01	-7.16E-04	4.11E-01	1.37E-01	-4.06E-01	2.30E-01	6.59E+01	-3.33E-02	1.51E-01	-	2.61E-06	2.99E+00	-1.85E-01	2.13E+00	-1.28E-01	9.16E+03	1.46E-02	-1.25E-01	-	0.89
SATNH/SMYS	-8.65E-01	7.55E-03	6.43E+00	2.51E+00	1.39E+01	-6.00E-01	4.33E+01	-3.68E-01	1.51E+00	-	-4.13E-05	9.10E+01	2.15E+00	4.15E+01	1.05E-01	1.32E+04	1.45E-01	1.45E+00	-	0.60

SAMNH/SMYS	2.10E+00	1.03E-02	2.97E+01	6.90E+00	1.16E+01	8.50E+00	6.38E+02	8.86E-01	1.37E+00	-	-6.39E-07	4.21E+01	6.58E+00	2.53E+01	4.56E+00	9.25E+04	-3.96E-01	1.89E+00	-	0.77
SABNH/SMYS	3.54E-01	-5.18E-03	1.20E+01	2.96E+00	1.38E+01	1.32E+00	2.85E+02	1.72E-01	1.92E+00	-	3.57E-05	1.01E+02	2.60E+00	3.90E+01	6.63E-01	3.37E+04	-6.53E-02	2.01E+00	-	0.69
SHTP/SMYS	1.17E+00	1.73E-02	2.78E+01	3.42E+00	9.05E+00	3.85E+00	5.99E+02	1.82E+00	2.72E+00	-	-1.11E-04	6.13E+02	1.48E+00	3.25E+00	2.36E+00	1.16E+05	7.84E-01	2.97E+00	-	0.70
SHMP/SMYS	5.63E-01	1.36E-02	2.38E+01	-8.75E-01	1.64E+00	1.17E+00	4.76E+02	1.60E+00	2.10E+00	-	-5.48E-05	5.99E+01	1.54E+00	7.43E-03	3.66E-01	7.01E+04	7.14E-01	2.27E+00	-	0.79
SHBP/SMYS	1.55E+00	-1.39E-02	2.06E+01	2.72E+00	1.13E+01	-7.93E-01	3.83E+02	2.82E-01	2.16E+00	-	7.77E-05	4.03E+02	1.51E+00	2.35E+01	6.81E-01	7.10E+04	-1.03E-01	2.25E+00	-	0.65
SHTNA_Z/D	8.68E-02	3.05E-04	-1.59E-01	6.85E-02	-2.39E-01	2.93E-01	3.38E+01	-6.44E-02	8.40E-02	-	-3.45E-06	5.61E+00	-6.38E-02	1.02E+00	-1.55E-01	3.91E+03	3.10E-02	-6.94E-02	-	0.78
SHTNA/SMYS	1.17E+00	1.29E-02	9.72E+00	3.04E+00	1.52E+01	4.25E-01	8.03E+01	-1.50E-01	1.10E+00	-	-7.34E-05	1.11E+02	2.55E+00	4.23E+01	-4.64E-01	2.25E+04	4.97E-02	1.06E+00	-	0.69
SHMNA/SMYS	-2.45E-01	4.67E-03	2.90E+01	4.74E+00	6.25E+00	7.73E+00	3.58E+02	3.23E-01	1.19E-01	-	4.52E-05	5.22E+01	4.05E+00	1.20E+01	4.08E+00	6.29E+04	-2.24E-01	-2.15E-01	-	0.60
SHBNA/SMYS	6.54E-01	-1.42E-02	9.74E+00	3.00E+00	1.53E+01	-7.88E-01	1.58E+02	5.50E-01	1.58E+00	-	8.26E-05	1.37E+02	2.43E+00	4.28E+01	7.56E-01	1.21E+04	-2.44E-01	1.43E+00	-	0.67
SHTXH_X/D	3.67E-01	-8.21E-04	2.92E+00	-1.41E-01	-3.49E-01	-1.98E-01	4.85E+01	-2.31E-03	-1.65E-01	-	3.61E-06	4.07E+01	1.47E-02	2.06E+00	1.36E-01	8.45E+03	6.70E-03	3.21E-02	-	0.58
SHTXH/SMYS	-8.05E-01	-4.73E-03	3.55E+01	3.96E+00	8.50E+00	-8.93E-01	2.62E+02	7.68E-01	4.77E-01	-	3.85E-05	3.36E+02	2.83E+00	1.05E+01	5.49E-01	3.82E+04	-4.26E-01	3.43E-01	-	0.90
SHMXH/SMYS	1.34E-02	1.03E-02	1.90E+01	2.29E+00	-3.32E-01	5.08E+00	4.22E+01	-8.04E-01	6.42E-01	-	-8.27E-05	1.97E+02	1.01E+00	2.26E+01	2.73E+00	1.47E+04	4.11E-01	1.21E+00	-	0.59
SHBXH/SMYS	1.01E+00	-5.84E-03	4.10E+01	4.85E+00	7.20E+00	4.15E+00	3.34E+02	1.17E+00	-6.10E-01	-	6.63E-05	4.05E+02	2.83E+00	6.10E+00	2.35E+00	3.92E+04	-6.09E-01	1.68E+00	-	0.78
SHTNH_X/D	-7.47E-03	1.45E-04	5.65E-02	6.45E-02	-1.60E-01	2.05E-01	1.39E+01	-4.50E-02	8.10E-02	-	-2.22E-06	1.47E+00	-3.38E-02	3.35E-01	-8.44E-02	2.76E+03	2.42E-02	-8.05E-02	-	0.78
SHTNH/SMYS	-9.20E-01	1.88E-02	4.54E+00	3.61E+00	1.27E+01	9.68E-01	8.83E+01	1.07E+00	1.19E+00	-	-1.09E-04	2.12E+02	2.07E+00	1.82E+01	-7.25E-01	2.85E+04	4.82E-01	1.25E+00	-	0.58
SHMNH/SMYS	1.20E+00	1.14E-02	3.67E+01	5.85E+00	5.35E+00	5.10E+00	8.46E+01	1.40E-01	6.33E-01	-	7.56E-06	9.80E+01	4.90E+00	4.98E+00	2.38E+00	2.71E+03	-1.10E-01	-3.29E-01	-	0.79
SHBNH/SMYS	8.39E-01	-1.41E-02	7.95E+00	3.62E+00	1.35E+01	-8.38E-01	9.47E+01	9.48E-01	1.22E+00	-	8.28E-05	1.76E+02	2.45E+00	2.58E+01	6.31E-01	2.51E+04	-4.41E-01	1.27E+00	-	0.62
SRP/SMYS	1.32E+00	3.00E-03	2.93E+00	1.38E+00	2.94E+00	1.29E+00	6.78E+02	6.22E-01	-4.27E-01	-2.94E-01	-1.63E-05	1.13E+01	9.65E-01	9.00E+00	-5.81E-01	9.34E+04	-2.38E-01	5.06E-01	5.37E-01	0.35
SMP/SMYS	1.55E+00	2.60E-03	7.32E+00	1.21E+00	5.75E+00	5.00E-01	1.63E+02	-9.73E-01	1.19E+00	-7.50E-01	-6.93E-06	1.66E+01	1.56E+00	2.88E+01	-1.41E-01	2.40E+04	4.06E-01	1.32E+00	7.74E-01	0.51
SRA_Z/D	1.93E-01	-6.10E-04	1.77E+00	-2.09E-01	-4.12E-01	-4.68E-01	8.04E+01	-1.89E-01	8.05E-02	6.69E-02	5.80E-06	1.73E+01	1.11E-01	4.98E+00	1.78E-01	1.16E+04	7.76E-02	3.10E-01	4.64E-02	0.60
SMA/SMYS	-1.10E-01	3.50E-03	3.15E+00	5.65E-02	3.70E-01	1.15E+00	6.89E+01	6.00E-03	-3.12E-02	-9.47E-01	-2.53E-05	7.04E+00	-4.68E-02	-	-3.86E-01	6.90E+00	-5.40E-03	6.06E-01	1.34E+00	0.63

			0											00		3				
SRA/SMYS	1.76E+0 0	-9.80E- 03	6.20E+0 0	1.42E+ 00	2.69E+ 00	-8.18E- 01	1.34E+0 2	7.22E- 01	1.73E+0 0	-9.53E- 02	6.40E- 05	4.88E+0 1	7.53E- 01	5.05E+ 00	4.23E- 01	2.00E+0 4	-3.47E- 01	7.81E- 01	-8.62E- 01	0.60
SRH_X/D	-4.26E- 02	-1.16E- 03	2.00E+0 0	1.76E- 01	-8.70E- 01	-3.08E- 01	9.41E+0 1	1.39E- 01	1.10E- 02	6.40E- 01	8.04E- 06	1.01E+0 1	-2.31E- 01	4.25E+ 00	9.19E- 02	1.53E+0 4	-7.12E- 02	1.66E- 01	-6.65E- 01	0.64
SMH/SMYS	-3.79E- 01	4.40E- 03	3.47E+0 0	6.15E- 01	-9.45E- 02	6.98E- 01	1.39E+0 2	1.65E- 01	1.57E- 01	1.35E+0 0	-3.13E- 05	4.07E+0 1	-3.03E- 01	2.49E+ 00	-1.63E- 01	2.16E+0 4	-7.41E- 02	-7.37E- 02	-9.58E- 01	0.53
SRH/SMYS	2.63E+0 0	-1.38E- 02	5.80E+0 0	1.96E+ 00	3.51E+ 00	1.30E- 01	1.66E+0 1	5.41E- 01	1.31E+0 0	4.54E+0 0	8.42E- 05	9.82E+0 1	7.73E- 01	5.03E+ 00	-3.69E- 02	6.29E+0 2	-2.78E- 01	1.03E+0 0	3.69E+0 0	0.46
N_log	1.13E+0 2	-2.72E- 01	9.61E+0 1	6.45E+ 01	2.03E+ 02	1.04E+ 02	4.17E+0 4	1.03E+0 1	3.37E+0 1	5.65E+0 1	1.90E- 03	3.84E+0 2	7.13E+ 01	9.95E+ 02	4.41E+ 01	5.88E+0 6	2.30E+0 0	3.65E+0 1	5.07E+0 1	0.31

Table B.4.1. List of random input variables and their statistical distribution for interaction of dent with longitudinal weld (μ = mean value, σ = standard deviation)

Variable	Distribution	μ	σ	Density function
MATERIAL INPUT PARAMETERS				
SMYS (MPa), SMYS (data collected from a local source for a list of pipeline purchase orders)	Lognormal	434	44	
E_l (MPa), EL	Normal	1.90×10^5	2.6×10^4	
E_t (MPa), ET	Normal	1.90×10^5	2.6×10^4	
σ_y @ $\varepsilon = 0.002$ (MPa), SY1=0.002*EI				
FSY2	Normal	1.15	0.075	
σ_y @ $\varepsilon = 0.005$ (MPa), SY2=FSY2*SMYS				
FSU	Normal	1.65	0.12	
σ_u (MPa), SU=FSU*SMYS				
GEOMETRY INPUT PARAMETERS				
D (mm), PIPEDIA=610				
D/t, DTRATIO (data collected from a local source for a list of pipeline purchase orders)	Uniform	85	± 55	
t (mm), THICK=DTRATIO*PIPDIA				
r (mm), DENTRAD	Lognormal	73	61	
INDENTATION AND PRESSURE LOADING INPUT PARAMETERS				
d/D (%), DENTPERCENT	Weibul		$\gamma=1.2689$ Char=2.6618 Offset=0	
d (mm), d=DENTPERCENT/100*PIPDIA				
P_{SMYS} (MPa), PSMYS=SMYS*2*THICK/PIPDIA				
FHYDRO	Normal	0.95	0.025	
FMIN	Uniform	0.2	± 0.1	
FMAX	Triangular	0.72	0.6-0.8	
P_{hydro} (MPa),				

PHYDRO=FHYDRO*PSMYS				
P_{\min} (MPa), PMIN=FMIN*PSMYS				
P_{\max} (MPa), PMAX=FMAX*PSMYS				
WELD RESIDUAL STRESS PARAMETERS				
FSINITIAL	Uniform	0.65	± 0.35	
σ_{residual} (MPa), SINITIAL= FSINITIAL*SY2				
X-offset, (mm)	Uniform	75	± 75	

Table B.4.2. Output parameters and their statistical distribution for interaction of dent with longitudinal weld (μ = mean value, σ = standard deviation)

NAME	DESCRIPTION			μ	σ
	Direction	Component	Location		
LENGTH	Dent length			268	233
WIDTH	Dent width			84	29
Strains at end of indentation phase					
EATP	Axial	Total	dent peak	-7.01E-02	6.64E-02
EAMP	Axial	Membrane	dent peak	4.75E-03	1.28E-02
EABP	Axial	Bending	dent peak	7.48E-02	7.36E-02
EATXA_Z	Location of maximum tensile value along dent longitudinal			169	416
EATXA	Axial	Total	maximum tensile in dent longitudinal	9.79E-03	1.23E-02
EAMXA	Axial	Membrane	maximum tensile in dent longitudinal	2.73E-03	4.79E-03
EABXA	Axial	Bending	maximum tensile in dent longitudinal	-4.32E-03	5.43E-03
EHTP	Hoop	Total	dent peak	-9.72E-02	8.40E-02
EHMP	Hoop	Membrane	dent peak	-7.08E-04	1.07E-02
EHBP	Hoop	Bending	dent peak	9.58E-02	8.99E-02
Stresses at end of indentation phase					
SATP	Axial	Total	dent peak	-467	268
SAMP	Axial	Membrane	dent peak	98	365
SABP	Axial	Bending	dent peak	543	195
SATNA_Z	Location of maximum compressive value along dent longitudinal			40	210
SATNA	Axial	Total	maximum tensile in dent longitudinal	-522	180
SAMNA	Axial	Membrane	maximum tensile in dent longitudinal	543	195
SABNA	Axial	Bending	maximum tensile in dent longitudinal	92	361
SATNH_X	Location of maximum compressive value along dent transverse			18	18
SATNH	Axial	Total	maximum tensile in dent transverse	-571	174
SAMNH	Axial	Membrane	maximum tensile in dent transverse	6	335
SABNH	Axial	Bending	maximum tensile in dent transverse	550	211
SHTP	Hoop	Total	dent peak	-556	261
SHMP	Hoop	Membrane	dent peak	-107	369
SHBP	Hoop	Bending	dent peak	578	200
SHTNA_Z	Location of maximum compressive value along dent longitudinal			12	17
SHTNA	Hoop	Total	maximum tensile in dent longitudinal	-622	192
SHMNA	Hoop	Membrane	maximum tensile in dent longitudinal	-144	317
SHBNA	Hoop	Bending	maximum tensile in dent longitudinal	584	191
SHTXH_X	Location of maximum tensile value along dent transverse			99	30
SHTXH	Hoop	Total	maximum tensile in dent transverse	224	170
SHMXH	Hoop	Membrane	maximum tensile in dent transverse	-110	111
SHBXH	Hoop	Bending	maximum tensile in dent transverse	-296	204
SHTNH_X	Location of maximum compressive value along dent transverse			6	12
SHTNH	Hoop	Total	maximum tensile in dent transverse	-600	193
SHMNH	Hoop	Membrane	maximum tensile in dent transverse	-107	375
SHBNH	Hoop	Bending	maximum tensile in dent transverse	586	194
Stress range and fatigue life at end of pressure cycle phase					
SRP	Von Mises	Range	dent peak	179	79
SMP	Von Mises	Mean	dent peak	312	96
SRA_Z	Location of maximum stress range in dent longitudinal direction			30	37
SRA	Von Mises	Range	maximum in dent longitudinal	461	122
SMA	Von Mises	Mean	maximum in dent longitudinal	94	307
SRH_X	Location of maximum stress range in dent transverse direction			19	23
SRH	Von Mises	Range	maximum in dent transverse direction	414	128
SMH	Von Mises	Mean	maximum in dent transverse direction	21	30
N_log	fatigye cycles to failure (in natural log)			10.72	9.851

Table B.4.3. Rank order Spearman Correlation factors between output and input parameters for interaction of dents with longitudinal weld

Out\Imp	SMYS	EL	ET	FSY2	FSU	THICK	DENTRAD	DENTPER CENT	FHYDRO	FMIN	FMAX	FSINITIA L	XOFFSE T
LENGTH	-0.02	-0.056	-0.149	0.185	-0.049	-0.372	0.39	-0.68	0.184	-0.163	-0.064	0.144	0.023
WIDTH	0.107	0.006	-0.059	0.178	0.053	-0.081	0.442	-0.485	0.227	-0.107	-0.119	0.108	-0.008
EATP	-0.093	-0.052	-0.091	0.043	-0.019	-0.163	0.349	-0.892	0.071	-0.061	-0.062	0.019	0.028
EAMP	0.111	0.061	-0.015	small	0.023	-0.261	-0.139	0.707	-0.11	0.194	-0.074	-0.093	-0.049
EABP	0.099	0.046	0.089	-0.034	0.007	0.113	-0.353	0.917	-0.075	0.068	0.055	-0.008	-0.016
EATXA_Z	0.025	-0.072	0.01	-0.012	-0.003	0.297	0.425	-0.687	0.043	0.008	-0.068	-0.105	-0.052
EATXA	0.116	0.085	0.112	-0.104	0.009	0.074	-0.195	0.955	-0.098	0.077	-0.015	0.01	-0.033
EAMXA	0.121	0.05	0.04	-0.074	0.053	-0.077	-0.116	0.805	-0.121	0.201	-0.084	-0.065	-0.081
EABXA	-0.024	-0.122	-0.084	0.121	-0.051	-0.403	0.156	-0.53	0.057	-0.016	-0.159	0.082	0.07
EHTP	-0.106	-0.053	-0.11	0.047	-0.004	-0.158	0.299	-0.913	0.077	-0.067	-0.04	0.019	0.03
EHMP	-0.048	0.081	-0.263	0.122	-0.03	-0.518	-0.128	-0.065	0.008	0.081	-0.106	-0.005	0.019
EHBP	0.111	0.052	0.098	-0.023	small	0.071	-0.332	0.938	-0.07	0.068	0.036	-0.004	-0.001
SATP	-0.352	0.002	-0.088	-0.094	-0.232	-0.247	0.232	-0.391	0.008	-0.009	-0.211	0.095	0.134
SAMP	0.166	0.038	-0.011	-0.038	0.113	-0.207	-0.131	0.727	-0.143	0.223	-0.054	-0.117	-0.023
SABP	0.461	0.023	0.093	0.09	0.279	0.063	-0.267	0.795	-0.066	0.101	0.053	-0.019	-0.041
SATNA_Z	0.124	0.021	0.023	-0.091	0.097	-0.065	0.273	0.364	-0.089	0.129	-0.147	-0.022	0.09
SATNA	-0.455	-0.027	-0.142	-0.078	-0.278	-0.203	0.241	-0.623	0.011	-0.121	-0.077	0.082	0.085
SAMNA	0.46	0.012	0.152	0.052	0.276	0.076	-0.229	0.815	-0.06	0.11	0.01	-0.041	-0.05
SABNA	0.157	0.056	small	-0.075	0.122	-0.179	-0.112	0.719	-0.123	0.272	-0.047	-0.15	-0.005
SATNH_X	-0.083	0.183	-0.115	-0.023	-0.286	-0.017	0.22	0.097	0.129	-0.131	-0.222	0.215	0.179
SATNH	-0.55	-0.083	-0.121	-0.165	-0.256	-0.119	0.203	-0.688	0.03	-0.023	-0.021	0.021	0.095
SAMNH	0.115	0.034	-0.027	-0.062	0.211	0.02	-0.192	0.427	-0.049	0.373	0.059	-0.223	-0.116
SABNH	0.431	0.036	0.116	0.095	0.244	0.135	-0.243	0.692	-0.035	0.097	0.044	-0.072	-0.053
SHTP	-0.428	-0.043	-0.082	-0.106	-0.27	-0.19	0.12	-0.464	0.016	-0.04	-0.172	0.109	0.102
SHMP	0.036	0.041	-0.085	-0.071	0.066	-0.288	-0.119	0.498	-0.081	0.25	-0.065	-0.122	0.033
SHBP	0.493	0.075	0.095	0.107	0.284	0.131	-0.174	0.685	-0.026	0.127	0.049	-0.077	-0.015
SHTNA_Z	0.044	0.108	0.089	0.015	-0.113	0.209	-0.079	0.073	0.164	-0.135	-0.088	0.019	-0.024
SHTNA	-0.56	-0.064	-0.143	-0.108	-0.312	-0.135	0.155	-0.72	0.05	-0.082	-0.031	0.058	0.102
SHMNA	-0.034	0.092	-0.12	-0.082	0.042	-0.329	-0.039	0.308	-0.056	0.302	-0.074	-0.162	0.057
SHBNA	0.481	0.018	0.103	0.131	0.272	0.131	-0.197	0.608	-0.022	0.06	0.097	-0.034	-0.096
SHTXH_X	-0.104	-0.068	-0.072	-0.044	-0.07	0.436	0.02	-0.488	0.021	-0.126	0.023	-0.047	-0.09
SHTXH	0.244	0.082	0.206	-0.014	0.024	-0.044	-0.089	0.966	-0.085	0.112	-0.101	0.018	0.025
SHMXH	-0.151	-0.109	-0.173	0.062	-0.055	-0.136	0.152	-0.933	0.078	-0.101	0.019	0.047	-0.015
SHBXH	-0.275	-0.108	-0.172	-0.04	-0.085	0.01	0.111	-0.937	0.072	-0.125	0.071	0.029	-0.004
SHTNH_X	0.099	-0.377	0.319	-0.051	-0.002	-0.099	0.023	0.02	-0.062	0.134	-0.125	0.047	0.029
SHTNH	-0.524	-0.03	-0.14	-0.109	-0.309	-0.123	0.129	-0.642	0.028	-0.093	-0.064	0.078	0.081
SHMNH	0.032	0.051	-0.089	-0.073	0.072	-0.288	-0.108	0.494	-0.078	0.26	-0.073	-0.133	0.046
SHBNH	0.543	0.029	0.142	0.115	0.3	0.096	-0.161	0.733	-0.057	0.074	0.027	-0.032	-0.065

SRP	0.269	-0.105	0.129	0.136	0.164	0.082	-0.246	0.186	0.017	-0.225	0.274	0.225	-0.123
SMP	0.384	-0.05	0.075	0.165	0.311	-0.139	-0.158	0.538	-0.115	-0.002	0.107	0.003	-0.099
SRA	0.173	-0.085	-0.085	0.13	0.16	-0.254	-0.057	-0.162	-0.089	-0.21	0.169	0.223	-0.081
SMA	0.458	0.207	0.176	0.161	0.174	0.061	-0.029	0.697	-0.003	0.16	-0.018	-0.199	-0.068
SRA_Z	-0.224	0.068	0.033	-0.136	-0.125	0.213	0.211	-0.218	-0.08	-0.018	-0.185	-0.086	0.166
SRH	-0.058	-0.228	-0.056	0.154	0.101	0.097	-0.179	-0.451	-0.061	-0.324	0.205	0.143	-0.082
SMH	0.454	0.131	0.154	0.129	0.091	-0.151	-0.036	0.758	-0.021	0.13	0.009	-0.04	-0.038
SRH_X	-0.134	-0.122	0.067	-0.104	-0.016	0.211	0.034	-0.145	-0.157	-0.029	-0.19	-0.027	0.117
N_log	-0.076	0.157	-0.166	-0.108	-0.1	-0.021	0.317	-0.346	0.02	0.183	-0.304	-0.201	0.115

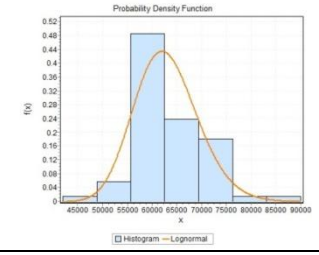
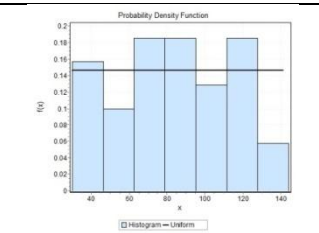
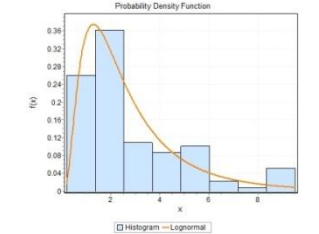
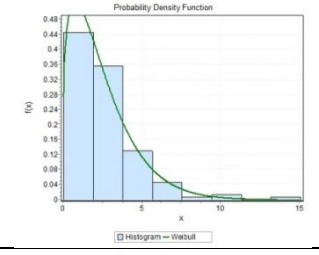
Table B.4.4. Regression analysis- Coefficients and R² value for interaction of dent with longitudinal weld

	a ₀	b ₁	b ₂	b ₃	b ₄	b ₅	b ₆	b ₇	b ₈	b ₉	b ₁₀	c ₁	c ₂	c ₃	c ₄	c ₅	c ₆	c ₇	c ₈	c ₉	c ₁₀	R ²
EATP	-5.41E-03	2.96E-05	1.15E+01	-1.53E-01	6.15E-01	4.10E-01	1.24E+01	2.35E-02	1.41E-02	2.84E-02	-	-2.48E-06	9.70E+01	2.50E-02	-5.38E-01	-1.81E-01	2.01E+03	-2.24E-02	-1.79E-02	2.31E-02	-	0.85
EAMP	3.95E-02	3.36E-04	6.94E-01	1.11E-02	-7.00E-02	-2.08E-02	4.56E+01	4.67E-02	1.10E-03	-5.33E-02	-	-1.18E-06	3.45E-01	-1.75E-03	6.83E-02	-2.57E-03	6.72E+03	-2.32E-02	2.50E-03	1.72E-01	-	0.59
EABP	4.49E-02	3.07E-04	1.22E+01	1.64E-01	-6.85E-01	-4.30E-01	5.81E+01	2.32E-02	-1.31E-02	-8.17E-02	-	1.30E-06	9.66E+01	-2.68E-02	6.05E-01	1.79E-01	8.73E+03	-7.65E-04	2.04E-02	1.49E-01	-	0.85
EATXA_Z/D	4.87E+00	6.50E-03	5.12E+01	-1.05E-01	2.14E+00	1.51E+00	1.63E+03	2.37E+00	2.48E+00	4.04E+00	-	2.08E-05	6.13E+02	7.15E-02	3.60E+00	2.23E-01	2.86E+05	9.34E-01	1.52E+00	1.59E+01	-	0.50
EATXA	-1.00E-03	2.15E-05	1.49E+00	2.59E-02	-1.04E-01	-5.65E-02	4.63E+00	1.63E-02	5.30E-03	-3.22E-02	-	3.11E-07	6.70E+00	-4.15E-03	8.95E-02	1.46E-02	4.10E+02	-8.20E-03	-4.90E-03	7.01E-02	-	0.90
EAMXA	3.95E-02	3.36E-04	6.94E-01	1.11E-02	-7.00E-02	-2.08E-02	4.56E+01	4.67E-02	1.10E-03	-5.33E-02	-	-1.18E-06	3.45E-01	-1.75E-03	6.83E-02	-2.57E-03	6.72E+03	-2.32E-02	2.50E-03	1.72E-01	-	0.59
EABXA	-1.05E-02	-4.98E-05	1.18E+00	1.99E-02	-7.75E-02	-4.38E-02	6.36E+00	3.40E-03	5.10E-03	-2.41E-02	-	5.15E-07	7.38E+00	-3.23E-03	6.53E-02	1.34E-02	1.14E+03	-1.80E-03	-4.30E-03	5.89E-02	-	0.86
EHTP	4.51E-02	1.18E-04	1.40E+01	-1.64E-01	6.55E-01	4.40E-01	2.20E+01	3.38E-02	-5.70E-03	9.53E-02	-	-3.00E-06	1.15E+02	2.65E-02	-5.68E-01	-1.90E-01	3.76E+03	-2.70E-02	-2.60E-03	-1.94E-01	-	0.90
EHMP	4.57E-02	4.47E-04	5.22E-02	5.65E-03	-5.45E-02	-4.68E-03	4.96E+01	3.99E-02	-5.30E-03	-8.50E-03	-	-1.87E-06	4.46E+00	-1.00E-03	5.63E-02	-8.75E-03	7.58E+03	-2.08E-02	7.50E-03	4.01E-02	-	0.43
EHBP	6.70E-04	3.29E-04	1.40E+01	1.70E-01	-7.05E-01	-4.45E-01	2.76E+01	6.10E-03	4.05E-04	-1.04E-01	-	1.13E-06	1.11E+02	-2.75E-02	6.23E-01	1.81E-01	3.82E+03	6.20E-03	1.01E-02	2.34E-01	-	0.90
SATP/SMYS	2.80E+00	1.58E-02	6.11E+01	-3.39E-01	1.64E+00	9.05E-01	2.70E+03	9.07E-01	1.48E+00	2.22E+00	-	-9.06E-05	9.77E+02	8.33E-02	1.96E+00	-7.25E-01	3.92E+05	-4.64E-01	-9.76E-01	7.27E+00	-	0.77
SAMP/SMYS	2.28E+00	2.45E-02	3.82E+01	1.38E-01	2.56E+00	1.81E+00	8.95E+02	-3.60E-01	2.94E-01	1.34E+00	-	-9.01E-05	1.38E+02	-1.37E-02	3.03E+00	6.50E-01	1.24E+05	1.26E-01	-3.97E-01	4.95E+00	-	0.88
SABP/SMYS	2.62E+00	-8.40E-03	5.38E+01	1.04E-01	2.29E+00	-3.00E-01	2.04E+03	2.75E-01	1.54E+00	1.29E+00	-	4.59E-05	7.43E+02	-4.13E-02	2.37E+00	3.48E-01	2.97E+05	-7.48E-02	1.04E+00	4.16E+00	-	0.81
SATNA_Z/D	-5.82E-01	-2.40E-03	1.07E+01	4.80E-01	5.20E-02	1.35E+00	1.18E+02	-2.02E-01	9.20E-01	6.31E-01	-	2.11E-05	4.20E+01	-7.90E-03	1.37E+00	6.63E-01	2.02E+04	8.40E-02	-6.65E-01	2.85E-01	-	0.62
SATNA/SMYS	1.27E+00	6.10E-03	4.18E+01	6.40E-02	3.21E+00	8.58E-02	1.20E+03	4.71E-02	1.36E+00	-7.67E-01	-	-3.24E-05	5.21E+02	1.05E-02	3.13E+00	-1.12E-01	1.75E+05	-1.16E-01	-8.97E-01	3.82E+00	-	0.78
SAMNA/SMYS	2.18E+00	1.99E-02	4.27E+01	2.23E-01	2.83E+00	1.87E+00	1.06E+03	-8.23E-01	4.05E-01	1.69E+00	-	-6.33E-05	2.55E+02	-2.78E-02	3.10E+00	6.38E-01	1.48E+05	3.43E-01	-5.06E-01	5.91E+00	-	0.84
SABNA/SMYS	1.26E+00	-4.70E-03	4.33E+01	-1.26E-01	3.26E+00	1.54E-01	1.07E+03	3.65E-01	1.60E+00	4.87E-01	-	2.26E-05	5.05E+02	9.00E-04	3.18E+00	2.14E-02	1.59E+05	-7.20E-02	1.08E+00	2.66E+00	-	0.83
SATNH_X/D	1.30E-01	-6.90E-04	1.94E-01	2.99E-04	7.15E-03	-6.33E-02	4.59E+01	-1.12E-01	1.05E-01	1.62E-02	-	3.80E-06	1.17E+01	1.25E-02	1.77E-01	5.51E-02	4.90E+03	4.64E-02	-7.03E-02	2.50E-01	-	0.89
SATNH/SMYS	-3.83E-01	6.10E-03	3.98E+01	5.90E-02	3.51E+00	-3.05E-01	3.44E+02	6.41E-02	1.66E+00	-9.76E-01	-	-2.53E-05	4.68E+02	1.20E-02	3.53E+00	-9.50E-02	5.96E+04	-7.01E-02	1.15E+00	4.31E+00	-	0.82
SAMNH/SMYS	1.07E+00	1.97E-02	4.78E+01	4.72E-01	2.94E+00	2.16E+00	9.38E+01	7.11E-01	-5.76E-01	1.48E+00	-	-7.67E-05	3.85E+02	-7.03E-02	3.20E+00	4.87E-01	3.92E+04	-3.13E-01	2.13E-01	3.86E+00	-	0.69
SABNH/SMYS	-4.01E-	-6.80E-	4.26E+	-1.03E-	3.27E+	7.15E-	6.85E+	3.25E-	-	5.42E-	-	2.87E-	-	-2.00E-	-	-4.08E-	-	-8.40E-	1.18E+	-	-	0.86

	01	03	01	01	00	01	02	01	1.69E+00	01		05	5.01E+02	03	3.35E+00	01	1.08E+05	02	00	3.09E+00		
SHTP/SMYS	3.85E+00	1.58E-02	5.50E+01	-1.59E-01	2.70E+00	8.13E-02	3.04E+03	3.27E-01	5.31E-01	2.27E+00	-	-8.71E-05	8.46E+02	5.80E-02	2.90E+00	-1.31E-01	4.44E+05	-1.66E-01	-2.20E-01	7.79E+00	-	0.74
SHMP/SMYS	-2.96E-01	2.48E-02	2.12E+01	3.14E-01	3.40E+00	2.08E+00	3.60E+02	-4.59E-01	3.95E-01	5.19E-02	-	-7.94E-05	9.89E+01	-4.35E-02	3.78E+00	5.53E-01	7.13E+04	1.25E-01	-4.38E-01	-9.84E-01	-	0.81
SHBP/SMYS	3.25E+00	-1.05E-02	4.92E+01	4.79E-02	3.03E+00	2.32E-01	2.26E+03	7.95E-01	1.05E+00	1.34E+00	-	5.31E-05	6.68E+02	-3.68E-02	3.10E+00	-6.94E-03	3.31E+05	-3.50E-01	6.34E-01	4.68E+00	-	0.78
SHTNA_Z/D	-3.22E-01	-7.11E-04	1.12E+01	3.70E-01	2.13E+00	-9.85E-01	1.27E+02	-1.67E-01	5.19E-01	1.80E-01	-	1.34E-05	6.80E+01	-6.28E-02	5.00E+00	4.73E-01	2.34E+04	7.38E-02	-3.69E-01	7.59E-01	-	0.85
SHTNA/SMYS	1.10E+00	3.10E-03	4.25E+01	1.12E-01	3.94E+00	-1.29E-01	1.09E+03	-3.27E-01	1.87E+00	-3.63E-01	-	-1.21E-05	4.82E+02	9.68E-03	3.70E+00	-1.15E-01	1.64E+05	8.00E-02	1.25E+00	2.03E+00	-	0.85
SHMNA/SMYS	1.48E+00	2.11E-02	1.87E+01	1.80E-01	2.31E+00	1.71E+00	1.09E+03	1.40E+00	6.55E-01	-2.60E-01	-	-6.33E-05	5.87E+01	-2.19E-02	2.80E+00	4.16E-01	1.75E+05	5.32E-01	-6.38E-01	3.80E-01	-	0.60
SHBNA/SMYS	1.02E+00	-3.70E-03	4.58E+01	-8.20E-02	3.71E+00	1.30E-01	1.00E+03	3.74E-01	1.94E+00	4.77E-01	-	1.46E-05	5.46E+02	-1.24E-02	3.48E+00	1.47E-01	1.51E+05	-1.00E-01	1.33E+00	2.38E+00	-	0.85
SHTXH_X/D	5.54E-01	-2.01E-03	7.76E+00	9.00E-03	-5.40E-02	1.14E-01	8.45E+01	-4.28E-02	1.64E-01	-1.43E-01	-	4.28E-06	8.84E+01	-1.13E-03	-3.45E-01	-6.18E-02	1.40E+04	1.83E-02	-1.38E-01	5.66E-01	-	0.77
SHTXH/SMYS	1.79E+00	8.20E-03	4.49E+01	-3.54E-02	1.45E-01	-8.93E-01	6.51E+02	4.23E-01	2.65E-01	2.14E-01	-	-3.20E-05	3.58E+02	1.23E-02	2.26E-01	4.99E-01	1.06E+05	-1.32E-01	-2.62E-01	-4.82E-01	-	0.96
SHMXH/SMYS	6.92E-01	-1.74E-04	2.02E+01	-1.16E-01	3.75E-01	5.28E-01	4.33E+02	9.50E-03	4.45E-02	2.58E-01	-	-4.09E-07	1.74E+02	1.70E-02	-3.30E-01	-2.64E-01	7.08E+04	-1.55E-02	-1.56E-02	1.34E+00	-	0.87
SHBXH/SMYS	2.09E+00	7.80E-03	5.01E+01	-1.27E-01	4.54E-01	-7.48E-01	9.14E+02	3.61E-01	1.51E-01	-3.06E-01	-	-3.24E-05	4.40E+02	2.78E-02	-9.88E-02	4.88E-01	1.47E+05	-1.13E-01	-1.64E-01	1.74E+00	-	0.96
SHTNH_X/D	1.27E-02	-4.77E-05	-3.13E-01	-5.15E-03	6.95E-03	-2.23E-03	3.17E+00	-2.54E-02	1.57E-02	3.24E-02	-	3.84E-07	9.21E+00	2.65E-03	4.35E-02	-4.99E-03	2.39E+02	1.39E-02	-1.11E-02	-8.57E-02	-	0.90
SHTNH/SMYS	1.30E+00	6.10E-03	4.45E+01	1.42E-01	3.97E+00	-1.27E-01	1.21E+03	-9.24E-02	1.39E+00	-1.72E-01	-	-3.13E-05	5.69E+02	2.28E-03	3.75E+00	-1.94E-01	1.78E+05	-6.21E-02	-8.88E-01	1.43E+00	-	0.82
SHMNH/SMYS	-5.89E-01	2.21E-02	2.07E+01	3.16E-01	3.36E+00	2.01E+00	1.99E+01	-8.78E-01	6.63E-01	-4.14E-01	-	-6.49E-05	7.30E+01	-4.45E-02	3.58E+00	5.18E-01	2.16E+04	3.02E-01	-6.43E-01	6.85E-01	-	0.78
SHBNH/SMYS	1.31E+00	-5.70E-03	4.29E+01	-1.64E-01	3.96E+00	3.93E-01	1.11E+03	5.10E-01	1.65E+00	2.31E-01	-	2.48E-05	5.23E+02	3.40E-03	3.83E+00	1.71E-02	1.65E+05	-1.40E-01	1.10E+00	1.35E+00	-	0.85
SRP/SMYS	-4.32E-01	-5.13E-04	1.41E+01	2.51E-01	-8.90E-01	-1.02E-01	1.62E+02	6.88E-01	-7.45E-01	3.68E-01	-2.82E-01	-6.20E-06	1.81E+02	-5.10E-02	7.03E-01	1.54E-01	1.63E+04	-2.16E-01	6.82E-01	1.40E+00	9.36E-01	0.47
SMP/SMYS	-8.93E-01	1.25E-02	2.57E+01	2.85E-01	-7.25E-01	-7.10E-01	5.98E+02	3.59E-01	-2.34E-01	-6.75E-01	1.86E+00	-7.43E-05	2.85E+02	-6.05E-02	8.80E-01	5.56E-01	7.71E+04	-8.13E-02	8.50E-02	3.59E+00	2.16E+00	0.55
SRA_Z/D	2.27E+00	-6.00E-03	7.21E-01	1.41E+00	1.28E+01	1.51E+00	4.40E+02	-6.61E-01	8.45E-01	8.14E-01	3.08E+00	2.11E-05	1.07E+02	-1.77E-01	1.06E+01	7.69E-01	6.42E+04	3.45E-01	-6.39E-01	1.39E+00	2.66E+00	0.77
SMA/SMYS	-1.84E-01	3.60E-03	4.83E+00	3.47E-01	2.06E+00	-1.63E-01	1.55E+02	1.71E-01	-4.64E-02	7.11E-01	1.30E+00	-2.36E-05	4.83E+01	-5.90E-02	1.68E+00	1.07E-01	1.29E+04	-4.80E-02	1.49E-01	2.52E+00	1.67E+00	0.35
SRA/SMYS	3.74E-01	2.20E-03	2.54E+01	-4.09E-02	2.04E+00	-3.55E-01	2.22E+02	-3.98E-01	-8.92E-01	-5.11E-01	8.71E-01	-6.53E-06	2.47E+02	-4.50E-03	1.70E+00	1.31E-01	3.79E+04	1.78E-01	4.66E-01	1.04E+00	-9.08E-01	0.71
SRH_X/D	2.69E-01	-2.01E-03	1.68E+00	8.15E-02	-7.20E-01	-7.23E-02	8.85E+01	3.14E-02	2.10E-03	1.99E-01	3.51E-01	9.59E-06	3.11E+01	-7.23E-03	4.25E-01	3.29E-02	1.28E+04	-8.00E-03	1.10E-02	-3.62E-01	-3.94E-01	0.64
SMH/SMYS	5.29E-01	-4.65E-01	-	1.66E-01	-2.24E-01	1.26E-01	-	7.76E-01	-4.85E-01	6.52E-01	-	-5.00E-01	2.67E+01	-3.28E-01	-1.46E-01	-8.56E-01	2.18E+01	6.90E-01	4.32E-01	-	1.85E+01	0.47

	01	04	3.74E+00	01	01	01	1.02E+02	02	01	01	1.35E+00	06	01	02	01	02	04	03	01	2.56E+00	00	
SRH/SMYS	-2.37E-01	6.20E-03	3.60E+01	2.10E-01	-6.75E-01	-6.48E-01	2.49E+02	-4.05E-01	-3.86E-02	-6.01E-01	1.54E+00	-2.72E-05	3.56E+02	-3.68E-02	8.35E-01	3.85E-01	3.61E+04	1.98E-01	-8.09E-02	1.79E+00	1.55E+00	0.64
N_log	7.09E+01	-2.29E-01	9.52E+02	1.17E+01	4.32E+01	1.39E+01	1.12E+04	3.40E+01	2.45E+01	1.71E+01	1.34E+02	1.70E-03	1.33E+04	2.60E+00	4.40E+01	1.76E+01	2.22E+06	9.26E+00	2.20E+01	3.73E+01	1.02E+02	0.53

Table B.5.1. List of random input variables and their statistical distribution for interaction of dent with girth weld (μ = mean value, σ = standard deviation)

Variable	Distribution	μ	σ	Density function
MATERIAL INPUT PARAMETERS				
SMYS (MPa), SMYS (data collected from a local source for a list of pipeline purchase orders)	Lognormal	434	44	
E_l (MPa), EL	Normal	1.90×10^5	2.6×10^4	
E_t (MPa), ET	Normal	1.90×10^5	2.6×10^4	
σ_y @ $\varepsilon = 0.002$ (MPa), SY1=0.002*E1				
FSY2	Normal	1.15	0.075	
σ_y @ $\varepsilon = 0.005$ (MPa), SY2=FSY2*SMYS				
FSU	Normal	1.65	0.12	
σ_u (MPa), SU=FSU*SMYS				
GEOMETRY INPUT PARAMETERS				
D (mm), PIPEDIA=610				
D/t, DTRATIO (data collected from a local source for a list of pipeline purchase orders)	Uniform	85	± 55	
t (mm), THICK=DTRATIO*PIPEDIA				
r (mm), DENTRAD	Lognormal	73	61	
INDENTATION AND PRESSURE LOADING INPUT PARAMETERS				
d/D (%), DENTPERCENT	Weibul		$\gamma=1.2689$ Char=2.6618 Offset=0	
d (mm), d=DENTPERCENT/100*PIPEDIA				
P_{SMYS} (MPa), PSMYS=SMYS*2*THICK/PIPDIA				
FHYDRO	Normal	0.95	0.025	
FMIN	Uniform	0.2	± 0.1	
FMAX	Triangular	0.72	0.6-0.8	
P_{hydro} (MPa),				

PHYDRO=FHYDRO*PSMYS				
P_{\min} (MPa), PMIN=FMIN*PSMYS				
P_{\max} (MPa), PMAX=FMAX*PSMYS				
WELD RESIDUAL STRESS PARAMETERS				
FSINITIAL	Uniform	0.65	± 0.35	
σ_{residual} (MPa), SINITIAL= FSINITIAL*SY2				
Z-offset, (mm)	Uniform	343	± 343	

Table B.5.2. Output parameters and their statistical distribution for interaction of dent with girth weld (μ = mean value, σ = standard deviation)

NAME	DESCRIPTION			μ	σ
	Direction	Component	Location		
LENGTH	Dent length			199	133
WIDTH	Dent width			75	22
Strains at end of indentation phase					
EATP	Axial	Total	dent peak	-7.22E-02	7.63E-02
EAMP	Axial	Membrane	dent peak	6.93E-03	2.08E-02
EABP	Axial	Bending	dent peak	7.91E-02	9.38E-02
EATXA_Z	Location of maximum tensile value along dent longitudinal			135	288
EATXA	Axial	Total	maximum tensile in dent longitudinal	1.17E-02	1.75E-02
EAMXA	Axial	Membrane	maximum tensile in dent longitudinal	3.44E-03	6.41E-03
EABXA	Axial	Bending	maximum tensile in dent longitudinal	-4.87E-03	7.67E-03
EHTP	Hoop	Total	dent peak	-1.01E-01	9.40E-02
EHMP	Hoop	Membrane	dent peak	5.37E-04	1.58E-02
EHBP	Hoop	Bending	dent peak	1.02E-01	1.16E-01
Stresses at end of indentation phase					
SATP	Axial	Total	dent peak	-477	233
SAMP	Axial	Membrane	dent peak	55	367
SABP	Axial	Bending	dent peak	541	156
SATNA_Z	Location of maximum compressive value along dent longitudinal			40	210
SATNA	Axial	Total	maximum tensile in dent longitudinal	-528	133
SAMNA	Axial	Membrane	maximum tensile in dent longitudinal	548	147
SABNA	Axial	Bending	maximum tensile in dent longitudinal	53	368
SATNH_X	Location of maximum compressive value along dent transverse			18	18
SATNH	Axial	Total	maximum tensile in dent transverse	-571	129
SAMNH	Axial	Membrane	maximum tensile in dent transverse	-54	345
SABNH	Axial	Bending	maximum tensile in dent transverse	545	162
SHTP	Hoop	Total	dent peak	-574	224
SHMP	Hoop	Membrane	dent peak	-124	393
SHBP	Hoop	Bending	dent peak	581	158
SHTNA_Z	Location of maximum compressive value along dent longitudinal			12	17
SHTNA	Hoop	Total	maximum tensile in dent longitudinal	-632	151
SHMNA	Hoop	Membrane	maximum tensile in dent longitudinal	-144	351
SHBNA	Hoop	Bending	maximum tensile in dent longitudinal	590	150
SHTXH_X	Location of maximum tensile value along dent transverse			99	30
SHTXH	Hoop	Total	maximum tensile in dent transverse	227	171
SHMXH	Hoop	Membrane	maximum tensile in dent transverse	-113	119
SHBXH	Hoop	Bending	maximum tensile in dent transverse	-287	201
SHTNH_X	Location of maximum compressive value along dent transverse			6	12
SHTNH	Hoop	Total	maximum tensile in dent transverse	-613	152
SHMNH	Hoop	Membrane	maximum tensile in dent transverse	-124	396
SHBNH	Hoop	Bending	maximum tensile in dent transverse	589	147
Stress range and fatigue life at end of pressure cycle phase					
SRP	Von Mises	Range	dent peak	175	71
SMP	Von Mises	Mean	dent peak	302	87
SRA_Z	Location of maximum stress range in dent longitudinal direction			30	37
SRA	Von Mises	Range	maximum in dent longitudinal	479	97
SMA	Von Mises	Mean	maximum in dent longitudinal	19	28
SRH_X	Location of maximum stress range in dent transverse direction			19	23
SRH	Von Mises	Range	maximum in dent transverse direction	428	109
SMH	Von Mises	Mean	maximum in dent transverse direction	10	23
N_log	fatigue cycles to failure (in natural log)			10.95	9.873

Table B.5.3. Rank order Spearman Correlation factors between output and input parameters for interaction of dents with girth weld

Out\Imp	SMYS	EL	ET	FSY2	FSU	THICK	DENTRAD	DENTPER CENT	FHYDRO	FMIN	FMAX	FSINITIA L	ZOFFSE T
LENGTH	0.113	-0.107	-0.073	0.173	0.048	-0.318	0.366	-0.503	0.01	0.145	-0.025	-0.13	0.142
WIDTH	0.087	-0.182	-0.101	0.177	0.111	-0.125	0.448	-0.247	0.031	0.206	0.002	-0.228	0.157
EATP	0.15	0.001	0.132	0.066	0.039	-0.079	0.2	-0.884	-0.058	0.174	0.065	-0.201	0.045
EAMP	0.005	0.013	-0.088	0.022	-0.103	-0.401	-0.042	0.636	0.025	-0.179	0.269	0.102	-0.006
EABP	-0.147	-0.007	-0.14	-0.061	-0.042	0.037	-0.192	0.91	0.059	-0.181	-0.043	0.177	-0.03
EATXA_Z	0.146	-0.08	0.156	0.07	0.093	0.171	0.304	-0.642	-0.034	0.181	0.169	-0.157	-0.024
EATXA	-0.12	small	-0.131	-0.087	-0.09	-0.009	-0.041	0.936	0.098	-0.145	-0.007	0.143	-0.01
EAMXA	-0.08	0.079	-0.082	-0.075	-0.063	-0.158	0.032	0.743	0.079	-0.112	0.185	0.034	0.031
EABXA	0.156	-0.048	0.08	0.093	0.028	-0.237	0.068	-0.679	-0.047	0.055	0.112	-0.215	0.074
EHTP	0.141	0.008	0.148	0.064	0.047	-0.069	0.115	-0.922	-0.073	0.144	0.027	-0.168	0.027
EHMP	-0.04	0.128	-0.049	0.151	-0.197	-0.379	-0.233	-0.012	-0.134	-0.166	0.227	0.057	0.025
EHBP	-0.137	-0.002	-0.162	-0.053	-0.062	0.004	-0.137	0.938	0.073	-0.175	-0.017	0.152	-0.01
SATP	-0.279	-0.025	0.095	-0.055	-0.209	-0.221	0.091	-0.395	-0.085	0.011	0.094	-0.171	0.181
SAMP	0.048	small	-0.129	0.002	-0.037	-0.317	0.057	0.694	0.039	-0.166	0.208	0.035	-0.051
SABP	0.297	-0.068	-0.18	0.053	0.173	0.02	-0.058	0.756	0.103	-0.122	-0.042	0.061	-0.092
SATNA_Z	0.092	0.142	-0.267	-0.019	-0.164	-0.135	0.119	0.357	0.047	-0.062	0.058	-0.178	0.011
SATNA	-0.317	-0.021	0.182	-0.06	-0.148	-0.144	0.096	-0.585	-0.075	0.089	0.073	-0.152	0.168
SAMNA	0.287	-0.032	-0.189	0.025	0.132	0.007	-0.053	0.807	0.1	-0.149	-0.044	0.07	-0.12
SABNA	0.02	0.01	-0.114	0.009	-0.045	-0.318	0.047	0.691	0.04	-0.175	0.193	0.052	-0.059
SATNH_X	-0.032	-0.072	-0.141	0.054	-0.142	0.15	0.325	0.328	-0.01	0.025	0.051	-0.203	0.175
SATNH	-0.409	0.04	0.222	-0.168	-0.101	-0.135	0.063	-0.631	-0.06	0.097	0.022	-0.067	0.077
SAMNH	-0.153	0.197	0.023	-0.018	-0.126	-0.185	-0.258	0.254	-0.094	-0.227	0.154	0.179	-0.104
SABNH	0.305	-0.029	-0.171	0.102	0.066	0.084	-0.109	0.663	0.056	-0.126	-0.066	0.102	-0.126
SHTP	-0.32	-0.01	0.117	-0.058	-0.208	-0.146	-0.063	-0.487	-0.093	0.004	0.046	-0.093	0.085
SHMP	-0.089	0.089	-0.046	0.061	-0.089	-0.332	-0.006	0.462	-0.074	-0.188	0.258	0.042	-0.064
SHBP	0.371	-0.056	-0.183	0.08	0.149	0.041	0.026	0.644	0.121	-0.093	-0.041	0.064	-0.064
SHTNA_Z	-0.232	-0.009	0.052	0.115	-0.153	0.256	0.072	0.054	-0.249	-0.003	0.055	-0.069	0.08
SHTNA	-0.387	0.07	0.193	-0.064	-0.192	-0.081	-0.047	-0.727	-0.125	0.081	-0.016	-0.031	0.053
SHMNA	-0.147	0.146	-0.028	0.05	-0.108	-0.243	-0.027	0.381	-0.066	-0.182	0.25	0.05	-0.064
SHBNA	0.344	-0.06	-0.149	0.091	0.167	0.112	0.005	0.601	0.124	-0.058	-0.047	0.065	-0.063
SHTXH_X	0.03	0.11	0.12	0.034	-0.003	0.495	-0.116	-0.397	-0.158	0.146	0.06	-0.158	0.175
SHTXH	0.034	-0.002	-0.181	-0.015	0.002	-0.046	0.136	0.955	0.084	-0.14	0.008	0.015	-0.045
SHMXH	0.029	-0.031	0.138	0.111	0.055	-0.034	-0.098	-0.923	-0.118	0.103	-0.059	-0.075	-0.008
SHBXH	-0.085	0.012	0.17	0.019	-0.018	0.077	-0.137	-0.925	-0.116	0.096	-0.067	0.008	-0.04
SHTNH_X	0.021	0.009	0.039	-0.21	-0.145	0.006	0.173	0.371	0.064	-0.112	0.053	0.146	-0.038
SHTNH	-0.356	0.032	0.163	-0.075	-0.196	-0.084	-0.082	-0.634	-0.112	0.05	0.035	-0.055	0.079
SHMNH	-0.09	0.099	-0.047	0.06	-0.099	-0.333	-0.003	0.462	-0.075	-0.196	0.253	0.041	-0.071
SHBNH	0.38	-0.059	-0.19	0.085	0.148	0.04	0.04	0.678	0.112	-0.098	-0.033	0.052	-0.077
SRP	0.227	-0.183	small	0.088	0.26	0.108	-0.243	0.112	0.029	-0.158	-0.098	0.27	-0.006
SMP	0.323	-0.211	-0.207	0.027	0.178	-0.041	-0.106	0.429	0.128	-0.056	0.001	0.192	0.017
SRA	0.163	-0.321	0.125	0.179	0.117	-0.314	0.016	-0.3	-0.002	-0.171	0.115	0.162	-0.076

SMA	0.161	0.182	-0.117	0.168	0.083	0.22	small	0.583	-0.015	0.023	0.137	0.069	-0.043
SRA_Z	0.07	-0.154	-0.005	0.066	0.022	-0.026	0.339	0.166	-0.122	0.087	-0.032	-0.348	0.105
SRH	0.138	-0.215	0.024	0.107	0.028	-0.136	-0.118	-0.535	-0.136	-0.106	-0.046	0.044	-0.02
SMH	0.145	0.139	-0.068	0.145	0.085	0.178	-0.044	0.577	0.04	0.045	0.202	0.126	-0.066
SRH_X	0.02	-0.009	0.046	-0.05	small	-0.132	0.136	0.52	0.043	0.012	0.163	-0.169	-0.005
N_log	0.04	0.247	0.043	-0.098	-0.152	-0.077	0.265	-0.319	-0.071	0.097	0.023	-0.348	-0.046

Table B.5.4. Regression analysis- Coefficients and R² value for interaction of dent with girth weld

	a ₀	b ₁	b ₂	b ₃	b ₄	b ₅	b ₆	b ₇	b ₈	b ₉	b ₁₀	c ₁	c ₂	c ₃	c ₄	c ₅	c ₆	c ₇	c ₈	c ₉	c ₁₀	R ²
EATP	-3.34E-01	1.10E-03	6.67E+00	-1.05E-01	-2.13E-01	2.38E-01	9.09E+01	2.75E-01	5.84E-02	9.27E-02	-	-4.51E-06	2.63E+01	-1.02E-02	1.78E+00	-1.67E-02	1.28E+04	-1.34E-01	-5.11E-02	-8.31E-02	-	0.84
EAMP	1.36E-01	-4.17E-04	1.33E+00	4.59E-02	-1.44E-01	-4.45E-02	4.10E+01	-9.92E-02	7.53E-04	-2.17E-02	-	3.34E-06	-4.59E-01	-6.15E-03	-2.60E-02	-3.16E-02	5.48E+03	4.50E-02	-3.30E-03	2.59E-02	-	0.68
EABP	4.69E-01	-1.50E-03	8.00E+00	1.51E-01	6.90E-02	-2.83E-01	1.32E+02	-3.73E-01	-5.79E-02	-1.14E-01	-	7.87E-06	2.68E+01	4.05E-03	1.81E+00	-1.50E-02	1.83E+04	1.79E-01	4.80E-02	1.09E-01	-	0.83
EATXA_Z/D	1.92E+00	2.65E-02	4.57E-01	-7.75E-01	2.98E+00	5.08E+00	3.11E+02	1.92E+00	9.54E-01	5.65E-01	-	-1.08E-04	8.99E+00	6.68E-01	1.46E+00	3.94E+00	6.18E+04	-8.68E-01	-7.22E-01	-1.98E-01	-	0.54
EATXA	7.76E-02	-2.09E-04	1.46E+00	2.60E-02	-6.65E-02	-6.05E-02	2.42E+01	-5.27E-02	-4.00E-03	-1.46E-02	-	1.40E-06	3.00E+00	8.50E-04	-7.48E-02	-3.13E-03	3.11E+03	2.32E-02	3.50E-03	1.40E-02	-	0.90
EAMXA	1.36E-01	-4.17E-04	1.33E+00	4.59E-02	-1.44E-01	-4.45E-02	4.10E+01	-9.92E-02	7.53E-04	-2.17E-02	-	3.34E-06	-4.59E-01	-6.15E-03	-2.60E-02	-3.16E-02	5.48E+03	4.50E-02	-3.30E-03	2.59E-02	-	0.68
EABXA	5.01E-02	-2.39E-04	1.16E+00	2.19E-02	-4.46E-02	-5.00E-02	1.61E+01	-2.91E-02	8.60E-04	-1.23E-02	-	1.37E-06	4.24E+00	4.50E-04	-8.40E-02	8.44E-03	2.10E+03	1.31E-02	-4.36E-04	1.16E-02	-	0.85
EHTP	-3.27E-01	1.30E-03	8.30E+00	-1.11E-01	-2.10E-01	2.05E-01	9.39E+01	2.67E-01	4.07E-02	8.00E-02	-	-6.00E-06	3.40E+01	-6.15E-03	1.78E+00	3.99E-02	1.34E+04	-1.30E-01	-4.24E-02	-7.34E-02	-	0.88
EHMP	1.07E-01	-1.47E-04	7.34E-01	3.50E-02	-1.29E-01	-3.05E-02	3.28E+01	-8.81E-02	7.10E-03	-1.81E-02	-	1.73E-06	1.39E+00	-5.30E-03	2.55E-02	-2.85E-02	4.42E+03	3.93E-02	-8.20E-03	2.27E-02	-	0.54
EHBP	4.34E-01	-1.50E-03	9.04E+00	1.46E-01	8.20E-02	-2.35E-01	1.27E+02	-3.55E-01	-3.38E-02	-9.82E-02	-	7.75E-06	3.26E+01	8.50E-04	1.76E+00	-6.88E-02	1.78E+04	1.69E-01	3.43E-02	9.61E-02	-	0.87
SATP/SMYS	-2.28E-01	-6.03E-04	3.59E+00	8.85E-01	9.25E+00	1.17E+00	5.15E+02	7.29E-01	7.46E-01	2.58E-02	-	6.29E-05	7.62E+01	-4.78E-01	2.05E+01	1.76E+00	5.23E+04	-2.96E-01	-7.23E-01	5.87E-02	-	0.50
SAMP/SMYS	1.58E+00	2.92E-02	3.34E+01	-2.36E-01	7.40E-02	1.80E+00	1.59E+02	1.45E-01	-9.99E-02	-1.12E-01	-	-1.37E-04	1.17E+02	1.23E-01	-8.43E-01	1.03E+00	1.90E+04	-7.12E-02	-4.48E-02	5.44E-02	-	0.89
SABP/SMYS	2.77E-01	-5.09E-04	5.98E+00	-8.05E-01	7.70E+00	1.06E+00	4.01E+02	-5.34E-01	-6.56E-01	3.90E-03	-	-4.27E-05	1.07E+02	3.95E-01	1.62E+01	1.08E+00	4.84E+04	2.77E-01	6.14E-01	-5.21E-02	-	0.55
SATNA_Z/D	-3.09E-02	2.50E-03	1.99E+00	2.77E-01	1.44E+00	-4.63E-01	1.95E+01	-9.12E-02	1.34E-01	2.04E-02	-	-1.05E-05	6.56E+00	-1.24E-01	2.60E+00	4.21E-01	1.46E+03	3.95E-02	-9.87E-02	-2.36E-02	-	0.66
SATNA/SMYS	-2.59E-01	-2.00E-03	1.77E+01	5.55E-01	5.15E+00	-1.07E-01	2.02E+02	-5.27E-02	2.78E-01	-5.49E-02	-	5.32E-05	1.83E+02	-3.43E-01	1.04E+01	-1.04E-01	3.02E+04	5.10E-03	-3.19E-01	7.87E-02	-	0.77
SAMNA/SMYS	1.71E+00	3.07E-02	3.31E+01	-2.52E-01	5.00E-01	2.01E+00	2.15E+02	3.31E-02	-3.92E-02	-8.61E-02	-	-1.49E-04	1.44E+02	1.40E-01	1.80E+00	1.16E+00	2.31E+04	-3.92E-02	-6.23E-02	2.21E-02	-	0.88
SABNA/SMYS	3.98E-01	2.95E-04	1.64E+01	-6.25E-01	5.30E+00	6.58E-01	1.79E+02	-2.10E-02	-4.13E-01	3.96E-02	-	-3.89E-05	1.49E+02	3.28E-01	1.06E+01	-4.45E-01	2.86E+04	5.42E-02	4.01E-01	-7.31E-02	-	0.80
SATNH_X/D	-3.18E-01	3.13E-02	-3.17E-01	1.79E-01	2.24E+01	1.28E-02	-3.83E-02	9.50E-03	7.87E-06	6.87E+00	-	-8.18E-02	2.49E+00	-5.50E-02	1.20E+03	-1.54E-03	2.22E-02	-1.02E-02	7.02E-02	-2.54E-01	-	0.75

SATNH/SMYS	1.49E+00	1.01E-02	8.69E+00	5.35E-01	4.98E+00	1.61E+00	9.38E+01	1.26E-01	4.88E-01	1.22E-01	-	-1.86E-05	6.87E+01	-2.90E-01	1.01E+01	1.22E+00	2.52E+03	-1.10E-01	-4.15E-01	-9.17E-02	-	0.77
SAMNH/SMYS	-1.40E-01	2.94E-02	2.72E+01	-3.29E-01	1.41E+00	2.60E+00	1.00E+02	1.75E+00	6.46E-02	-2.68E-02	-	-1.41E-04	1.17E+02	2.93E-01	5.15E+00	6.38E-01	1.55E+04	7.55E-01	-3.20E-02	3.10E-03	-	0.72
SABNH/SMYS	6.40E-01	-6.50E-03	1.17E+01	-6.70E-01	5.65E+00	1.76E+00	1.60E+02	1.16E-01	-3.93E-01	-1.92E-01	-	-5.30E-06	1.02E+02	3.65E-01	1.21E+01	1.60E+00	2.70E+04	1.93E-02	3.64E-01	1.56E-01	-	0.77
SHTP/SMYS	4.09E-01	1.40E-03	8.45E+00	9.10E-01	7.40E+00	1.52E+00	5.26E+02	-6.23E-01	3.72E-01	-1.01E-01	-	4.96E-05	1.73E+02	-4.78E-01	1.52E+01	1.84E+00	6.04E+04	3.31E-01	-4.01E-01	1.41E-01	-	0.56
SHMP/SMYS	-3.89E-01	3.50E-02	3.19E+01	-8.50E-02	2.73E+00	3.25E+00	9.42E+01	1.13E+00	-4.48E-01	-2.77E-01	-	-1.47E-04	7.36E+01	8.90E-02	7.10E+00	1.79E+00	9.44E+03	4.31E-01	2.39E-01	1.74E-01	-	0.79
SHBP/SMYS	2.10E-01	-4.80E-03	7.61E+00	-8.90E-01	6.85E+00	2.04E+00	3.55E+02	1.31E-01	-3.85E-01	4.50E-02	-	-1.94E-05	1.18E+02	4.25E-01	1.37E+01	2.26E+00	4.31E+04	-3.96E-02	3.89E-01	-6.75E-02	-	0.68
SHTNA_Z/D	2.50E-01	-5.59E-04	1.41E-01	1.09E-02	-1.68E-01	-7.03E-02	1.06E+02	1.09E-02	-6.88E-02	8.60E-03	-	3.20E-06	5.09E-01	-8.73E-03	6.53E-01	1.34E-01	1.28E+04	-6.10E-03	4.52E-02	-7.90E-03	-	0.60
SHTNA/SMYS	-8.58E-01	6.00E-03	1.12E+01	8.55E-01	6.15E+00	1.62E+00	1.35E+02	1.21E-01	5.74E-01	-7.30E-02	-	5.29E-06	8.02E+01	-4.10E-01	1.16E+01	1.44E+00	2.25E+04	-1.54E-01	-4.84E-01	6.26E-02	-	0.82
SHMNA/SMYS	8.09E-01	3.12E-02	2.09E+01	-2.62E-01	3.24E+00	2.23E+00	5.64E+02	1.28E+00	-2.38E-01	-2.23E-01	-	-1.30E-04	2.08E+01	1.10E-01	9.78E+00	1.20E-01	7.66E+04	4.14E-01	5.77E-02	1.34E-01	-	0.68
SHBNA/SMYS	8.46E-01	-7.10E-03	1.03E+01	-8.00E-01	6.15E+00	1.81E+00	1.78E+02	-3.28E-01	-4.38E-01	-8.40E-03	-	6.32E-07	8.44E+01	3.75E-01	1.18E+01	1.67E+00	2.80E+04	2.53E-01	3.94E-01	6.80E-03	-	0.79
SHTXH_X/D	3.79E-01	-2.10E-03	3.35E+00	-1.15E-01	1.17E+00	1.07E-01	1.84E+01	-2.69E-01	4.38E-02	1.29E-01	-	4.88E-06	2.44E+01	6.13E-02	2.60E+00	-1.76E-02	3.83E+03	1.37E-01	-5.41E-02	-8.29E-02	-	0.45
SHTXH/SMYS	-7.37E-01	7.00E-03	3.11E+01	-2.87E-01	-3.65E-01	-2.31E-01	1.80E+02	4.77E-01	1.23E-01	-9.00E-03	-	-2.44E-05	1.75E+02	1.51E-02	4.08E+00	-1.38E-01	3.40E+04	-2.43E-01	-1.04E-01	-6.63E-02	-	0.93
SHMXH/SMYS	5.11E-02	-8.17E-04	1.30E+01	-2.19E-02	1.06E+00	2.14E-01	1.23E+01	3.08E-01	2.50E-03	-2.03E-01	-	1.18E-05	7.40E+01	-5.03E-02	3.90E+00	-7.25E-02	6.29E+02	-1.70E-01	-9.30E-03	1.52E-01	-	0.78
SHBXH/SMYS	-7.90E-01	6.30E-03	3.13E+01	-2.61E-01	1.14E+00	1.70E-01	1.84E+02	2.42E-01	2.05E-01	2.26E-01	-	-2.93E-05	1.84E+02	1.59E-02	-8.33E-01	-4.03E-01	2.98E+04	-1.00E-01	-1.76E-01	-2.22E-01	-	0.92
SHTNH_X/D	-3.45E-02	1.88E-04	2.39E-01	3.10E-03	-3.98E-02	-6.38E-02	8.08E+00	2.05E-02	1.47E-02	6.30E-03	-	-1.11E-06	1.08E-01	-1.98E-03	1.74E-01	1.15E-01	1.61E+03	-8.30E-03	-9.60E-03	-5.50E-03	-	0.92
SHTNH/SMYS	-1.73E-01	4.40E-03	1.39E+01	7.90E-01	5.70E+00	1.40E+00	2.83E+02	-3.83E-01	3.09E-01	-1.11E-01	-	1.46E-05	1.35E+02	-3.75E-01	1.05E+01	1.14E+00	4.16E+04	1.05E-01	-3.09E-01	9.92E-02	-	0.79
SHMNH/SMYS	-5.91E-01	3.63E-02	3.05E+01	-1.36E-01	2.39E+00	3.18E+00	7.28E+01	-8.75E-01	-3.72E-01	-2.70E-01	-	-1.60E-04	7.82E+01	1.27E-01	6.15E+00	1.59E+00	1.05E+04	2.77E-01	1.82E-01	1.48E-01	-	0.77
SHBNH/SMYS	3.26E-01	-5.30E-03	1.33E+01	-7.85E-01	5.65E+00	1.55E+00	2.53E+02	1.55E-01	-2.37E-01	7.87E-02	-	-8.79E-06	1.28E+02	3.63E-01	1.03E+01	1.24E+00	3.86E+04	8.80E-03	2.60E-01	-7.26E-02	-	0.81
SRP/SMYS	4.85E-02	-2.60E-03	1.84E+00	-6.30E-02	2.97E+00	4.18E-01	1.02E+02	-4.01E-01	-5.18E-01	-1.13E-02	4.59E-01	-7.23E-06	1.69E+00	1.11E-01	8.55E+00	-1.80E-01	2.92E+03	3.16E-01	5.79E-01	7.18E-02	-4.53E-01	0.40
SMP/SMYS	1.54E+00	3.00E-03	6.04E+00	-6.05E-02	3.02E+00	-4.83E-01	3.70E+01	-9.13E-01	-7.47E-02	7.14E-02	4.39E+00	-3.11E-05	2.04E+01	1.32E-01	8.60E+00	4.75E-01	1.49E+04	5.29E-01	2.06E-01	3.65E-02	3.85E+00	0.45

SRA_Z/D	-1.94E-01	2.40E-03	3.55E+00	3.61E-01	1.49E+00	-4.48E-01	3.59E+01	5.28E-02	4.53E-02	1.39E-02	4.34E-01	-1.33E-05	1.99E+01	-1.51E-01	2.68E+00	3.96E-01	5.09E+03	-3.32E-02	-5.47E-02	-1.79E-02	-4.80E-01	0.59
SMA/SMYS	-1.48E-01	1.10E-03	7.04E+00	-1.97E-02	1.33E+00	5.08E-01	1.91E+01	-3.18E-01	1.76E-01	-1.11E-02	1.63E-01	-9.34E-06	5.09E+01	1.52E-02	3.85E+00	-3.38E-01	1.94E+03	2.24E-01	-8.35E-02	-2.37E-02	1.34E-01	0.48
SRA/SMYS	3.02E+00	4.91E-05	1.34E+01	-3.70E-01	2.27E+00	-5.05E-01	5.23E+02	-2.01E-01	-2.98E-01	-3.10E-02	3.94E+00	-2.14E-05	9.58E+01	2.55E-01	5.13E+00	4.46E-01	7.17E+04	7.15E-02	2.68E-01	4.54E-02	3.72E+00	0.58
SRH_X/D	1.51E-01	-5.55E-04	1.70E-01	2.24E-02	-5.60E-02	-7.23E-03	7.04E+01	6.06E-02	-1.32E-01	-3.10E-03	9.18E-02	4.92E-06	4.74E+00	-1.68E-02	3.40E-01	-2.71E-02	9.04E+03	-2.88E-02	7.04E-02	-9.70E-03	-1.03E-01	0.29
SMH/SMYS	-1.87E-01	2.40E-03	4.62E+00	1.14E-01	4.21E-01	-4.80E-02	2.08E+01	4.42E-02	7.31E-02	-3.03E-02	2.29E-01	-1.63E-05	3.73E+01	-1.64E-02	-4.40E-01	-2.73E-02	5.64E+03	2.42E-02	-3.24E-02	1.00E-03	3.70E-03	0.57
SRH/SMYS	3.13E+00	-5.20E-03	1.04E+01	-3.90E-01	3.20E+00	2.90E-01	4.89E+02	-6.90E-01	-2.41E-01	-1.98E-04	3.75E+00	5.51E-06	9.37E+01	2.36E-01	9.58E+00	1.37E-01	6.76E+04	3.45E-01	2.69E-01	1.57E-02	3.70E+00	0.53
N_log	6.66E+00	3.26E-01	1.05E+02	6.65E+00	1.36E+02	3.08E+00	1.36E+04	5.20E+01	3.62E+01	-7.26E-01	8.69E+01	-7.79E-04	9.36E+02	3.93E+00	4.50E+02	1.60E+01	1.19E+06	3.15E+01	3.60E+01	5.63E+00	7.87E+01	0.35

REFERENCES

1. 01-SAMSS-035, 2009, *API Line Pipe*, Saudi Aramco.
2. Adams, K. and J. Zhou, “In-Service Dent Management Program from an Operator’s Perspective”, *Proceedings of the International Pipeline Conference*, ASME, IPC04-0437, Calgary, Alberta, Canada, 2004.
3. Advantica Ltd., 2004, *Risk Assessment of Selected Saudi Aramco Pipelines*, Report 6725, Advantica, United Kingdom.
4. Advantica, to be published by *United Kingdom Onshore Pipeline Association (UKOPA)*, UK, 2009, www.UKOPA.co.uk, Also, Francis, A. et al. “Development of a New Limit State Function for the Failure of Pipelines due to Mechanical Damage”, PRCI/EPRG/APIA Joint Technical Meeting, Orlando, USA, 2005.
5. ANSYS Inc., 2007, *Theory Reference for ANSYS and ANSYS Workbench 11.0*.
6. API 1156, 1999, *Effects of Smooth and Rock Dents on Liquid Petroleum Pipelines (Phase II)*, American Petroleum Institute.
7. API 579, *Fitness for Service*, American Petroleum Institute, October 2005.
8. API 5L, 2007, *Specification for Line Pipe*, American Petroleum Institute, 44th Edition.
9. API RP 579, 2000, *Recommended Practice for Fitness-For-Service*, American Petroleum Institute.
10. Arunakumar, G., 2007, *UKOPA Pipeline Fault Database, Pipeline Product Loss Incidents (1962-2006)*, UKOPA Report No: 6957, Issue: 1.0.
11. ASME B31.4, *Pipeline Transportation Systems for Liquid Hydrocarbons and Other Liquids*, ASME, 2006.

12. ASME B31.8, *Gas Transmission and Distribution Piping Systems*, ASME, 2007.
13. ASME B31.8, *Gas Transmission and Distribution Piping Systems*, ASME, 2003.
14. ASTM A 370, 2009, Standard Test Methods and Definitions for Mechanical Testing of Steel Products, American Society of Testing Materials.
15. Been, J., Carroll, B., Dinovizer, A. and R. Sutherby, “Stress Intensification and Crack Growth in the Presence of Dents on Pipelines”, *Proceedings of the International Pipeline Conference*, ASME, IPC2006-10415, Calgary, Alberta, Canada, 2006.
16. Belanger, A. A., and R. Narayanan, “Direct Strain Calculation of Pipe Line Dent from Knot Migration using a Kinematic Model Free of Material Properties”, *Proceedings of the International Pipeline Conference*, ASME, IPC2008-64143, Calgary, Alberta, Canada, 2008.
17. Bolton, B., Semiga, V., Dinovitzer, A., Tikku, S. and C. Alexander, 2008 “Towards a Validated Pipeline Dent Integrity Assessment Model”, *Proceedings of the International Pipeline Conference*, ASME, IPC2008-64621, Calgary, Alberta, Canada.
18. Broggiato, G. B., Campana, F., and L. Cortese, 2008 “The Chaboche Nonlinear Kinematic Hardening Model: Calibration Methodology and Validation”, *Meccanica*, **43**, pp 115-124.
19. BS 7910, 2005, *Guide to Methods for assessing the acceptability of Flaws in Metallic Structures*, British Standard Institution.
20. Caleyó, F., Alfonso, L., Alcantara, J. A, Hallen, J. M., Lagos, F. and H. Chow, 2006 “On The Estimation of Failure Rates of Multiple Pipeline Systems”,

- Proceedings of the International Pipeline Conference*, ASME, IPC2006-105265, Calgary, Alberta, Canada.
21. Carroll, L. B., 2007, *Full Scale Demonstration of the Interaction of Dents with Localized –Task 3 Material characterization*, updated report to Pipeline Research Council International, Project MD-4B Task 3, BMT Fleet Technology Limited.
 22. Carroll, L. B., Tiku, S., and A. Dinovitzer, 2006, *Full Scale Demonstration of the Interaction of Dents with Localized Effects- State of the Knowledge Review*, quarterly progress report to Pipeline Research Council International, Project MD 4-2B Task 1, BMT Fleet Technology Limited.
 23. Chaboche, J. L., 2008 “A Review of Some Plasticity and Viscoplasticity constitutive Theories”, *International Journal of Plasticity*, **24**, pp 1642-1693.
 24. Choi, Y., Son, D., Jang, J., Park, J., Kim, W. and D. Kwon, “Advanced Indentation Techniques; NDE for Flow Properties and Residual Stresses of Pipelines”, *Proceedings of the International Pipeline Conference*, ASME, IPC2002-27404, Calgary, Alberta, Canada, 2002.
 25. Clapham, L., Babbar, V., Rahim, T., and D. Atherton, “Detection of Mechanical Damage using the Magnetic Flux Leakage Technique”, *Proceedings of the International Pipeline Conference*, ASME, IPC2002-27142, Calgary, Alberta, Canada, 2002.
 26. Cosham, A., and P. Hopkins, “The Pipeline Defect Assessment Manual”, *Proceedings of the International Pipeline Conference*, ASME, IPC2002-27067, Calgary, Alberta, Canada, 2002.
 27. CSA Z662, *Oil and Gas Pipeline Systems*, Canadian Standards Association, 2003.

28. Cunha, S. B., Netto, T. A., Neto, F. Q. and O. S. X. Pinto, "Stress, Strain and Plastic Instability of Internally Pressurized Pipes with Axis-Symmetric and Narrow Volumetric Flaws- Analysis and Experiments", *Proceedings of the International Pipeline Conference*, ASME, IPC2006-10081, Calgary, Alberta, Canada, 2006.
29. D'Agostino, R. B. and Stephens, M. A., 1986. *Goodness-of-Fit Techniques*. Marcel-Dekker: New York.
30. Dawson, S. J., Russel, A., and A. Patterson, 2006 "Emerging Techniques for Enhanced Assessment and Analysis of Dents", *Proceedings of the International Pipeline Conference*, ASME, IPC2006-10264, Calgary, Alberta, Canada.
31. Dinovitzer, A. Lazor, R., Carroll, L.B., Zhou, J, McCarver, F., Ironside, S., Raghu, D., and K. Keith, "Geometric Dent Characterization", *Proceedings of the International Pipeline Conference*, ASME, IPC2002-27076, Calgary, Alberta, Canada, 2002.
32. Dinovitzer, A., Fredj, A., Carroll, B., Semiga, V., Asavare M., and S. Tiku, 2007, *Evaluation of the Interaction of Mechanical Damage on Welds*, Final Report prepared to Pipeline Research Council International, Report No. PR-214-0326, Catalogue No. L52048, BMT Fleet Technology Limited.
33. EGIG, 1999, *Gas Pipeline Incidents Report 1970-1998*, The 4th Report of the European Gas Pipeline Incident Data Group.
34. Fowler, J. R., Alexander, C. R., Kovach, P. J., and L. M. Connelly, 1994, *Cyclic Pressure Fatigue Life of Pipelines with Plain Dents, Dents with Gouges, and Dents with Welds*, Final Report prepared to Pipeline Research

- Council International, Report No. PR-201-927/201-9324, Catalogue No. L51705, Stress Engineering Services Inc.
35. Fowler, J. R., Katsounas, A. T., and R. Boubenider, 1992, *Criteria for Dent Acceptability of Offshore Pipelines*, Final Report prepared to Pipeline Research Council International, Report No. PR-201-927, Catalogue No. L51671, Stress Engineering Services Inc.
36. Francini, R. B. and N Yoosef-Ghodsi, 2008, *Development of a Model for Predicting the Severity of Pipeline Damage Identified by In-Line Inspection*, final report to Pipeline Research Council International, Report No. PR-218-063511-B, Kiefner & Associates, Inc.
37. Fuglem, M. K., Chen, Q., and M. J. Stephens, October 2001, *Pipeline Design for Mechanical Damage*, final report to Pipeline Research Council International, Report No. PR-244—9910, Catalogue No. L51860, CFER Technologies.
38. Gao, M., McNealy, R., Krishnamurthy, R. and I. Colquhoun, 2008 “Strain-Based Models for Dent Assessment- A Review”, *Proceedings of the International Pipeline Conference*, ASME, IPC2008-64565, Calgary, Alberta, Canada.
39. Green, S. B., 1991, "How many subjects does it take to do a regression analysis?", *Multivariate Behavioral Research*, **26** (3), pp. 499-510.
40. Halinski, R. S. and L. S. Feldt, 1970, “The Selection of Variables in Multiple Regression Analyses”, *Journal of Educational Management*, **7** (3), pp. 151-158.

41. Hertz-Clemens, S., “Experimental and Numerical Modelling of Pipeline Denting”, *Proceedings of the International Pipeline Conference*, ASME, IPC2006-10138, Calgary, Alberta, Canada, 2006.
42. Hines, W. W., and D. C. Montgomery, 1990, *Probability Statistics in Engineering and Management Sciences*, 3rd edition, John Wiley & Sons: New York.
43. Hopkins, P. and A. Cairns, *A Fracture Model to Predict the Failure of Defects in Dented Linepipe*, British Gas Engineering Research Station, December 1981
44. Ironside, S. and L. Carroll, “Pipeline Dent Management Program”, *Proceedings of the International Pipeline Conference*, ASME, IPC2002-27260, Calgary, Alberta, Canada, 2002.
45. Jandu, C., Francini, B., Taylor, M., and A. Francis, 2008 “Towards a New Limit State Function for Determining the Failure Pressure of a Pipeline Containing Mechanical Damage”, *Proceedings of the International Pipeline Conference*, ASME, IPC2008-64304, Calgary, Alberta, Canada.
46. Jaske, C. E., Hart, B. O. and W. A. Bruce, *Updated Pipeline Repair Manual Revision 6*, Final Report prepared to Pipeline Research Council International, Report No. PR-186-0324, Catalogue No. L52047, August 28, 2006.
47. Jinheng, L., Xinwei, Z., Qingren, X., and H. Chunyong, “Defective Pipeline Fatigue-Life Prediction Using Failure Assessment Diagram Technique”, *Proceedings of the International Pipeline Conference*, ASME, IPC04-0487, Calgary, Alberta, Canada, 2004.
48. Kececioglu, D. B., 2002. *Reliability Engineering Handbook: Volume 2*. DEStech Publications, Inc: Pennsylvania.

49. Kiefner, J. F., Melosh, R. E., and B. A. Kiefner, 2000, *Analysis of DOT Reportable Incidents for Gas Transmission and Gathering System Pipelines, Incident Data – 1985 to 1997*, final report to Pipeline Research Council International, PR-218-9801, Catalogue No. L51830.
50. Kiefner, J. F., Kolovich, C. E., Zelenak, P. A. and T. Wahjudi, “Estimating Fatigue Life for Pipeline Integrity Management”, *Proceedings of the International Pipeline Conference*, ASME, IPC04-0167, Calgary, Alberta, Canada, 2004.
51. Knoop, F. M. and R. Sommer, “Manufacturing and Use of Spiral Welded Pipes for High Pressure Service- State of the Art”, *Proceedings of the International Pipeline Conference*, ASME, IPC04-0257, Calgary, Alberta, Canada, 2004.
52. Lazor, R., and S. Verbit, “Using Pipeline Operating History for Integrity Management”, *Proceedings of the International Pipeline Conference*, ASME, IPC04-0399, Calgary, Alberta, Canada, 2004.
53. Le Bastard, A., 2006 “Influence of Internal Pressure for Depth Measurement on Dent”, *Proceedings of the International Pipeline Conference*, ASME, IPC2006-10103, Calgary, Alberta, Canada.
54. Lee, H. Y., Nikbin, K. M. and N. P. O’Dowd, “Simplified Method for Profiling Residual Stress Distributions in Plate and Pipe Components”, *Proceedings of the International Pipeline Conference*, ASME, IPC04-0648, Calgary, Alberta, Canada, 2004.
55. Leis, B. N., Forte, T. P., and X. Zhu, 2004 “Integrity Analysis for Dents in Pipelines”, *Proceedings of the International Pipeline Conference*, ASME, IPC04-0061, Calgary, Alberta, Canada.

56. Leis, N. B. and R. B. Francini, *Line Pipe Resistance to Outside Force, Volume 2: Assessing Serviceability of Mechanical Damage*, Final Report prepared to Pipeline Research Council International, Report No. PR-3-9305, Catalogue No. L51832, Battelle Memorial Institute, 1999.
57. Lyons, C., Haswell, J. V., Hopkins, P., Ellis, R. and N. Jackson, 2008 “A Methodology for the Prediction of Pipeline Failure Frequency Due to External Damage”, *Proceedings of the International Pipeline Conference*, ASME, IPC2008-64375, Calgary, Alberta, Canada.
58. Mannuci, G., Guagnelli, M., Vittori, O., and C. Spinelli, “An Experimental Approach to Evaluate the Resistance of Gas Pipeline to Dent and Gouge Damage by an Excavator”, *Proceedings of the International Pipeline Conference*, ASME, IPC2002-27069, Calgary, Alberta, Canada, 2002.
59. McCoy, J. and S. Ironside, “Dent Management Program”, *Proceedings of the International Pipeline Conference*, ASME, IPC04-0393, Calgary, Alberta, Canada, 2004.
60. Noronha Jr., D. B., Martins, R. R., Jacob, B. P. and E. de Souza, “The Use of B-Splines in the Assessment of Strain Levels Associated with Plain Dents”, *Proceedings of the Rio Pipeline Conference & Exposition*, ASME, Rio de Janeiro, Brazil, 2005.
61. Noronha Jr., D. B., Martins, R. R., Jacob, B. P. and E. de Souza, 2008 “Some Remarks on the Strain Based Assessment of Pipeline Dents”, *Proceedings of the International Pipeline Conference*, ASME, IPC2008-64136, Calgary, Alberta, Canada.
62. O’Neil, G., Besserer, M., Moore, D., and L. Fenyvesi, “A Satellite-Based Mechanical Damage Management Solution”, *Proceedings of the International*

- Pipeline Conference*, ASME, IPC2002-27320, Calgary, Alberta, Canada, 2002.
63. Pinheiro, B., Pasqualino, I., and S. da Cunha, 2006 “Stress Concentration Factors of Dented Pipelines”, *Proceedings of the International Pipeline Conference*, ASME, IPC2006-10598, Calgary, Alberta, Canada.
64. Pinheiro, B., Pasqualino, I., and S. da Cunha, 2008 “Fatigue Life Analysis of Steel Pipelines with Plain Dents under Cyclic Internal Pressure”, *Proceedings of the International Pipeline Conference*, ASME, IPC2008-64690, Calgary, Alberta, Canada.
65. ROSEN Group, *CDP Corrosion Detection Tool*. TF-CDP-E-02-2007-09. www.roseninpsection.net. 2007.
66. ROSEN Group, *RoCD² EMAT Crack Detection & Coating Disbondment Tool*. TF-RoCD2-E-02-2007-09. www.roseninpsection.net. 2007.
67. ROSEN Group, *RoGeo·Xt XYZ Mapping Tool*. TF-RoGeoXt-E-02-2007-09. www.roseninpsection.net. 2007.
68. Rosenfeld, M. J., Beckett, A., Neogi, B. Baskurt, U. J., and J. Elden, “Deterministic Assessment of Minor Mechanical Damage in Pipelines”, *Proceedings of the International Pipeline Conference*, ASME, IPC2006-10513, Calgary, Alberta, Canada, 2006.
69. Rosenfeld, M. J., *Development of a Model for Fatigue Rating Shallow Unrestrained Dents*, Final Report prepared to Pipeline Research Council International, Report No. PR-218-9405, Catalogue No. L51741, Kiefner Associates Inc., September 1997.

70. Rosenfled, M. J., *Guidelines for the Assessment of Dents on Welds*, Final Report prepared to Pipeline Research Council International, Report No. PR-218-9822, Catalogue No. L51810, Kiefner Associates Inc., December 1999.
71. Rosenfled, M. J., Warman, D. J., and R. C. McGregor, "Toward and Acceptance Criterion for Shallow Dents Affecting Girth Welds in Gas Transmission Pipelines", PVP-Vol. 353, *PVP Conference*, July 27-31, 1997.
72. SAE-L-131, 2009, *Fracture Control of Line Pipe*, Saudi Aramco.
73. SAEP-310, *Piping and Pipeline Repair*, Saudi Aramco, January 13, 2008.
74. SAES-L-450, *Pipeline Construction*, Saudi Aramco, 2003.
75. Seevam, P., Leyons, C., Hopkins, P., and M. Toft, 2008 "Modelling of Dent Gouges, and the Effect on the Failure Probability of Pipelines", *Proceedings of the International Pipeline Conference*, ASME, IPC2008-64061, Calgary, Alberta, Canada.
76. Semiga, V., December 2007, *Inventory of Types of Mechanical Damage Experienced by Gas and Oil Pipelines*, final draft report to Pipeline Research Council International, Project MD 2-1, Report No. PR-218—63511, BMT Fleet Technology, Ltd.
77. Semiga, V., November 2007, *Full Scale Demonstration of the Interaction of Dents with Localized Effects, task 4*, interim report to Pipeline Research Council International, Project MD 4-2, BMT Fleet Technology, Ltd.
78. Shigley, J. E., and C. R. Mischke, *Mechanical Engineering Design*, 1989, International Edition, 5th edition, Mc-Graw Hill Book Co., Singapore, pp. 276-299, Chap. 7.
79. STATGRAPHICS, 2010, *STATGRAPHICS Centurion XVI Vsession 16.1.03*, Statpoint Technologies Inc., Copyright 1982-2010.

80. Vieth, P. H., Maier, C. J., and C. E. Jaske, "Pressure Cycle Fatigue- A Statistical Assessment Approach", *Proceedings of the International Pipeline Conference*, ASME, IPC04-0556, Calgary, Alberta, Canada, 2004.
81. Warman, D. J., Johnston, D., Mackenzie, J. D., Rapp, S. and B. Travers, "Management of Pipeline Dents and Mechanical Damage in Gas Pipelines", *Proceedings of the International Pipeline Conference*, ASME, IPC2006-10407, Calgary, Alberta, Canada, 2006.
82. Westwood, S., and P. Hopkins, "Smart Pig Defect Tolerances: Quantifying the Benefits of Standard and High Resolution Pigs", *Proceedings of the International Pipeline Conference*, ASME, IPC04-0514, Calgary, Alberta, Canada, 2004.
83. Wolvert, G., Zarea, M., Rousseau, D. and C. Andrieux, 2004 "Probabilistic Assessment of pipeline Resistance to Third Party Damage: Use of Surveys to Generate Necessary Input Data", *Proceedings of the International Pipeline Conference*, ASME, IPC04-0656, Calgary, Alberta, Canada.

Active projects

84. Dinovitzer, A., Zarea, M., Wood, I., and M Piazza., *Structural Significance of Mechanical Damage*, quarterly progress report to Pipeline Research Council International, Project MD 4, November 30, 2008.
85. Zarea, M., Batisse, R., and P. Cardin, *Full Scale Experimental Validation of Mechanical Damage Assessment Models*, update presentation to Pipeline Research Council International, Project MD 4-1, February 12, 2008.
86. [MD-4-3](#). *Improved Model for Predicting the Burst Pressure of Dent + Gouge Damage*. Project funded by Pipeline Research Council International.
87. [MD-4-4](#). *Improved Model for Predicting the Time/Cycle Dependent Behavior of Dent + Gouge Model*. Project funded by Pipeline Research Council International.
88. [MD-4-6](#). *Full-Scale Experimental Validation of Mechanical Damage Assessment Models-Extension of MD-4-1*. Project funded by Pipeline Research Council International.
89. [MD-4-7](#). *Full-Scale Experimental Validation of Mechanical Damage Assessment Models-Options MD-1*. Project funded by Pipeline Research Council International.
90. [MD-1](#). *Development of a Dual Field Magnetic Flux Leakage Inspection Technology to Detect Mechanical Damage*. Project funded by Pipeline Research Council International.
91. [MD-1-1](#). *Dual Field Magnetic Flux Leakage Inspection Technology to Detect Mechanical Damage*. Project funded by Pipeline Research Council International.

92. [MD-1-2](#). *Performance Characterization of Current In-Line Inspection Technologies for Mechanical Damage Detection*. Project funded by Pipeline Research Council International.
93. [MD-1-3](#). *Understanding Magnetic Flux Leakage Signals “from Mechanical Damage in Pipelines*. Project funded by Pipeline Research Council International.
94. [MD-1-4](#). *Field Testing and Verification of Existing Tool Capabilities for Mechanical Damage Detection and Characterization*. Project funded by Pipeline Research Council International.
95. [MD-1-5](#). *Enhanced Mechanical Damage Database by Improving Mechanical Damage Assessment in the Ditch*. Project funded by Pipeline Research Council International.
96. [MD-1-6](#). *Ultrasonic Measurements of Strains in Pipelines*. Project funded by Pipeline Research Council International.
97. [MD-5A](#). *Inspection Procedures for Dent+Gouge Damage*. Project funded by Pipeline Research Council International.
98. [MD-5B](#). *Easy Repair Procedures for Dent+Gouge Damage*. Project funded by Pipeline Research Council International.

VITA

Name: Husain Muhammed Al-Muslim

Birth: 11 Sep, 1977, Hofuf, Saudi Arabia

Education: - Completed BS Degree in Mechanical Engineering with First Honors from King Fahd University of Petroleum and Minerals, Dhahran, Saudi Arabia in May 2000.

- Completed MS Degree in Mechanical Engineering with from King Fahd University of Petroleum and Minerals, Dhahran, Saudi Arabia in Feb 2003.

- Completed PhD Degree requirements in Mechanical Engineering from King Fahd University of Petroleum and Minerals, Dhahran, Saudi Arabia in May 2010.

Professional: Mechanical Engineer, Saudi Aramco, 2000-2005

Pipeline Engineer, Saudi Aramco, 2005-present

Contact: Husain.muslim.2@aramco.com; muslimhm@hotmail.com